Lappeenrannan teknillinen yliopisto
*Lappeenranta University of Technology*

Ivan Zakharchuk

# MANIFESTATION OF THE PAIRING SYMMETRY IN THE VORTEX CORE STRUCTURE IN IRON-BASED SUPERCONDUCTORS

Thesis for the degree of Doctor of Science (Technology) to be presented with due permission for public examination and criticism in the Auditorium 1382 at Lappeenranta University of Technology, Lappeenranta, Finland on the 17th of June, 2013, at noon.

Acta Universitatis
Lappeenrantaensis 520

Supervisors Professor Erkki Lähderanta and
D. Sc. Konstantin Traito
Department of Mathematics and Physics
Lappeenranta University of Technology
Finland

Reviewers Professor Nikolai Kopnin
O.V. Lounasmaa Laboratory
Aalto University School of Science
Finland

Professor Sergey Saveliev
Department of Physics
Loughborough University
United Kingdom

Opponent Professor Alexander Granovsky
Department of Magnetism
Faculty of Physics
Moscow State University
Russia

ISBN 978-952-265-418-2
ISBN 978-952-265-419-9 (PDF)
ISSN-L 1456-4491
ISSN 1456-4491

Lappeenrannan teknillinen yliopisto
Digipaino 2013

## Abstract

Ivan Zakharchuk
**MANIFESTATION OF THE PAIRING SYMMETRY IN THE VORTEX CORE STRUCTURE IN IRON-BASED SUPERCONDUCTORS**
Lappeenranta, 2013
179 p.
Acta Universitatis Lappeenrantaensis 520
Diss. Lappeenranta University of Technology
ISBN 978-952-265-418-2, ISBN 978-952-265-419-9 (PDF), ISSN-L 1456-4491, ISSN 1456-4491

The superconducting gap is a basic character of a superconductor. While the cuprates and conventional phonon-mediated superconductors are characterized by distinct $d$- and $s$-wave pairing symmetries with nodal and nodeless gap distributions respectively, the superconducting gap distributions in iron-based superconductors are rather diversified. While nodeless gap distributions have been directly observed in $Ba_{1-x}K_xFe_2As_2$, $BaFe_{2-x}Co_xAs_2$, LiFeAs, $K_xFe_{2-y}Se_2$, and $FeTe_{1-x}Se_x$, the signatures of a nodal superconducting gap have been reported in LaOFeP, LiFeP, FeSe, $KFe_2As_2$, $BaFe_{2-x}Ru_xAs_2$, and $BaFe_2(As_{1-x}P_x)_2$. Due to the multiplicity of the Fermi surface in these compounds $s^{\pm}$ and $d$ pairing states can be both nodeless and nodal. A nontrivial orbital structure of the order parameter, in particular the presence of the gap nodes, leads to effects in which the disorder is much richer in $d_{x^2-y^2}$-wave superconductors than in conventional materials. In contrast to the $s$-wave case, the Anderson theorem does not work, and nonmagnetic impurities exhibit a strong pair-breaking influence. In addition, a finite concentration of disorder produces a nonzero density of quasiparticle states at zero energy, which results in a considerable modification of the thermodynamic and transport properties at low temperatures. The influence of order parameter symmetry on the vortex core structure in iron-based pnictide and chalcogenide superconductors has been investigated in the framework of quasiclassical Eilenberger equations. The main results of the thesis are as follows.

The vortex core characteristics, such as, cutoff parameter, $\xi_h$, and core size, $\xi_2$, determined as the distance at which density of the vortex supercurrent reaches its maximum, are calculated in wide temperature, impurity scattering rate, and magnetic field ranges. The cutoff parameter, $\xi_h(B, T, \Gamma)$, determines the form factor of the flux-line lattice, which can be obtained in $\mu$SR, NMR, and SANS experiments. A comparison among the applied pairing symmetries is done. In contrast to $s$-wave systems, in $d_{x^2-y^2}$-wave superconductors, $\xi_h/\xi_{c2}$ always increases with the scattering rate $\Gamma$. Field dependence of the cutoff parameter affects strongly on the second moment of the magnetic field distributions, resulting in a significant difference with nonlocal London theory.

It is found that normalized $\xi_2/\xi_{c2}(B/B_{c2})$ dependence is increasing with pair-breaking impurity scattering (interband scattering for $s^{\pm}$-wave and intraband impurity scattering for $d$-wave superconductors). Here, $\xi_{c2}$ is the Ginzburg-Landau coherence length determined from the upper critical field $B_{c2} = \Phi_0/2\pi\xi_{c2}^2$, where $\Phi_0$ is a flux quantum. Two types of $\xi_2/\xi_{c2}$ magnetic field dependences are obtained for $s^{\pm}$ superconductors. It has a minimum at low temperatures and small impurity scattering transforming in monotonously decreasing function at strong scattering and high temperatures. The second kind of this dependence has been also found for $d$-wave superconductors at intermediate and high temperatures. In contrast, impurity scattering results in decreasing of $\xi_2/\xi_{c2}(B/B_{c2})$ dependence in $s_{++}$ superconductors.

A reasonable agreement between calculated $\xi_h/\xi_{c2}$ values and those obtained experimentally in non-

stoichiometric $BaFe_{2-x}Co_xAs_2$ ($\mu$SR) and stoichiometric LiFeAs (SANS) was found. The values of $\xi_h/\xi_{c2}$ are much less than one in case of the first compound and much more than one for the other compound. This is explained by different influence of two factors: the value of impurity scattering rate and pairing symmetry.

Keywords: iron-based superconductors, quasiclassic, Eilenberger, vortex core structure, flux-line lattice, pair-breaking, impurity scattering, spin fluctuation

UDC 538.945:537.312.6:621.38:53:621.3

*To my wife*

## Acknowledgements

This thesis is a result of research performed at the Department of Mathematics and Physics of Lappeenranta University of Technology. I would like to express my gratitude to my supervisors Professor Erkki Lähderanta and D. Sc. Konstantin Traito for introduction to the subject and guidance throughout the research work. Their valuable discussions and support are highly appreciated. I am grateful to my colleagues Mikhail Safonchik and Polina Belova for cooperation and inestimable help. I also would like to thank Alexandr Lashkul and other colleagues from the Department of Mathematics and Physics of Lappeenranta University of Technology for interesting and pleasant atmosphere.

I wish to thank my beloved family for support during my studies. And I am sincerely and heartily grateful to my wife Maria for her understanding, care and love.

I would like to thank preliminary examiners Professor Nikolai Kopnin and Professor Sergey Saveliev and my opponent Professor Alexander Granovsky for their discreet critique, valuable remarks and suggestions.

I acknowledge financial support from the Research Foundation of LUT (LTY:n Tukisäätiö) and Finnish Cultural Foundation (Etelä-Karjalan rahasto).

Lappeenranta, 2013

*Ivan Zakharchuk*

## Preface

The pairing mechanism of high-$T_c$ iron-based superconductors has been a significant open problem and is still far from well understood. The nesting between hole and electron Fermi surface pockets is one of the main characters of FeAs compounds. In such systems hole-pockets are located in the Brillouin zone center and electron-pockets at the zone corners. The spin fluctuation theories predict fully-gaped sign reversing $s^{\pm}$-wave symmetry [Mazin et al. (2008b)] by focusing on the intra-orbital nesting, whereas inter-orbital nesting can initiate large orbital fluctuations which lead to the $s$-wave state without sign reversal ($s_{++}$). The latter behavior has been supported by the random-phase approximation [Saito et al. (2010)] and the fluctuation-exchange approximation [Onari and Kontani (2010)]. On the other hand, experimental reports on the alkali-intercalated iron-selenide materials of base composition $A_x\mathrm{Fe}_2\mathrm{Se}_2$ indicated an absence of the hole-like Fermi sheets for some dopings [Qian et al. (2011)]. The lack of hole pockets near the zone center excludes the $s^{\pm}$ pairing symmetry, which is based on scattering between the hole and electron Fermi surface sheets in the iron-pnictides. The computations based on the scattering among the electron pockets have pointed out that this band structure is nodeless $d$-wave [Kuroki et al. (2008)], since the symmetry-enforced nodal lines fall between the Fermi surfaces [Maier et al. (2012a)]. The calculations in the random-phase approximation (RPA) by Maiti *et al* show competing $d$- and $s$-wave orders for large electron doping, but only $d$-wave symmetry stabilizes in the absence of hole Fermi pockets [Maiti et al. (2011b)]. While experiments show contradictory results, recent angle-resolved photoemission spectroscopy (ARPES) measurements [Xu et al. (2012)] report of detecting an isotropic superconducting gap, which promotes the $s$-wave pairing symmetry. And the investigation of the thermal conductivity of $\mathrm{K}(\mathrm{Fe}_{1-x}\mathrm{Co}_x)_2\mathrm{As}_2$ samples with various $x$ point to the $d$-wave nature of superconductivity [Wang et al. (2012)]. Hence, the problem is still under debates.

This thesis describes the investigation of order parameter symmetry influence on the vortex core structure in iron-based superconductors, such as, pnictides and chalcogenides. The $s^{\pm}$-, $s_{++}$-, and $d_{x^2-y^2}$-wave pairing symmetries are the most plausible options for the novel materials and are examined for applicability. Here, the magnetic field distribution of the vortex lattice is calculated via the nonlocal generalized London model with the effective cutoff parameter $\xi_h$. The cutoff parameter is introduced into the model through the modified Bessel function, with the purpose to account for the finiteness of the core size and its magnetic field and temperature dependences. In the London equation (see, for example, **Paper 1**) the magnetic field penetration depth is calculated from the microscopic theory of the Meissner state. The cutoff parameter, $\xi_h$, is found from comparison of the generalized London equation, describing the vortex state in the superconductors, with numerically obtained solution of the quasiclassical Eilenberger equations for the mixed state. The advantage of the quasiclassical approach is that it contains nonlocal, nonlinear and the core effects simultaneously, which allows the investigation of their influence on electrodynamic and magnetic properties of high-$\kappa$ superconductors.

The model developed in **Papers 1-5** can be applied to data extraction from the muon spin rotation ($\mu$SR) and small-angle neutron scattering (SANS) studies of the vortex cores in the type-II superconductors [Sonier (2007)]. The data obtained throughout the research is of interest for interpretation of the experimental results and as a reference. The model employed in the computations is presented thoroughly for $s_{++}$ and $s^{\pm}$ symmetries in **Paper 1** and for the $d_{x^2-y^2}$-wave case in **Paper 2**. The influence of the pair-breaking impurity scattering on the cutoff parameter is examined in **Paper 4**. For comparison the order parameter coherence length, $\xi_1$, is also calculated, and different behavior with impurity introduction is found. The coherence length $\xi_1$ is defined as

$1/\xi_1 = (\partial|\Delta(r)|/\partial r)_{r=0}/|\Delta_{NN}|$, where index NN means nearest-neighbor (here and all through the text term "nearest-neighbor" is applied to the neighboring vortices of a flux-line lattice). **Paper 5** is paying attention to the vortex lattice form factor calculated using Eilenberger equations considering all relevant pairing symmetries.

### List of publications and author's contribution

Throughout the original publications the author was involved in the formulation of the problems and calculation processes. He also participated in discussions of the results and in writing the manuscripts.

The thesis includes an introductory part, a review of the subject, and comments to the following publications, which are referred to in the text by their numerals:

**1** **I. Zakharchuk, P. Belova, M. Safonchik, K. B. Traito and E. Lähderanta**, Vortex core size in unconventional superconductors, *Journal of applied physics*, **113**, 013906, 2013 DOI: 10.1063/1.4772670

**2** **I. Zakharchuk, P. Belova, K. B. Traito and E. Lähderanta**, Eilenberger approach to the vortex state in iron pnictide superconductors, *Supercondutors - Materials, Properties and Applications*, chapter 9, ISBN 979-953-307-798-6, 2012 DOI: 10.5772/48571

**3** **P. Belova, I. Zakharchuk, K. B. Traito and E. Lähderanta**, Impact of the order parameter symmetries on the vortex core structure in iron-based superconductors, *Modern Physics Letters B*, **26**, 1230013, 2012 DOI: 10.1142/S021798491230013X

**4** **P. Belova, I. Zakharchuk, K. B. Traito and E. Lähderanta**, Cutoff parameter versus Ginzburg-Landau coherence length in the mixed state of high-$\kappa$ superconductors with impurities: quasiclassical approach, *Journal of Physics: Conference Series*, **400**, 022007, 2012 DOI: 10.1088/1742-6596/400/2/022007

**5** **P. Belova, I. Zakharchuk,, M. Safonchik, K. B. Traito and E. Lähderanta**, Vortex lattice form factor in stoichiometric and nonstoichiometric iron pnictide superconductors, *Physica C*, submitted.

# PART I: OVERVIEW OF THE THESIS

CHAPTER I

# Introduction

The iron-arsenide superconductor LaFeAsO with critical temperature $T_c = 26$ K was discovered in 2008 by Hideo Hosono group [Kamihara et al. (2008)], which captured the attention of the high-temperature superconductivity community. Within two months, materials based on substitution of La with other rare earths had been synthesized, raising the critical temperature of Fe-based superconductors (FeBS) to 55 K. During the following five years several related families of materials were revealed, the rapid calculation of the electronic structure within density functional theory (DFT), and the development of microscopic models substantially based on these calculations were performed. The presence of another class of high-temperature superconductors is important due to the possibility of existence of materials with even higher $T_c$'s within the same class of Fe-based materials. But more important is that the comparison with the cuprates can allow one to potentially understand the essential ingredients of high-temperature superconductivity.

The structure and symmetry of the superconducting gap is one of the most fascinating issues surrounding the Fe-based superconductors. After five years of intensive research on the Fe-based superconductors, no consensus on any universal gap structure has been reached, and there is strong evidence that small differences in electronic structure can lead to strong diversity in superconducting gap structures, including gaps with nodes in some and full gaps in other materials. The actual symmetry class of most of the materials may be the same, of generalized $A_{1g}$ ($s$-wave) type, probably involving a sign change of the order parameter between Fermi surface sheets ($s^{\pm}$-wave). In addition, there have been suggestions that some related materials, furthest from the nearly compensated semimetal band structure of the originally discovered compounds, may have $d$-wave symmetry. Understanding of the symmetry character of the superconducting ground states and the detailed structure should provide clues to the microscopic pairing mechanism in the FeBS and, thus, a deeper conception of the high-temperature superconductivity phenomenon.

Fe-based superconductors like cuprates have two-dimensional $3d$ transition metal ions as the building blocks. In both cases small doping can introduce orthorombic distortions. The main structural difference in these planes is that in cuprates the $2p$-ligands lie very nearly in the plane with the Cu, while in Fe-based superconductors As, P, Se, or Te lie in nearly tetrahedral positions above and below the Fe plane [Lynn and Dai (2009)]. The in-plane subset of Cu $d$-orbitals $e_g$ are both present near the Fermi level, making the planar $d_{x^2-y^2}$ dominant in the system [Sakakibara et al. (2010)]. This allows the reduction of the multiband electronic structure to a low-energy effective one-band model. In FeBS, on the other hand, out-of-plane As hybridize well with the $t_{2g}$ Fe $d$-orbitals and all

three of them have weight at the Fermi surface. A substantial overlap between the $d$-orbitals favors a multiband model.

The phase diagrams of many FeBS look similar to cuprates'. In both classes of materials the undoped compounds exhibit antiferromagnetism, which vanishes with doping. Superconductivity appears at some nonzero doping and then disappears [Basov and Chubukov (2011)]. In cuprates the long range ordered Néel phase vanishes before superconductivity appears, while in FeBS the competition between these orders can take several forms. In LaFeAsO (1111 system), for instance, there appears to be a first order transition between the magnetic and superconducting states at a critical doping value, whereas in the $A_x Fe_2As_2$ (122 system, where $A$ is an alkaline earth metal) the superconducting phase coexists with magnetism over a finite range and then persists to higher doping [Hirschfeld et al. (2011)].

It seems that the two classes of superconducting materials show generally very similar behavior, but there are profound differences as well. The first difference is that the undoped cuprates are Mott insulators, but FeBS are metals, which suggests that the Mott-Hubbard physics of a half-filled Hubbard model is not a good starting point for pnictides. Another important difference between cuprates and FeBS is related to normal state properties. Underdoped cuprates manifest pseudogap behavior in both one-particle and two-particle charge and spin observables, as well as a variety of competing orders. For holedoped cuprates, a strange metal phase near optimal doping is characterized by linear resistivity over a wide temperature range. In FeBS, different temperature power law for the resistivity, including linear, have been observed near optimal doping and interpreted as being due to multiband physics and interband scattering [Golubov et al. (2011)]. The FeBS do not develop a robust pseudogap behavior in a wide variety of observable properties.

The nature of doping in Fe-based superconductors is not completely understood. Similar phase diagrams are obtained by replacing the spacer ion as in $LaFeAsO_{1-x}F_x$ and $Sr_{1-x}K_xFe_2As_2$, or by in-plane substitution of Fe with Co or Ni as in $Ba(Fe_{1-x}Co_x)_2As_2$ and $Ba(_{1-x}Ni_x)_2As_2$, or by replacing Ba with K, $Ba_{1-x}K_xFe_2As_2$. Whether these heterovalent substitutions dope the FeAs or FeP plane as in the cuprates is not initially clear [Sawatzky et al. (2009)], but now it is well established that they affect the Fermi surface consistent with the formal electron count doping [Nakamura et al. (2011)]. Another mechanism to vary electronic and magnetic properties is via the possibility of isovalent doping with phosphorus in $BaFe_2(As_{1-x}P_x)_2$ or ruthenium in $BaFe_2(As_{1-x}Ru_x)_2$. The dopants can act as potential scatterers and change the electronic structure by differences in ionic sizes or diluting magnetic ions with nonmagnetic ones. But roughly the phase diagrams of all FeBS are quite similar, challenging to find a systematic structural observable which correlates with the variation of $T_c$. Among several proposals, the height of the pnictogen or chalcogenide atom above the Fe plane has been noted as playing some role in the doping dependence [Kuroki et al. (2009)].

Probes of specific heat, penetration depth, nuclear magnetic resonance (NMR) relaxation rate, *etc* imply multiband nature with strongly coupled bands in many FeBS. Another manifestation of multiband superconductivity in FeBS is found in the thermal conductivity. The reduced thermal conductivity $\kappa/T$ is zero at $T = 0$, if the Fermi surface is fully gapped in the superconducting state, although pair-breaking effects due to magnetic impurities may create mobile quasiparticle states with zero energy [Glatz and Koshelev (2010)]. Many of FeBS, as well as $MgB_2$, display this behavior. Abrikosov vortices start to appear in the system upon applying magnetic field. At fields on the order of $H_{c2}/3$, the vortices begin to overlap, resulting in the increase of the thermal conductivity. Now, if there are two gaps in the system, one substantially smaller than the other, one may assume that the vortex overlap will start at much smaller fields. Indeed, the distance between the vortices

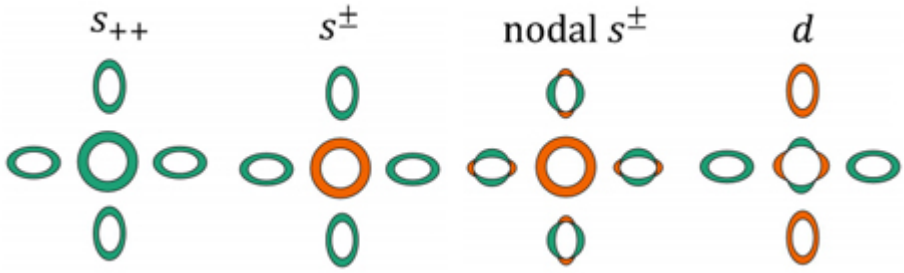


**Figure 1.1**: Pattern of order parameters under discussion in the Fe-pnictide superconductors represented in the 2D, 1-Fe Brillouin zone. Different colors stand for different signs of the gap [Hirschfeld et al. (2011)].

is proportional to $H^{-1/2}$, while their size is defined by the coherence length and, thus, inversely proportional to the order parameter, $\Delta$. So, the critical field where the weaker band will be smaller than that for the stronger band by a factor of, roughly, $(\Delta_1/\Delta_2)^2$, which is about 10 for $MgB_2$. Experimentally the dependence looks linear at the smallest accessible $H$ and nobody has observed the flattening of $\kappa(H)/T$ at fields $H \lesssim H_{c2}/30$. Many FeBS studied by this technique show a linear increase of $\kappa/T|_{T\to 0}$ at small fields, which suggests a considerable disparity between the large and the small gaps, or strong gap anisotropy.

Until late 1970s all known superconductors could be accounted for in terms of a condensate of Cooper pairs, where the Cooper pairs form due to electron-phonon interactions. The discovery of the superfluid phases of $^3$He changed this conception by providing an example of a non-electron-phonon-mediated pairing and of a superfluid condensate that breaks additional symmetries [Osheroff et al. (1972)]. On the other hand, the discovery of heavy-fermion superconductivity as a prime candidate for a complex order parameter symmetries and non-electron-phonon-mediated pairing in $f$-electron compounds played an important role in understanding of superconductivity. A complete analysis of the possible superconducting classes in heavy-fermion systems for cubic, hexagonal, tetragonal, rhombohedral groups was extensively studied by Volovik and Gor'kov [Volovik and Gor'kov (1985)]. The group theoretical classification of gap structures in unconventional superconductors has been circumstantially reviewed in [Sigrist and Ueda (1991)]. In the absence of spin-orbit coupling in Fe-based superconductors, the total spin of the Cooper pair can be either $S = 1$ or $S = 0$. Experimental data rules out spin triplet states, so the spin singlet case attracts attention. The focus is on tetragonal point group symmetry relevant for FeBS. In a 3D tetragonal system, group theory allows only four one-dimensional irreducible representations: $A_{1g}$ ($s$-wave), $B_{1g}$ ($d$-wave [$x^2-y^2$]), $B_{2g}$ ($d$-wave [$xy$]), and $A_{2g}$ ($g$-wave [$xy(x^2-y^2)$]) according to how the order parameter transforms under $90^\circ$ rotations and other operations of the tetragonal group [Volovik and Gor'kov (1985)]. In Figure 1.1 two of these symmetries are illustrated, namely $s$-wave and $d_{x^2-y^2}$-wave. The $s_{++}$ and $s^{\pm}$ states represented in Fig. 1.1 all have the same symmetry, neither of them changes sign if the crystal axes are rotated by $90^\circ$. Contrary, the $d$-wave state changes sign under a $90^\circ$ rotation. The mere existence of the single hole and single electron pockets leads to new ambiguities in the sign structure of the various states. In addition to a global sign change, which is equivalent to a gauge transformation, one can have individual rotations on single pockets and still preserve the symmetry. For instance, rotation of the gap on the hole pocket for the $d$-wave case (Fig. 1.1) by $90^\circ$ but keeping

the electron pocket sign fixed, still represents a $B_{1g}$ state [Hirschfeld et al. (2011)].

These symmetry properties are distinct from gap structure. Gaps with the same symmetry may have very different structures, as also illustrated in Figure 1.1. The isotropic fully gapped $s_{++}$ and $s^{\pm}$ states differ only by a relative phase of $\pi$ in the latter case between the hole and electron pockets. On the other hand, in the nodal $s$-wave case, the gap is shown vanishing at certain points on the electron pockets. This is the case of nodal $s^{\pm}$, in that the sign on the hole pockets is opposite to the average sign on the electron pockets. Nodes of this type are sometimes described as "accidental", since their existence is not dictated by symmetry, but rather by the details of the pair interaction. As such, they can be removed continuously, resulting in either an $s_{++}$ or an $s^{\pm}$ state.

CHAPTER II

# Bardeen-Cooper-Schrieffer theory

A general Hamiltonian has the form $\mathcal{H}_{BCS} = \hat{H}_0(\mathbf{r}) + H_{int}$, where

$$\hat{H}_0(\mathbf{r}) = \sum_{\alpha} \int d^d\mathbf{r} \psi^\dagger_\alpha(\mathbf{r})[\epsilon(-i\boldsymbol{\nabla}_\mathbf{r}) - \mu]\psi_\alpha(\mathbf{r}) \tag{2.1}$$

is the band Hamiltonian of quasiparticles with dispersion $\epsilon(\mathbf{k})$, $\mu$ is the chemical potential, and the interaction part

$$H_{int} = -\frac{1}{2}\sum_{\substack{\alpha,\beta \\ \gamma,\delta}} \int d^d\mathbf{r} d^d\mathbf{r}' \psi^\dagger_\alpha(\mathbf{r})\psi^\dagger_\alpha(\mathbf{r}')V_{\alpha\beta\gamma\delta}(\mathbf{r},\mathbf{r}')\psi_\gamma(\mathbf{r}')\psi_\delta(\mathbf{r}'). \tag{2.2}$$

Here $\mathbf{r}$ is the real space coordinate, $\alpha$, $\beta$, $\gamma$, and $\delta$ are the spin indices, and $\psi^\dagger$ and $\psi$ are the fermionic creation and annihilation operators, respectively. The mean field approximation consists of decoupling the four-fermion interaction into a sum of all possible bilinear terms, so that

$$H_{int} = \sum_{\alpha,\beta} \int d^d\mathbf{r} d^d\mathbf{r}' \Big( \tilde{V}_{\alpha\beta}(\mathbf{r},\mathbf{r}')\psi^\dagger_\alpha(\mathbf{r})\psi_\beta(\mathbf{r}') + \Delta_{\alpha\beta}(\mathbf{r},\mathbf{r}')\psi^\dagger_\alpha(\mathbf{r})\psi^\dagger_\beta(\mathbf{r}') + \Delta^*_{\alpha\beta}(\mathbf{r},\mathbf{r}')\psi_\beta(\mathbf{r})\psi_\alpha(\mathbf{r}') \Big). \tag{2.3}$$

The effective potential, $\tilde{V}_{\alpha\beta}(\mathbf{r},\mathbf{r}')$, is the sum of the Hartree and Fock exchange terms, and the last two terms account for superconducting pairing. The pairing field, $\Delta$, is determined self-consistently from

$$\Delta_{\alpha\beta}(\mathbf{r},\mathbf{r}') = \frac{1}{2}V_{\alpha\beta\gamma\delta}(\mathbf{r},\mathbf{r}')\langle\psi_\gamma(\mathbf{r}')\psi_\delta(\mathbf{r})\rangle. \tag{2.4}$$

The pairing occurs only below the transition temperature, $T_c$. Above $T_c$ the average of the two annihilation operators in Eq. (2.4) vanishes, and, therefore, $\Delta_{\alpha\beta} = 0$. In contrast, Hartree and Fock terms are finite at all temperatures, and can be incorporated in the quasiparticle dispersion, $\epsilon(\mathbf{k})$. These terms change below $T_c$, upon entering the superconducting state. Their relative change is of the order of the fraction of electrons participating in superconductivity, and therefore is small for weak coupling superconductors ($\sim \Delta/W \ll 1$, where $W$ is the electron bandwidth). Hence, the effective potential, $\tilde{V}$, is not included explicitly.

Therefore, the reduced mean field BCS Hamiltonian is

$$\mathcal{H}_{BCS} = \sum_{\alpha} \int d^d\mathbf{r} \psi^\dagger_\alpha(\mathbf{r}) \hat{H}_0(\mathbf{r}) \psi_\alpha(\mathbf{r}) + \sum_{\alpha,\beta} \int d^d\mathbf{r} d^d\mathbf{r}' \left\{ \Delta_{\alpha\beta}(\mathbf{r},\mathbf{r}') \psi^\dagger_\alpha(\mathbf{r}) \psi^\dagger_\beta(\mathbf{r}') + \text{H.c.} \right\}. \quad (2.5)$$

The spatial and spin structure of $\Delta_{\alpha\beta}(\mathbf{r},\mathbf{r}')$ determines the type of superconducting pairing. Here the singlet pairing is considered, when $\Delta$ has only the off-diagonal matrix elements in spin space, and it is common to write $\Delta_{\alpha\beta}(\mathbf{r},\mathbf{r}') = (i\sigma^y)_{\alpha\beta}\Delta(\mathbf{r},\mathbf{r}')$, where $\Delta$ is now a scalar function.

In a uniform superconductor the interaction depends only on the relative position of the electrons, so that $V(\mathbf{r},\mathbf{r}') = V(\boldsymbol{\rho} \equiv \mathbf{r} - \mathbf{r}')$. Thus, in the absence of impurities, the structure of the order parameter in real space depends on the symmetry properties of $V(\boldsymbol{\rho})$. These are easier to consider in momentum, rather than coordinate space. In models with local attraction, when $V(\boldsymbol{\rho}) = V_0\delta(\boldsymbol{\rho})$, the Fourier transform of the interaction is featureless, and $\Delta(\mathbf{k}) = \Delta_0$, which is an example of an isotropic ($s$-wave) superconductor.

### Bogoliubov transformation

Since the effective Hamiltonian of Eq. (2.5) is bilinear in fermion operators, $\psi$ and $\psi^\dagger$, it can be diagonalized by a canonical transformation of the form

$$\psi_\alpha(\mathbf{r}) = \sum_n \left[ u_{n\alpha}(\mathbf{r})\gamma_n + v_{n\alpha}(\mathbf{r})\gamma^\dagger_n \right], \quad (2.6)$$

subject to condition $|u_{n\alpha}(\mathbf{r})|^2 + |v_{n\alpha}(\mathbf{r})|^2 = 1$. The coefficients $u$ and $v$ are determined by solving the Bogoliubov-de Gennes equations [de Gennes (1989)]

$$E u_\alpha(\mathbf{r}) = H_0(\mathbf{r}) u_\alpha(\mathbf{r}) + \int d^d\mathbf{r}' \Delta_{\alpha\beta}(\mathbf{r},\mathbf{r}') v_\beta(\mathbf{r}'), \quad (2.7)$$

$$-E v_\alpha(\mathbf{r}) = H^*_0(\mathbf{r}) v_\alpha(\mathbf{r}) + \int d^d\mathbf{r}' \Delta^*_{\alpha\beta}(\mathbf{r},\mathbf{r}') u_\beta(\mathbf{r}'). \quad (2.8)$$

Here, label $n$ is omitted for conciseness. Clearly, when $\Delta = 0$, coefficients $u$ and $v$ do not couple, and there is no particle-hole mixing.

For each $n$ there are four functions, $u_\uparrow(\mathbf{r}), u_\downarrow(\mathbf{r}), v_\uparrow(\mathbf{r}), v_\downarrow(\mathbf{r})$ that need to be determined. However, for a singlet superconductor the matrix $\Delta_{\alpha\beta}$ is off-diagonal in the spin indices, so that $u_\uparrow(u_\downarrow)$ couples only to $v_\downarrow(v_\uparrow)$, and hence only two of the equations are coupled. In the presence of the impurity potential, however, in general all four components become independent.

Equations (2.7) and (2.8) are coupled integro-differential equations for the functions $u_{n\alpha}(\mathbf{r})$ and $v_{n\alpha}(\mathbf{r})$ [Balatsky et al. (2006)]. They have to be complemented by the self-consistency equations on $\Delta_{\alpha\beta}$, which can be obtained directly from Eq. (2.4),

$$\Delta_{\alpha\beta}(\mathbf{r},\mathbf{r}') = -\frac{1}{2} V_{\alpha\beta\gamma\delta}(\mathbf{r},\mathbf{r}') \sum_n \left[ u_{n\gamma}(\mathbf{r}') v^*_{n\delta}(\mathbf{r}) f(E_n) + v^*_{n\gamma}(\mathbf{r}') u_{n\delta}(\mathbf{r})(1 - f(E_n)) \right]. \quad (2.9)$$

Here, the Fermi function $f(E) = [\exp(E/T) + 1]^{-1}$.

In a uniform superconductor the Fourier transform of the Bogoliubov equations, Eqs. (2.7) and (2.8), into the momentum space gives

$$(\xi_{\mathbf{k}} - E_{\mathbf{k}})u_{\mathbf{k}\alpha} + \Delta_{\alpha\beta}(\mathbf{k})v_{\mathbf{k}\beta} = 0, \tag{2.10}$$

$$(\xi_{\mathbf{k}} + E_{\mathbf{k}})v_{\mathbf{k}\alpha} + \Delta^*_{\alpha\beta}(-\mathbf{k})u_{\mathbf{k}\beta} = 0, \tag{2.11}$$

where $\xi_{\mathbf{k}}$ is the bare quasiparticle energy, measured with respect to the chemical potential, $\xi_{\mathbf{k}} = \epsilon(\mathbf{k}) - \mu$. In a singlet superconductor

$$(\xi_{\mathbf{k}} - E_{\mathbf{k}})u_{\mathbf{k}\uparrow} + \Delta(\mathbf{k})v_{\mathbf{k}\downarrow} = 0, \tag{2.12}$$

$$(\xi_{\mathbf{k}} + E_{\mathbf{k}})v_{\mathbf{k}\downarrow} + \Delta^*(\mathbf{k})u_{\mathbf{k}\uparrow} = 0, \tag{2.13}$$

and one recovers the energy spectrum $E_{\mathbf{k}} = \sqrt{\xi^2_{\mathbf{k}} + |\Delta(\mathbf{k})|^2}$, with the coefficients $u$ and $v$ given by

$$\begin{pmatrix} u^2_{\mathbf{k}} \\ v^2_{\mathbf{k}} \end{pmatrix} = \frac{1}{2}\left[1 \pm \frac{\xi_{\mathbf{k}}}{E_{\mathbf{k}}}\right]. \tag{2.14}$$

**BCS variational wave function**

Superconductivity originates from the instability of the Fermi sea towards pairing of time-reversed quasiparticle states. Therefore, a variational wave function approach is to restrict the trial wave function to the subspace of either empty or doubly occupied states,

$$|\Psi(\mathbf{r})\rangle = \prod_n (a_n + b_n c^\dagger_{n\uparrow} c^\dagger_{\overline{n}\downarrow})|0\rangle, \tag{2.15}$$

and to minimize the energy, $E_{BCS} = \langle\Psi|H|\Psi\rangle$. This is a reasonable approximation at low temperatures. In Eq. (2.15) the vacuum state $|0\rangle$ denotes the filled Fermi sea, and $c^\dagger_{n\uparrow}$ ($c^\dagger_{\overline{n}\downarrow}$) creates a quasiparticle with spin up (down) and with the wave function $\phi_n(\mathbf{r})$ ($\phi^*_n(\mathbf{r})$) that is the eigenfunction of the single particle Hamiltonian. Normalization requires that $|a_n|^2 + |b_n|^2 = 1$.

In the absence of impurities these eigenfunctions can be labeled by the same indices, $\mathbf{k}$ and $\alpha$. Consequently, the variational approach is completely equivalent to the Bogoliubov analysis with the choice $u_n(\mathbf{r}) = a_n\phi_n(\mathbf{r})$, and $v_n(\mathbf{r}) = b_n\phi_n(\mathbf{r})$. In general interaction with impurities may lead to the appearance of the single particles states in the ground state wave function. Moreover, it is worth remembering that energy of the state described by the BCS wave function is greater or equal to that of the exact ground state obtained by solving the Bogoliubov equations.

**Green's functions**

The third approach is the Green's function method, which originates with the work of Gor'kov [Gor'kov (1959)]. Following Nambu notation a 4-vector, that is a spinor representation of the particle and hole states, is introduced,

$$\Psi^\dagger(\mathbf{r}) = (\psi^\dagger_\uparrow, \psi^\dagger_\downarrow, \psi_\uparrow, \psi_\downarrow). \tag{2.16}$$

The matrix Green's function is defined as the imaginary-time ordered average

$$\hat{G}(x,x') = -\langle T_\tau \Psi(x)\Psi^\dagger(x')\rangle, \tag{2.17}$$

where the four-vector $x = (\mathbf{r}, \boldsymbol{\tau})$ combines the real space coordinate, $\mathbf{r}$, and the imaginary time, $\tau$. The time evolution of the creation and annihilation operators in the Heisenberg approach is given by $\partial\psi/\partial\tau = [\mathcal{H}_{BCS} - \mu N, \psi]$.

For a singlet homogeneous superconductor the Hamiltonian of Eq. (2.5) in the Nambu notation takes the form

$$H_{BCS} = \int d\mathbf{r}\Psi^\dagger(\mathbf{r})(\xi(-i\nabla)\tau_3 + \Delta\tau_1\sigma_2)\Psi(\mathbf{r}), \tag{2.18}$$

and one finds [Maki (1969)]

$$\hat{G}_0^{-1}(\mathbf{k},\omega) = i\omega_n - \xi(\mathbf{k})\tau_3 - \Delta(\mathbf{k})\sigma_2\tau_1. \tag{2.19}$$

Here, $\omega_n = \pi T(2n+1)$ is the Matsubara frequency, $\sigma_i$ are the Pauli matrices acting in spin space, $\tau_i$ are the Pauli matrices in the particle-hole space, and $\tau_i\sigma_j$ denotes a direct product of the matrices operating in the 4-dimensional Nambu space. The self-consistency equation for a singlet superconductor takes the form

$$\Delta(\mathbf{k}) = -T\sum_{\omega_n}\int d\mathbf{k}' V(\mathbf{k},\mathbf{k}')\mathrm{Tr}[\tau_1\sigma_2 G_0]. \tag{2.20}$$

In BCS the interaction is restricted to a thin shell of electrons near the Fermi surface, and thus

$$\Delta(\hat{\Omega}) = -TN_0\sum_{\omega_n}\int d\hat{\Omega}' V(\hat{\Omega},\hat{\Omega}')\mathrm{Tr}\left[\tau_1\sigma_2\int d\xi_{\mathbf{k}} G_0\right], \tag{2.21}$$

where $\hat{\Omega}$ denotes a direction on the Fermi surface, and $N_0$ is the normal state density of states.

The off-diagonal component of $(\hat{G}_0)_{12} = F$ is often called the Gor'kov anomalous Green's function, since it describes the pairing average

$$F_{\alpha\beta}(x,x') = -\langle T_\tau \psi_\alpha(x)\psi_\beta(x')\rangle. \tag{2.22}$$

In general $F_{\alpha\beta}(x,x') = \mathrm{g}_{\alpha\beta}F(x,x')$, where g is the matrix describing the spin structure of the superconducting order. For the singlet pairing $\mathrm{g} = i\sigma^{(y)}$, where $\sigma^{(y)}$ is the Pauli matrix. Therefore, normal and anomalous components of $\hat{G}_0$ in a singlet spatially uniform superconductor are

$$G(\omega_n,\mathbf{k}) = \frac{i\omega_n + \xi_{\mathbf{k}}}{(i\omega_n)^2 - \xi_{\mathbf{k}}^2 - |\Delta(\mathbf{k})|^2}, \tag{2.23}$$

$$F(\omega_n,\mathbf{k}) = \frac{\Delta(\mathbf{k})}{(i\omega_n)^2 - \xi_{\mathbf{k}}^2 - |\Delta(\mathbf{k})|^2}. \tag{2.24}$$

The connection with the Bogoliubov's transformation is provided by rewriting the Green's functions as

$$G(\omega_n,\mathbf{k}) = \frac{u_{\mathbf{k}}^2}{i\omega_n - E_{\mathbf{k}}} + \frac{v_{\mathbf{k}}^2}{i\omega_n + E_{\mathbf{k}}}, \tag{2.25}$$

$$F(\omega_n, \mathbf{k}) = u_{\mathbf{k}} v_{\mathbf{k}}^* \left( \frac{1}{i\omega_n - E_{\mathbf{k}}} - \frac{1}{i\omega_n + E_{\mathbf{k}}} \right), \tag{2.26}$$

where $u_{\mathbf{k}}$ and $v_{\mathbf{k}}$ are given by Eq. (2.14) [Balatsky et al. (2006)].

For inhomogeneous problems, where the interesting part is the spatial variations of the superconducting order and electron density, both Bogoliubov equations and Green's functions are often used. The derivation of equations of motion for the energy integrated Green's functions can now proceed as originally described by Eilenberger [Eilenberger (1968)]. In this method only wave vectors close to the Fermi surface are assumed to be important.

### Vortex state in quasiclassical approach

Much attention has been focused on a vortex structure in $d_{x^2-y^2}$-wave superconductors. The main reason for it is to investigate the impact of the energy gap anisotropy on the vortex structure. The zero-energy density of states (DOS) $N(0)$ dependence on a magnetic field $H$ as $N(0) \propto \sqrt{H}$ in the $d_{x^2-y^2}$-wave pairing and $N(0) \propto H$ in the $s$-wave pairing was theoretically suggested by Volovik [Volovik (1993)]. While a $\sqrt{H}$-like behavior was observed in specific heat experiments [Moler et al. (1994)], it is uncertain whether it is exactly $\sqrt{H}$ or not. Deviations from $N(0) \propto H$ were also reported for $s$-wave superconductors [Hedo et al. (1998)]. Low-energy excitations in the vortex state can be divided conceptually into three groups: (i) those from the continuum states associated with the nodal structure, (ii) the core excitations from the bound states localized in a vortex core, and (iii) the quasiparticle transfer between vortices (vortex lattice effect). Volovik's calculation has accounted for only the first item, which is valid near the lower critical field $H_{c1}$, nevertheless, the other two play an essential role when considering the low-energy physics of the vortex state in general. Therefore, the calculation of the vortex structure should account for these three contributions on an equal footing in order to establish the general features of the mixed state in $d_{x^2-y^2}$- and $s$-wave superconductors.

Ichioka, Hasegawa, and Machida [Ichioka et al. (1999)] has obtained the pair potential and vector potential self-consistently by solving the Eilenberger equation in the Matsubara frequency, $\omega_n = (2n+1)\pi T$, and considered the quasiclassical Green's functions, $\mathrm{g}(i\omega_n, \theta, \mathbf{r})$, $f(i\omega_n, \theta, \mathbf{r})$, and $f^\dagger(i\omega_n, \theta, \mathbf{r})$. The $\mathbf{r}$ designates the center-of-mass coordinate of a Cooper pair. The direction of the relative momentum of the Cooper pair, $\widehat{\mathbf{k}} = \mathbf{k}/|\mathbf{k}|$, is denoted by an angle $\theta$ measured from the $a$ axis in the $ab$ plane. The Eilenberger equations are given by

$$\begin{aligned} \left[ \omega_n + \frac{i}{2} \mathbf{v}_F \cdot \left( \frac{\nabla}{i} + \frac{2\pi}{\phi_0} \mathbf{A}(\mathbf{r}) \right) \right] f(i\omega_n, \theta, \mathbf{r}) &= \Delta(\theta, \mathbf{r}) \mathrm{g}(i\omega_n, \theta, \mathbf{r}), \\ \left[ \omega_n - \frac{i}{2} \mathbf{v}_F \cdot \left( \frac{\nabla}{i} - \frac{2\pi}{\phi_0} \mathbf{A}(\mathbf{r}) \right) \right] f^\dagger(i\omega_n, \theta, \mathbf{r}) &= \Delta^*(\theta, \mathbf{r}) \mathrm{g}(i\omega_n, \theta, \mathbf{r}), \end{aligned} \tag{2.27}$$

where $\mathrm{g}(i\omega_n, \theta, \mathbf{r}) = [1 - f(i\omega_n, \theta, \mathbf{r}) f^\dagger(i\omega_n, \theta, \mathbf{r})]^{1/2}$, $\mathrm{Re}\mathrm{g}(i\omega_n, \theta, \mathbf{r}) > 0$, and $\mathbf{v}_F = v_F \widehat{\mathbf{k}}$ is the Fermi velocity. The vector potential is written as $\mathbf{A}(\mathbf{r}) = \frac{1}{2}\mathbf{H} \times \mathbf{r} + \mathbf{a}(\mathbf{r})$ in the symmetric gauge, where $\mathbf{H} = (0, 0, H)$ is an external field and $\mathbf{a}(\mathbf{r})$ is related to the internal field $\mathbf{h}(\mathbf{r}) = [0, 0, h(\mathbf{r})]$ as $\mathbf{h}(\mathbf{r}) = \nabla \times \mathbf{a}(\mathbf{r})$. As for the pair potential $\Delta(\theta, \mathbf{r}) = \Delta(\mathbf{r})\phi(\theta)$, where $\phi(\theta) = \sqrt{2}\cos 2\theta$ is set for the $d_{x^2-y^2}$-wave pairing and $\phi(\theta) = 1$ for the $s$-wave pairing. The self-consistent conditions for $\Delta(\mathbf{r})$ and $\mathbf{a}(\mathbf{r})$ are given as

$$\Delta(\theta, \mathbf{r}) = N_0 2\pi T \sum_{\omega_n > 0} \int_0^{2\pi} \frac{d\theta'}{2\pi} V(\theta', \theta) f(i\omega_n, \theta', \mathbf{r}), \tag{2.28}$$

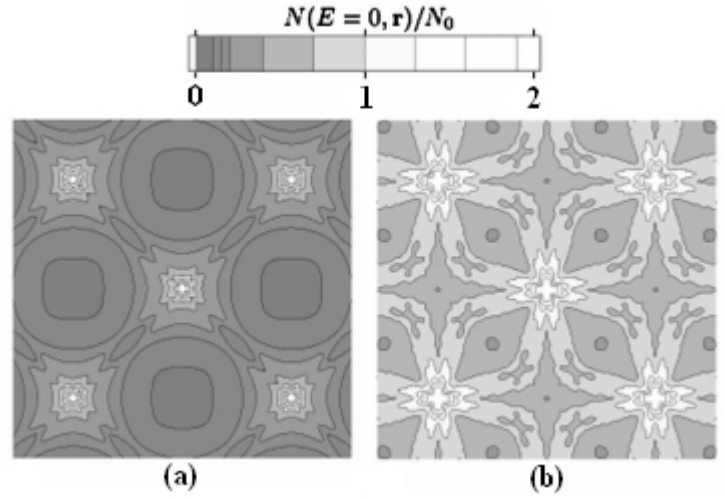


**Figure 2.1**: Spatial variation of the LDOS for $E = 0$ in the $d_{x^2-y^2}$-wave pairing. Contour plot of $N(E = 0, \mathbf{r})/N_0$ is presented in the region $14\xi_0 \times 14\xi_0$. (a) At low field $H/H_{c2} = 0.021$ and (b) high field $H/H_{c2} = 0.54$ [Ichioka et al. (1999)].

$$\nabla \times \nabla \times \mathbf{a}(\mathbf{r}) = -\frac{\pi}{\kappa^2} 2\pi T \sum_{\omega_n > 0} \int_0^{2\pi} \frac{d\theta'}{2\pi} \frac{\widehat{\mathbf{k}}}{i} \mathrm{g}(i\omega_n, \theta, \mathbf{r}), \tag{2.29}$$

where $N_0$ is the density of states at the Fermi surface, $V(\theta', \theta) = \overline{V}\phi(\theta')\phi(\theta)$ is the pairing interaction, $\kappa = [7\zeta(3)/72]^{1/2}(\Delta_0/T_c)\kappa_{BCS}$ with Rieman's zeta function $\zeta(3)$, $\kappa_{BCS}$ is the GL parameter in the BCS theory, and $\Delta_0$ is the uniform gap at $T = 0$. The material parameters appropriate to YBCO were used, i.e., $\xi_{BCS} = 16$Å and $\kappa_{BCS} = 100$. Then, $H_{c2} = 66.7$ T in the $s$-wave pairing and 93.2 T in the $d_{x^2-y^2}$-wave pairing for $T/T_c = 0.5$ [Ichioka et al. (1999)]. The local density of states was calculated for energy $E$ as

$$N(E, \mathbf{r}) = N_0 \int_0^{2\pi} \frac{d\theta}{2\pi} \mathrm{Re}\mathrm{g}(i\omega_n \to E + i\eta, \theta, \mathbf{r}). \tag{2.30}$$

The zero-energy LDOS $N(E = 0, \mathbf{r})$ may be directly observed in the STM experiment. In the $s$-wave pairing at lower fields, $N(E = 0, \mathbf{r})$ is localized circularly in a small region around each vortex core, as in the single vortex case. Since the inter-vortex distance decreases with increasing $H$, the vortex lattice effect appears in $N(E = 0, \mathbf{r})$ at higher fields [Ichioka et al. (1997)]. Therefore, $N(E = 0, \mathbf{r})$ is suppressed along the lines connecting two nearest-neighbor vortex centers.

These features are contrasted with those of the $d_{x^2-y^2}$-wave pairing. In the single vortex case, as shown in Fig. 8(d) in Ref. [Golubov and Hartmann (1994)], $N(E = 0, \mathbf{r})$ consists of the vortex core contribution and four element tails extended from the vortex center along lines of the node direction ($\theta = \pi/4$ and its equivalent directions). Strictly speaking, this low-energy state is not a bound state as the tails extend toward infinite points [Franz and Tesănović (1998)]. These tails arisen from the nodal structure of the $d_{x^2-y^2}$-wave pairing can be seen in Fig. 2.1 (a) in the vortex lattice case at low field. It is noted, however, that each tail slightly splits into two ridges between vortices. This split is due to the vortex lattice effect, i.e. the suppression along the line between nearest-neighbor vortex

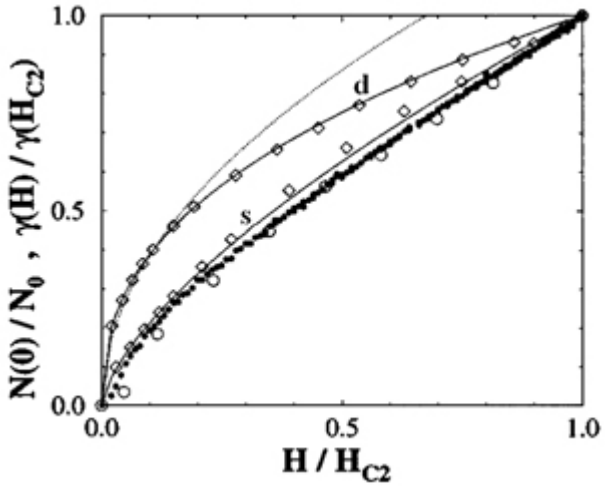


**Figure 2.2**: Field dependence of $N(0)/N_0$ in the $d_{x^2-y^2}$- and $s$-wave pairings ( $\diamondsuit$ ). Solid and dotted lines are fitting lines. Experimental data $\gamma(H)/\gamma(H_{c2})$ are plotted for $CeRu_2$ ( $\bullet$ ) [Hedo et al. (1998)] and $NbSe_2$ ( $\circ$ ) [Ichioka et al. (1999)].

centers. The vortex lattice effect appears even from the lower fields in the $d_{x^2-y^2}$-wave pairing. It means that the quasiparticle transfer between vortices is large in the $d_{x^2-y^2}$-wave case due to the tail structure of $N(E=0,\mathbf{r})$. The split is enhanced on raising the field, as shown in Fig. 2.1 (b) for $H = 0.54H_{c2}$. Therefore, the tail structure along the node directions in $N(E=0,\mathbf{r})$ is smeared by the vortex lattice effect at higher field, where the tails extend toward rather different directions.

According to Volovik [Volovik (1993)] for the $d_{x^2-y^2}$-wave case, the contribution to $N(0)$ mainly comes from the tail structure along the node direction in $N(E=0,\mathbf{r})$. The length of the tail is the order of $H^{-1/2}$ (lattice constant of the vortex lattice). As the vortex density is proportional to $H$, $N(0)$ is roughly estimated as $N(0) \sim H^{-1/2}H = \sqrt{H}$. This estimate becomes uncertain at higher field, since the tail structure along the node directions is smeared by the vortex lattice effect as shown in Fig. 2.1. The difference between the $d_{x^2-y^2}$ and $s$ states is clearly seen in Fig. 2.2, where the latter has no tail structure in $N(E=0,\mathbf{r})$. However, the dependence in the $d_{x^2-y^2}$-wave pairing deviates from $\sqrt{H}$ behavior, the curve for $\sqrt{H}$ is plotted by dotted line [Wang and MacDonald (1995)]. The fit, $N(0)/N_0 = (H/H_{c2})^{0.41}$, is presented in Fig. 2.2 by solid line. Its exponent 0.41 is slightly smaller than 0.5 of the Volovik theory. Experimentally, $N(0)$ is obtained from the coefficient of the $T$-linear term in the specific heat $C(T)$, i.e., $N(0) \propto \gamma(H) = \lim_{T\to 0} C(T)/T$. So far, the $\sqrt{H}$ behavior of $\gamma(H)$ was examined within the low-field region [Moler et al. (1994)].

As for the $s$-wave pairing case, the data in Fig. 2.2 deviates from the expected relation that $N(0)$ is proportional to the vortex density, i.e., $N(0) \propto H$. The best fit is $N(0)/N_0 = (H/H_{c2})^{0.67}$ (solid line). In Fig. 2.2 the field dependence of $\gamma(H)/\gamma(H_{c2})$, which corresponds to $N(0)/N_0$, is plotted, for $CeRu_2$ [Hedo et al. (1998)] and $NbSe_2$ [Nohara et al. (1997)]. These experimental data for typical $s$-wave superconductors apparently deviate from $H$-linear behavior and fit with a similar curve to calculated for $s$-wave pairing [Ichioka et al. (1999)]. The borocarbide superconductor $LuNi_2B_2C$ shows $\sqrt{H}$-like behavior of $\gamma(H)$ [Nohara et al. (1997)], that is, $d$-wave-like behavior of Fig. 2.2. While it is considered to be an $s$-wave superconductor, it has a highly anisotropic Fermi surface with fourfold symmetry [Wilde et al. (1997)]. Then, $\sqrt{H}$-like behavior may occur due to

the Fermi surface anisotropy instead of the gap anisotropy, both of which give rise to a similar effect on $N(0)$ in the result.

### Multiband BCS theory

The BCS formula has been derived in the assumption that the superconducting gap is the same at all points on the Fermi surface. The variational character of the BCS theory makes one think that giving the system an additional variational freedom of varying the order parameter over the Fermi surface should always lead to a higher transition temperature. For a case of two bands with uniform order parameters in each of them this problem was solved first in Ref. [Suhl et al. (1959)]. It can be easily generalized onto a $\mathbf{k}$-dependent order parameter. In the weak coupling limit it reads

$$\Delta(\mathbf{k}) = \int \Lambda(\mathbf{k}, \mathbf{k}')\Delta(\mathbf{k}')F[\Delta(\mathbf{k}'), T]d\mathbf{k}', \tag{2.31}$$

where summation over $\mathbf{k}$ implies also summation over all bands crossing the Fermi level. A strong coupling generalization is straightforward. Here, the matrix $\Lambda$ characterizes the pairing interaction, and

$$F = \int_0^{\omega_B} dE \tanh(\frac{\sqrt{E^2+\Delta^2}}{2T})/\sqrt{E^2+\Delta^2}. \tag{2.32}$$

The intermediate boson frequency sets the cut-off frequency. Assuming that the order parameter $\Delta$ varies slightly within each sheet of the Fermi surface, while differing between the sheets, Eq. (2.31) is reduced to the original expression of [Suhl et al. (1959)]:

$$\Delta_i = \sum_j \Lambda_{ij}\Delta_j F[\Delta_j, T], \tag{2.33}$$

where $i$, $j$ are band indices and $\Lambda$ is an asymmetric matrix related to the symmetric matrix of the pairing interaction $V$, $\Lambda_{ij} = V_{ij}N_j$, where $N_i$ is the contribution of the $i$-th band to the total DOS. It can be shown that in the BCS weak coupling limit the critical temperature is given by the standard BCS relation, $kT_c = \hbar\omega_D \exp(-1/\lambda_{eff})$, where $\lambda_{eff}$ is the largest eigenvalue of the matrix $\Lambda$. The ratios of the individual order parameters are given by the corresponding eigenvector.

Moreover, it is evident from Eq. (2.33) that unless all $V_{ij}$ are the same, the temperature dependence of individual gaps does not follow the canonical BCS behavior. For instance, in a two-band superconductor, where the intraband coupling dominates, the smaller gap opens initially at a very small value. And only at a temperature corresponding to its own superconducting transition it starts to grow. This effect is gradually suppressed as the interband coupling approaches the geometrical average of the intraband couplings, but as the interband coupling becomes dominant the gaps again show non-BCS temperature dependence. In this limit the larger gap deviates more from the BCS behavior.

Aronov and Sonin [Aronov and Sonin (1973)] realized that Eqs. (2.31) and (2.33) may have solutions even when all elements of the interaction matrices $\Lambda$ are negative, displaying repulsive behavior. The simplest example is an off-diagonal repulsion: $V_{11} = V_{22} = 0$, $V_{12} = V_{21} = -V < 0$. In this case the solution is $\lambda_{eff} = \sqrt{\Lambda_{12}\Lambda_{21}} = |V_{12}\sqrt{N_1 N_2}|$, $\Delta_1(T_c)/\Delta_2(T_c) = -\sqrt{N_2/N_1}$. At lower temperatures the gap ratio becomes closer to 1 [Hirschfeld et al. (2011)]. However, it is important to bear in mind that actual FeBS materials have five bands, each possibly having different gap magnitudes and angular dependences.

CHAPTER III

# Spin fluctuation pairing

Electronic spin fluctuations are widely believed to be critical to superconductivity in the new Fe-based high-temperature superconductors due to the proximity between the superconducting and the magnetic ordered phases. The driving mechanisms of both magnetic ordering and superconductivity are currently under intensive debate, mainly between two approaches: a weak coupling approach where both magnetic and SC orders are conducted by the enhanced spin susceptibility near the Fermi surface, and a strong coupling approach where the two orders are caused by local magnetic exchange interactions between neighboring electrons. The weak coupling approach has found support from the observation of quasi-nesting between hole FS pockets at the Brillouin zone center and electron FS pockets located at the antiferromagnetic wave vector in most ferropnictides [Ding et al. (2008)]. However, this approach has encountered difficulty in explaining the bicollinear magnetic ordering pattern in the ferrochalcogenide FeTe [Bao et al. (2009)] and it has been seriously challenged by the recent observation of isotropic SC gaps in a new ferrochalcogenide superconductor, $A_x\mathrm{Fe}_2\mathrm{Se}_2$ ($A$ = K, Rb, Cs, Tl), without FS nesting on the particle-hole channel [Mou et al. (2011); Miao et al. (2012)].

The Berk-Schrieffer [Berk and Schrieffer (1966)] type spin fluctuation theories are popular because they are relatively simple to express and have given some qualitatively correct results in the case of cuprates. In the Fe-based superconductors, the early understanding that the Fermi surface consisted of small, nearly nested electron and hole pockets led to the expectation of a strongly peaked susceptibility near $\mathbf{Q} = (\pi, 0)$, and a corresponding pairing instability with sign change between electron and hole sheets.

Spin fluctuations exchange in the singlet channel always leads to a repulsive interaction, and, therefore, only sign-changing superconducting states can be implemented. If this interaction is sufficiently strong at some particular momentum it will necessarily result in superconductivity. For a single Fermi surface this superconductivity will be nodal, usually of a $d$-wave symmetry. This is the case of high-$T_c$ cuprates and, possibly, overdoped $\mathrm{KFe}_2\mathrm{As}_2$ compounds. On the other hand, a multiband system may exhibit lack of nodes, while still preserving a sign-changing structure. As an illustration to this situation can be $d$-wave superconductivity that can develop in a cubic system with Fermi surface pockets around the X points and in a hexagonal system with pockets around the M points [Agterberg et al. (1999)], $d$-wave superconductivity in a tetragonal system with FS pockets near X/Y points [Kuroki et al. (2008)], $s^{\pm}$ superconductivity proposed for bilayered cuprates [Liechtenstein et al. (1995)], and the electron-hole $s^{\pm}$ superconductivity that can develop

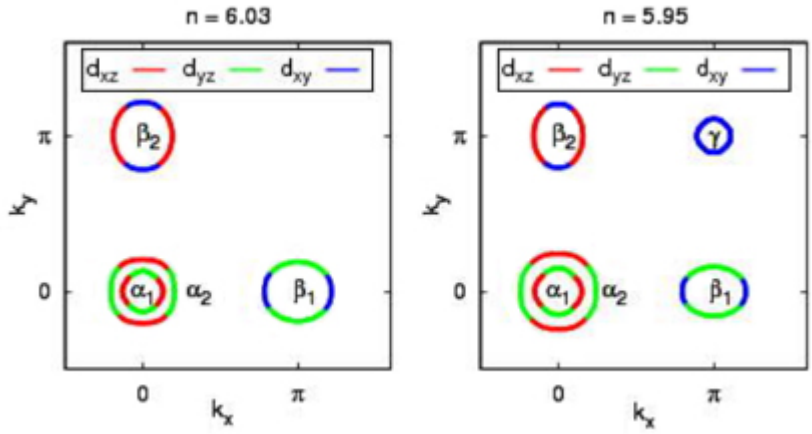


**Figure 3.1**: Fermi sheets of the five-band model in the unfolded BZ for $n = 6.03$ (left) and $n = 5.95$ (right) with colors indicating major orbital character (red = $d_{xz}$, green = $d_{yz}$, blue = $d_{xy}$). The $\gamma$ Fermi surface sheet is a hole pocket which appears at $\sim 1\%$ hole doping [Kemper et al. (2010)].

in semimetals [Aronov and Sonin (1973)].

The last alternative is now the leading candidate for the majority of pnictides and chalcogenides, while $d$-wave superconductivity has been suggested for overdoped $KFe_2As_2$. A version of the nodeless $d$-wave state has been suggested for Se-based 122 materials [Kuroki et al. (2008)], and the bonding-antibonding nodeless $s^{\pm}$ state has been also proposed for them [Liechtenstein et al. (1995)]. Therefore, one may think that as long as the spin fluctuations are strong and nonuniform, some superconducting state will unavoidably form, and the details of the electronic structure and of the pairing interaction will decide which particular symmetry will form, often in close competition with other symmetries.

### Antiferromagnetic spin fluctuations

In the context of heavy fermion systems it has been realized that strong antiferromagnetic spin fluctuations in either the weak or strong coupling limit lead naturally to spin singlet, $d$-wave pairing [Scalapino et al. (1986)]. Assuming that the susceptibility is strongly peaked near some wave vector $\mathbf{Q}$, the form of the singlet interaction is

$$\Gamma_s(\mathbf{k},\mathbf{k}') = \frac{3}{2}U^2\frac{\chi_0(\mathbf{q})}{1-U\chi_0(\mathbf{q})}, \tag{3.1}$$

if to neglect the terms which are small near the RPA instability $U\chi_0(\mathbf{q}) \to 0$ [Nakajima (1973)]. This implies that $\Gamma_s(\mathbf{q})$ is also peaked at this wavevector, but is always repulsive. Nevertheless, the examination of the BCS gap equation for this interaction

$$\Delta_{\mathbf{k}} = -\sum_{\mathbf{k}'}\Gamma_s(\mathbf{k},\mathbf{k}')\frac{\Delta'_{\mathbf{k}}}{2E'_{\mathbf{k}}}\tanh\frac{E'_{\mathbf{k}}}{2T} \tag{3.2}$$

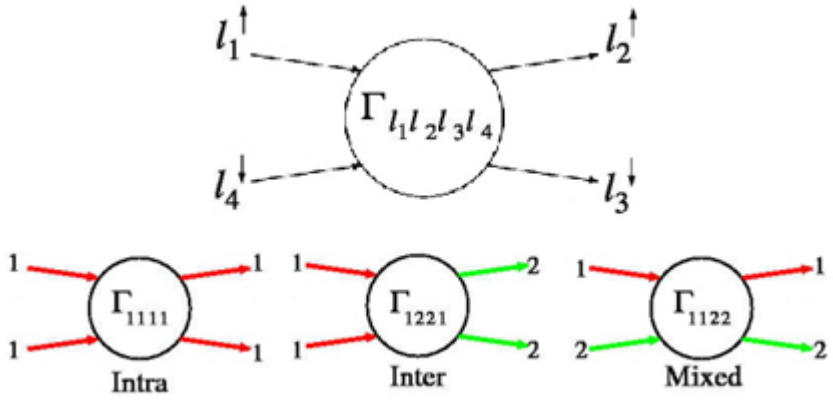


**Figure 3.2**: (Top) Pairing vertex $\Gamma_{l_1,l_2,l_3,l_4}$ defined in terms of orbital states $l_i$ of incoming and outgoing electrons. (Bottom) Representative examples of classes of intra-, inter-, and mixed orbital vertices [Kemper et al. (2010)].

leads to a conclusion that an isotropic state cannot be a solution, but in case of sign changing

$$\Delta_{\mathbf{k}} = -\Delta_{\mathbf{k}+\mathbf{Q}}, \tag{3.3}$$

a solution will be allowed.

In the cuprates, $\chi$ is peaked at $\mathbf{Q} \simeq (\pi, \pi)$, and the two possible states of this type which involve pairing on the nearest neighbor bonds only are

$$\Delta_{\mathbf{k}}^{d,s} = \Delta_0(\cos \mathrm{k}_x a \mp \cos \mathrm{k}_y a). \tag{3.4}$$

The Fermi surface then defines which state will be stabilized. So the states close to the Fermi surface are the most important in Eq. (3.2), thus, the pairing kernel should be examined for these momenta. For example, for $(\pi/a, 0) \rightarrow (0, \pi/a)$ scattering, $\Delta_{\mathbf{k}}^s$ satisfies Eq. (3.3) by being zero, whereas $\Delta_{\mathbf{k}}^d$ is nonzero and changes sign, contributing to the condensation energy.

The proximity of the Fe $d$-states to the Fermi level in the Fe-based superconductors leads one to consider a Hamiltonian with kinetic energy $H_0$, consisting of the bands derived from the 5 Fe $d$-orbitals found in DFT, approximated within some tight-binding scheme. Figure 3.1 depicts such obtained 2D Fermi surface in the 1-Fe zone. This model Fermi surface is similar to DFT and is characterized by small concentric hole pockets around the $\Gamma$ point and slightly elliptical electron pockets around the M points. In a weak-coupling approach, the near-nesting of the hole and electron pockets suggested the existence of a peak in the spin susceptibility at $\mathbf{Q} = (\pi, 0)$ in the 1-Fe zone. The gap equation (Eq. (3.2)) then admits a solution with the property (Eq. (3.3)) if there is a sign change of $\Delta_{\mathbf{k}}$ between electron and hole pockets [Hirschfeld et al. (2011)]. Small size of the pockets allows one to simplify the model by neglecting the anisotropy on each electron sheet. This leads to the isotropic $s^{\pm}$ state (Fig. 1.1), which has the full symmetry of the crystal lattice and is, therefore, formally an $\mathrm{A}_{1g}$ ($s$-wave) state, but with fundamentally different gap structure.

**Spin fluctuation pairing in multiorbital systems**

The Hamiltonian consisting of a kinetic energy $H_0$ for the effective Fe bands as described above, plus an interaction $H_{int}$ containing all possible two-body on-site interactions between electrons in Fe orbitals, is a good starting point for a microscopic description of this system (pairing by electronic interactions),

$$H = H_0 + \overline{U}\sum_{i,l} n_{il\uparrow}n_{il\downarrow} + \overline{U}'\sum_{i,l'<l} n_{il}n_{il'} + \overline{J}\sum_{i,l'<l}\sum_{\sigma,\sigma'} c^\dagger_{il\sigma}c^\dagger_{il'\sigma'}c_{il\sigma'}c_{il'\sigma} + \\ + \overline{J}'\sum_{i,l'\neq l} c^\dagger_{il\uparrow}c^\dagger_{il\downarrow}c_{il'\downarrow}c_{il'\uparrow}, \tag{3.5}$$

where $n_{il} = n_{il\uparrow} + n_{il\downarrow}$. The Coulomb parameters $\overline{U}$, $\overline{U}'$, $\overline{J}$, and $\overline{J}'$ are in the notation employed in Ref. [Kuroki et al. (2008)], and are related to those used in Ref. [Graser et al. (2009a)] by $\overline{U} = U$, $\overline{J} = J/2$, $\overline{U}' = V + J/4$, and $\overline{J}' = J'$. The noninteracting $H_0$ is given by a tight-binding model spanned by the 5 Fe $d$-orbitals, Eq. (3.6), which give rise to the Fermi surfaces shown in Fig. 3.1. The kinetic energy is given by the Hamiltonian

$$H_0 = \sum_{\mathbf{k}\sigma}\sum_{ll'}(\xi_{ll'}(\mathbf{k}) + \epsilon_l\delta_{ll'})d^\dagger_{lk\sigma}d_{l'k\sigma}, \tag{3.6}$$

where $d^\dagger_{lk\sigma}$ creates a particle with momentum $\mathbf{k}$ and spin $\sigma$ in the orbital $l$, $\xi_{ll'}(\mathbf{k})$ are the hoppings, and $\epsilon_l$ are the single-site level energies.

The effective pair scattering vertex $\Gamma(\mathbf{k},\mathbf{k}')$ between bands $i$ and $j$ in the singlet channel is

$$\Gamma_{ij}(\mathbf{k},\mathbf{k}') = \mathrm{Re}\Big[\sum_{l_1l_2l_3l_4} a^{l_2,*}_{\nu_i}(\mathbf{k})a^{l_3,*}_{\nu_i}(-\mathbf{k}) \times \Gamma_{l_1l_2l_3l_4}(\mathbf{k},\mathbf{k}',\omega=0)a^{l_1}_{\nu_j}(\mathbf{k}')a^{l_4}_{\nu_j}(-\mathbf{k}')\Big], \tag{3.7}$$

where the momenta $\mathbf{k}$ and $\mathbf{k}'$ are confined to the various Fermi surface sheets with $\mathbf{k} \in C_i$ and $\mathbf{k}' \in C_j$. In Eq. (3.7), the intra- and interorbital Coulomb repulsions are distinguished, as well as the Hund's rule exchange $\overline{J}$ and pair-hopping term $\overline{J}'$ for generality, but if they are generated from a single two-body term with spin rotational invariance they are related by $\overline{U}' = \overline{U} - 2\overline{J}$ and $\overline{J}' = \overline{J}$. In a real crystal, such a local symmetry will not always hold [Kubo (2007)]. As illustrated in Fig. 3.2, there are intra-orbital, inter-orbital and mixed-orbital pair scattering processes. The contributions of each to the total pair scattering vertex $\Gamma_{ij}$ in Eq. (3.8) are quite different. In particular, the orbital matrix elements for $\mathbf{k}$ and $-\mathbf{k}$ states on the Fermi surface favor pairs that are formed from electrons in the same orbital state. Although the mixed-orbital scattering can be significant, its contribution to the pairing interaction is negligible [Kemper et al. (2010)]. The orbital vertex functions $\Gamma_{l_1l_2l_3l_4}$ describe the particle-particle scattering of electrons in orbitals $l_1, l_4$ into $l_2, l_3$ (Fig. 3.2). In the fluctuation exchange formulation [Kubo (2007)] they are given by

$$\Gamma_{l_1l_2l_3l_4}(\mathbf{k},\mathbf{k}',\omega) = \Big[\frac{3}{2}\overline{U}^s\chi_1^{RPA}(\mathbf{k}-\mathbf{k}',\omega)\overline{U}^s + \frac{1}{2}\overline{U}^s - \\ \frac{1}{2}\overline{U}^c\chi_0^{RPA}(\mathbf{k}-\mathbf{k}',\omega)\overline{U}^c + \frac{1}{2}\overline{U}^c\Big]_{l_1l_2l_3l_4}, \tag{3.8}$$

where each of the quantities $\overline{U}^s$, $\overline{U}^c$, $\chi_1$, *etc* represent matrices in orbital space which depend on the interaction parameters. Here, $\chi_0^{RPA}$ describes the orbital charge-fluctuation contribution and $\chi_1^{RPA}$

the spin-fluctuation contribution, determined by Dyson-type equations as

$$(\chi_0^{RPA})_{st}^{pq} = \chi_{st}^{pq} - (\chi_0^{RPA})_{uv}^{pq}(U^c)_{wz}^{uv}\chi_{st}^{wz} \tag{3.9}$$

and

$$(\chi_1^{RPA})_{st}^{pq} = \chi_{st}^{pq} - (\chi_1^{RPA})_{uv}^{pq}(U^s)_{wz}^{uv}\chi_{st}^{wz}, \tag{3.10}$$

where repeated indices are summed over. Here, $\chi_{st}^{pq}$ is a generalized multiorbital susceptibility [Kemper et al. (2010)].

The microscopic approach uses the linearized gap equation to calculate the critical temperature $T_c$ and determine the symmetry of the pairing instability there. The superconducting order parameter $\Delta(\mathbf{k})$ can be written as $\Delta g(\mathbf{k})$, with $g(\mathbf{k})$ as a dimensionless function describing the momentum dependence on the Fermi surface. Then $g(\mathbf{k})$ is given as the stationary solution of the dimensionless pairing strength functional [Graser et al. (2009a)]

$$\lambda[g(\mathbf{k})] = -\frac{\sum_{ij} \oint_{C_i} \frac{dk_\parallel}{v_F(\mathbf{k})} \oint_{C_j} \frac{dk'_\parallel}{v_F(\mathbf{k}')} g(\mathbf{k})\Gamma_{ij}g(\mathbf{k}')(\mathbf{k},\mathbf{k}')}{(2\pi)^2 \sum_i \oint_{C_i} \frac{dk_\parallel}{v_F(\mathbf{k})}[g(\mathbf{k})]^2} \tag{3.11}$$

with the largest eigenvalue $\lambda$, which provides a dimensionless measure of the pairing strength. Here, $\mathbf{k}$ and $\mathbf{k}'$ are restricted to the various Fermi surfaces $\mathbf{k} \in C_i$ and $\mathbf{k}' \in C_j$, and $v_{F,\nu}(\mathbf{k}) = |\nabla_{\mathbf{k}} E_\nu(\mathbf{k})|$ is the Fermi velocity on a given Fermi sheet.

The leading dimensionless gap function $g(\mathbf{k})$ derived from the RPA theory around the electron $\beta_1$ sheet is plotted in Fig. 3.3 for two different values of the doping, for spin-rotationally invariant parameters $U = 1.3$ and $J = 0.2$. The gap on the hole sheets is found to be isotropic, while on the electron sheets the average of the gap is of opposite sign compared to the hole sheets, and is highly anisotropic, with nodes in the case of electron doping.

The spin fluctuation pairing analysis based on Eq. (3.7) shows that the orbital structure of the Fermi surface can have a significant impact on the anisotropy of the pairing state. The intra-orbital scattering of $d_{xz}$ and $d_{yz}$ pairs between the $\alpha$ and $\beta$ Fermi surfaces by $(\pi, 0)$ and $(0, \pi)$ spin fluctuations (Fig. 3.2) leads to a gap which changes sign between the $d_{xz}/d_{yz}$ parts of the $\alpha$ Fermi surfaces and the $d_{yz}$ and $d_{xz}$ parts of the $\beta_1$ and $\beta_2$ electron pockets [Mazin et al. (2008b)], see Fig. 3.1. However, scattering between the $\beta_1$ and $\beta_2$ Fermi surfaces prevents from the formation of an isotropic $s^\pm$ gap there [Kuroki et al. (2009)]. Furthermore, this anisotropy can also be driven by the effect of the intraband Coulomb interaction. Finally, inter-orbital pair scattering can also occur, depending upon $\overline{U}'$ and $\overline{J}'$. The contributions to the total pairing interaction arising from mixed and interorbital processes may be shown explicitly to be subdominant to the intraorbital processes but important for nodal formation [Kemper et al. (2010)].

On the other hand, the $\beta_1 - \beta_2$ $d_{xy}$ orbital frustration is weaker or does not occur if an additional hole pocket $\gamma$ of $d_{xy}$ character is present (Fig. 3.1). These scattering processes take place at $(\pi, 0)$ in the unfolded zone and therefore support isotropic $s^\pm$ pairing (Fig. 3.3). Kuroki *et al* [Kuroki et al. (2009)] tried to relate the crystal structure, electronic structure, and pairing, by noting that the As height above the Fe plane in the 1111 family was a crucial variable controlling the appearance of the $\gamma$ pocket and thus driving the anisotropy of the $s^\pm$ state. It is important to note that the transition between nodal and nodeless $A_{1g}$ gap structures does not involve any symmetry change and relies only on the details of the pairing interaction [Chubukov et al. (2009)].

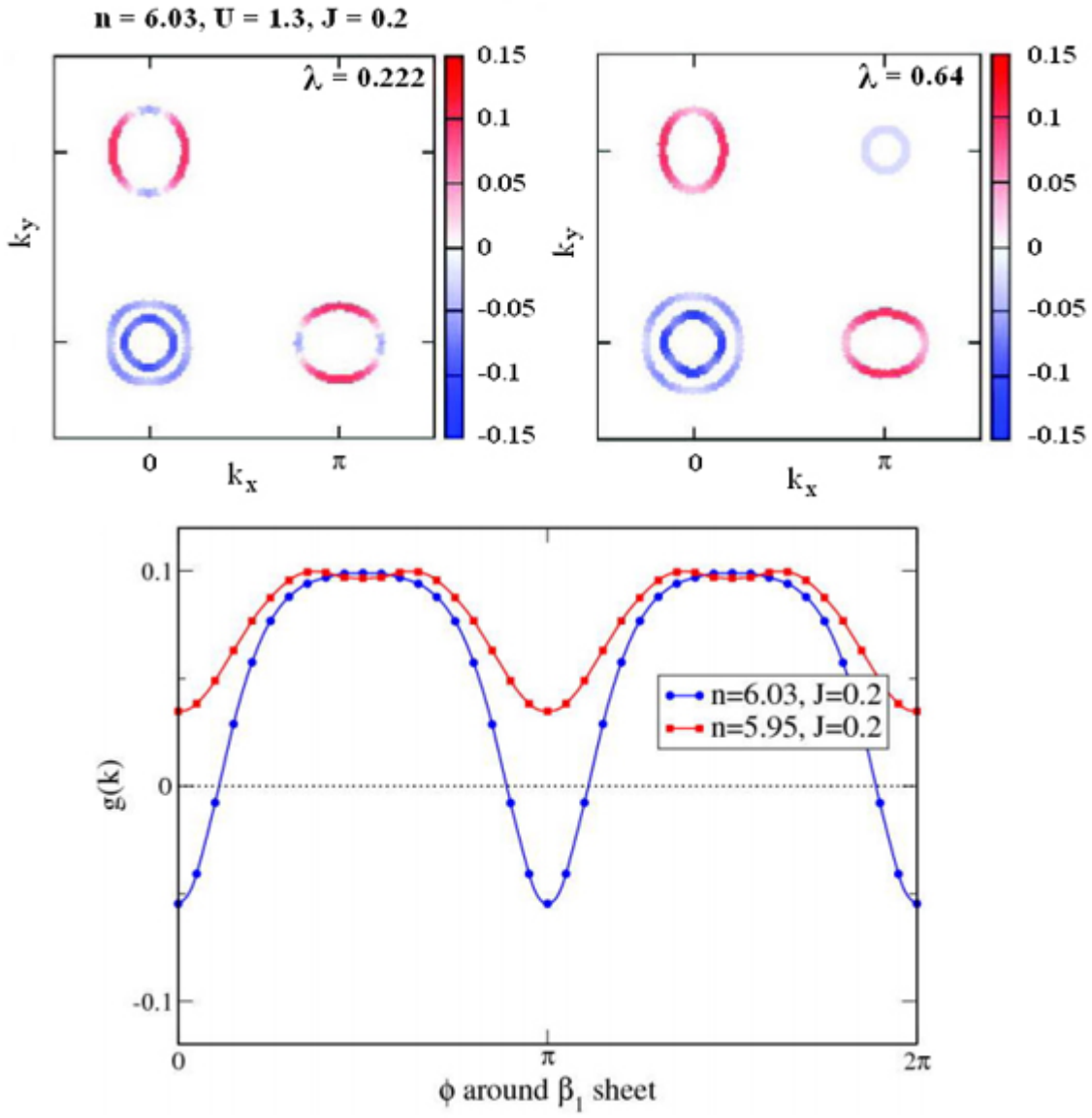


**Figure 3.3**: (Top) False color plots of dimensionless gap function $g(k)$ on various Fermi surface sheets for electron doped case $n = 6.03$ (left) and hole doped case $n = 5.95$ (right). (Bottom) Detail of $g(k)$ on $\beta_1$ pocket for $U = 1.3$ and $n = 5.95$, and $\overline{J} = 0.2$ (red squares) and $n = 6.01$, $\overline{J} = 0.2$ (blue circles). Here, the angle $\phi$ is measured from the $k_x$-axis [Kemper et al. (2010)].

The term of strong coupling frequently appears in reference to the large size of the Hubbard interaction relative to the bandwidth, which in the 1-band case at half-filling allows for a description in terms of the spin degrees of freedom as the charge degrees of freedom become localized. The spin dynamics can become more localized in situations other than the canonical Mott-Hubbard case and, however, are well described by DFT, which for the FeBS gives a typical energy scale for the magnetic interactions of order 100 meV or larger. Thus, the moments are large and quite localized. This is not a contradiction, even in genuinely itinerant systems magnetic interactions are essentially local, decaying with distance as a power law. This magnetic model leads to a competition between the Néel and stripe-collinear orders, also present in the itinerant DFT calculation, corresponding to the same ground state magnetic pattern and to a similar structure of spin fluctuations in the reciprocal state (a maximum near $(\pi, 0)$) [Hirschfeld et al. (2011)]. In Ref. [Seo et al. (2008)], a $t - J_1 - J_2$ model with two bands was studied, and the exchange terms were decoupled in mean field in the pairing channel. In this procedure, the nearest-neighbor exchange $J_1$ induces competing $\cos k_x + \cos k_y$ and $\cos k_x - \cos k_y$ ($s$- and $d$-wave, respectively) pairing harmonics, while the next-nearest-neighbor exchange leads to $\cos k_x \cos k_y$ and $\sin k_x \sin k_y$ ($s$- and $d$-wave, respectively). In the region of the general phase diagram with $J_2 \gtrsim J_1$, $\cos k_x \cos k_y$ was the leading instability for the 2-band Fermi surface, leading to a nodeless $s^{\pm}$ state, and a similar ground state was also found for a 5-orbital model [Goswami et al. (2010)].

ARPES experiments [Miao et al. (2012)] have revealed isotropic superconducting gaps on both electron-like and hole-like FS pockets in high-quality $FeTe_{0.55}Se_{0.45}$ samples. The pairing has been found to be stronger on the electron-like FSs, which can be naturally explained by the enhanced antiferromagnetic exchange between the third nearest neighbors ($J_3$) in this material. All the different SC gaps can be fitted by a single gap function that is fully consistent with the strong coupling $J_1$-$J_2$-$J_3$ approach [Miao et al. (2012)]. Figures 3.4 (a) (3.4 (c)) and 3.4 (b) (3.4 (d)) show the intensity plots near $\Gamma$ (M) along the $\Gamma$-M direction in the normal state (25 K) and SC state (6 K), respectively. The corresponding energy distribution curves (EDCs) are given below each panel. Around the $\Gamma$ point, the normal state data show clearly two intense hole-like bands. While the inner one ($\alpha$) sinks $\sim 14$ meV below $E_F$, the outer one ($\alpha'$) crosses $E_F$ very close to $\Gamma$. A third weaker hole-like band with a larger Fermi wave vector ($k_F$) and a larger effective mass, named $\beta$ band, is also visible. Around the M point, one electron pocket ($\gamma$) with a smaller effective mass is also resolved. At temperatures below $T_c = 14.5$ K, SC coherent peaks develop on the $\alpha'$, $\beta$, and $\gamma$ bands, as well evidenced by the low temperature EDCs shown in Figs. 3.4 (f) and 3.4 (h). The temperature evolution of the coherent peaks is drastic and confirms their superconducting origin.

The temperature dependence of the EDC recorded at a particular $k_F$ of the $\beta$ band is displayed in Fig. 3.5 (a), which shows dramatic line shape across $T_c$. Figure 3.5 (b) compares EDCs recorded in the SC state at the $k_F$ of the $\alpha'$, $\beta$, and $\gamma$ bands [Miao et al. (2012)]. The gap sizes are 1.7, 2.5, and 4.2 meV for the $\alpha'$, $\beta$, and $\gamma$ bands, respectively.

Existence of the gap nodes at the M point in the superconducting state is a highly debated issue in the study of Fe-based superconductors. An angle-resolved specific heat (ARSH) experiment claims nodes or minimal gaps in $FeTe_{0.55}Se_{0.45}$ samples [Zeng et al. (2010)]. Figures 3.5 (c) and 3.5 (d) show the symmetrized EDCs of the $\beta$ and $\gamma$ bands, respectively, at different $k_F$ positions indicated on the FS which is displayed in Fig. 3.5 (e). As illustrated by the polar in Fig. 3.5 (f), the gap sizes on both pockets are nodeless and quite isotropic. It has been proposed that the orbital character may be important to determine the pairing strength and the symmetry for this multiorbital system [Graser et al. (2009a); Mazin and Schmalian (2009); Miao et al. (2012)]. Experimental data [Chen et al. (2010); Miao et al. (2012)] suggests that the $\alpha$ ($\alpha'$) band has an even (odd) symmetry along

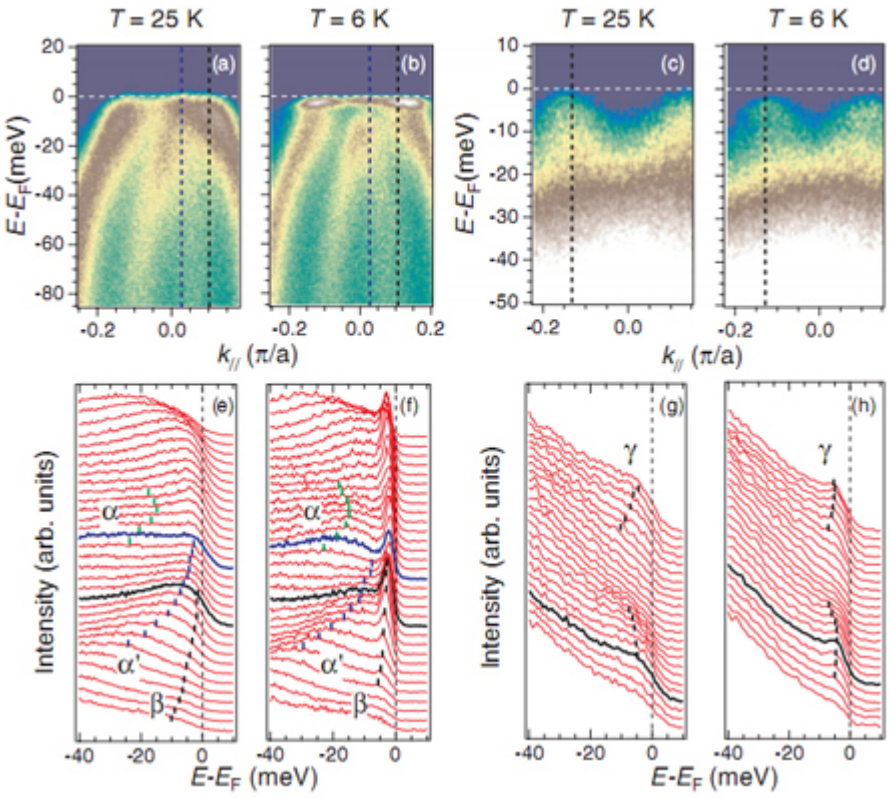


**Figure 3.4**: (a)-(d) ARPES intensity plots along Γ-M. (a) Near Γ, in the normal state ($T = 25$ K). Blue and black dotted lines indicate the $k_F$ positions of the $\alpha'$ and $\beta$ bands, respectively. (b) Same as (a) but in the SC state ($T = 6$ K). (c) Near M, normal state ($T = 25$ K). (d) Near M, SC state ($T = 6$ K). The corresponding EDCs are given below each panel in (e)-(h) [Miao et al. (2012)].

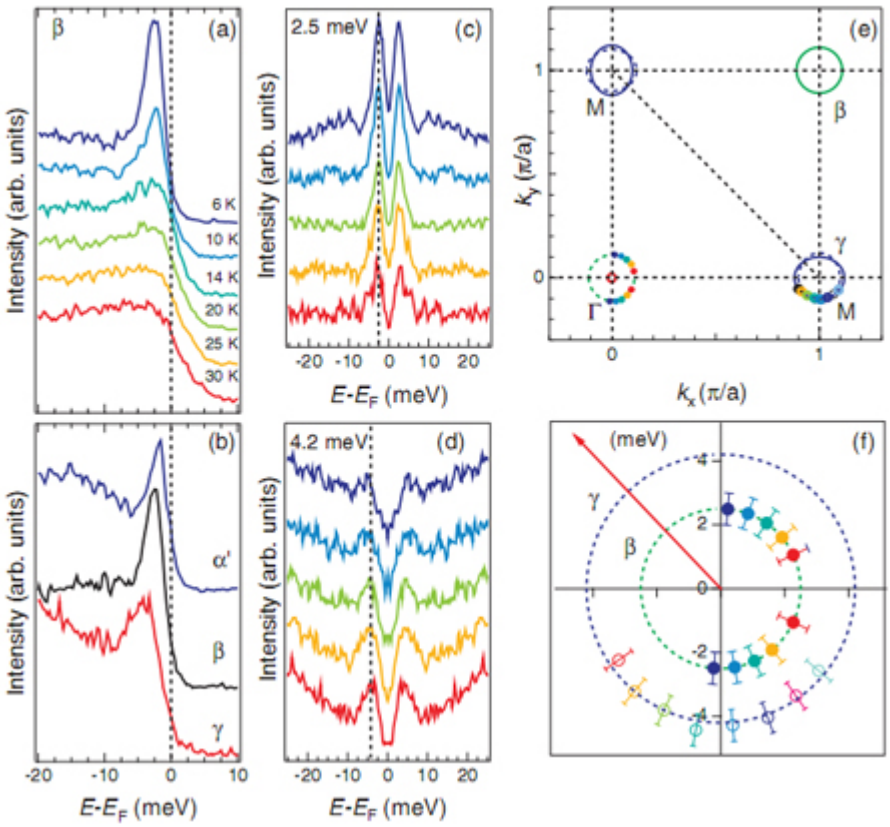


**Figure 3.5**: (a) Temperature dependence of the SC gap of the $\beta$ band. (b) Comparison of the SC gaps of the $\alpha'$, $\beta$, and $\gamma$ bands. (c) and (d) $k$ dependences of symmetrized EDCs along the $\beta$ and $\gamma$ FSs, respectively. (e) Schematic FS indicating positions of measured SC gap size. Dotted FSs are folded from the BZ of a pure Fe plane due to the alternate position of the chalcogen atoms above and below the Fe plane. (f) Polar plot of the SC gaps with dotted circles indicating the average values on each FS pocket [Miao et al. (2012)].

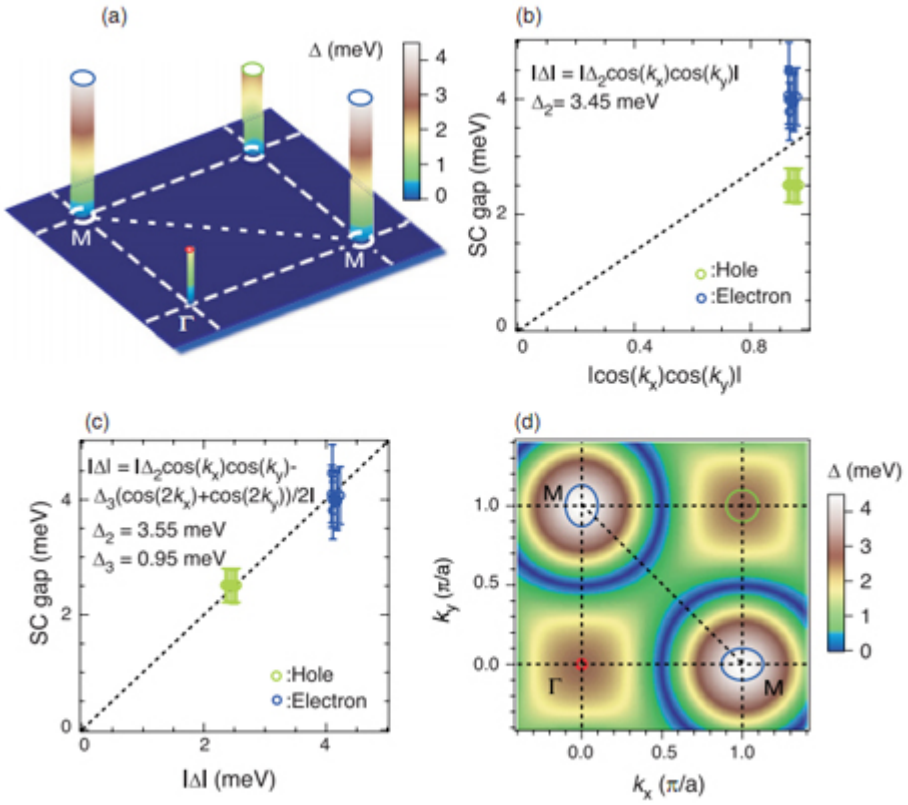


**Figure 3.6**: (a) 3D representation of the SC gap with the FS topology. (b) Fit of the SC gap data with a $|\Delta_2 \cos k_x \cos k_y|$ gap function. (c) Fit of the SC gap data with a $|\Delta_2 \cos k_x \cos k_y| - \Delta_3(\cos 2k_x + \cos 2k_y)/2$ gap function. The horizontal and vertical error bars represent the uncertainties on $k_F$ positions and their corresponding SC gap values. (d) In-plane $k$ distribution of the $|\Delta_2 \cos k_x \cos k_y| - \Delta_3(\cos 2k_x + \cos 2k_y)/2$ SC gap function along with the FSs [Miao et al. (2012)].

both Γ-M and Γ-X directions, while the $\beta$ band is even along Γ-X but is odd along Γ-M.

The gap amplitude has been found to be stronger on the electron FS, as can be seen in Fig. 3.6 (a). In contrast, iron-pnictide superconductors have similar gap size on the quasi-nested hole-like and electron-like FSs [Ding et al. (2008)], which can be captured by the $s^{\pm}$ gap function $\cos k_x \cos k_y$ naturally derived from the effective $J_1$-$J_2$ model [Seo et al. (2008)], where $J_1$ and $J_2$ are the nearest- and next-nearest-neighbor magnetic exchange interaction strengths, respectively. Figure 3.6 (b) shows that a simple $\cos k_x \cos k_y$ function cannot fit the gaps on both hole and electron FSs. However, the exchange parameters in iron-chalcogenides differ from the ones in iron-pnictides in such a way that (i) $J_1 < 0$ (ferromagnetic) and (ii) $J_3$ (next-next-nearest-neighbor exchange) is no longer negligible. A sizable AF $J_3$ ($\sim$ 7 meV) that may play a critical role in forming the bicollinear magnetic pattern in FeTe has been reported from inelastic neutron scattering (INS) measurements [Lipscombe et al. (2011)]. The shape of $s$-wave pairing induced by AF $J_3$ is $\Delta_3(\cos 2k_x + \cos 2k_y)/2$. Combined with $\cos k_x \cos k_y$ induced by AF $J_2$, the pairing form in this material should be $|\Delta_2(\cos k_x \cos k_y) - \Delta_3(\cos 2k_x + \cos 2k_y)/2|$. As demonstrated in Fig. 3.6 (c), this gap function fits all gaps reasonably well, with $\Delta_2 = 3.55$ meV and $\Delta_3 = 0.95$ meV. The ratio

between $\Delta_2$ and $\Delta_3$ is similar to $J_2/J_3$ (22/7) given by an INS study [Lipscombe et al. (2011)].

Strong and isotropic pairing on the electron FS sheets of $FeTe_{1-x}Se_x$ has important implications to superconductivity in another iron-chalcogenide, $AFe_2Se_2$ (A = K, Rb, Cs, Tl), with $T_c$ up to 31 K [Fang et al. (2011b)]. Several ARPES studies [Lipscombe et al. (2011)] revealed an isotropic SC gap on its electron FS. Interestingly, the $2\Delta/T_c$ ratios are similar in these two iron-chalcogenides (7 in $AFe_2Se_2$ [Wang et al. (2011c)] against 6.7 in $FeTe_{1-x}Se_x$ [Lipscombe et al. (2011)]). A recent INS study indicates a large $J_3 \sim 9$ meV for $K_{0.8}Fe_{1.6}Se_2$ as well [Wang et al. (2011b)]. As shown in Fig. 3.6 (d), the enhanced pairing on the electron FS around M accompanies the reduced pairing on the hole FS around $\Gamma$. For $AFe_2Se_2$, which does not have hole Fermi surface at $\Gamma$, this effect may have no impact on $T_c$ [Miao et al. (2012)]. Clearly, the observation of isotropic SC gaps with strong pairing on the electron-like FS pocket in the iron-chalcogenide supports the strong coupling local pairing picture for the Fe-based superconductors.

CHAPTER IV

# Impurities in iron-based superconductors

Grain and surface boundaries, twinning planes, and other structural inhomogeneities scatter conduction electrons and thereby affect the resulting order parameters. However, here only impurity atoms are of particular interest.

An impurity atom has a different electronic configuration than the host solid. Its interaction with the density of conduction electrons via a Coulomb potential has the form

$$H_{imp} = \sum_{\alpha} \int d\mathbf{r} \psi^{\dagger}_{\alpha}(\mathbf{r}) U_{pot}(\mathbf{r}) \psi_{\alpha}(\mathbf{r}). \tag{4.1}$$

In metals the Coulomb interaction is screened at the length scales comparable to the lattice spacing, hence, the resulting scattering potential is often assumed to be completely local, $U_{pot}(\mathbf{r}) = U_0 \delta(\mathbf{r} - \mathbf{r_0})$, with the impurity at $\mathbf{r_0}$. The resulting scattering occurs only in the isotropic, $s$-wave, angular momentum channel. If finite range of the interaction is relevant, scattering in $l \neq 0$ channels needs to be considered. In that case the treatment is similar to that of magnetic scattering in conventional superconductors [Kampf and Devereaux (1997)].

In the 4-vector notation of the Chapter 2 the potential scattering has to have the same matrix structure as the chemical potential, or $\epsilon(\mathbf{k})$ in Eq. (2.19), so that

$$H_{imp} = \int d\mathbf{r} \Psi^{\dagger}(\mathbf{r}) U_{pot}(\mathbf{r}) \tau_3 \Psi(\mathbf{r}), \tag{4.2}$$

or, in Nambu notation,

$$\hat{U}_{pot} = U_0 \tau_3 \delta(\mathbf{r} - \mathbf{r}_0). \tag{4.3}$$

In addition to the electrostatic interactions, if the impurity atom has a magnetic moment, there is an exchange interaction between the local spin on the impurity site and the conduction electrons,

$$H_{imp} = \sum_{\alpha\beta} \int d\mathbf{r} J(\mathbf{r}) \psi^{\dagger}_{\alpha}(\mathbf{r}) \mathbf{S} \cdot \boldsymbol{\sigma}_{\alpha\beta} \psi_{\beta}(\mathbf{r}). \tag{4.4}$$

The range of interaction here is determined by the quantum mechanical structure of the electron cloud associated with the localized spin. Again, in reality a simplified exchange Hamiltonian with

$J(\mathbf{r}) = J\delta(\mathbf{r} - \mathbf{r_0})$ is often considered, which captures the essential physics of the problem. In the 4-vector notations the electron spin operator becomes

$$\boldsymbol{\alpha} = \frac{1}{2}\Big[(1+\tau_3)\boldsymbol{\sigma} + (1-\tau_3)\sigma_3\boldsymbol{\sigma}\sigma_3\Big]. \tag{4.5}$$

Therefore,

$$H_{imp} = \int d\mathbf{r}\Psi^\dagger(\mathbf{r})J(\mathbf{r})\mathbf{S}\cdot\boldsymbol{\alpha}\Psi(\mathbf{r}), \tag{4.6}$$

or, in Nambu notation,

$$\hat{U}_{mag} = J(\mathbf{r})\mathbf{S}\cdot\boldsymbol{\alpha}. \tag{4.7}$$

When considering many noninteracting impurities the net impurity potential is simply

$$\hat{U}_{imp}(\mathbf{r}) = \sum_i \hat{U}_{imp}(\mathbf{r}-\mathbf{r}_i) = \int d\mathbf{r}'\rho_{imp}(\mathbf{r}')\hat{U}_{imp}(\mathbf{r}-\mathbf{r}_i). \tag{4.8}$$

Here, $\hat{U}$ denotes the matrix structure of the potential in both spin and particle-hole space, and the impurity density is introduced,

$$\rho_{imp}(\mathbf{r}) = \sum_i \delta(\mathbf{r}-\mathbf{r}_i). \tag{4.9}$$

The dilute impurity limit of the average impurity concentration $n_i \ll 1$ is also assumed, where

$$n_i = \int \frac{d\mathbf{r}}{V}\rho(\mathbf{r}). \tag{4.10}$$

For magnetic scatterers it has been explicitly shown that that effect of the Ruderman-Kittel-Kasuya-Yosida (RKKY) interaction between scattering centers on the superconducting properties is small [Galitskii and Larkin (2002)].

If one computes a local physical quantity, such as the density of states measured by the STM at the position $\mathbf{r}$, it will depend on the distance from nearby impurities, and therefore will be different for different realization of impurity distributions. In contrast, thermodynamic quantities, such as the density of states measured in planar junctions, or the specific heat, average the density of states over many random local configurations of impurities. Hence, in computing their values one averages all impurity configurations [Abrikosov et al. (1963)], so that

$$\overline{G}(\omega_n, \mathbf{k}) = \prod_{i=1}^{N_i}\left[\frac{1}{V}\int d\mathbf{r}_i G(\omega_n, \mathbf{k}, \mathbf{r}_1, \ldots, \mathbf{r}_{N_i})\right]. \tag{4.11}$$

Here, a bar denotes such an impurity average. By definition $\bar{\rho}_{imp} = n_i$. An uncorrelated (random) impurity distribution has the form

$$\overline{\rho(\mathbf{r})\rho(\mathbf{r}')} = \prod_{i=1}^{N_i}\left[\frac{1}{V}\int d\mathbf{r}_i\rho(\mathbf{r}, \mathbf{r}_1, \ldots, \mathbf{r}_{N_i})\rho(\mathbf{r}, \mathbf{r}_1, \ldots, \mathbf{r}_{N_i})\right] = n_i\delta(\mathbf{r}-\mathbf{r}') + n_i^2. \tag{4.12}$$

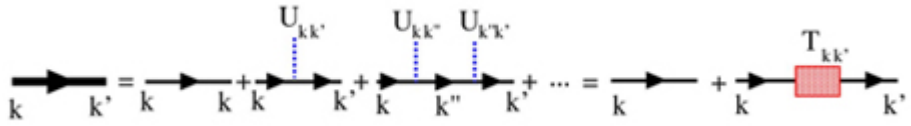


**Figure 4.1**: Multiple scattering on a single impurity. The thick line denotes the full Green's function, the thin line is the bare Green's function, and the dashed line symbolizes the scattering process. The rightmost part defines the $T$ matrix according to Eq. (4.15) [Balatsky et al. (2006)].

Since the impurities are dilute, $n_i^2 \ll n_i$, and the second term can be neglected compared to the first.

In practice to compute the Green's function in the presence of impurities the $T$-matrix approximation is often employed [Hirschfeld and Goldenfeld (1993)]. For a single impurity with the scattering potential $\hat{U}_{\mathbf{k},\mathbf{k}'}$ in the momentum space, the $T$-matrix accounts exactly for multiple scattering of one impurity. In the language of Feynman diagrams, the corresponding process is shown in Fig. 4.1. The hat over a letter in equations means that it denotes a matrix in Nambu space. Therefore, the full Green's function is

$$\hat{G}(\mathbf{k},\mathbf{k}') = \hat{G}_0(\mathbf{k}) + \hat{G}_0(\mathbf{k})\hat{U}_{\mathbf{k},\mathbf{k}'}\hat{G}_0(\mathbf{k}') + \sum_{\mathbf{k}''} \hat{G}_0(\mathbf{k})\hat{U}_{\mathbf{k},\mathbf{k}''}\hat{G}_0(\mathbf{k}'')\hat{U}_{\mathbf{k}'',\mathbf{k}'}\hat{G}_0(\mathbf{k}') + \dots . \tag{4.13}$$

The frequency index in the Green's function is omitted due to the elasticity of the scattering. The series can be summed to write according to Fig. 4.1

$$\hat{G}(\mathbf{k},\mathbf{k}') = \hat{G}_0(\mathbf{k}) + \hat{G}_0(\mathbf{k})\hat{T}_{\mathbf{k},\mathbf{k}'}\hat{G}_0(\mathbf{k}'), \tag{4.14}$$

where the $T$-matrix is given by an infinite series

$$\hat{T}_{\mathbf{k},\mathbf{k}'} = \hat{U}_{\mathbf{k},\mathbf{k}'} + \sum_{\mathbf{k}''} \hat{U}_{\mathbf{k},\mathbf{k}''}\hat{G}_0(\mathbf{k}'')\hat{U}_{\mathbf{k}'',\mathbf{k}'} + \ldots = \hat{U}_{\mathbf{k},\mathbf{k}'} \sum_{\mathbf{k}''} \hat{U}_{\mathbf{k},\mathbf{k}''}\hat{G}_0(\mathbf{k}'')\hat{T}_{\mathbf{k}'',\mathbf{k}'}. \tag{4.15}$$

This equation needs to be solved for $\hat{T}$. If the impurity scattering is purely local, $\hat{U}(\mathbf{r}-\mathbf{r}')$, the scattering is isotropic, $\hat{U}_{\mathbf{k},\mathbf{k}'} = \hat{U}$, greatly simplifying the process of solving the equation for the $T$-matrix, as $\hat{T}$ depends only on frequency.

The main observation here is that, in the vicinity of the impurity, the translational invariance is broken, and the Green's function depends on two momenta, $\mathbf{k}$ and $\mathbf{k}'$

$$\hat{G}(\mathbf{r},\mathbf{r}';\omega) = \hat{G}_0(\mathbf{r},\mathbf{r}';\omega) + \hat{G}_0(\mathbf{r},\mathbf{r}_0;\omega)\hat{T}(\omega)\hat{G}_0(\mathbf{r}_0,\mathbf{r}';\omega). \tag{4.16}$$

The $T$-matrix lends itself easily to describe the effect of an ensemble of impurities. The self-consistent $T$-matrix approach considers multiple scattering on a single site of an electron that has already been scattered on all other impurity sites [Hirschfeld et al. (1986)]. This results in replacing the bare Green's function in Eq. (4.15) by its impurity-averaged counterpart, $\hat{G}(\mathbf{k},\omega)$. The translational invariance restores after averaging over the random impurity distribution, so that the Green's function depends on a single momentum $\mathbf{k}$ [Balatsky et al. (2006)]. The combined effect of impurities is given by the self-energy, $\hat{\sum}(\mathbf{k},\omega) = n_i\hat{T}_{\mathbf{k},\mathbf{k}'}$, so that

$$\hat{G}^{-1}(\mathbf{k},\omega) = \hat{G}_0^{-1}(\mathbf{k},\omega) - \hat{\Sigma}(\mathbf{k},\omega). \tag{4.17}$$

In contrast to the single impurity case, where Eq. (4.14) with the $T$-matrix given by Eq. (4.15) is the exact solution of the problem, the Green's function given above is an approximation. Much recent research is motivated by questions about how accurately it describes the properties of nodal superconductors with impurities.

### Anderson's theorem

One of the most important early results was the robustness of the conventional superconductivity to small concentrations of non-magnetic impurities. Theoretical underpinning of this result is known as Anderson's theorem [Anderson (1959)]. Anderson's observation was that, since superconductivity is due to the instability of the Fermi surface to pairing of time-reversed quasiparticle states, any perturbation that does not lift the Kramers degeneracy of these states does not affect the mean field superconducting transition temperature.

This is most clearly seen from the BCS analysis according to Ma and Lee [Ma and Lee (1985)]. Here an isotropic pairing potential is considered, $V_{\alpha\beta\gamma\delta}(\mathbf{r},\mathbf{r}') = V\delta(\mathbf{r}-\mathbf{r}')$. In the absence of magnetic field the coefficients $a_n = \sin\theta_n$ and $b_n = \cos\theta_n$ can be taken real without loss of generality, so that the self-consistency condition, Eq. (2.9), reads

$$\Delta_n = V\sum_{m\neq n}\frac{\Delta_m}{(\xi_m^2+\Delta_m^2)}\int d^d\mathbf{r}\phi_n^2(\mathbf{r})\phi_m^2(\mathbf{r}), \tag{4.18}$$

where

$$\Delta_n = \int d^d\mathbf{r}\Delta(\mathbf{r})\phi_n^2(\mathbf{r}). \tag{4.19}$$

As noted above, in the BCS approach $\phi$'s are eigenfunctions of the single particle Hamiltonian. In the absence of impurities the system is translationally invariant, so that $\Delta(\mathbf{r}) = \Delta_n = \Delta_0$. The most important assumption underlying Anderson's theorem is that the superconducting order parameter can be taken to be uniform, $\Delta(\mathbf{r}) = \Delta_1$, even in the presence of impurities. In that case the individual eigenfunctions of the single particle Hamiltonian including impurities are rather complicated. Then the gap equation, Eq. (4.18), takes the form

$$\frac{1}{V} = \int \epsilon\frac{N(\epsilon,\mathbf{r})}{\sqrt{\epsilon^2+\Delta_1^2}}. \tag{4.20}$$

If the density of states of the system with impurities,

$$N(\epsilon,\mathbf{r}) = \sum_n \phi_m^2(\mathbf{r})\delta(\epsilon-\epsilon_m), \tag{4.21}$$

is unchanged compared to the pure metal, then $N(\epsilon,\mathbf{r}) \approx \rho_0$. If this condition is satisfied, the solution $\Delta_1 = \Delta_0$ of the gap equation (Eq. (4.20)) must be identical to that of the BCS equation in the absence of impurities, and therefore the transition temperature and the gap are insensitive to the impurity scattering at the mean field level.

Anderson's theorem helped to explain the robustness of superconductivity to impurities in early experiments. However, it is important to keep in mind that the thermodynamic averages of the

system is an approximate statement. Anderson's theorem introduces the need to separate the study of impurity effects on different length scales, from lattice spacing to the coherence length, to sample size.

In weakly disordered systems the density of states remains nearly constant as a function of disorder. Ma and Lee [Ma and Lee (1985)] argued that Anderson's theorem remains valid in the form above even in a strongly disordered system provided the localization length, $L \gg (\rho_0 \Delta_0)^{1/d}$. In that case there is a large number of states localized within energy $\Delta_0$ of the Fermi surface, and these states form a local superconducting patch. The Josephson interaction between the patches then leads to global phase coherence at zero temperature. Moreover, they argued that the theorem holds all the way to the limit of site localization.

It is important to note that the superfluid stiffness, i.e. the ability of the superconductor to screen out the magnetic field, is affected by disorder. In particular, when the quasiparticle lifetime, $\tau$, becomes sufficiently short, $\Delta_0 \tau \ll 1$, the superfluid density $\rho_s \approx \Delta_0 \tau$. Consequently the superconductor is sensitive to the local phase fluctuations of the order parameter, and the experimentally observed transition temperature may be severely suppressed compared to the mean field $T_c$, as it is, for instance, in granular superconductors [Balatsky et al. (2006)]. Therefore, for dilute impurities Anderson's theorem is valid provided the superconducting order parameter can be taken to be nearly uniform. The distance at which the order parameter $\Delta(\mathbf{r})$ varies significantly is the coherence length, $\xi_0 \simeq v_F/\Delta_0$, where $v_F$ is the Fermi velocity, while the Coulomb screening length for the charged impurities in metals is of the order of the lattice spacing, $a$. Hence, for $\xi_0 \gg a$ the order parameter remains essentially uniform, and Anderson's theorem holds. Recently, it has been shown that in case when the superconducting pairing is of the order of the electron bandwidth, Anderson's theorem is violated [Ghosal et al. (1998), Moradian et al. (2001)]. Ghosal *et al* [Ghosal et al. (1998)] have explored in detail the discrepancy between the single particle excitation gap and the superconducting order parameter as a function of disorder in these circumstances. Beyond Anderson's regime of the constant density of states, both quantities decrease at first, since the disorder depletes the density of states. Then the spectral gap persists while the superconducting order vanishes. As pointed out in Ref. [Ma and Lee (1985)] in the limit of strong disorder, the models with on-site pairing show the on-site spectral gap (so-called Anderson negative-$U$ glass) without the off-diagonal long range order and without symmetry breaking.

The Green's function formalism is well suited for the analysis of the combined effect of many uncorrelated impurities in the bulk of a superconductor. The first treatment of the superconducting properties using this technique was given by Abrikosov and Gor'kov [Abrikosov and Gor'kov (1960)]. After averaging over different impurity distributions following Eq. (4.11), the translational symmetry in the system is restored, and therefore the Green's function takes the general form

$$\hat{G}^{-1}(\mathbf{k}, \omega) = i\omega_n - \xi(\mathbf{k})\tau_3 - \Delta_0 \sigma_2 \tau_2 - \hat{\Sigma} \equiv i\tilde{\omega} - \tilde{\epsilon}(\mathbf{k})\tau_3 - \tilde{\Delta}\sigma_2\tau_2. \tag{4.22}$$

Here, the rightmost part of the equation explicitly takes into account the matrix structure of the self-energy, $\hat{\Sigma}$. The superconducting gap in the presence of impurities is determined by the self-consistency condition, Eq. (2.21), which reads here

$$\Delta(\hat{\Omega}) = \pi T N_0 \sum_{\omega_n} \int d\hat{\Omega}' V(\hat{\Omega}, \hat{\Omega}') \frac{\tilde{\Delta}\hat{\Omega}'}{\sqrt{\tilde{\omega}_n^2 + \Delta^2(\hat{\Omega}')}}. \tag{4.23}$$

The transition temperature is the temperature at which a non-trivial solution of the self-consistency equation first appears. Together with the self-energy equations these equations form a general basis

for treating ensembles of impurities in superconductors. It should be noted that the contribution of $\Sigma_3$ is ignored, which is equivalent to the renormalization of the chemical potential. This is always allowed when computing the density of states, although the corrections may need to be taken into account in evaluating the response functions [Hirschfeld et al. (1988)]. The basic assumption for computing the self-energy is that, in addition to neglecting the interaction between spins on different impurity sites, the interference effects of scattering on different impurities also can be neglected. This is of order $(p_F l)^{-1}$, where $l$ is the mean free path.

**Born approximation**

Abrikosov and Gor'kov (AG) analyzed the effect of the impurity scattering on superconductivity in the Born approximation [Abrikosov and Gor'kov (1960)]. Here it is presented in the treatment of Maki [Maki (1969)]. General impurity potential combining the potential and the magnetic scattering is considered as

$$\hat{U}_{imp}(\mathbf{k}-\mathbf{k}') = U_{pot}(\mathbf{k}-\mathbf{k}')\tau_3 J(\mathbf{k}-\mathbf{k}')\mathbf{S}\cdot\boldsymbol{\alpha}, \tag{4.24}$$

where $\boldsymbol{\alpha}$ is defined in Eq. (4.5). AG considered the self-energy in the Born approximation,

$$\hat{\Sigma}(\omega,\mathbf{k}) = n_i \int \frac{d\mathbf{k}'}{(2\pi)^3}\hat{U}_{imp}(\mathbf{k}-\mathbf{k}')\hat{G}(\mathbf{k}',\omega)\hat{U}_{imp}(\mathbf{k}'-\mathbf{k}). \tag{4.25}$$

Integrating over $\mathbf{k}'$ one finds

$$\tilde{\omega} = \omega_n + \frac{1}{2}\left(\frac{1}{\tau_p}+\frac{1}{\tau_s}\right)\frac{\tilde{\omega}}{\sqrt{\tilde{\omega}_n^2+\Delta^2}}, \tag{4.26}$$

$$\tilde{\Delta} = \Delta + \frac{1}{2}\left(\frac{1}{\tau_p}-\frac{1}{\tau_s}\right)\frac{\tilde{\Delta}}{\sqrt{\tilde{\omega}_n^2+\Delta^2}}, \tag{4.27}$$

where the potential ($\tau_p$) and spin-flip ($\tau_s$) scattering times are given by

$$\frac{1}{\tau_p} = n_i N_0 \int d\hat{\Omega}|U_{pot}(\mathbf{k}-\mathbf{k}')|^2, \tag{4.28}$$

$$\frac{1}{\tau_s} = n_i N_0 S(S+1)\int d\hat{\Omega}|J(\mathbf{k}-\mathbf{k}')|^2. \tag{4.29}$$

Here, everything is averaged over all possible directions of the impurity spin.

In the absence of spin-flip scattering both $\Delta$ and $\omega$ are renormalized identically, and it follows from Eq (4.23) that the gap remains unchanged compared to the pure case. This is in accordance with Anderson's theorem. The spin-flip scattering time, which violates the time-reversal symmetry, enters the equations for $\tilde{\omega}$ and $\tilde{\Delta}$ with the opposite sign. Therefore, introducing $u = \tilde{\omega}/\tilde{\Delta}$, one finds

$$\frac{\omega}{\Delta} = u\left(1-\frac{(\Delta\tau_2)^{-1}}{\sqrt{1+u^2}}\right). \tag{4.30}$$

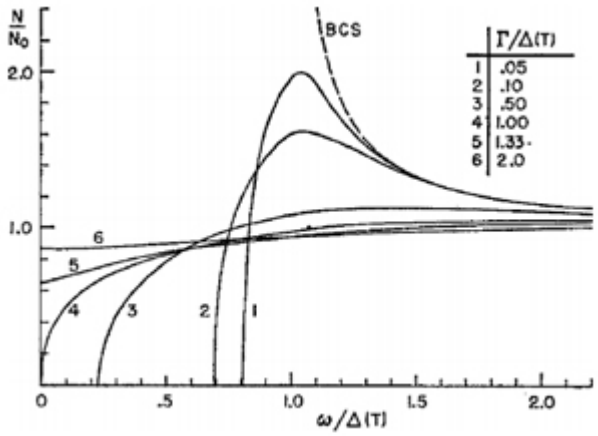


**Figure 4.2**: Density of states in the Abrikosov-Gor'kov theory of magnetic impurities in superconductors. Here scattering rate has the form of $\Gamma = \tau_s^{-1}$ [Betbeder-Matibet and Weiss (1964)].

It follows that the gap in the single particle spectrum is $E_{gap} = \Delta(1 - (\delta\tau_s)^{-2/3})^{3/2}$ for $\Delta\tau_s > 1$, and vanishes for $\Delta\tau_s < 1$. This gapless region starts at the value of pair-breaking parameter $\alpha$,

$$\alpha' = \tau_s^{-1} = \Delta_{00} \exp\left(-\frac{\pi}{4}\right), \tag{4.31}$$

where $\Delta_{00}$ is the gap in the pure material at $T = 0$. The transition temperature is determined from

$$\psi\left(\frac{1}{2} + \frac{1}{2\pi\tau_s T_c}\right) - \psi\left(\frac{1}{2}\right) = \ln\frac{T_{c0}}{T_c}, \tag{4.32}$$

where $\psi(x)$ is the digamma function and $T_{c0}$ is the transition temperature of the pure material. Consequently, superconductivity is destroyed ($T_c = 0$) when

$$\alpha_c = \tau_s^{-1} = \pi T_{c0}/2\gamma = \Delta_{00}/2 > \alpha', \tag{4.33}$$

where $\gamma \approx 1.78$. As $\alpha' \approx 0.912\alpha_c$ AG predicted that a regime of gapless superconductivity exists for a range of impurity scattering [Abrikosov and Gor'kov (1960)]. This was first confirmed in experiments by [Woolf and Reif (1965)]. The evolution of the density of states with increasing disorder has been investigated in detail by authors of Ref. [Betbeder-Matibet and Weiss (1964)], and is shown in Fig. 4.2. For $\alpha < \alpha'$ a hard gap in the single particle spectrum persists up to the critical impurity concentration, as shown in Fig. 4.3. This result shows that even a single magnetic impurity creates a localized state in the superconducting gap.

### Impurities in $d$-wave superconductors

The growth of the impurity band with finite concentration of the impurities is considered. As was mentioned above, scalar non-magnetic impurities have a pair-breaking effect on any unconventional superconductor, and substantially change the low-energy spectrum of superconducting quasiparticles. This problem has been considered in great detail in the framework of the self-consistent

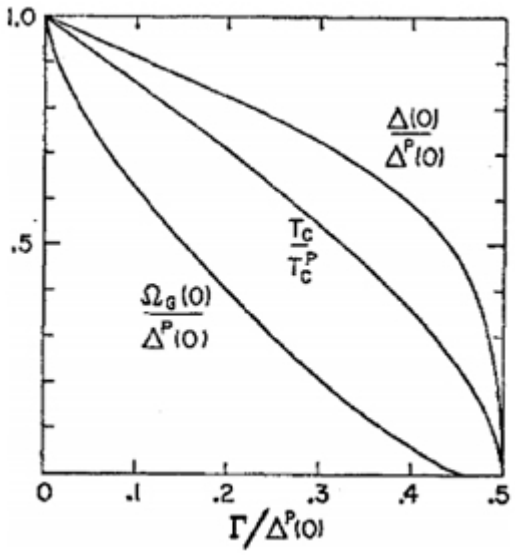


**Figure 4.3**: Dependences of the order parameter $\Delta$, transition temperature $T_c$, and the single-particle spectral gap $\Omega_G$ on the scattering rate, $\Gamma = \tau_s^{-1}$ [Betbeder-Matibet and Weiss (1964)].

$T$-matrix approximation [Hirschfeld and Goldenfeld (1993)], which leads to the finite density of states at the Fermi level.

For finite impurity concentration, the self-consistent Green's function, averaged over impurity positions, is given in Eq. (4.17) as

$$\hat{G}^{-1}(\mathbf{k},\omega) = \hat{G}_0^{-1}(\mathbf{k},\omega) - \hat{\Sigma}(\omega), \tag{4.34}$$

with $\hat{\Sigma}(\omega) = n_i \hat{T}(\omega)$. In the case of particle-hole symmetry [Hirschfeld et al. (1988)], and unconventional gap (defined as having a zero average over the Fermi surface) the only non-vanishing component of the $T$-matrix is proportional to $\tau_0$,

$$T_0(\omega) = \frac{g_0(\omega)}{c^2 - g_0(\omega)}. \tag{4.35}$$

The $T$-matrix has to be determined self-consistently with $g_0(\omega) = \frac{1}{2\pi N_0} \sum_{\mathbf{k}} \mathrm{Tr}\hat{G}(\mathbf{k},\omega)\hat{\tau}_0$.

Solution of this equation leads to a finite density of states at the Fermi level. This result was first obtained for Born scattering [Gor'kov and Kalugin (1985)], leading to an exponentially small $N(0)/N_0 \approx 4\tau^2\Delta_0^2 \exp(-2\Delta_0\tau)$, where $\tau$ is the normal state scattering rate. The results are much more dramatic for unitary scattering ($c = 0$) [Hirschfeld et al. (1986)]

$$\gamma \simeq \sqrt{n_i(\Delta_0/\pi N_0)}, \tag{4.36}$$

where $\gamma = -\mathrm{Im}\sum(\omega \to 0)$ is the scattering rate for low-energy quasiparticles. For $\omega \lesssim \gamma$, the density of states is determined by impurities and is finite: $N_i(0)/N_0 = 2\gamma/\pi\Delta_0$. The characteristic width of the impurity-dominated region is $\omega^* \simeq \gamma \propto \sqrt{n_i}$.

The origin of the finite density of states is the impurity band, grown from the impurity-induced states ($c = 0$). Scaling of the impurity bandwidth $\gamma \propto \sqrt{n_i}$ has been obtained earlier for the case

of paramagnetic impurities in an $s$-wave superconductor [Shiba (1968)]. The fact that $\gamma \propto \sqrt{n_i}$ is obeyed in the case of a $d$-wave superconductor with scalar impurities as well is consistent with the claim that the low-energy states in a disordered $d$-wave superconductor are formed from the bound states at finite concentration [Balatsky et al. (2006)]. The results above are for isotropic impurity scattering. Anisotropic impurities may preferentially scatter electrons between regions with the same, or close values of the gap, so that the scattering is inefficient in suppressing $T_c$.

## Pair breaking in iron-based superconductors

Iron-pnictide superconductors have a number of peculiar properties. Among which is the specific-heat-jump $\Delta C$ proportionality to $T_c^3$ as demonstrated on 122 series of $Ba(Fe_{1-x}Co_x)_2As_2$ and $Ba(Fe_{1-x}Ni_x)_2As_2$ [Bud'ko et al. (2009)]. This behavior cannot be explained within the conventional BCS theory domain [Zaanen (2009)]. Similar behavior is observed in 122 crystals with Ba substituted partially by K and with Fe substituted by Pd and Rh [Ni et al. (2008)]. Another uncommon character is that slopes of the upper critical field $dH_{c2}/dT$ at $T_c$ are approximately proportional to $T_c$ across both 1111 and 122 series.

These two behaviors can be understood within the weak-coupling BCS model provided a strong pair-breaking is present in the materials. In fact, these features should also be present in conventional superconductors with magnetic impurities as discussed by Abrikosov and Gor'kov in their work on the pair-breaking for the nearly critical concentration of these impurities when $T_c \ll T_{c0}$, where $T_{c0}$ is the critical temperature of a clean material [Abrikosov and Gor'kov (1960)]. AG considered isotropic materials with a spherical Fermi surface and the $s$-wave order parameter constant along this surface. The symmetry of the order parameter in multiband pnictides is not yet determined with certainty, however, the $s^{\pm}$ structure is in favor [Mazin and Schmalian (2009); Zhang et al. (2009)]. The critical temperature in materials with a strongly anisotropic order parameter is suppressed not only by scattering breaking the time reversal symmetry (spin-flip), in fact, any scattering reduces $T_c$.

The evaluation of $dH_{c2}/dT$ and $\Delta C$ at $T_c$ for an arbitrary anisotropy of the order parameter $\Delta$ and of the Fermi surface in the presence of pair-breaking has been performed within the weak-coupling scheme by Kogan [Kogan (2009)]; where the main focus has been on the situation when the average $\langle\Delta\rangle$ over the FS is close to zero that presumably is the case of pnictides [Mazin and Schmalian (2009); Zhang et al. (2009)]. The energy dependence of the total density of states and the specific heat jump at $T_c$ in this limit read

$$\frac{N(\epsilon)}{N(0)} = 1 - 2\Delta^2\tau_+^2\frac{1-\eta^2}{(1+\eta^2)^2}, \quad \eta = 2\tau_+\epsilon \tag{4.37}$$

and

$$\Delta C = C_s - C_n = \frac{16\pi^4 k_B^4 N(0)\tau_+^2}{3\hbar^2(3\langle\Omega^4\rangle - 2)}T_c^3, \tag{4.38}$$

respectively [Kogan (2009)].

Figure 4.4 is a compilation of data on the slopes $H'_{c2}$ for 1111 compounds with various dopants and, therefore, with various $T_c$'s. An approximate scaling $H'_{c2} \propto T_c$ is evident despite the fact that the presented compounds have critical temperatures varying from 6 to 46 K. From this data one can

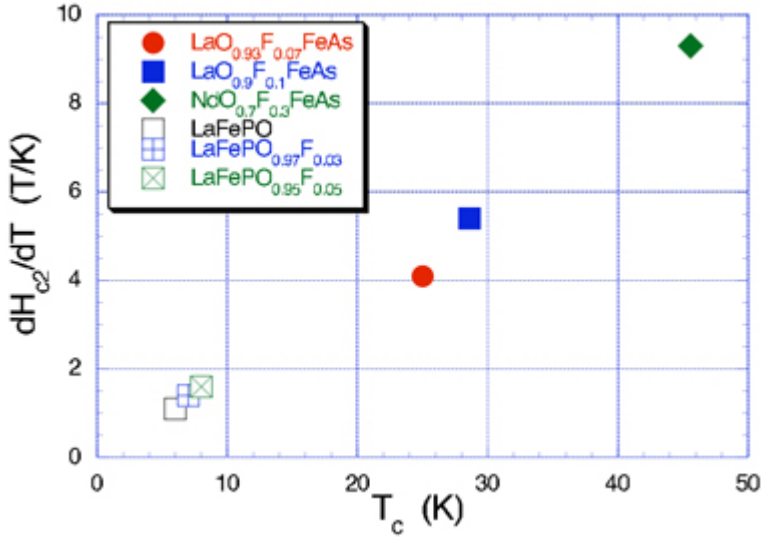


**Figure 4.4**: The slopes of $H'_{c2}(T)$ near $T_c$ for several 1111 compounds. The two rightmost points are for $H'_{c2,ab}$ of crystalline samples, the rest are for polycrystals, so that all points reflect $H'_{c2,ab}$ [Kogan (2009)].

estimate the slope of $dH_{c2}/dT_c$ as approximately equal to 0.2 T/K$^2$. Then, the order of magnitude of the Fermi velocity follows from $|dH_{c2}/dT_c| \sim \pi\phi_0 k_B^2/\hbar^2 v_F^2$ as $v_F \sim 10^7$ cm/s, a reasonable order that can be taken as yet another argument in favor of the picture presented. In Fig. 4.5, the data for the 122 family are collected. The same approximate scaling is seen although with a considerable scatter. The latter might be caused by variety of reasons: different criteria in extracting $H_{c2}$ from resistivity data, unavoidable uncertainties rooted in sample inhomogeneities in determination of $T_c$ and the slopes of $H_{c2}(T)$ near $T_c$, possible differences in Fermi velocities and the order parameter anisotropies, *etc*. Moreover, the model employing only two scattering parameters for multiband iron-pnictides is a far-reaching simplification [Kogan (2009)]. Nevertheless, the observed scaling seems robust. One can take this as evidence in favor of a strong pair-breaking present in all compounds examined. It should be stressed again that for strongly anisotropic order parameters, $\langle\Delta\rangle \approx 0$, the critical temperature suppression (pair-breaking) is caused by the combined effect of the transport and the spin-flip scatterings. On the other hand, in the well-studied $MgB_2$ with two $s$-type gaps of the same sign, the slopes of $H'_{c2}$ do not show a similar behavior: one can suppress $T_c$ by neutron irradiation leaving the $H'_{c2}$-slopes nearly unchanged [Wilke et al. (2006)]. Furthermore, carbon doping enhances $H'_{c2}(T_c)$ without causing a substantial reduction of $T_c$ [Chu et al. (2009)].

Figure 4.6 shows the specific heat jump measured in a number of compounds [Bud'ko et al. (2009)]. The scaling $\Delta C \propto T_c^3$ suggested by Bud'ko, Ni, and Canfield is evident. Again, it is worth noting that only the combined rate enters the coefficient in front of $T_c^3$ of Eq. (4.38), so that the source of $T_c$ suppression is not necessarily the spin-flip AG pair-breaking. The ever present transport scattering suppresses $T_c$ as well, provided the order parameter is strongly anisotropic. This is presumably the case of iron-pnictides.

The scalings $H'_{c2} \propto T_c$ and $\Delta C \propto T_c^3$ seem to hold across the whole class of iron-pnictides for compounds with different couplings, Fermi surfaces, *etc*. Clearly, the source of this scaling should be universal across the pnictide family of materials. The pair-breaking has been offered by Kogan

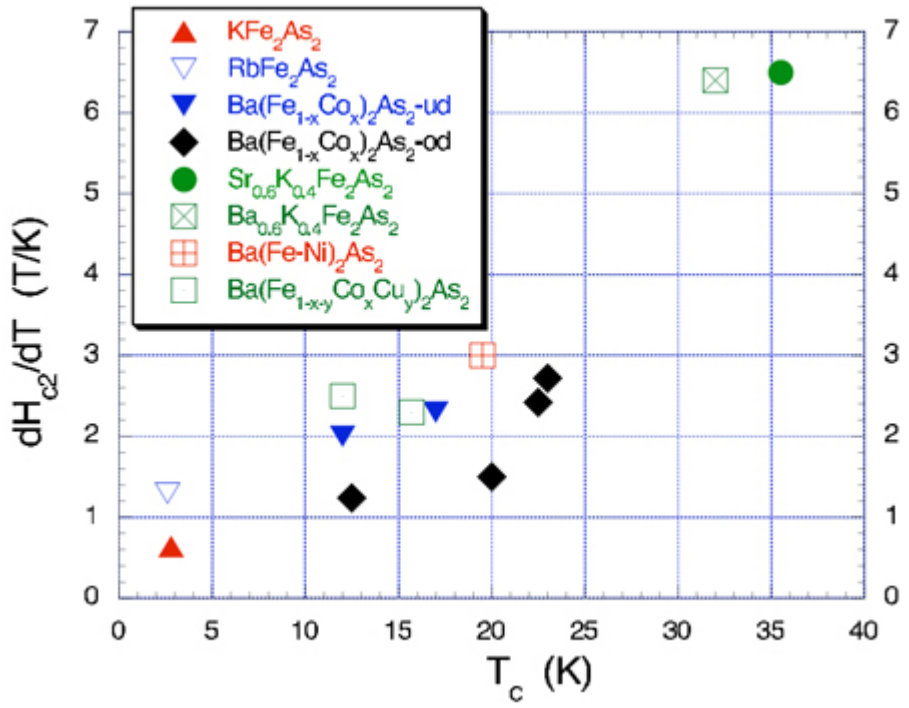


**Figure 4.5**: The slopes of $H'_{c2,c}(T)$ near $T_c$ for several 122 iron-pnictides [Kogan (2009)].

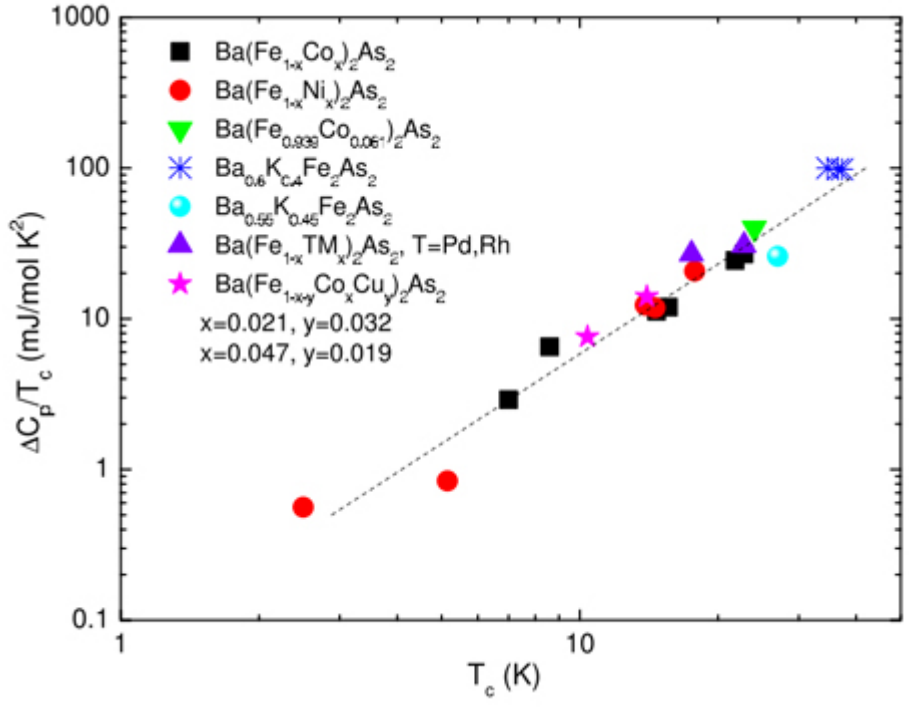


**Figure 4.6**: The specific heat jump versus $T_c$ for several 122 compounds depicted on a log-log plot. The dashed line corresponds to $\Delta C \propto T_c^3$ [Kogan (2009)].

[Kogan (2009)] as such a universal source.

The fact that $BaFe_2As_2$ superconducts only being doped shows that dopants play much more important role than just to provide extra scattering. Hence, for each compound listed in Fig. 4.6, the material characteristics entering Eq. (4.38) ($N(0)$, $\tau_+$, the anisotropy parameter $\langle\Omega^4\rangle$) differ. On the other hand, the scaling shown in this figure implies that the combination $N(0)\tau_+^2/(3\langle\Omega^4\rangle - 2)$ in all these compounds is roughly the same. This might be rationalized by notions that in the gapless state with $T_c \ll T_{c0}$ in which all of them presumably reside, the pair-breaking parameter $\tau_+$ is close to the critical value where $T_c = 0$. According to Eq. (4.37), tunneling experiments are likely to show the ratio of the apparent gap $\epsilon_m$, where the total density of states $N(\epsilon)$ is maximum, to $T_c$ varying as $1/T_c$ across the family of iron-pnictides.

Applying the approach as with $\Delta C \propto T_c^3$ [Kogan (2009)] one may investigate the low-temperature behavior of the London penetration depth $\lambda(T) = \lambda(0) + \Delta\lambda$, for which the pair-breaking results in

$$\Delta\lambda \propto \frac{T^2}{T_c^3}. \tag{4.39}$$

Despite some initial disagreements in experimental reports, most precision measurements of the in-plane London penetration depth of iron-based superconductors have found the power-law $\Delta\lambda(T) \propto T^n$ with $n \approx 2$ [Gordon et al. (2009)]; for some compounds $n \approx 1$ is claimed [Fletcher et al. (2009)]. Commonly, a nonexponential behavior is taken as evidence of an unconventional order parameter, possibly having a nodal gap structure [Gordon et al. (2009)]. However, such a direct correspondence between the nodes and the exponent $n$ should exist only in clean materials. Usually scattering breaks this connection. For example, in $d$-wave superconductors, the linear low-$T$ dependence of $\lambda$ in the clean case changes to $T^2$ in the presence of moderate scattering [Hirschfeld and Goldenfeld (1993)]. In fact, the connection between the power-law behavior of $\Delta\lambda(T)$ and scattering in iron-based superconductors was suggested in Ref. [Gordon et al. (2009)]. Figure 4.7 (a) shows examples of the quadratic variation in $\Delta\lambda$ that appear as straight lines when plotted versus $(T/T_c)^2$ for $T < T_c/3$ in compounds with $T_c$ varying from approximately 12 to 23 K. The exponent $n$ in $\Delta\lambda \propto T^n$ extracted by fitting the low-temperature data is shown for six compounds in Fig. 4.7 (b). One may see that $\Delta\lambda \propto T^2$ holds for the $(AE)(Fe_{1-x}TM_x)_2As_2$ (122), the $(RE)FeAs(O_{1-x}F_x)$ (1111), and $FeTe_{1-x}Se_x$ (11) families. Here, $AE$ stands for an alkali earth element, $TM$ for a transition metal, and $RE$ for a rare earth. Thus, the four lines shown in Fig. 4.7 (a) are not merely for different doping levels of the same compound but rather belong to four different families of the iron-based materials.

Godon *et al* [Gordon et al. (2010)] employed for strong pair-breaking description the quasiclassical version of the weak-coupling Gor'kov theory, which holds for a general anisotropic Fermi surface and for any gap symmetry [Eilenberger (1968)]. The theory is formulated in terms of functions $f(\mathbf{r}, \mathbf{k}_\mathrm{F}, \omega)$, $f^+$, and $\mathrm{g}$ which originate from Gor'kov-Green's functions and are normalized by $\mathrm{g}^2 + ff^+ = 1$. The Matsubara frequencies are $\omega = \pi T(2\nu + 1)$ with integer $\nu$ and $\hbar = k_B = 1$. The order parameter is taken in the form $\Delta(\mathbf{r}, \mathbf{k}_\mathrm{F}) = \Psi(\mathbf{r}, T)\Omega(\mathbf{k}_\mathrm{F})$, where $\Omega(\mathbf{k}_\mathrm{F})$ describes the variation of $\Delta$ along the Fermi surface and is conveniently normalized so that the average over the whole Fermi surface $\langle\Omega^2\rangle = 1$.

The scattering in the Born approximation is characterized by two scattering times, the transport $\tau$ responsible for the normal conductivity and $\tau_m$ for processes breaking the time-reversal symmetry

$$\frac{1}{\tau_\pm} = \frac{1}{\tau} \pm \frac{1}{\tau_m}. \tag{4.40}$$

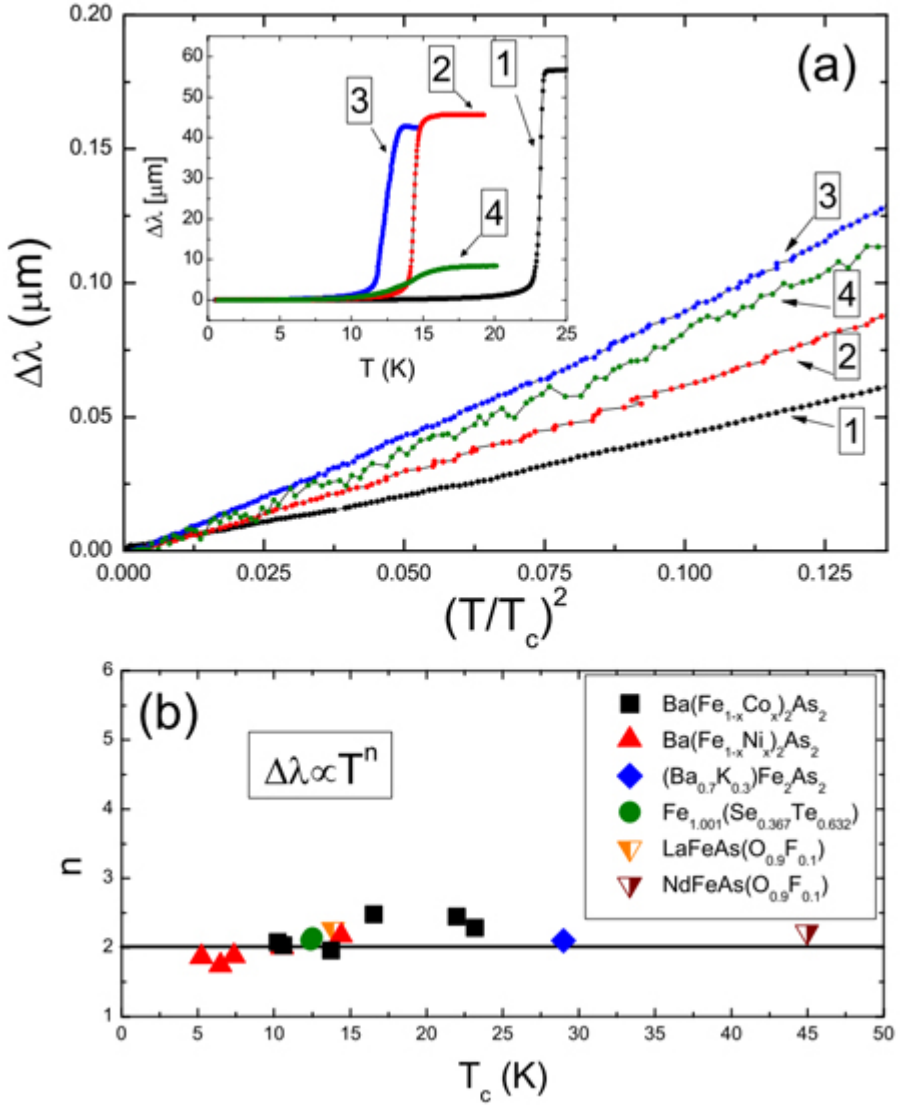


**Figure 4.7**: $\Delta\lambda$ versus $(T/T_c)^2$ for (1) $Ba(Fe_{0.942}Co_{0.058})_2As_2$, (2) $Ba(Fe_{0.941}Ni_{0.059})_2As_2$, (3) $Fe_{1.001}Se_{0.367}Te_{0.632}$, (4) $LaFeAsO_{0.9}F_{0.1}$. Inset of (a) depicts $\Delta\lambda$ in the full temperature range. (b) Fitted exponent $n$ in $\Delta\lambda \propto T^n$ [Gordon et al. (2010)].

Commonly, two dimensionless parameters are used for simplification

$$\rho = \frac{1}{2\pi T_c \tau} \quad \text{and} \quad \rho_m = \frac{1}{2\pi T_c \tau_m}, \tag{4.41}$$

or equivalently $\rho_\pm = \rho \pm \rho_m$. For multiband Fermi surfaces one may need more parameters for various intraband and interband processes, which are hardly controllable and their number is too large for a useful theory.

It is well-known that the formal scheme of the Abrikosov-Gor'kov work on magnetic impurities [Abrikosov and Gor'kov (1960)] applies to various situations with different pair-breaking causes, not necessarily the AG spin-flip scattering [Maki (1969)]. In each particular situation, the parameter $\rho_m$ must be properly defined. Evaluation of $\lambda(T, \tau, \tau_m)$ for arbitrary $\tau$'s and arbitrary anisotropy of $\Delta$ is difficult analytically. However, for a strong-$T_c$ suppression, the problem is manageable. Within the microscopic theory, penetration of weak magnetic fields into superconductors is evaluated by first solving for the unperturbed zero-field state and then treating small fields as perturbations. It was shown by AG [Abrikosov and Gor'kov (1960)] that for strong pair-breaking the formalism for the derivation of the Ginzburg-Landau equations near critical temperature applies at all temperatures. Within the Eilenberger approach this means that $f \ll 1$ and $\mathrm{g} \approx 1 - ff^+/2$ at all temperatures. The calculation then proceeds in a manner similar to that near $T_c$.

Within a two-band model for iron-based materials, the order parameter is believed to have an $s^\pm$ structure [Mazin and Schmalian (2009)] so that $\langle\Delta\rangle \ll |\Delta_{\max}|$ [Zhang et al. (2009)]. The problem simplifies considerably if one assumes $\langle\Delta\rangle = 0$. In the zero-field state, one looks for solutions of Eilenberger equations as $f_0 = f^{(1)} + f^{(2)} + \ldots$, where $f^{(1)} \sim \Delta$, $f^{(2)} \sim \Delta^2$, *etc*. The Eilenberger equation for $f$ then yields [Kogan (2009)]

$$f_0 = \frac{\Delta}{\omega_+} + \frac{\Delta}{2\omega_+^3}\left(\frac{\langle\Delta^2\rangle}{2\tau_{+\omega_+}} - \Delta^2\right) + \mathcal{O}(\Delta^5), \tag{4.42}$$

where $\omega_+ = \omega + 1/2\tau_+$. One can see that even at low temperatures $f_{0,\max} \sim \tau_+ T_c \sim 1/\rho_+ \ll 1$ because for strong pair-breaking $T_c \to 0$. This is a quasiclassical justification for the AG statement that $f \ll 1$ at all temperatures.

The temperature dependence of $\Delta$ (or $\Psi$) is obtained from the self-consistent gap equation. For a strong pair-breaking, this equation takes form [Kogan (2009)]

$$\frac{\Psi(1-t^2)}{12\pi T\rho_+^2} = \sum_{\omega>0}^{\infty}\left(\frac{\Psi}{\omega^+} - \langle\Omega f\rangle\right). \tag{4.43}$$

Substituting here $f$ with Eq. (4.42), one obtains the order parameter in the field-free state

$$\Psi^2 = \frac{2\pi^2(T_c^2 - T^2)}{3\langle\Omega^4\rangle - 2}, \tag{4.44}$$

which for $\Omega = 1$ reduces to the AG form.

One can now consider the response to a small current

$$\mathbf{j} = -4\pi|e|N(0)T\mathrm{Im}\sum_{\omega>0}\langle \boldsymbol{v}\mathrm{g}\rangle, \tag{4.45}$$

where $N(0)$ is the density of states at the Fermi level per one spin. Weak supercurrents leave the order parameter modulus unchanged but cause the condensate to acquire an overall phase $\theta(\mathbf{r})$. One then looks for perturbed solutions as

$$\Delta = \Delta_0 e^{i\theta}, \quad f = (f_0 + f_1)e^{i\theta}, \quad f^+ = (f_0 + f_1^+)e^{-i\theta}, \quad \mathrm{g} = \mathrm{g}_0 + \mathrm{g}_1, \tag{4.46}$$

where the subscript 1 denotes small corrections to the uniform state functions $f_0$ and $\mathrm{g}_0$. In London limit, the only coordinate dependence is that of the phase $\theta$; i.e., $f_1$, $\mathrm{g}_1$ are spatially independent. The Eilenberger equations provide the corrections, among which only $\mathrm{g}_1$ is needed [Kogan (2009)]

$$\mathrm{g}_1 = \frac{i f_0^2 \boldsymbol{v}\boldsymbol{P}}{2\omega_+} = \frac{i\Delta^2 \boldsymbol{v}\boldsymbol{P}}{2\omega_+^3}. \tag{4.47}$$

Here, $\boldsymbol{P} = \nabla\theta + 2\pi\boldsymbol{A}/\phi_0 \equiv 2\pi\boldsymbol{a}/\phi_0$ with the gauge invariant vector potential $\boldsymbol{a}$.

One needs to substitute $\mathrm{g}_0 + \mathrm{g}_1$ in Eq. (4.45) and compare the result with $4\pi j_i/c = -(\lambda^2)_{ik}^{-1} a_k$ to obtain

$$(\lambda^2)_{ik}^{-1} = \frac{8\pi^2 e^2 N(0) T}{c^2} \langle v_i v_k \Omega^2 \rangle \Psi^2 \sum_{\omega>0} \frac{1}{\omega_+^3}. \tag{4.48}$$

The sum here is expressed in terms of the poly-gamma function

$$\sum_{\omega>0} \frac{1}{\omega_+^3} = -\frac{1}{16\pi^3 T^3} \psi''\left(\frac{\rho^+}{2t} + \frac{1}{2}\right) \approx \frac{\tau_+^2}{\pi T}, \tag{4.49}$$

where $\rho_+ \gg 1$ has been used [Gordon et al. (2010)]. Taking into account Eq. (4.44), one obtains

$$(\lambda^2)_{ik}^{-1} = \frac{16\pi^3 e^2 N(0) k_B^2 \tau_+^2}{c^2 \hbar^2 (3\langle\Omega^4\rangle - 2)} \langle v_i v_k \Omega^2 \rangle (T_c^2 - T^2) \tag{4.50}$$

in common units. Now it is easy to obtain the low-temperature behavior of $\Delta\lambda_{ab} = \lambda_{ab}(T) - \lambda_{ab}(0)$ for a uniaxial material

$$\Delta\lambda_{ab} = \eta \frac{T^2}{T_c^3}, \quad \eta = \frac{c\hbar}{8\pi K_B \tau_+} \sqrt{\frac{3\langle\Omega^4\rangle - 2}{\pi e^2 N(0) \langle v_a^2 \Omega^2 \rangle}}. \tag{4.51}$$

Here $\tau_+$ is close to the critical value for which $T_c \to 0$. Then, one obtains for $T = 0$

$$\lambda_{ab}(0) = \frac{2\eta}{T_c}. \tag{4.52}$$

The factor $\beta$ in $\Delta\lambda = \beta T^2$ has been obtained by fitting the low temperature $\Delta\lambda$ for 122, 1111, and 11 compounds of Fig. 4.7 with $\beta$ being the only fitting parameter. The $\beta$'s are plotted in Fig. 4.8 versus $T_c$. The error bars in this graph reflect the fact that each sample has a certain transition width, which is the prevailing source of error in determination of $\beta$. According to the strong pair-breaking scenario, $\beta = \eta/T_c^3$. To compare experiment with theory, $\beta$ is plotted on the log-log scale in Fig. 4.8 along with the line $\beta = (8.8 \pm 1.0)/T_c^3$ obtained by fitting the data. Moreover, by substituting $v \sim 10^7$ cm/s and $N(0) \sim 10^{33}$ erg$^{-1}$cm$^{-3}$ in Eq. (4.39) one roughly estimates $\tau^+ \sim 3 \times 10^{-14}$ s. This value corresponds to the parameter $\rho^+ \approx 5$ for $T_c = 40$ K and to larger values for lower $T_c$'s, an observation consistent with the major model assumption of $\rho^+ \gg 1$ [Gordon et al. (2010)].

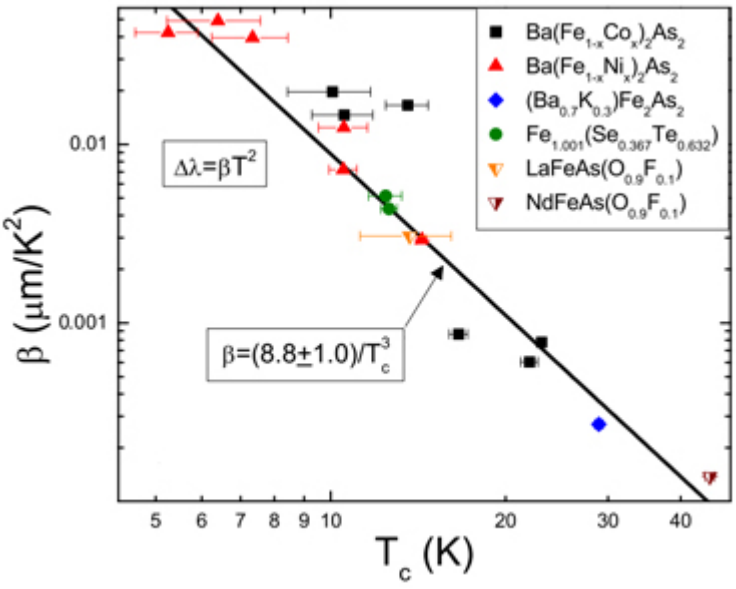


**Figure 4.8**: The factor $\beta$ is obtained by fitting the data to $\Delta\lambda = \beta T^2$ and plotted versus $T_c$ on a log-log scale. The solid line is a fit to $\beta = \eta/T_c^3$, motivated by Eq. (4.39) for a strong pair-breaking [Gordon et al. (2010)].

The degree to which experimental values follow the theory is remarkable, a substantial scatter of the data points notwithstanding. It is worth noting that $1/T_c^3$ scaling in $\Delta\lambda \propto T^2/T_c^3$ is a result of a strong pair-breaking and does not follow from any other currently discussed model. It should be stressed that the penetration depth scalings are approximate by design since their derivation involves a number of simplifying assumptions. Still they are robust in showing that the pair-breaking is an important factor for superconductivity of iron pnictides.

Consideration of iron-based materials being free of the pair-breaking scattering leads one to conclude that these materials would have had much higher critical temperatures. For instance, if $\rho_+ \approx 5$ and $T_c \approx 20$ K, the clean material would have $T_{c0} = T_c \exp[\psi(\rho_+/2 + 1/2) - \psi(1/2)]$ in the range of room temperatures, which is too doubtful. The pair-breaking scattering is probably inherent for the iron-based superconductors because the same interactions (presumably, spin fluctuations) cause both the pairing and the pair-breaking, and the both effects ought to be considered on the same footing.

The strong pair-breaking in the isotropic case leads to gapless superconductivity with the in-plane thermal conductivity data showing $\kappa/T(T \to 0) = 0$ [Luo et al. (2009)]. The strong pair-breaking model for anisotropic order parameters states that the total density of states $N(\epsilon)$ integrated over all pockets of the Fermi surface is finite at zero energy [Kogan (2009)]. This does not exclude the possibility that $N = 0$ for some parts on the Fermi surface. The superfluid density $\propto 1/\lambda^2$ depends only on the Fermi surface averages so that it is less sensitive to the $\Delta$ behavior on a particular set of directions [Gordon et al. (2010)].

Analysis of the low-temperature behavior of London penetration depth shows that a strong pair-breaking is likely to be responsible for the nearly universal temperature dependence $\Delta\lambda_{ab} \propto T^2/T_c^3$, along with reported $\Delta C \propto T_c^{-3}$ and $[dH_{c2}/dT]_{T_c} \propto T_c$, in nearly all iron-based superconductors.

CHAPTER V

# Comments on original publications

## Paper 1. Vortex core size in unconventional superconductors

Recently a new family of Fe-based chalcogenide superconductors $A_x Fe_{2-y} Se_2$ ($A$ = K, Ca) with $T_c \propto 30$ K has been discovered [Guo et al. (2010)]. These compounds are heavily electron doped, such that there are only electron Fermi surface pockets left, according to ARPES studies [Qian et al. (2011)]. The usual argument [Mazin et al. (2008b); Kuroki et al. (2008); Graser et al. (2009a)] leading to the most popular $s^{\pm}$ gap structure in the FeBS requires a $\Gamma$-centered pocket to enhance spin fluctuation pairing with wave vector $\mathbf{Q} \sim (\pi, 0)$ in the unfolded 1-Fe Brillouin zone. In the absence of these hole pockets a gap of the $s^{\pm}$ type is unfeasible. Therefore, the question of the pairing interaction was associated with the exchange of spin-fluctuations, as considered for the older materials [Kuroki et al. (2008); Graser et al. (2009a); Ishida et al. (2009); Ikeda et al. (2010)], but that the effective interaction peaked at a wave vector $\mathbf{Q} = (\pi, \pi)$ rather than at $(\pi, 0)$. In this case one would expect that the gap would have $B_{1g}$ symmetry, changing sign between the $(\pi, 0)$ and $(0, \pi)$ electron Fermi surfaces [Maier et al. (2011)]. The random phase approximation calculations [Maier et al. (2011)] (discussed in Chapter 3) showed competing $s$- and $d$-wave order for large electron doping, but only $d$-wave pairing stabilized in the absence of hole pockets [Maiti et al. (2011b)]. A strong peak was found in the dynamical susceptibility not at the wave vector $\mathbf{Q} \sim (\pi, 0)$ corresponding to the nesting wave vector of the two electron pockets in the 1-Fe BZ, but rather close to $(\pi, 0.6\pi)$, the vector connecting the closest flat sides of the rather square electron pockets [Maier et al. (2011)]. A number of authors [Mazin (2011); Khodas and Chubukov (2012)] have discussed the role of hybridization and the appearance of an $s^{\pm}$ state, in which the gap changes sign between the hybridized electron pockets. Other authors considered weak-coupling models involving proximity to or coexistence with simple magnetic stripes [Das and Balatsky (2011a)], with the $\sqrt{5} \times \sqrt{5}$ block state [Das and Balatsky (2011b)], or considered similar electronic structure in orbital fluctuation pairing models [Saito et al. (2011)].

Important experimental information was obtained from the inelastic neutron scattering measurements on $Rb_x Fe_{2-y} Se_2$ performed by Park *et al* [Park et al. (2011)]. They reported a resonance in the superconducting state similar to that observed in other Fe-pnictide and Fe-chalcogenide superconductors [Lumsden and Christianson (2010)] except that it was observed not at $\mathbf{Q} = (\pi, 0)$ but at $\mathbf{Q} \simeq (\pi, \pi/2)$, very close to the value predicted by Maier *et al* [Maier et al. (2011)]. Friemel *et al* [Friemel et al. (2012)] then observed a dispersion of the resonant mode consistent with band

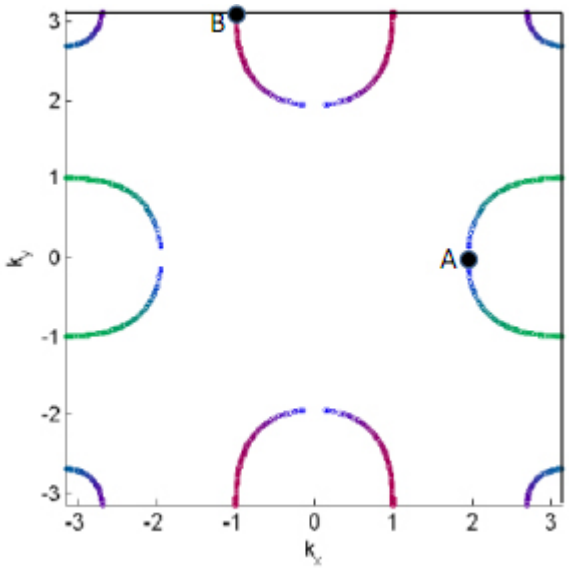


**Figure 5.1**: The Fermi surface used to represent the chalcogenides. Colors indicate the orbital components: red $d_{xz}$, green $d_{yz}$, and blue $d_{xy}$ [Fang et al. (2011a)].

structure calculations on $RbFe_2Se_2$, within RPA $d$-wave spin fluctuation picture. However, over a range of doping the $s^{\pm}$ and $d$ states are nearly degenerate. In Ref. [Maier et al. (2012b)] the imaginary part of the magnetic spin susceptibility was calculated for these gaps and how the evolution of neutron scattering resonances with doping can be distinguished between them was discussed.

A strong coupling approach predicts an $s$-wave pairing symmetry in the iron-pnictides. It was shown that the pairing symmetry is determined mainly by the next-nearest neighbor (NNN) AFM exchange coupling $J_2$ together with a renormalized narrow band width [Seo et al. (2008)]. The superconducting gap is close to a $\cos k_x \cos k_y$ form in momentum space, higher harmonic contributions are neglected in this approach. This result is model independent as long as the dominating interaction is $J_2$ and the Fermi surfaces are located close to the $\Gamma$ and M points in the folded BZ. The $\cos k_x \cos k_y$ form factor changes sign between the electron and hole pockets in the BZ, similar to the order parameters of $s^{\pm}$ proposed from weak-coupling scheme [Mazin et al. (2008a)].

Comparing the predictions from weak and strong couplings, the 122 iron-chalcogenides provide an interesting opportunity to address the difference between the two perspectives. The $s$-wave pairing symmetry is robust even in extremely electron-overdoped ferrochalcogenides because the AFM $J_2$ is the main factor for pairing and the $J_1$ is ferromagnetic, which is corroborated from neutron scattering experiments [Lipscombe et al. (2011)] and the magnetic structure associated with 245 vacancy ordering [Fang et al. (2012)]. The FM $J_1$ significantly reduces the competitiveness of $d$-wave pairing symmetry. The competition between $s$- and $d$-wave weakens the superconducting instability scale.

The mean-field diagram of an effective model for the $AFe_2Se_2$ compounds was calculated by Fang *et al* [Fang et al. (2011a)]. As the main relevant orbital weight is given by the $d_{xz}$, $d_{yz}$, and $d_{xy}$ orbitals, a three-orbital kinetic model with $J_1$ and $J_2$ interactions was employed. The specific kinetic theory utilized for the mean-field analysis is a modified three-band model [Daghofer et al. (2010)], given

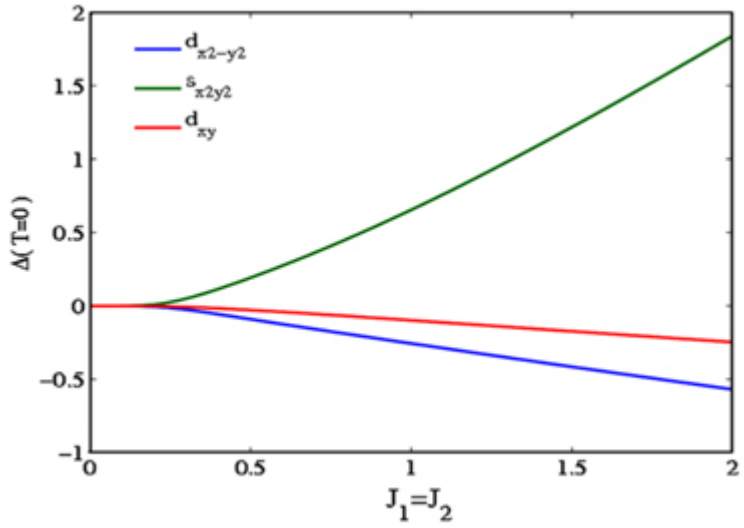


**Figure 5.2**: The intra-orbital, $s_{x^2y^2}$ ($s^{\pm}$), $d_{x^2-y^2}$ and the inter-orbital, $d_{xy}$, pairing order parameter, as a function of $J = J_1 = J_2$ when the chemical potential is $\mu = 1.8$ [Seo et al. (2008)].

by

$$\hat{T}(\mathbf{k}) = \begin{pmatrix} T_{11}(\mathbf{k}) - \mu & T_{12}(\mathbf{k}) & T_{13}(\mathbf{k}) \\ T_{21}(\mathbf{k}) & T_{22}(\mathbf{k}) - \mu & T_{23}(\mathbf{k}) \\ T_{31}(\mathbf{k}) & T_{32}(\mathbf{k}) & T_{33}(\mathbf{k}) - \mu \end{pmatrix}, \tag{5.1}$$

where

$$\begin{aligned} T_{11}(\mathbf{k}) &= 2t_2\cos(k_x) + 2t_1\cos(k_y) + 4t_3\cos(k_x)\cos(k_y), \\ T_{22}(\mathbf{k}) &= 2t_1\cos(k_x) + 2t_2\cos(k_y) + 4t_3\cos(k_x)\cos(k_y), \\ T_{33}(\mathbf{k}) &= 2t_5(\cos(k_x) + \cos(k_y)) + 4t_6\cos(k_x)\cos(k_y) + \delta, \\ T_{12}(\mathbf{k}) &= 4t_4\sin(k_x)\sin(k_y),\ T_{21}(\mathbf{k}) = T_{12}^{\star}(\mathbf{k}), \\ T_{13}(\mathbf{k}) &= 2it_7\sin(k_x) + 4it_8\sin(k_x)\cos(k_y), \\ T_{23}(\mathbf{k}) &= 2it_7\sin(k_y) + 4it_8\sin(k_y)\cos(k_x). \end{aligned} \tag{5.2}$$

The other matrix elements are given by hermiticity. The parameters in the model are taken to be $t$ = (0.02, 0.06, 0.03, -0.01, 0.35, 0.3, -0.2, 0.1), $\delta = 0.4$, and $\mu = 0.412$. Energies are expressed in units of eV. The parameter set provides the Fermi surface shown in Fig. 5.1 with a filling factor of 4.41 electrons per site. Aside from a negligibly small electron pocket at the M point in the unfolded Brillouin zone, the main features are the large electron pockets at X which dictate the physics of the mean-field phase diagram at this electron doping regime (Fig. 5.1). In the three-band model, the small electron pocket appears around the M-point in the unfolded Brillouin zone which may be related to the resonance feature experimentally discussed for the $\Gamma$ point in the folded zone. In contrast, the 5-band fit to the chalcogenides suggests small electron pocket features around the $\Gamma$-point of the unfolded Brillouin zone.

Despite this discrepancy, both appearances have a similar effect and can hence be discussed on the same footing. The interaction part in the present mean-field analysis is the pairing energy obtained by decoupling the magnetic exchange coupling [Seo et al. (2008)], which can be written as

$$\hat{V} = -\sum_{\alpha,r}(J_1 b^{\dagger}_{\alpha,r,r+x} b_{\alpha,r,r+x} + J_1 b^{\dagger}_{\alpha,r,r+y} b_{\alpha,r,r+y} + J_2 b^{\dagger}_{\alpha,r,r+x+y} b_{\alpha,r,r+x+y} + \\ + J_2 b^{\dagger}_{\alpha,r,r+x-y} b_{\alpha,r,r+x-y}), \tag{5.3}$$

where $b_{\alpha,r,r'} = c_{\alpha,r,\uparrow} c_{\alpha,r',\downarrow} - c_{\alpha,r,\downarrow} c_{\alpha,r',\uparrow}$ represents singlet pairing operators between the $r$, $r'$ sites. The pairing order parameters are defined as follows: in real space, the pairing on two NN bonds and two NNN bonds are represented by $\Delta^{\alpha}_{x} = J_1 \langle b_{\alpha,r,r+x} \rangle$, $\Delta^{\alpha}_{y} = J_1 \langle b_{\alpha,r,r+y} \rangle$, $\Delta^{\alpha}_{x+y} = J_2 \langle b_{\alpha,r,r+x+y} \rangle$, and $\Delta^{\alpha}_{x-y} = J_2 \langle b_{\alpha,r,r+x+y} \rangle$, where $\alpha$ denotes the orbital index and $x$, $y$ are the two unit lattice vectors [Fang et al. (2011a)]. The influence of the orbital-crossing exchange antiferromagnetic, $J_{1,12}$, $J_{2,12}$, and Hund's couplings, $J_H$, were considered for iron oxypnictides [Seo et al. (2008)]. Because Fe-based oxypnictides together with ternary iron chalcogenides are electron-doped systems, Fang *et al* [Fang et al. (2011a)] have suggested similar role of inter-orbital pairing in these compounds. The orbital-crossing exchange coupling was decoupled in four spin-singlet orbital-crossing pairing order parameters, $\Delta'(\mathbf{k}) = \Delta'_{x^2+y^2}(\mathbf{k}) + \Delta'_{x^2-y^2}(\mathbf{k}) + \Delta'_{x^2y^2}(\mathbf{k}) + \Delta'_{xy}(\mathbf{k})$. It has been found that in the region where Hund's coupling, $J_H \sim \mathrm{Max}(J_1, J_2)$, the corresponding pairing function, $\Delta_H$, is extremely small. Hence, Hund's coupling has little effect on the pairing symmetry. In the mixed $s^{\pm}$ and $d_{x^2-y^2}$ phase, for $J_{1,12} \leq J_1$ and $J_{2,12} \leq J_2$, the orbital-crossing pairing order $\Delta'$ is zero within computing error except for $d_{xy}$ with symmetry $\Delta'(\mathbf{k}) = \Delta'_0 \sin(k_x) \sin(k_y)$. In Fig. 5.2, the results for the intra-orbital pairing order parameters $s_{x^2y^2} \sim \cos k_x \cos k_y$ ($s^{\pm}$) and $d_{x^2-y^2} \sim (\cos k_x - \cos k_y)$, and the inter-orbital pairing order parameter $d_{xy}$ are plotted as functions of $J = J_1 = J_2 = J_{1,12} = J_{2,12}$, when the chemical potential is $\mu = 1.8$ corresponding to 18% electron doping [Seo et al. (2008)]. As can be seen in Fig. 5.2 the inter-orbital pairing is small, therefore, only intra-orbital pairing has been taken into account in Ref. [Fang et al. (2011a)]. The smallness of inter-orbital $\Delta'_0$ with $d_{xy}$ symmetry does not imply that the intra-orbital pairing on $d_{xy}$ orbital is also small (see Figs. 5.3, 5.4, 5.5).

Considering the $C_4$ symmetry of the lattice, the pairing symmetries can be classified according to the one-dimensional irreducible representations of the $C_4$ symmetry. Since the pairing is a spin singlet, the classification can be the following: an order parameter is of $A$-type ($B$-type) if it is even (odd) under a 90-degree rotation. This classification leads to six candidate pairings with $A$-symmetry and another six candidates with $B$-symmetry as the SC pairings include NN from $J_1$ and NNN from $J_2$ bonds [Fang et al. (2011a)], which manifests as the $A$-type symmetry

$$\begin{aligned}
\Delta^{A}_{NN,s} &= (\Delta^{xz}_{x} + \Delta^{xz}_{y} + \Delta^{yz}_{x} + \Delta^{yz}_{y})/4, \\
\Delta^{A}_{NN,d} &= (\Delta^{xz}_{x} - \Delta^{xz}_{y} - \Delta^{yz}_{x} + \Delta^{yz}_{y})/4, \\
\Delta^{A}_{NNN,s} &= (\Delta^{xz}_{x+y} + \Delta^{xz}_{x-y} + \Delta^{yz}_{x+y} + \Delta^{yz}_{x-y})/4, \\
\Delta^{A}_{NNN,d} &= (\Delta^{xz}_{x-y} - \Delta^{xz}_{x+y} + \Delta^{yz}_{x+y} - \Delta^{yz}_{x-y})/4, \\
\Delta^{xy}_{NN,s} &= (\Delta^{xy}_{x} + \Delta^{xy}_{y})/2, \\
\Delta^{xy}_{NNN,s} &= (\Delta^{xy}_{x+y} + \Delta^{xy}_{x-y})/2.
\end{aligned} \tag{5.4}$$

and the B-type symmetry

$$\begin{aligned}
\Delta^B_{NN,s} &= (\Delta^{xz}_x + \Delta^{xz}_y - \Delta^{yz}_x - \Delta^{yz}_y)/4, \\
\Delta^B_{NN,d} &= (\Delta^{xz}_x - \Delta^{xz}_y + \Delta^{yz}_x - \Delta^{yz}_y)/4, \\
\Delta^B_{NNN,s} &= (\Delta^{xz}_{x+y} + \Delta^{xz}_{x-y} - \Delta^{yz}_{x+y} - \Delta^{yz}_{x-y})/4, \\
\Delta^B_{NNN,d} &= (\Delta^{xz}_{x-y} - \Delta^{xz}_{x+y} - \Delta^{yz}_{x+y} + \Delta^{yz}_{x-y})/4, \\
\Delta^{xy}_{NN,d} &= (\Delta^{xy}_x - \Delta^{xy}_y)/2, \\
\Delta^{xy}_{NNN,d} &= (\Delta^{xy}_{x-y} - \Delta^{xy}_{x+y}/2.
\end{aligned} \tag{5.5}$$

In reciprocal lattice space, the mean-field Hamiltonian is given by

$$\hat{T} = \sum_{\mathbf{k}} \begin{pmatrix} \hat{T}(\mathbf{k}) & \hat{\Delta}(\mathbf{k}) \\ \hat{\Delta}^\dagger(\mathbf{k}) & -\hat{T}^\star(-\mathbf{k}) \end{pmatrix}, \tag{5.6}$$

where

$$\hat{\Delta}(\mathbf{k}) = \begin{pmatrix} \Delta_{11}(\mathbf{k}) & 0 & 0 \\ 0 & \Delta_{22}(\mathbf{k}) & 0) \\ 0 & 0 & \Delta_{33}(\mathbf{k}) \end{pmatrix}, \tag{5.7}$$

and

$$\begin{aligned}
\Delta_{11}(\mathbf{k}) &= (\Delta^A_{NN,s} + \Delta^B_{NN,s})(\cos(k_x) + \cos(k_y)) + (\Delta^A_{NN,d} + \Delta^B_{NN,d})(\cos(k_x) - \cos(k_y)) \\
&\quad +2(\Delta^A_{NNN,s} + \Delta^B_{NNN,s})\cos(k_x)\cos(k_y) + 2(\Delta^A_{NNN,d} + \Delta^B_{NNN,d})\sin(k_x)\sin(k_y), \\
\Delta_{22}(\mathbf{k}) &= (\Delta^A_{NN,s} - \Delta^B_{NN,s})(\cos(k_x) + \cos(k_y)) + (\Delta^B_{NN,d} - \Delta^A_{NN,d})(\cos(k_x) - \cos(k_y)) \\
&\quad +2(\Delta^A_{NNN,s} - \Delta^B_{NNN,s})\cos(k_x)\cos(k_y) + 2(\Delta^B_{NNN,d} - \Delta^A_{NNN,d})\sin(k_x)\sin(k_y), \\
\Delta_{33}(\mathbf{k}) &= \Delta^{xy}_{NN,s}(\cos(k_x) + \cos(k_y)) + \Delta^{xy}_{NN,d}(\cos(k_x) - \cos(k_y)) \\
&\quad +2\Delta^{xy}_{NNN,s}\cos(k_x)\cos(k_y) + 2\Delta^{xy}_{NNN,d}\sin(k_x)\sin(k_y).
\end{aligned} \tag{5.8}$$

The symbols $s$ and $d$ merely represent the geometric factor of pairing in $k$-space. As can be seen from Eqs. (5.4), (5.5), and (5.8), $\Delta_{11} \propto \Delta^{xz}$, $\Delta_{22} \propto \Delta^{yz}$, and $\Delta_{33} \propto \Delta^{xy}$, i.e. $\hat{\Delta}$ is represented by orbital pairing functions, therefore it is diagonal. In general, there are more than one self-consistent set of $\{\Delta\}$'s as self-consistent mean-field solutions. The free energies in each solution have to be compared to find the solution with the lowest free energy.

First, pure NNN-pairings stemming from $J_2$ are considered, which is a reasonable limit to start with since $J_1$ in FeTe(Se) has been shown to be ferromagnetic, thus, not contributing to pairing in the singlet pairing channel. $J_2$ is increased from zero to $J_2 = 1.5$ while the band width is $W \sim 4$. The robust superconductivity solution with purely $A$-type $s$-wave pairing is obtained when $J_2$ is larger than $0.4$. So the pairing remains the same as in iron-pnictides with the geometric factor $\cos(k_x)\cos(k_y)$ [Seo et al. (2008)]. The Bogoliubov particle spectrum is completely gapped in this state. When $J_2$ becomes larger than 1, the ground state is a mixture of $A$- and $B$-type pairings. The nonzero $B$-type pairings all have the geometric factor $\sin(k_x)\sin(k_y)$ as in the phase diagram depicted in Fig. 5.3. In the coexistence phase, the quasiparticle spectrum shows nearly gapless features at several points, and, moreover, the dispersion explicitly breaks $C_4$ rotation symmetry (see Fig. 5.3 displaying the quasiparticle spectrum of the lowest branch).

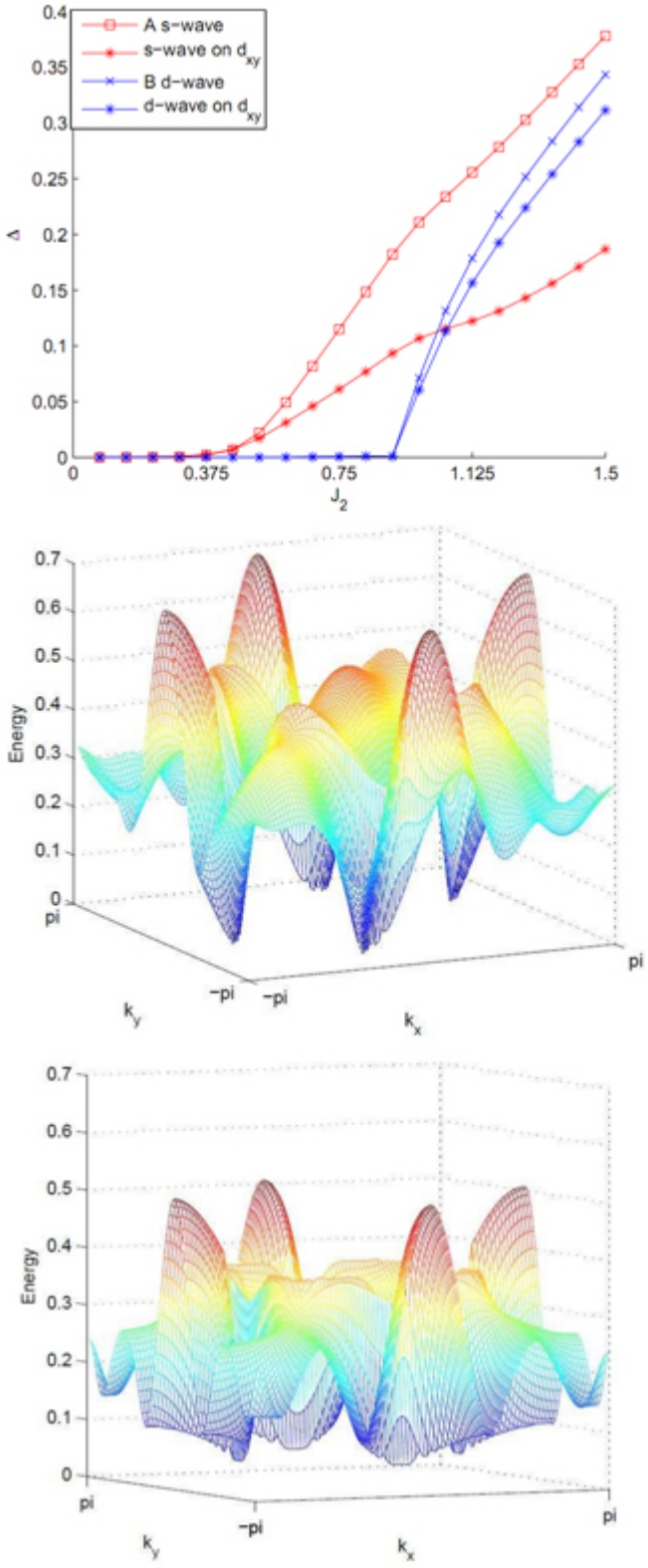


**Figure 5.3**: (Top) The mean field phase diagram along $J_1 = 0$ in the parameter space. (Middle) The quasiparticle spectrum at $J_2 = 1$ and (Bottom) $J_2 = 0.75$. The quasiparticle spectrum explicitly breaks $C_4$ symmetry because of mixing of $A$- and $B$-type pairing symmetries at $J_2 = 1$ [Fang et al. (2011a)].

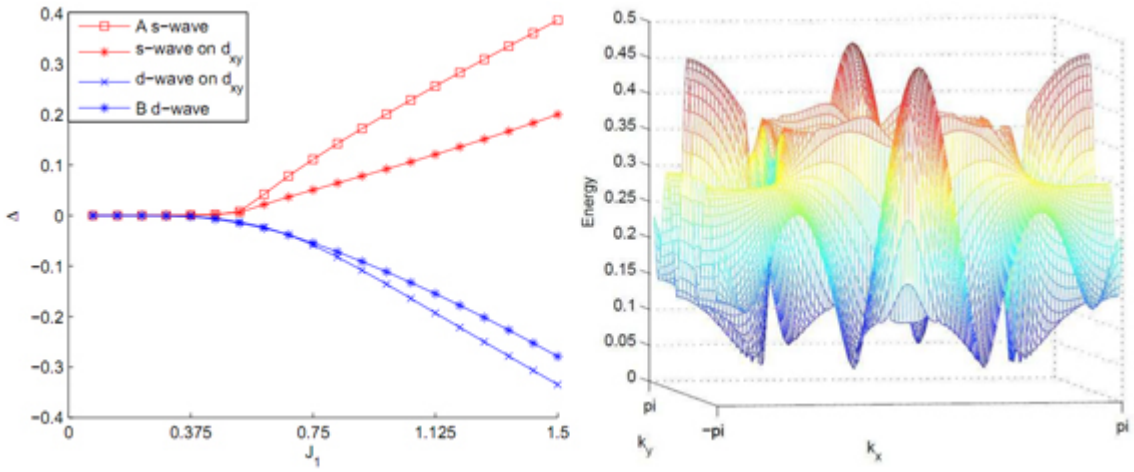


**Figure 5.4**: (Left) The mean field phase diagram along $J_2 = 0$ in the parameter space. (Right) The quasiparticle spectrum at $J_1 = 0.75$. The quasiparticle spectrum explicitly breaks $C_4$ symmetry because of mixing of $A$- and $B$-type pairing symmetries at $J_1 = 0.75$ [Fang et al. (2011a)].

Second, the phase diagram is studied when only antiferromagnetic $J_1$ is present. In this case, only NN pairings are nonzero and there are six SC gaps. If one increases $J_1$ from $J_1 = 0$ to $J_1 = 1.5$ where the band width is $W \sim 4$, the SC order becomes non-zero from $J_1 = 0.4$ on. However, in this case, the $B$-type SC order arises slightly earlier than $A$-type SC order. The ground state is always a mixture of $A$- and $B$-type pairings. The two leading orders are $A$-type $s$-wave and $B$-type $d$-wave in $xz$, $yz$ orbitals while the sub-leading ones are $s$- and $d$-waves in the $xy$ orbitals (Fig. 5.4). Due to strong mixing of $A$- and $B$-type pairings, the quasiparticle spectrum is very anisotropic. It is still nodeless, in contrast to a pure $s$-wave pairing $\cos(k_x) + \cos(k_y)$, where there are nodes [Thomale et al. (2011a)] on the electron pockets seen in Fig. 5.4.

Finally, when $J_1$ and $J_2$ are antiferromagnetic, $J_1 + J_2 = 1$ is fixed, and $J_1 - J_2$ is changed as a parameter, one observes that NNN pairings dominate for $J_1 - J_2 < -0.1$ and NN pairings dominate for $J_1 - J_2 > 0.2$ presented in Fig. 5.5 (a). In the intermediate range, there is only weak $B$-type pairing. A schematic phase diagram within the range $0 < J_1, J_2 < 1$ is shown in Fig. 5.5 (b). In the whole parameter region of $(J_1, J_2)$, the SC order parameters always have the same sign for all three orbitals. This can be seen in Fig. 5.6, where the orbital resolved pairing amplitude is shown along electron pockets around X. This result is essentially consistent with the functional renormalization group (FRG) result [Fang et al. (2011a)]. It is, however, different from what one would expect from the very strong coupling limit.

The strong inter-orbital repulsion favors different signs of pairing for the $d_{xy}$ orbital and the $d_{xz/yz}$ orbitals [Lu et al. (2012)]. Some quantitative differences between Fig. 5.6 and FRG results [Fang et al. (2011a)] may be explained as the incompleteness of a three-orbital model and the fact that the mean-field pairing is not constrained to the FS. It is clearly seen in Fig. 5.6 that the orbital resolved pairing amplitude is highly anisotropic. This is a natural reflection of different orbital composition on different parts of the Fermi surface. Following the Fermi surface topology in Fig. 5.1, these mean-field results correspond to the case, where a small electron pocket is still present at the M-point. Without the M pocket, one sees that $s$-wave pairings are less favored than before, as its

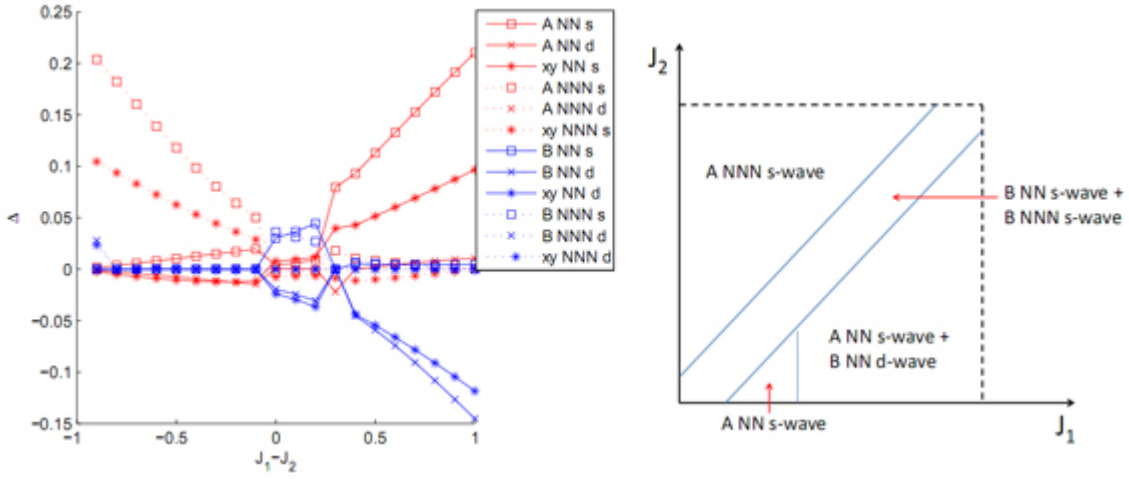


**Figure 5.5**: (Left) The mean field phase diagram with $J_1 + J_2 = 1$ in the parameter space. (Right) A schematic phase diagram for the model (Eq. (5.6)) within $0 < J_1, J_2 < 1$ [Fang et al. (2011a)].

geometric factor is $\cos(k_x)\cos(k_y)$ or $\cos(k_x) + \cos(k_y)$, both being maximized around M. With the two-pocket FS, taking $J_1 = 0$ and increasing $J_2 > 0$, $B$-type pairings blend in at smaller $J_2$ than shown in Fig. 5.3; taking $J_2 = 0$ and increasing $J_1 > 0$, $A$-type pairings appear at slightly larger $J_1$ than shown in Fig. 5.4 [Fang et al. (2011a)]. It can be seen from the Fig. 5.7 that the $s$-wave pairing symmetry is always robust when the AFM NNN $J_2$ is strong, while the $d$-wave pairing can be strong if $J_1$ is AFM for the electron overdoped region. Moreover, if they are both AFM, there is a strong competition between the $s$- and $d$- wave pairings. When there are hole pockets, even in a range of $J_1 \sim J_2$, the contribution from $J_1$ to the pairing is much weaker than the one from $J_2$. In that case, an AFM $J_1$ will not generate strong $d$-wave pairing so that the $s$-wave wins easily. From neutron scattering experiments, it has been shown that a major difference between iron-pnictides and iron-chalcogenides is that the NN coupling $J_1$ change from AFM in the former [Zhao et al. (2008)] to FM in the latter [Lipscombe et al. (2011)]. In fact, $J_1$ is rather strongly FM in the latter, which explains the high magnetic transition temperature ($\sim$ 500 K) in the 245 vacancy ordering state as shown in Ref. [Fang et al. (2012)].

Combining these results, one can partially answer the question regarding the different behaviors between iron-pnictides and iron-chalcogenides in the electron-overdoped region. The reason of the high SC transition temperature in ferrochalcogenides, but not in ferropnictides. Since $J_1$ acts in iron-pnictides as AFM while it is FM in iron-chalcogenides, $J_1$ will weaken the SC pairing in the former but not in the latter. This model suggests that there is no difference between ferropnictides and ferrochalcogenides in terms of pairing symmetry. Both of them are dominated by $s$-wave pairing. If both hole and electron pockets are present, the signs of the SC order in hole and electron pockets are opposite ($s^{\pm}$-wave). However, the mechanism causing $s^{\pm}$ is different in the weak and strong coupling approaches. In the weak coupling approach, the sign change is due to the scattering between the hole and electron pockets while in the strong coupling approach, the sign change is due to the form factor of the SC order parameters which is specified to be $\cos k_x \cos k_y$ since the pairing mainly originates from the AFM $J_2$. Therefore, to obtain $s^{\pm}$ pairing symmetry, the existence of both

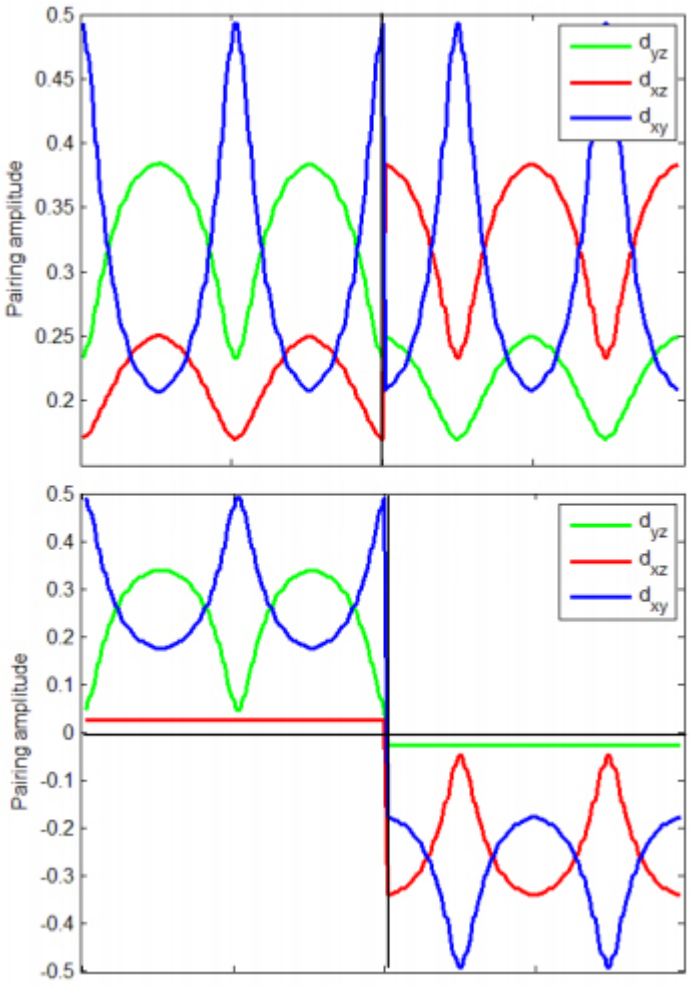


**Figure 5.6**: The orbital resolved pairing amplitude on the FS for a typical $s$-wave ($d$-wave) pairing state in the upper (lower) panel, calculated within mean-field approximation. The interaction parameters are $J_1 = 0$, $J_2 = 0.8$ for the upper panel and $J_1 = 0.5$, $J_2 = 0$ for the lower panel. In the left half of these figures, the k-point traces the electron pocket around $X$-point counterclockwise from point A in Fig. 5.1 and in the right half, it traces the electron pocket around the $Y$-point counterclockwise from point B in Fig. 5.1 [Fang et al. (2011a)].

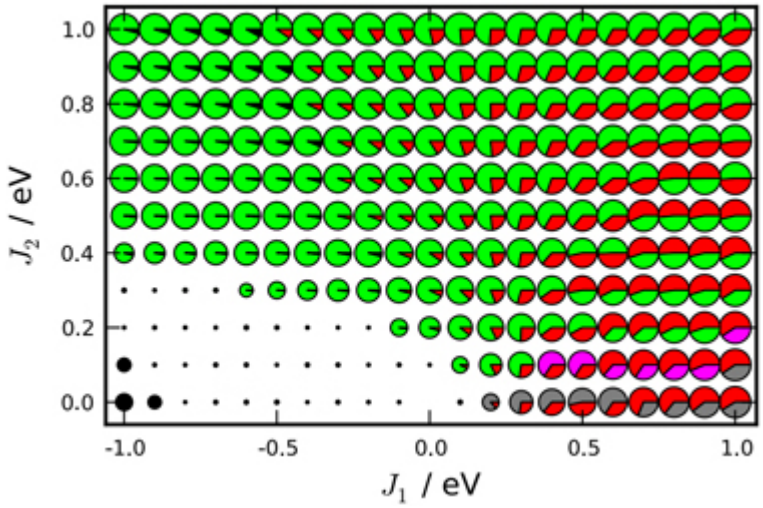


**Figure 5.7**: The phase diagram of the three-pocket model. The different pairing channels are depicted as constant $s$-wave (grey), extended $s_{x^2y^2}$-wave (green), the nodal $s_{x^2+y^2}$-wave (purple), and the $d_{x^2-y^2}$-wave (red). Parameter sets with $J_1 \sim -1$ and $J_2 \sim 0$ have highly oscillating form factors so the triplet channel should be considered in these cases [Fang et al. (2011a)].

hole and electron pockets is necessary in the weak coupling approach, but not in the strong coupling one.

The unit-cell of iron-based superconductors contains two Fe atoms. However, except for 122-systems, a single-Fe model can be constructed from the original two-Fe model by applying the gauge transformation on $d$-orbitals [Miyake et al. (2010)]. By this procedure, the original Brillouin zone is enlarged to the unfolded BZ. Based on the single-Fe model, spin-fluctuation-mediated $d$-wave state ($B_{1g}$ representation) without nodes has been proposed [Wang et al. (2011a); Maier et al. (2011); Das and Balatsky (2011a)], by focusing on the nesting between electron pockets. However, a single-Fe model for 122 systems cannot be constructed since finite hybridization between electron pockets prevents the unfolding procedure [Miyake et al. (2010)].

Saito *et al* [Saito et al. (2011)] have investigated the superconducting state in $K_xFe_2Se_2$ based on the ten-orbital Hubbard-Holstein model without hole-pockets. When the Coulomb interaction is large, spin-fluctuation mediated $d$-wave state appears due to the nesting between electron-pockets. Interestingly, the symmetry of the body-centered tetragonal structure in $K_xFe_2Se_2$ requires the existence of nodes in the $d$-wave gap, although fully-gapped $d$-wave state is realized in the case of simple tetragonal structure. In the presence of moderate electron-phonon interaction due to Fe-ion optical modes, on the other hand, orbital fluctuations give rise to the fully-gapped $s_{++}$-wave state without sign reversal. Therefore, both superconducting states are distinguishable by careful measurements of the gap structure or the impurity effect on $T_c$. The dispersion of the model and the primitive BZ are shown in Figs. 5.8 (a) and (b). Suzuki *et al* [Suzuki et al. (2011a)] also studied the $s^{\pm}$-wave gap structure for $BaFe_2As_2$ based on a ten-orbital model.

Figure 5.8 presents the Fermi surfaces of $KFe_2Se_2$ for $k_z = 0$ (Fig. 5.8(c)) and $k_z = \pi$ (Fig. 5.8(d)) planes, when the electron number per Fe-ion is $n = 6.5$ (each plane has four large and heavy e-

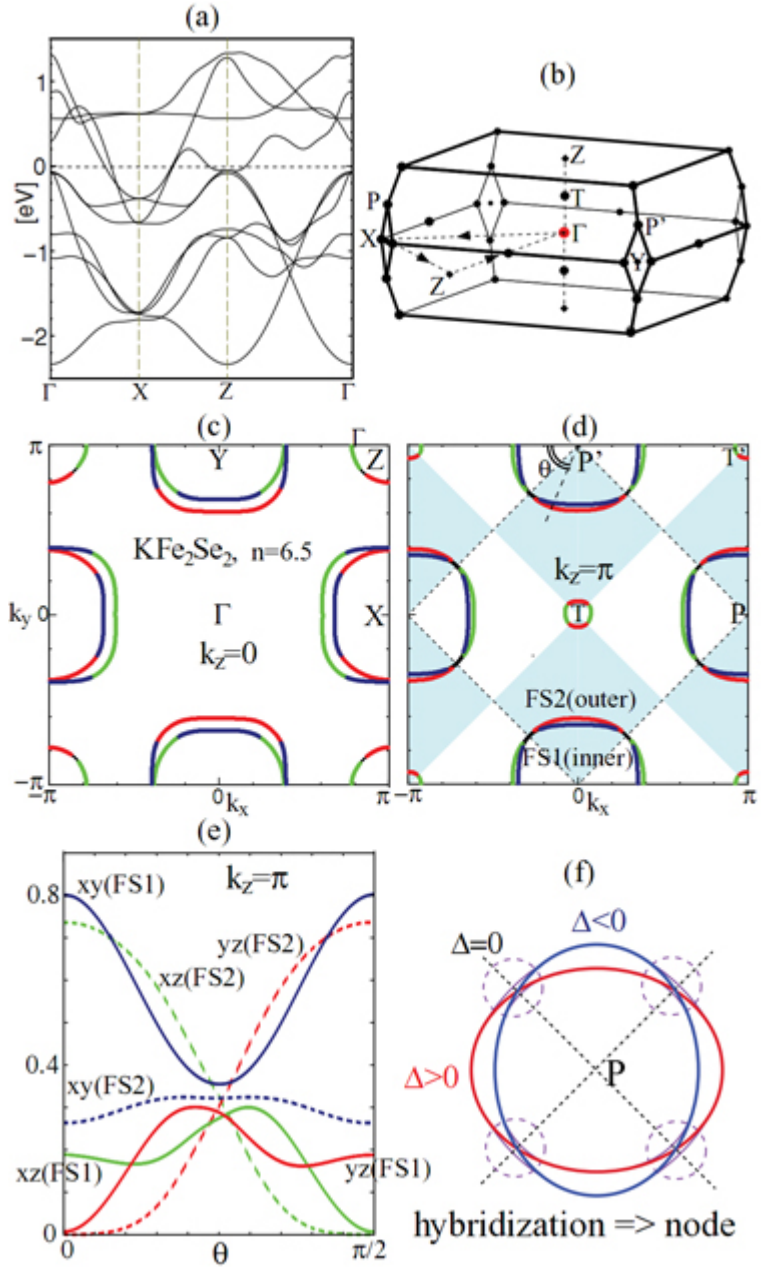


**Figure 5.8**: (a) Dispersion of the ten-orbital model for $KFe_2Se_2$. $\Gamma$, $X$, and $Z$ points are on the $k_z = 0$ plane. (b) Primitive BZ for body-centered tetragonal lattice. (c) and (d) FSs on the $k_z = 0$ and $k_z = \pi$ planes, correspondingly. The green, red, and blue lines correspond to $xz$, $yz$, and $xy$ orbitals, respectively. The diamond-shaped shadows in (d) panel indicate the sign of basis function for $B_{1g}$ representation. (e) Weight of each orbital on the inter FS (FS1) and the outer FS (FS2) as function of $\theta$; $\theta$ is defined in (d). (f) Hybridization between two e-pockets in 122 systems should create the nodal $d$-wave gap [Saito et al. (2011)].

pockets around X and Y points, and one small and light e-pocket around Z point). In this case, the energy of the hole-band at $\Gamma$ point from the Fermi level, $E_h$, is $\sim -0.07$ eV, which is consistent with

recent ARPES reports [Zhang et al. (2011); Qian et al. (2011); Zhao et al. (2011)]. In the presented in Fig. 5.8 (b) Brillouin zone, Γ and Z points and X and Y points in Fig. 5.8 (c) are not equivalent, and $k_z = 2\pi$ plane is given by $(\pi, \pi)$ shifting of the points in Fig. 5.8 (c). The T and T' points and P and P' points are equivalent in representation of Fig. 5.8 (d), meaning that the reciprocal wave vector on the $k_z = \pi$ plane is $(\pi, \pi)$ and $(\pi, -\pi)$. The diamond-shaped shadows in the $k_z = \pi$ plane indicates the sign of the basis function for $B_{1g}$ ($(x^2 - y^2)$-type) representation, which has nodes on the P-P' line on both FS1 (inner FS) and FS2 (outer FS).

Large hybridization of FS1 and FS2 in $KFe_2Se_2$ confirms the existence of nodes. In fact, the weights of $d$-orbitals on FS1 and FS2 depicted in Fig. 5.8 (e) are smooth functions of $\theta$, which shows a strong evidence for the hybridization in wide momentum space. This hybridization disappears when interlayer hoppings are neglected. Then, both $xy$ (FS1) and $xy$ (FS2) show apexes at $\theta = \pi/4$, and $xz$ (FS2) drops rapidly to almost zero for $\theta \geq \pi/4$. The origin of nodal gap based on the fully-gapped $d$-wave solution in the single-Fe model is explained in Fig. 5.8 (f) [Wang et al. (2011a); Maier et al. (2011); Das and Balatsky (2011a)]. By introducing interlayer hoppings, two elliptical e-pockets with positive and negative $\Delta$ in the unfolded BZ are hybridized to form FS1 and FS2 with four-fold symmetry. It results in appearance of nodal lines on FS1 and FS2, at least near the $|k_z| = \pi$ plane.

Figures 5.9 (a)-(c) show the gap functions of the $d$-wave solution at $T = 0.03$ eV for $k_z = 0$, $\pi/2$, and $\pi$, respectively. In case of $U = 1.1$ eV, the eigenvalue $\lambda_E$ is $0.61$ for Fig. 5.9 (a), $0.63$ for Fig. 5.9 (b), and $0.62$ for Fig. 5.9 (c). The relation $\lambda_E \geq 1$ corresponds to the superconducting state. The $\lambda_E$ values are relatively small since the SC condensation energy becomes small, when the gap has complicated nodal line structure. On the $k_z = \pi$ plane (Fig. 5.9 (c)), the nodal lines rest along $\theta = \pi/4$ and $3\pi/4$ directions, which is correspondent to the basis of $B_{1g}$ representation in Fig. 5.8 (d). These nodes move to the BZ boundary, $\theta = 0$ and $\pi$, on the $k_z = \pi/2$ plane in Fig. 5.9 (b), and diverge from the Fermi surfaces on $k_z = 0$ plane in the Fig. 5.9 (a), resulting in the nodal gap emergence for $\pi/2 < |k_z| < 3\pi/2$ in the whole BZ ($|k_z| \leq 2\pi$).

Figure 5.9 (d) features the $s^{\pm}$-wave state for $k_z = \pi$. In this case, the sign reversal of the SC gap takes place between electron pockets and the "hidden" hole pockets below the Fermi level given by the valence bands 5 and 6. Interestingly, the eigenvalue in $s^{\pm}$ case is $\lambda_E = 0.99$ for $U = 1.1$ eV, which is larger than $\lambda_E$ for $d$-wave state in Figs. 5.9 (a)-(c). Such large $\lambda_E$ arises from the scattering of Cooper pairs between electron and the "hidden" hole pockets.

The temperature dependence of $\lambda_E$ can be analyzed through a simple two-band model with inter-band repulsion [Yada and Kontani (2008)]. The set of gap equations is given by $\lambda_E \Delta_h = -V N_e L_e \Delta_e$ and $\lambda_E \Delta_e = -V N_h L_h \Delta_h$, where $V > 0$ is the repulsive interaction between electron and hole pockets, and $N_{e,h}$ is the density of states near the Fermi level. The first situation is when the top of the h-pocket is well above the Fermi level, corresponding to $L_e = L_h = \ln(1.13\omega_c/T)$, where $\omega_c$ is the cutoff energy. Hence, the eigenvalue is given as $\lambda_E = V\sqrt{N_e N_h}\ln(1.13\omega_c/T) \propto -\ln T$, similar to single-band BCS superconductors. The second case occurs when the h-pocket is slightly below the Fermi level, $L_h = (1/2)\ln(\omega_c/|E_h|)$, where $E_h < 0$ is the energy of the top of hole band [Yada and Kontani (2008)]. Thus, the eigenvalue is given as $\lambda_E = V\sqrt{N_e N_h L_h}\sqrt{\ln(1.13\omega_c/T)} \propto \sqrt{-\ln T}$. Therefore, the temperature dependence of $\lambda_E$ is much moderate in the second case. Monotonic growth at decreasing temperature of $\lambda_E$ for $d$-wave state is clearly seen in Fig. 5.10 (a) [Saito et al. (2011)]. Contrary to that, $\lambda_E$ for $s^{\pm}$-wave state saturates at low temperatures. This result suggests that the $d$-wave state overcomes the $s^{\pm}$-wave state at $T_c \sim 30$ K in $K_xFe_2Se_2$.

According to inelastic neutron scattering measurement of $Ba(Fe,Co)_2As_2$ [Inosov et al. (2010a)],

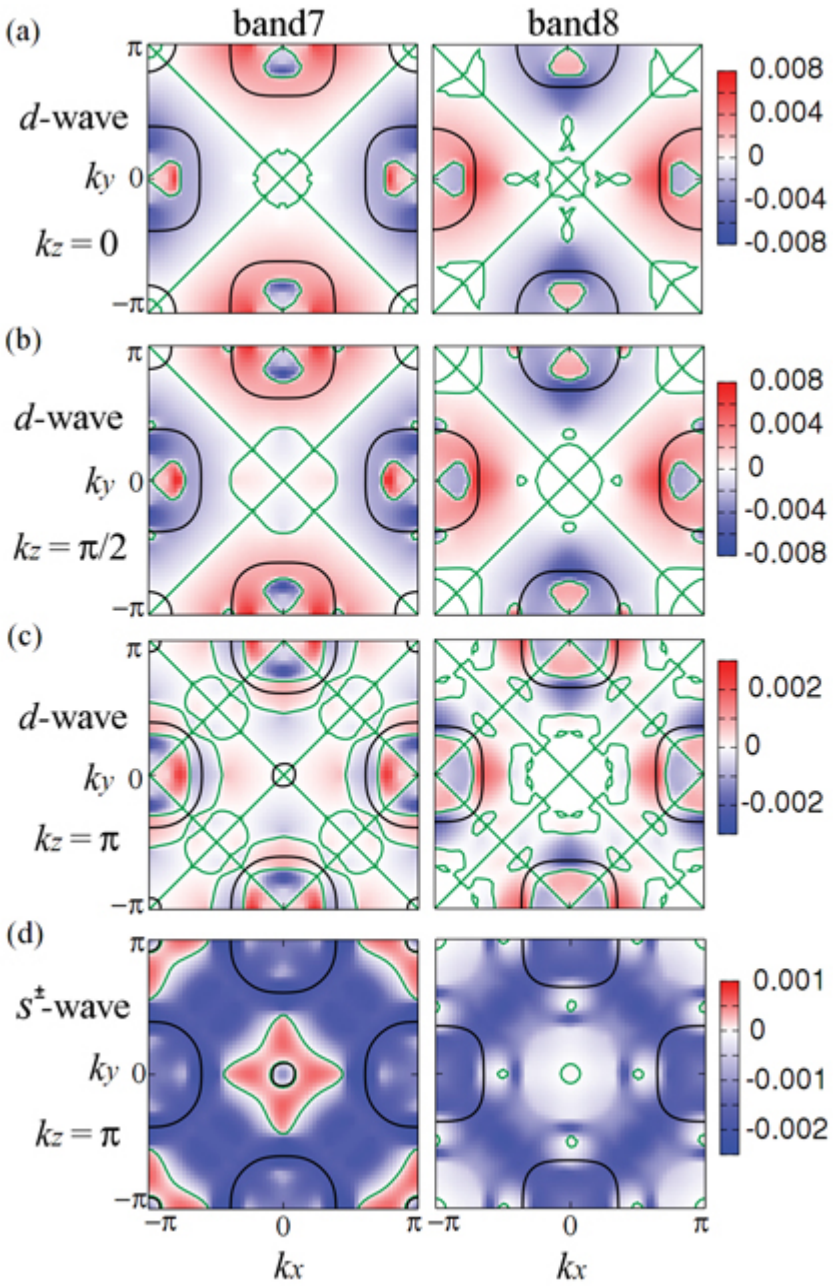


**Figure 5.9**: Superconducting gap functions for outer FS (FS2) on band 7 and inner FS (FS1) on band 8. The $d$-wave gap functions on the (a) $k_z = 0$, (b) $k_z = \pi/2$, and (c) $k_z = \pi$ planes. Black and green lines represent the FSs and gap nodes. (d) An $s^{\pm}$-wave gap function on the $k_z = \pi$ plane [Saito et al. (2011)].

the characteristic spin-fluctuation energy is $\omega_{sf} \sim 100$ K, which is above $T_c$ (∼30 K). Assuming a similar $\omega_{sf}$ in $KFe_2Se_2$ since critical temperatures of the materials are almost equal, one may obtain the relation $\omega_c \sim \omega_{sf} \ll |E_h|$ in $KFe_2Se_2$. Since $L_h$ is a monotonic decrease function of $|E_h|/\omega_c$ and $L_h$ is less than one for $-E_h/\omega_c > 0.15$, the $d$-wave state can be considered as overcoming the $s^{\pm}$-wave state in $KFe_2Se_2$, as long as the spin-fluctuation mediated superconductivity is engaged.

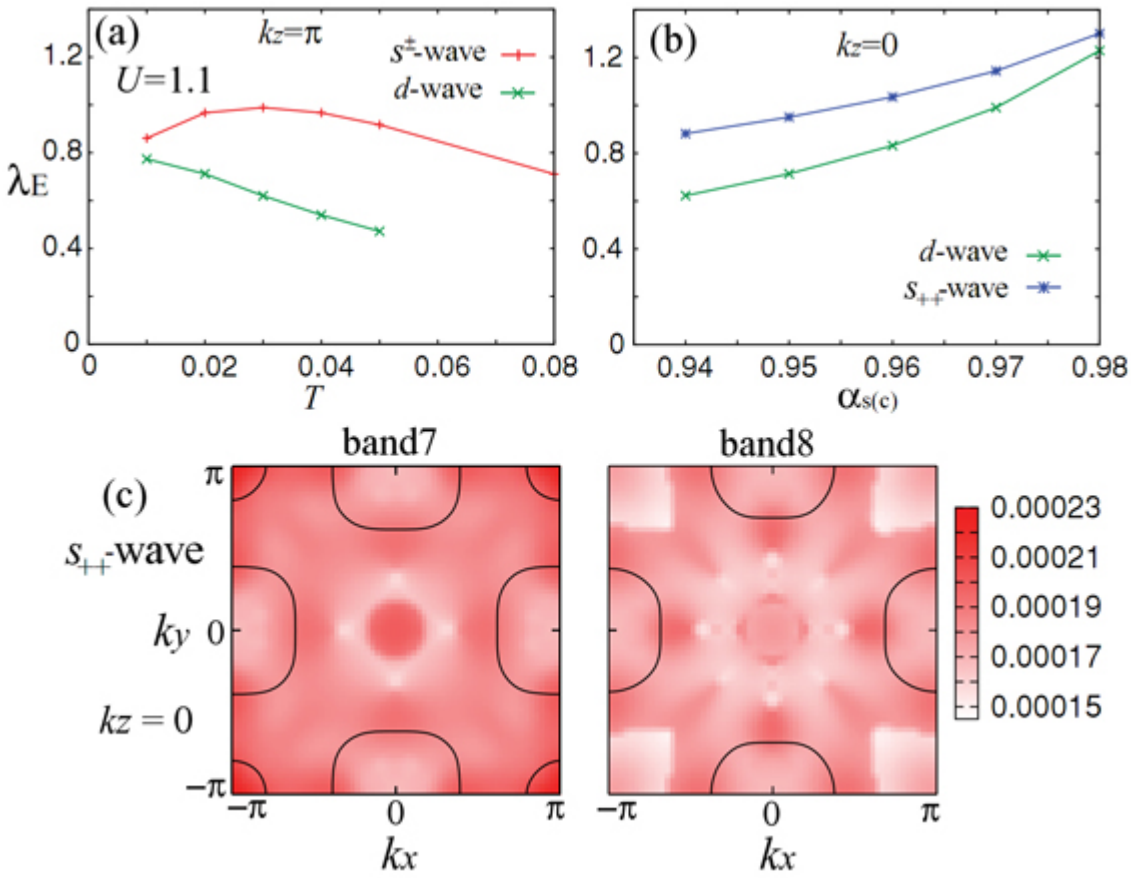


**Figure 5.10**: (a) The temperature dependence of $\lambda_E$ for $d$- and $s^{\pm}$-wave states. (b) $\alpha_s$- ($\alpha_c$-) dependence of $\lambda_E$ for $d$-wave ($s_{++}$-wave) state at $T = 0.03$ eV. (c) Superconducting gap functions for $s_{++}$-wave state [Saito et al. (2011)].

Although high-$T_c$ $s^{\pm}$-wave state can be realized for $|E_h|/\omega_c < 0.1$, then the implemented $T_c$ will be very sensitive to $E_h$ or the filling $n$ [Yada and Kontani (2008)].

The $s_{++}$-wave state due to orbital fluctuations on the $k_z = 0$ plane with $n = 6.5$ is presented in Figs. 5.10 (b) and (c). In Fig. 5.10 (b), the $\alpha_c$-dependence of $\lambda_E$ is shown at $T = 0.03$ for the $s_{++}$-wave state with $U = 0$, and the $\alpha_s$-dependence of $\lambda_E$ for the $d$-wave state with $g = 0$. Here, $\alpha_c$ ($\alpha_s$) is the charge (spin) Stoner factor introduced in Ref. [Kontani and Onari (2010)]. The $\alpha_c = 1$ and $\alpha_s = 1$ correspond to the ODW and SDW states, respectively [Saito et al. (2011)]. The SC gap functions for $s_{++}$-wave state are rather isotropic, as shown in Fig. 5.10 (c). However, the presented SC gap becomes more anisotropic when $U > 0$ [Onari and Kontani (2010)].

An isotropic superconducting gap distribution on the small electron Fermi pocket around the Z point in $K_{0.77}Fe_{1.65}Se_2$, which favors the $s$-wave pairing symmetry, has been detected by ARPES measurements (see Fig. 5.11) [Xu et al. (2012)]. However, due to the fact that the properties of $K_xFe_{2-y}Se_2$ compounds are strongly dependent on doping [Li et al. (2012)] the pairing symmetry of different phases is still an open question. It should be noted that this model was also used for description of the superconducting state in LiFeAs (see comment to **Paper 3**).

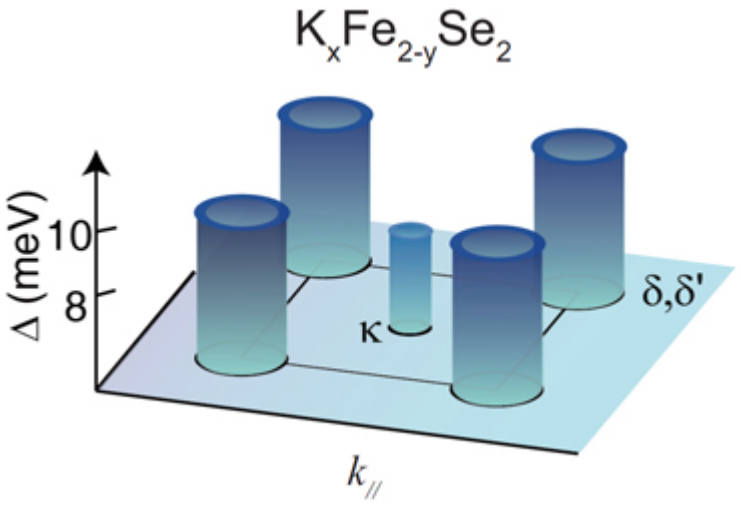


**Figure 5.11**: Summary of the gap distribution at $\kappa$, $\delta$, and $\delta'$ pockets in $K_xFe_{2-y}Se_2$ [Xu et al. (2012)].

The investigation of the impurity scattering effects on the superconducting state is a powerful method of pairing state studying in ternary chalcogenides [Zhu et al. (2011)]. In **Paper 1** we study vortex core size, $\xi_2$, and cutoff parameter, $\xi_h$ in the mixed state of type-II superconductors with impurities. The vortex core radius is defined as the distance from the vortex center at which the current density reaches its maximum value, and the cutoff parameter is determined by Eq. (1) of **Paper 1**. The correlation between these parameters is discussed in the comment to **Paper 4**. We note, that our results for $\xi_2$ length in conventional $s$-wave clean superconductors agree well with those obtained in Ref. [Ichioka et al. (1999)]. The field dependence of $\xi_2$ from this paper is presented in Fig. 5.20. The $\xi_h$ and $\xi_2$ can be found from $\mu$SR and SANS measurements. The obtained in **Paper 1** magnetic field and impurity scattering dependences of $\xi_h$ and $\xi_2$ for various pairing states can be useful for understanding of a superconducting state in $K_xFe_{2-y}Se_2$.

## Paper 2. Eilenberger approach to the vortex state in iron pnictide superconductors

Since the symmetry and structure of the superconducting gap may reflect the underlying electron pairing mechanism, many works have been done to clarify it [Hirschfeld et al. (2011)]. However, so far there is still no consensus on this issue, particularly the doping evolution of the superconducting gap [Maiti et al. (2011a)]. The symmetry and the structure of the gap in Fe-based superconductors were studied by decomposing the pairing interaction obtained in the RPA into $s$-wave and $d$-wave components and into contributions from scattering between different Fermi surfaces [Maiti et al. (2011b)]. It was shown that each interaction is well approximated by the lowest angular harmonics. Using this simplification the competition between $s$- and $d$-wave solutions was analyzed, and $d$-wave pairing in heavily hole-doped $KFe_2As_2$ was predicted. The investigation of the superconducting phase in $Ba_{1-x}K_xFe_2As_2$ (Ba122) compounds at moderate to strong hole-doping regimes using the functional renormalization group has shown that while the system develops a nodeless anisotropic $s^{\pm}$ order parameter in the moderately doped regime, gapping out the electron pockets

at strong hole-doping drives the system into a nodal $d$-wave superconducting state in $KFe_2As_2$. For the hole-doped $Ba_{1-x}K_xFe_2As_2$ system, the angle-resolved photon emission spectroscopy experiment revealed multiple nodeless gaps at optimal doping $x \sim 0.4$ [Ding et al. (2008)], which was confirmed by bulk thermal conductivity measurements [Luo et al. (2009)]. On the overdoped side, nodeless gaps were observed at $x = 0.7$ by ARPES [Nakayama et al. (2011)], and at $x = 0.77$ by point contact Andreev reflection spectroscopy [Zhang et al. (2010)]. However, further increasing of doping to the end member $KFe_2As_2$ with only hole pockets [Sato et al. (2009)] results in a nodal superconducting gap, which was detected by thermal conductivity [Dong et al. (2010a)], penetration depth [Hashimoto et al. (2010)], and NMR [Fukazawa et al. (2009)].

It is now under debate whether this is a $d$-wave gap with symmetry-imposed nodes [Thomale et al. (2011b)] or an $s$-wave gap with accidental nodes [Maiti et al. (2011a); Suzuki et al. (2011b)]. The ultrahigh-resolution laser angle-resolved photoemission spectroscopy unveils that $KFe_2As_2$ is a nodal $s$-wave superconductor with highly unusual FS-selective multigap structure: a nodeless gap on the inner FS, an unconventional gap with octet-line nodes on the middle FS, and an almost-zero gap on the outer FS [Okazaki et al. (2012)]. This gap structure may arise from the frustration between competing pairing interactions on the hole FSs causing the eightfold sign reversal. A model for such behavior was suggested in Ref. [Maiti et al. (2012)].

Influence of impurities on a superconducting state can give important information about the gap pairing symmetry [Balatsky et al. (2006)]. Figure 5.12 shows the temperature dependence of resistivity down to 50 mK for $K(Fe_{1-x}Co_x)_2As_2$ single crystals. For the pure $KFe_2As_2$, $T_c = 4.4$ K (transition temperature $T_c$ is defined when the resistivity drops to 90% of the normal-state value) and resistivity reaches zero at 4.2 K. A power-law fit between 5 and 25 K yields a residual resistivity $\rho_0 = 0.11 \pm 0.01$ $\mu\Omega$ cm for this crystal and a residual resistance ratio (RRR) equal to 2017 is estimated, suggesting the crystal is extremely close to the clean limit. The RRR decreases dramatically from 2017 to 19 with increasing Co doping from 0 to 0.050 (see Table 5.1). This suggests that the Co doping leads to large impurity scattering. At the same time, $T_c$ decreases rapidly to zero around $x = 0.042$.

Taking into account the dramatic enhancement of $\rho_0$ and rapid reduction of $T_c$ at very low Co concentration, the main role of Co dopants is as impurities to scattering carriers in $KFe_2As_2$, instead of injecting electrons to form electron Fermi surfaces and rise the $T_c$. In order to study the pair breaking effect of Co dopants, in Fig. 5.13 (a), a comparison of the evolution of $T_c$ with Co concentration is plotted for $K(Fe_{1-x}Co_x)_2As_2$ and $Ba_{0.5}K_{0.5}(Fe_{1-x}Co_x)_2As_2$, where $Ba_{0.5}K_{0.5}Fe_2As_2$ has isotropic superconducting gaps. The slope $dT_c/dx$ of $K(Fe_{1-x}Co_x)_2As_2$ is much steeper than that of $Ba_{0.5}K_{0.5}(Fe_{1-x}Co_x)_2As_2$. This difference may come from the pairing symmetry. Indeed, the impurity scattering is very effective in the $T_c$ suppression in case of $d$-wave superconductors.

The normal-state scattering rate $\Gamma = e\rho/(m^*R_H)$ is listed in Table 5.1 [Wang et al. (2012)]. Here, $e$ is the electronic charge and $m^*$ is the effective mass ($m^* = 6m_e$ is inferred from ARPES [Sato et al. (2009)] and de Haas-van Alpha effect measurements [Terashima et al. (2010)]). The $\Gamma$ was estimated [Wang et al. (2012)] from the residual resistivity $\rho_0$ (as presented in Table 5.1) and the extrapolated zero-limiting Hall coefficient $R_H$ (as shown in the inset of Fig. 5.13 (b)).

The Abrikosov-Gor'kov formula [Abrikosov and Gor'kov (1960)] was used in Ref. [Wang et al. (2012)] to describe the suppression of $T_c$ for different impurity scattering rates $\Gamma$ and extract a value of $\Gamma_c$, as plotted in Fig. 5.13 (b), where $\Gamma_c$ is the critical scattering rate required for reducing $T_c$ to zero. The $\hbar\Gamma_c \approx 2.2k_BT_{c0}$ was found, where $T_{c0}$ (4.55K for $KFe_2As_2$) is the extrapolating value to the clean limit by using Abrikosov-Gor'kov formula. This $\hbar\Gamma_c$ is slightly larger than that estimated

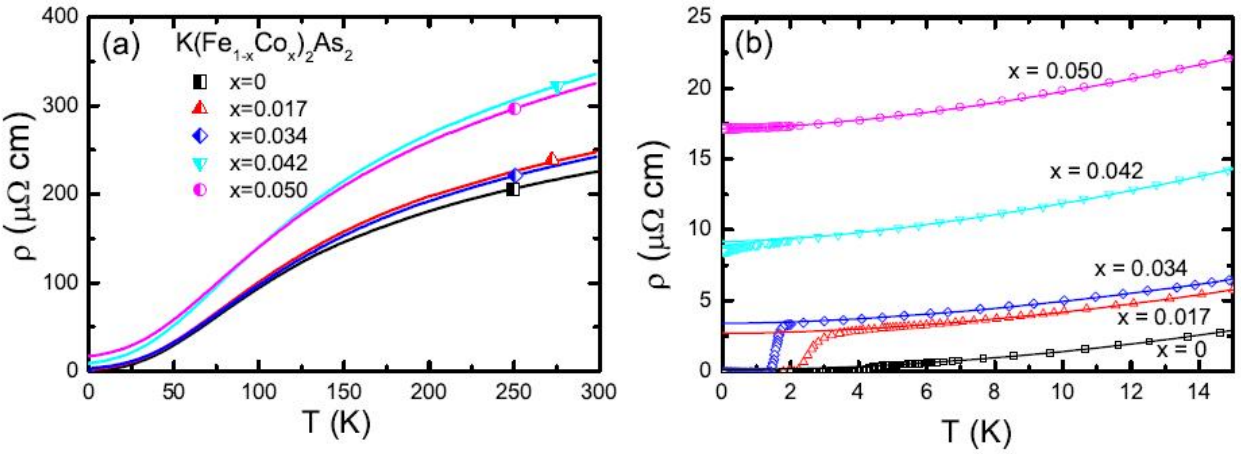


**Figure 5.12**: (a) Temperature dependence of resistivity for $K(Fe_{1-x}Co_x)_2As_2$ single crystals. (b) The zoomed plot for the data shown in (a). The lines are the fits to $\rho = \rho_0 + \alpha T^{\alpha}$, from which the residual resistivity $\rho_0$ is extrapolated [Wang et al. (2012)].

**Table 5.1**: Lattice parameter $c$, residual resistivity $\rho_0$, power-law exponent $\alpha$, impurity scattering rate $\Gamma$, residual resistance ratio RRR and superconducting transition temperature $T_c$, varying with Co content $x$ [Wang et al. (2012)].

| $x$ | $c$ (Å) | $\rho_0$ ($\mu\Omega$ cm) | $\alpha$ | $\Gamma$ ($10^{10}$ $s^{-1}$) | RRR | $T_c$ (K) |
|---|---|---|---|---|---|---|
| 0 | 13.876 | 0.11 | 1.89 | 1.34 | 2017 | 4.4 |
| 0.017 | 13.871 | 2.69 | 1.79 | 57.6 | 92 | 2.9 |
| 0.034 | 13.866 | 3.39 | 1.71 | 100 | 72 | 1.7 |
| 0.042 | 13.864 | 9.18 | 1.60 | 296 | 37 | 0 |
| 0.050 | 13.862 | 17.1 | 1.62 | | 19 | 0 |

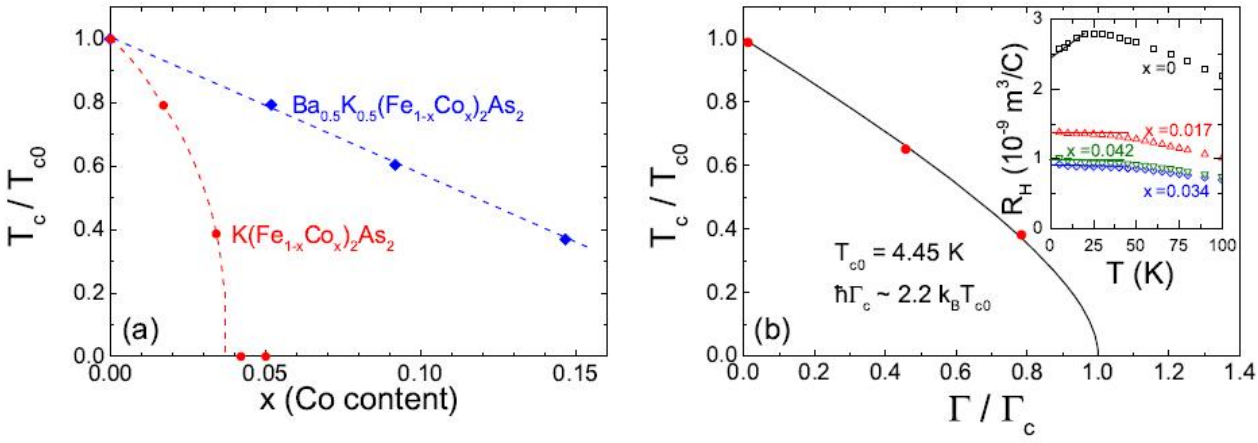


**Figure 5.13**: (a) The normalized $T_c$ plotted against Co content $x$ for $K(Fe_{1-x}Co_x)_2As_2$. As a comparison, $x$ dependence of the normalized $T_c$ for $Ba_{0.5}K_{0.5}(Fe_{1-x}Co_x)_2As_2$ is also plotted. (b) $T_c$ for $K(Fe_{1-x}Co_x)_2As_2$ plotted as a function of scattering rate. The solid line is calculated by the Abrikosov-Gorkov formula. Inset: Low-temperature Hall coefficient for $x = 0, 0.017, 0.034$ and 0.042 [Wang et al. (2012)].

by Reid *et al* on the impurity scattering from disorders in $KFe_2As_2$ ($1.3k_BT_{c0}$) [Reid et al. (2012)], but far smaller than that of $45k_BT_{c0}$ in $BaFe_2As_2$ and $SrFe_2As_2$ at optimal Co, Pt, Pd, Cu, Ni, and Ru doping [Kirshenbaum et al. (2012)]. This indicates that the pairing symmetry of $KFe_2As_2$ is distinctly different from the $s$-wave symmetry in the optimally doped 122 systems.

Due to the strong suppression of $T_c$ in $K(Fe_{1-x}Co_x)_2As_2$ by Co doping, this system provides a great opportunity to determine whether the superconducting state in $KFe_2As_2$ is a $d$-wave or an accidental nodal $s$-wave. For a $d$-wave superconductor, there is a universal heat conduction upon increasing the impurity level. This has been clearly demonstrated in $YBa_2(Cu_{1-x}Zn_x)_3O_{6.9}$ [Taillefer et al. (1997)]. The universal heat conduction results from the compensation between the increase of quasiparticle density induced by impurities and the decrease of mean free path. For an accidental nodal $s$-wave superconductor, the heat conduction is not universal.

Figure 5.14 shows the thermal conductivity of $K(Fe_{1-x}Co_x)_2As_2$ with $x = 0$ and 0.034 in zero magnetic field. For clean $KFe_2As_2$ with $\rho_0 = 0.116$ $\mu\Omega$ cm, the data below 0.3 K can be fitted by quadratic function $\kappa/T = a + bT^2$, with the residual linear term $\kappa_0/T = a = 4.94 \pm 0.09$ mW $K^{-2}$ cm$^{-1}$ and $b = 283 \pm 2$. However, for the $x = 0.034$ sample with $\rho_0 = 3.56$ $\mu\Omega$ cm, the data below 0.4 K obeys linear law $\kappa/T = a + bT$, with $\kappa_0/T = a = 3.95 \pm 0.01$ mW $K^{-2}$ cm$^{-1}$ and $b = 2.43 \pm 0.06$. Previously, for a dirty $KFe_2As_2$ with $\rho_0 = 3.32$ $\mu\Omega$ cm, similar temperature dependence of $\kappa/T = a + bT$ was observed, with $b = 3.04$ [Dong et al. (2010b)]. Therefore, the $T^2$ term of $\kappa$ is attributed to phonons, and the huge $T^3$ term observed in the clean $KFe_2As_2$ must come from the nodal quasiparticles. Indeed, for a clean $d$-wave superconductor, theoretical calculation shows that the leading-order finite-temperature correction will contribute a $T^3$ term to the electronic thermal conductivity [Graf et al. (1996)]. Such an electronic cubic term has been observed in the ultraclean $YBa_2Cu_3O_7$ [Hill et al. (2004)]. Apparently, the $T^3$ term is rapidly suppressed by impurities or magnetic field.

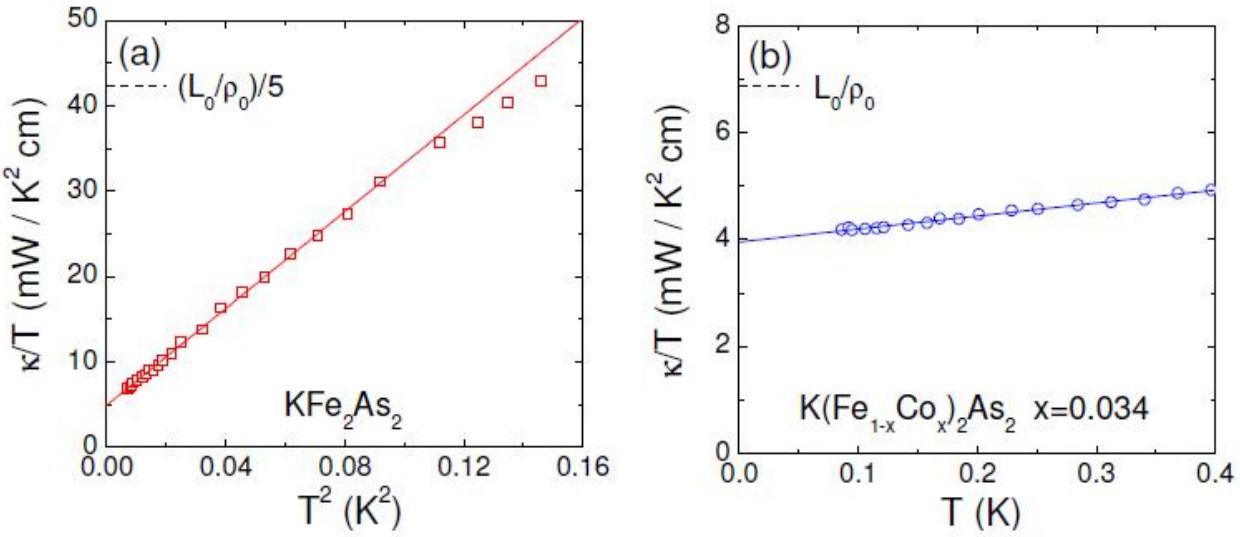


**Figure 5.14**: The thermal conductivity of $K(Fe_{1-x}Co_x)_2As_2$ with (a) $x = 0$, and (b) $x = 0.034$ in zero magnetic field. The solid lines are fits to $\kappa/T = a + bT^2$ for $x = 0$ sample, and $\kappa/T = a + bT$ for $x = 0.034$ sample, respectively. The dash lines are the normal-state Wiedemann-Franz law expectation $L_0/\rho_0$, with $L_0$ the Lorenz number $2.45 \times 10^{-8}$ W $\Omega$ $K^{-2}$ and normal-state $\rho_0 = 0.116$ and 3.56 $\mu\Omega$ cm, respectively. For the $x = 0$ sample, its $L_0/\rho_0$ is divided by 5 to put into the panel [Wang et al. (2012)].

Figure 5.14 shows that while the resistivity $\rho_0$ and scattering rate are increased by 30 and 70 times, respectively, the $\kappa_0/T$ of the $x = 0$ and 0.034 samples in zero magnetic field remains comparable (4.94 and 3.95 mW $K^{-2}$ $cm^{-1}$, correspondingly). For the clean $x = 0$ sample, the value is less than 3% of its normal-state $\kappa/T$, while for the dirty $x = 0.034$ sample, the value is more that 50% of its normal-state $\kappa/T$ [Wang et al. (2012)]. Considering the experimental error mainly coming from the uncertainty associated with the geometric factor, the heat conduction in the $x = 0$ and 0.034 samples is universal. Such a universal heat conduction strongly suggests that the superconducting gap in $KFe_2As_2$ is $d$-wave, not accidental nodal $s$-wave. The same tendency of heat conduction has been also observed in Ref. [Reid et al. (2012)] by comparing clean and dirty $KFe_2As_2$ single crystals with 10 times difference of $\rho_0$.

The effects connected with $d$-wave pairing were widely discussed under analysis of experimental data in high-$T_c$ cuprates. Another clear difference is the presence of extended states. These extended states give rise to the Volovik effect [Volovik (1993)], which has been observed as the $\sqrt{H}$-term in the specific heat [Moler et al. (1994); Kopnin and Volovik (1996)] and as the $H$-linear term in the thermal conductivity [Kübert and Hirschfeld (1998); Chiao et al. (1999)]. Delocalized quasiparticles in the vortex state were also probed by $^{63}$Cu NMR in the high-$T_c$ superconductor $TlSr_2CaCu_2O_{6.8}$ in magnetic fields up to 28 T [Zheng et al. (2002)]. At low temperatures well below $T_c$, both the spin Knight shift and the nuclear spin-lattice relaxation rate measured around the middle point between the two nearest vortices (saddle point) have increased substantially with increasing field, which indicate that the quasiparticle states with an ungapped spectrum are extended outside the vortex cores in a $d$-wave superconductor. The density of states around the saddle point was found to be proportional to $\kappa N_0\sqrt{H/H_{c2}}$, with $\kappa = 0.5 - 0.7$ and $N_0$ being the normal-state DOS.

Additionally, nonlocal corrections to the relation between the supercurrent and the superfluid velocity become important for the response of electrons with momenta on the Fermi surface close to the gap nodes, even in strongly type-II materials. This can be understood by realizing that the coherence length, being inversely proportional to the gap, becomes very large close to the node and formally diverges at the nodal point. Thus, quite generally, there exists a locus of points on the Fermi surface, where $\xi \gg \lambda_0$, and the response becomes highly nonlocal. This effect was first discussed in Refs. [Franz et al. (1997); Kosztin and Leggett (1997)] in the mixed state. The advantage of the quasiclassical approach use is that it includes nonlocal, nonlinear and the core effects simultaneously, which allows the investigation of their influence on electrodynamic and magnetic properties of unconventional superconductors.

We also mention Gor'kov and Schrieffer's prediction [Gorkov and Schrieffer (1998)] that in a $d_{x^2-y^2}$-wave superconductor at intermediate fields $B_{c1} \ll B \ll B_{c2}$ the quasiparticles form Landau levels with a discrete energy spectrum $E_n = \pm\hbar\omega_H\sqrt{n}$, where $n = 0, 1, \ldots$, $\omega_H = 2\sqrt{\omega_c\Delta_0/\hbar}$, with $\omega_c = eB/mc$ being the cyclotron frequency and $\Delta_0$ the maximum superconducting gap. However, using a singular gauge transformation [Franz and Tesănović (2000)] it was shown that for a periodic vortex lattice the natural low-energy quasiparticle states are Bloch waves rather than Landau levels.

Taking into account all these effects, the applicability of EHC theory (Eq. (1) in **Paper 2**) regarding the description of the vortex state $d_{x^2-y^2}$-wave superconductors is not evident *apriori*. In **Paper 2**, we numerically solve the quasiclassical Eilenberger equations for the mixed state of a $d_{x^2-y^2}$-wave superconductor. Good fitting of the Eilenberger equations solution to EHC theory is obtained in **Paper 2**. It means that all effects mentioned above are included in our effective theory correctly, i.e. the cutoff parameter includes both the bound states (vortex core effect) and the extended states (nonlinear Volovik and nonlocal effects). It fundamentally differs from Hao-Clem theory [Hao et al. (1991)], where the cutoff parameter was responsible only for vortex core effect. We specially check the importance of nonlocal effects separately in Section 4 of **Paper 2**, fitting the Eilenberger equations solution to the NGLE approximation (Eq. (27) in **Paper 2**). In this approximation the nonlocal effects are included in the theory explicitly, replacing London penetration depth by anisotropic electromagnetic response tensor $L_{ij}$ (Eq. (28) in **Paper 2**). It does not essentially improve quality of the fitting, but this approximation is much more time consuming than the local EHC theory. A comparison between our results and Franz-Affleck-Amin (FAA) theory [Franz et al. (1997)] is done. The importance of proper calculated cutoff parameter is demonstrated in Fig. 12 of **Paper 2**.

The $\mu$SR investigation of the flux-line lattice in $KFe_2As_2$ compounds with different impurity concentrations and various scattering potentials, and comparison with theoretical results of **Paper 2** can provide additional information about the pairing state in this system. We note, that in **Paper 2** besides $d$-wave pairing other symmetries ($s_{++}$, $s^{\pm}$) are also considered.

## Paper 3. Impact of the order parameter symmetries on the vortex core structure in iron-based superconductors

LiFeAs is a very remarkable member in the family of iron-based superconductors. The compound demonstrates superconducting properties in its stoichiometric composition. It is not magnetic [Taylor et al. (2011)] and its surface electronic structure is the same as in the bulk [Lankau et al. (2010)]. The Fermi surface of LiFeAs consists of two hole-like and two electron-like sheets around the center and corners of the Brillouin zone, respectively [Borisenko et al. (2010)]. The values of $\Delta$ have been

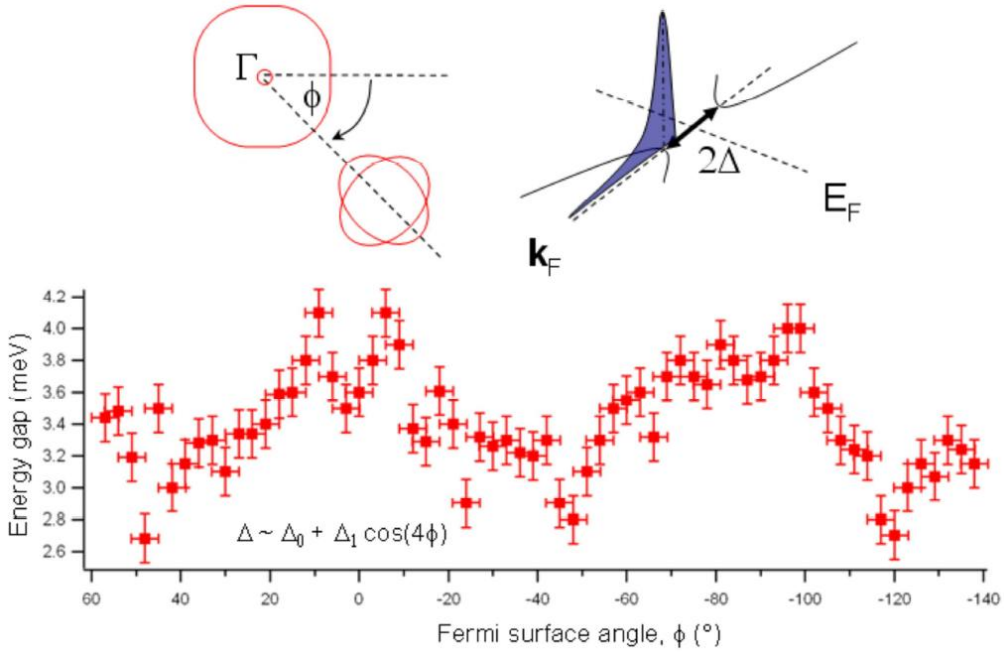


**Figure 5.15**: Strong anisotropy of the superconducting gap. Gap function from the peak positions of $\mathbf{k}_F$-EDCs [Borisenko et al. (2012)].

determined for many ($\mathbf{k}_F$) along the large Fermi surface in Ref. [Borisenko et al. (2012)] and the result is shown in Fig. 5.15. An oscillating behavior, with the functional form $\Delta \sim \Delta_0 + \Delta_1 \cos 4\phi + ...$ is clearly seen. Even the presence of higher harmonics, $\cos 8\phi$ ($\sim 12\%$) and $\cos 12\phi$ ($\sim 20\%$) can be noticed as local extrema at $\phi = \pi n/4$ and asymmetric shape of global maxima and minima. The latter are oriented towards the sides and the corners of the BZ, respectively. The gap on the outer FS contour is smaller than on the inner one and the gaps change in-phase, i.e. both increase when going from $\phi = 0$ to the direction towards the $\Gamma$ point. This behavior is confirmed by the more detailed scanning of the angle and plotting the angular dependence for the two gaps, which is presented in Fig. 5.16.

Borisenko *et al* [Borisenko et al. (2012)] has determined the superconducting energy gap on the small FS at $\Gamma$ point. Closest to $\Gamma$, hole-like $d_{xz,yz}$ feature strongly disperses towards the Fermi level but never crosses it, approaching as close as 10 meV at particular $k_z$. A detailed photon energy dependent study showed that the middle hole-like feature supports even smaller FS than it had been initially thought [Borisenko et al. (2010)]. A significant BZ-dependent intensity distribution seen in the vicinity of $\Gamma$ point is caused by the Van Hove singularity, but the actual Fermi-surface crossing has been found only for certain $k_z$ intervals as is demonstrated in Fig. 5.17. In Fig. 5.18 (a) the gap function is presented schematically for the whole BZ. The largest gap ($\sim$6 meV) corresponds to the small hole-like FS at $\Gamma$ point. Along the large 2D hole-like FS the gap varies around $\sim$3.4 meV roughly as $0.5 * \cos 4\phi$ meV being minimal at the direction towards the electron-like FS. The gap on the outer electron pocket is smaller than on the inner one. But both vary around $\sim$3.6 meV as $0.5 * \cos 4\phi$ meV having maximal values at the direction towards $\Gamma$ point. Since ARPES is not sensitive to the sign of the gap, the other possible gap function is shown (Fig. 5.18 (b)), which is in the agreement with observations.

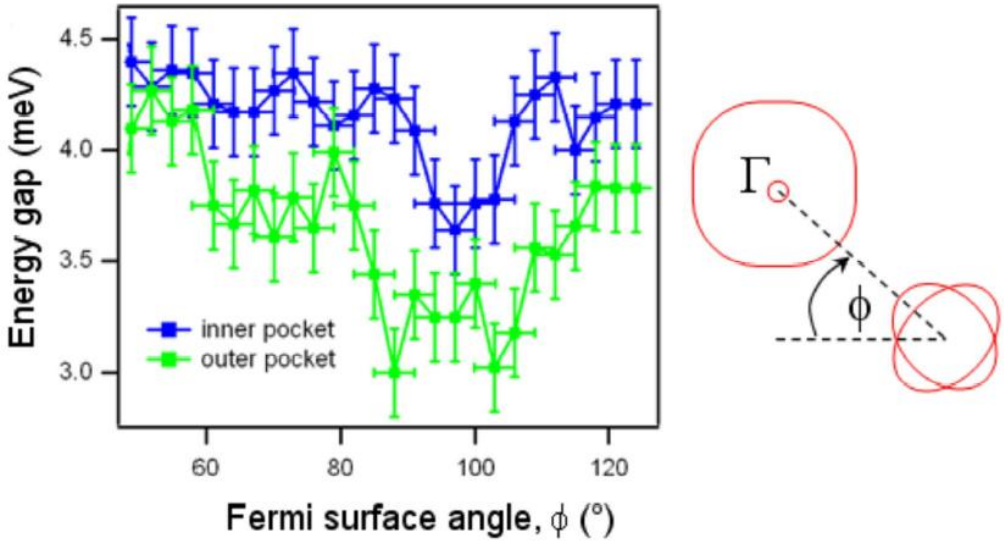


**Figure 5.16**: Superconducting gap on the electron-like pockets. Gap functions in a limited angular interval showing in-phase variation of the gaps on both FSs [Borisenko et al. (2012)].

There are two main possibilities for the realization of the $s^{\pm}$ scenario in terms of gap functions [Mazin et al. (2008a)]. It can be either nodeless and have a dominant functional form $\cos k_x * \cos k_y$ term or nodal having a functional form with dominant $\cos k_x + \cos k_y$ term, depending on the details of the pair interaction. In real space the latter corresponds to the direct Fe-Fe exchange interaction while the former to the next-nearest-neighbor exchange interaction via As atoms. The Fe-Fe distance in LiFeAs is one of the smallest among all families of pnictides and thus the second variant is more likely. Moreover, many model calculations of the gap function predict nodal $s^{\pm}$ behavior for strongly electron doped materials [Kuroki et al. (2008); Graser et al. (2009b)]. This is natural since upon electron doping the size of hole-like FSs becomes negligible in comparison with the size of electron-like FSs, nesting is destroyed and spin-fluctuation mechanism can only be established when dominant interaction between electron-like pockets would change sign of the order parameter between them.

The system should adjust the magnitude of the angle-dependent, $\pm \cos 2\phi$ gap component along the two electron FSs to minimize the effect of the inter-electron-pocket repulsion [Graser et al. (2009b)]. Stoichiometric LiFeAs due to large $d_{xy}$ FS should adopt this scenario for strongly electron-doped systems because the proportion between the $d_{xz,yz}$ originated FSs is exactly the same. Only one of the hole-like FSs with this orbital composition is present (the other one being completely below the Fermi energy), whereas the electron-like pockets are very large with absolutely no sign of $(\pi, \pi)$-nesting [Borisenko et al. (2010)]. These considerations inevitably imply the presence of nodes and anti-phase behavior of the gaps on electron-like FSs of LiFeAs (Fig. 5.18 (d)). Also, in the simplest case of $\cos k_x + \cos k_y$ order parameter one would expect the maximal gaps on the large hole-like FS to be oriented in the direction of electron pockets (Fig. 5.18 (d)). The results demonstrate just the opposite (Fig. 5.18 (a) and Fig. 5.15) [Borisenko et al. (2012)].

One can assume that nodeless $s^{\pm}$ order parameter takes place. Indeed, this would fix the in-phase/anti-phase discrepancy and the orientation of the gap maxima on the large hole pocket (Fig.

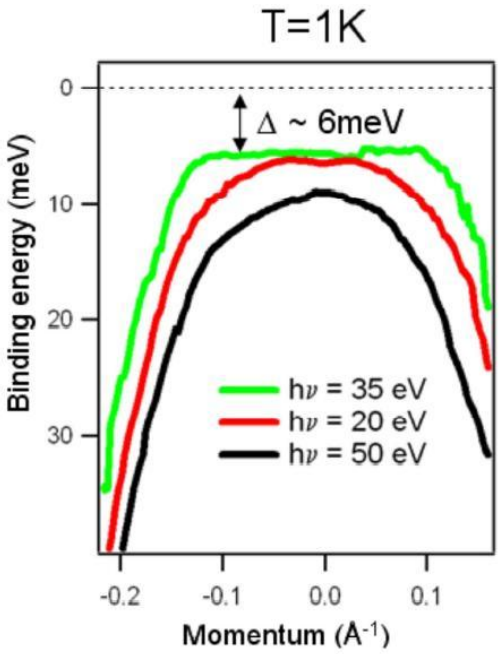


**Figure 5.17**: Gap at Γ and kinks. Dispersion of the middle hole-like feature near G for different $k_z$, set by various excitation energies [Borisenko et al. (2012)].

5.18 (c)). However, the orientation of the extrema of the in-phase oscillating gaps on electron FSs would then be in conflict with the experimentally observed one (Fig. 5.18 (b)). It is known that the orbital character of small portions of electron FSs oriented towards Γ points is $d_{xy}$ and the inter-orbital pairing with $d_{xz,yz}$ states on hole FSs is weaker than the intraorbital pairing for the major parts of electron pockets. On the contrary, the data show that the gaps on these portions are maximal (Fig. 5.18 (a), (b)).

Another ingredient necessary for realization of spin-fluctuation scenario is apparently missing in LiFeAs. Recent neutron-scattering experiments on single crystals demonstrate that the strength of spin fluctuations in LiFeAs is an order of magnitude weaker than in Co-doped 211 system [Qureshi et al. (2012)]. As a consequence, there is no evidence of electron-magnon coupling in LiFeAs contrary to the case of optimally doped 122 compounds and cuprates [Dahm et al. (2009)]. Moreover, the detected energy spectrum of magnetic fluctuations does not contain any features that can explain the dispersion kinks in electronic spectrum observed in Refs. [Kordyuk et al. (2011); Taylor et al. (2011); Qureshi et al. (2012)]. More evidence for strong electron-boson coupling was found in Ref. [Borisenko et al. (2012)]. All typical energy scales derived by Kordyuk *et al* [Kordyuk et al. (2011)] correspond to phonon modes [Jishi and Alyahyaei (2010)], detected experimentally for the center of the BZ by Raman scattering [Um et al. (2012)]. In spite of the noticeable renormalization kinks implying considerable electron-phonon coupling, the largest gap in LiFeAs is twice larger than in a weak coupling BCS scheme and its momentum dependence is very peculiar implying that conventional electron-phonon coupling mechanism is not operational in this material.

This brings one to an alternative approach to superconductivity in pnictides based on the orbital fluctuations model [Kontani and Onari (2010)]. A general consensus exists regarding the important

role of orbital degrees of freedom played in physics of iron-based superconductors. Together with the possibility of Fe $3d$ orbital ordering at structural transition [Krüger et al. (2009)], one of the most remarkable and robust experimental evidences for this importance is the universal bandwidth renormalization of the factor of 2-3 found in all families of pnictides and chalcogenides [Zabolotnyy et al. (2009); Chen et al. (2010); Borisenko et al. (2010)]. This renormalization is captured by DMFT calculations which take into account the Hund's rule coupling [Skornyakov et al. (2010)]. Therefore, it is not surprising that fluctuations of orbital order can drive the pairing. It was shown that for this interaction to be attractive, a moderate electron-phonon coupling should be present [Kontani and Onari (2010)].

The hallmark of the orbital-fluctuations-mediated-by-phonons scenario is the $s_{++}$ order parameter, i.e. the superconducting gap of one sign for the whole BZ. According to Kontani and Onari [Kontani and Onari (2010)], this superconducting state is likely to be realized exactly in electron-doped FeBS even without impurities (see Fig. 4 (c) in Ref. [Kontani and Onari (2010)]). Taking into account the above remark about the classification of LiFeAs in terms of doping and directly determined gap function for all FSs, this is in perfect agreement with data obtained by Borisenko and collaborators [Borisenko et al. (2012)]. The gap function in band representation calculated in Ref. [Yanagi et al. (2010)] (Fig. 7) captures all the peculiarities of experimentally observed one: gaps on electron pockets oscillate in phase, their maxima are oriented towards $\Gamma$ point. Even the orientation of the extrema on large hole-like $d_{xy}$ FS match the experimental observation.

Scanning tunneling spectroscopy of superconducting LiFeAs single crystals was used for study of the quasiparticles spectrum [Chi et al. (2012)]. A dip-hump structure was observed below $T_c$ with an energy scale consistent with a broad magnetic excitation peaked around 5-8 meV reported by inelastic neutron scattering [Taylor et al. (2011); Qureshi et al. (2012)]. Ummarino *et al* [Ummarino et al. (2013)] have proposed a model, which reproduce superconducting and normal properties of the iron-pnictide LiFeAs in the framework of the four-band $s^{\pm}$-wave Eliashberg theory. A confirmation of the multiband nature of the system rises from the experimental measurements of the superconducting gaps and resistivity as a function of temperature. The antiferromagnetic spin fluctuation was found to be the most plausible mechanism of pairing [Ummarino et al. (2013)].

Eilenberger approach was used in **Paper 3** to calculate cutoff parameter in superconductors with different pairing symmetries. In particular, we study the case of weak intraband scattering. This can be realized in stoichiometric pnictides such as LiFeAs. It is found that at some scatterings parameters the $\xi_h/\xi_{c2}$ ratio is larger than the AGL values for $s^{\pm}$-wave state, as observed in SANS measurements on stoichiometric LiFeAs compound [Inosov et al. (2010b)].

## Paper 4. Cutoff parameter versus Ginzburg-Landau coherence length in the mixed state of high-$\kappa$ superconductors with impurities: quasiclassical approach

The structural and electronic properties of the flux-line lattice state in high-$T_c$ cuprates have been extensively studied by microscopic techniques, including scanning tunneling spectroscopy, small-angle neutron scattering, nuclear magnetic resonance, and muon spin rotation. Rich information has been provided not only on the superconductivity itself, but also on the unique FLL state as a vortex matter realized in $YBa_2Cu_3O_{7-\delta}$ and $Bi_2Sr_2CaCu_2O_{8+\delta}$ systems. In particular, recent developments concerning the $\mu$SR experimental technique have made it feasible to obtain micriscopic details of the spatial field distribution $B(\mathbf{r})$ in the FLL state directly from the $\mu$SR time spectra [Sonier (2007)].

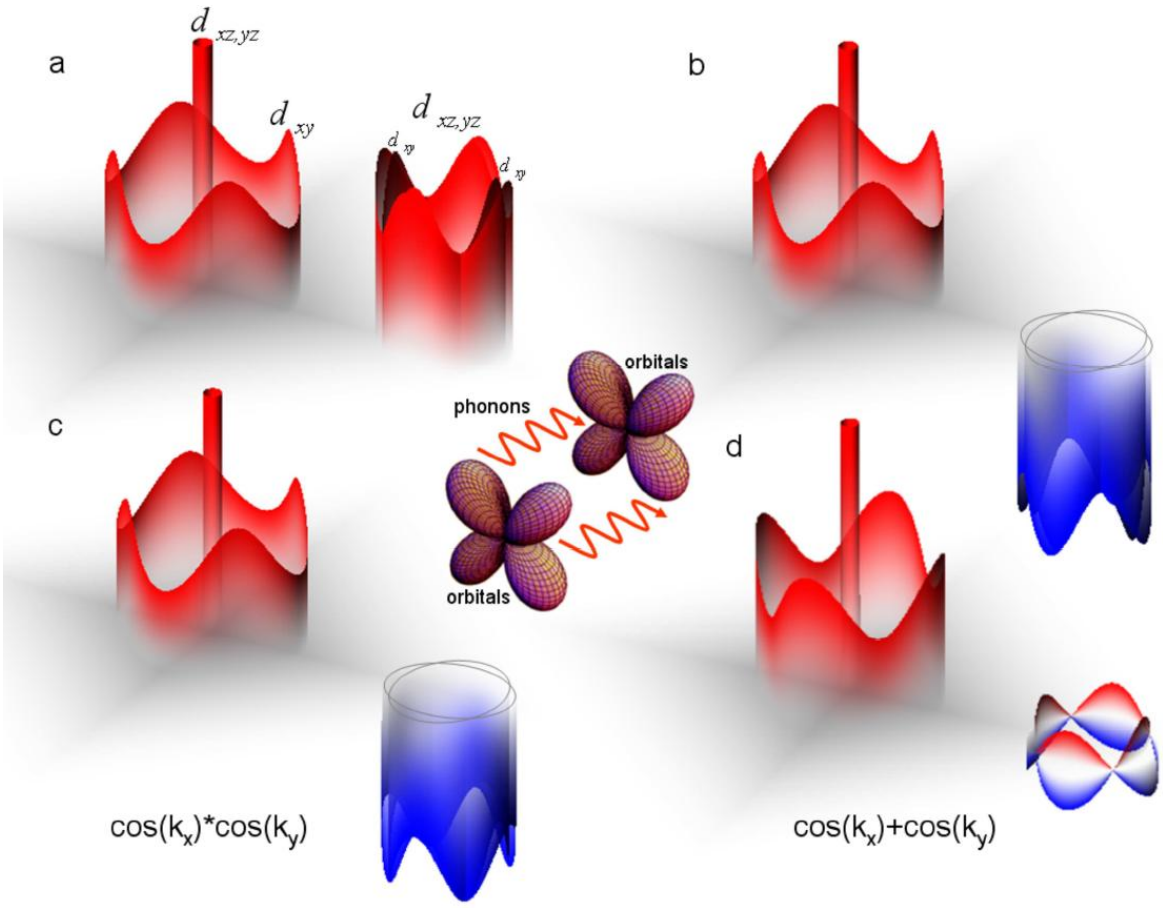


**Figure 5.18**: Symmetry of the order parameter in LiFeAs. (a) 3D representation of the gap function as it follows from ARPES measurements. Only two sets of the Fermi surfaces are shown: those centered at Γ point and at the corner of the BZ. Note the orientation of the extrema of all FSs and in-phase behavior of the electron-like sheets. Orbital composition of the FSs is indicated as well. (b) Same as (a), but taking into account the possibility of different sign between hole- and electron-like FSs. (c) Gap function corresponding to the nodeless $s^{\pm}$ order parameter, usually discussed for hole-doped FeBS with nested FSs. Though similar to the case shown in (b), the orientation of the extrema on the electron-like FSs is different. (d) Nodal $s^{\pm}$ order parameter which should apply to LiFeAs according to the calculations within the spin-fluctuation scenario. Inset schematically represents the orbital-fluctuations model with electron-phonon interaction [Borisenko et al. (2012)].

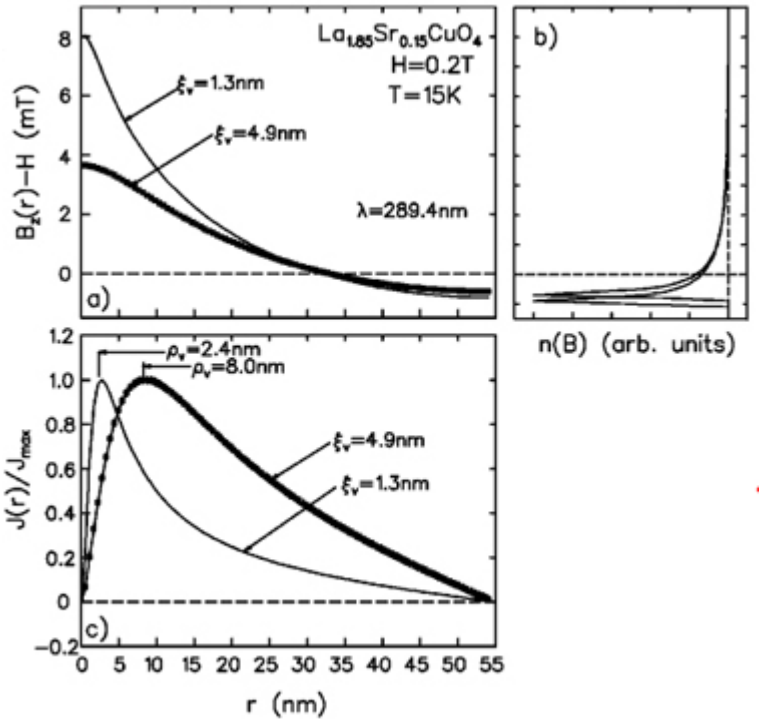


**Figure 5.19**: (a) Example of the reconstructed field distribution $B_z(r)$, which yields the spectral density $n(B)$ in (b). The radial distribution of the supercurrent density, $J(r) = |\mathrm{rot}\mathbf{B}(\mathbf{r})|$ is depicted in (c) along with the definition of the core radius $\rho_v$ [Kadono et al. (2004)].

The analysis of the field distribution experimental results on mixed state of type-II superconductors uses different approximations. In the modified London model, $B(\mathbf{r})$ is approximated as the sum of the magnetic induction from isolated vortices to yield

$$B(\mathbf{r}) = B_0 \sum_{\mathbf{G}} \frac{e^{-i\mathbf{G}\cdot\mathbf{r}}}{1+G^2\lambda^2} F(G,\xi_v), \tag{5.9}$$

where $\mathbf{G}$ are the vortex reciprocal-lattice vectors, $B_0$ ($\simeq H$) is the average internal field, $\lambda$ is the London penetration depth, and $F(G,\xi_v)$ is a nonlocal correction term with $\xi_v$ being the cutoff parameter for the magnetic field distribution. The $\xi_v$ parameter describes the electromagnetic response of a vortex, thereby it is not necessarily equivalent to the core radius $\rho_v$. Considering small anisotropy predicted by the theory [Ichioka et al. (1999)], an isotropic vortex core and associated field distribution near the vortex center are assumed. It is found that the $\mu$SR spectra in LSCO at lower fields are much better reproduced by the Lorentzian cutoff, $F(G,\xi_v) = \exp(-\sqrt{2}G\xi_v)$, compared with the conventional Gaussian cutoff, $F(G,\xi_v) = \exp(-G^2\xi_v^2/2)$. While the fitting analysis of the $\mu$SR data is performed entirely in time domain, one can reconstruct $B(\mathbf{r})$ by Eq. (5.9) using the physical parameters deduced from the fitting analysis. An example of the reconstructed field distribution, $B(\mathbf{r}) = B_z(r)$, along the radial direction from the core center to a saddle point is shown in Fig. 5.19 (a), together with the corresponding $n(B)$ (Fig. 5.19 (b)) and supercurrent density $J(r) = |\mathrm{rot}\mathbf{B}(\mathbf{r})|$ (Fig. 5.19 (c)). As shown in Fig. 5.19 (c), the core radius defined by $J(\rho_v) = J_{max}$, where $J_{max}$ denotes the maximum of $J(r)$, is considerably larger than the magnetic

cutoff parameter $\xi_v$, indicating the need for a special precaution in interpreting $\xi_v$ directly as the core radius. However, the result of a data analysis for various fields/temperatures indicates that $\rho_v$ is always proportional to $\xi_v$ [Kadono et al. (2004)].

Analyzed with this method, $\mu$SR experimental results in $V_3Si$, $NbSe_2$, and $LuNi_2B_2C$ in intermediate magnetic fields and low temperatures showed that $\xi_h/\xi_{c2}(\sim 0.7)$ is less than 1 (see Fig. 7 in Ref. [Sonier (2007)]). These small values differ from the prediction of the analytical Ginzburg-Landau theory ($\xi_v/\xi_{c2} = \sqrt{2}$), which is described in the comment to **Paper 5**. In **Paper 4** we calculate the $\xi_h/\xi_{c2}(B)$ dependence in $s$-wave superconductors at different impurity scattering rates, $\Gamma$, and temperatures, $T/T_c$. Small values of $\xi_h/\xi_{c2}$ are obtained at high $\Gamma$ values and low $T/T_c$. The results can be relevant to low temperature superconductors mentioned above.

## Paper 5. Vortex lattice form factor in stoichiometric and nonstoichiometric iron pnictide superconductors

To understand the origin of the deviation of the zero-energy density of states $N(0)$ from $H$-linear behavior in the $s$-wave pairing, the field dependence of the vortex core radius is depicted in Fig. 5.20. The radius $\xi_1$ is defined from the initial slope of the pair potential by fitting as $|\Delta(\mathbf{r})| = \Delta_1 r/\xi_1$ at the vortex center. Here, $\Delta_1$ is defined as the maximum of $|\Delta(\mathbf{r})|$ along the line connecting the nearest-neighbor vortex centers. The radius $\xi_2$ is defined as the one where the screening current around a vortex reaches its maximum. In increasing magnetic field $H$, both $\xi_1$ and $\xi_2$ decrease similarly as seen in Fig. 5.20. The $d_{x^2-y^2}$-wave case shows the similar decrease about the core radius. The shrinkage of the core radius was also observed by the experiments of STM [Golubov and Hartmann (1994)] and $\mu$SR [Sonier et al. (1997)]. In the calculation of a single vortex [Fetter and Hohenberg (1969)], the zero-energy DOS per vortex $N(0)/H$ is proportional to an area of the vortex core $\pi\xi_3^2$. In Ref. [Fetter and Hohenberg (1969)], the radius $\xi_3$ corresponds to $\xi_1$. If $\xi_3$ is independent of $H$, one obtains the expected relation $N(0) \propto H$. However, it is not the case.

Figure 5.20 shows the core radius $\xi_3$ estimated from $N(0)$, where $\xi_3 = a[(N(0)/N_0)(H/H_{c2})]^{1/2}$ with a fitting parameter $a = 0.35$. The radius $\xi_3$ decreases similarly as $\xi_1$ with increasing $H$. It means that the deviation from $H$-linear in $N(0)$ does reflect the field dependence of the core radius. The spatial variations of $h(\mathbf{r})$ are characterized by the form factor $h_{m,n}$, where $m$ and $n$ are integer. It is the Fourier component $h(\mathbf{r})$ defined as $h(\mathbf{r}) = H\sum_{m,n} h_{m,n}\exp(i\mathbf{g}_{m,n}\cdot\mathbf{r})$ with reciprocal lattice vector $\mathbf{g}_{m,n} = -n\mathbf{k}_1 + m\mathbf{k}_2$. The spatial variation of $h(\mathbf{r})$ shows fourfold symmetry around a vortex core in the $d_{x^2-y^2}$-wave pairing, while it is circular in the $s$-wave pairing [Ichioka et al. (1996)]. This difference becomes clear at higher field, and reflects the field dependence of $h_{1,1}$ and $h_{2,0}$ as shown in Fig. 5.21 [Ichioka et al. (1999)]. It is worth noting that clear difference does not appear in $h_{1,0}$, $h_{2,1}$, and $h_{3,0}$. These differences can be detected by SANS and $\mu$SR.

The three low-energy features are (i) from the continuum state associated with the nodal structure, (ii) the core excitations from the bound states, and (iii) the quasiparticle transfer between vortices. These features give rise to the clear difference between $d_{x^2-y^2}$- and $s$-wave pairings in the field dependence of $N(0)$ and the form factors $h_{1,1}$ and $h_{2,0}$. The vortex lattice effect gives the deviation from $\sqrt{H}$-behavior of $N(0)$ in the $d_{x^2-y^2}$-wave pairing. As the vortex core radius decreases with increasing field, $N(0)$ deviates from $H$-linear behavior in the $s$-wave pairing.

A widely used analytical GL expression was obtained by Clem [Clem (1975)] for isotropic superconductors at low inductions $B \ll B_{c2}$. Using a Lorentzian trial function for the order parameter

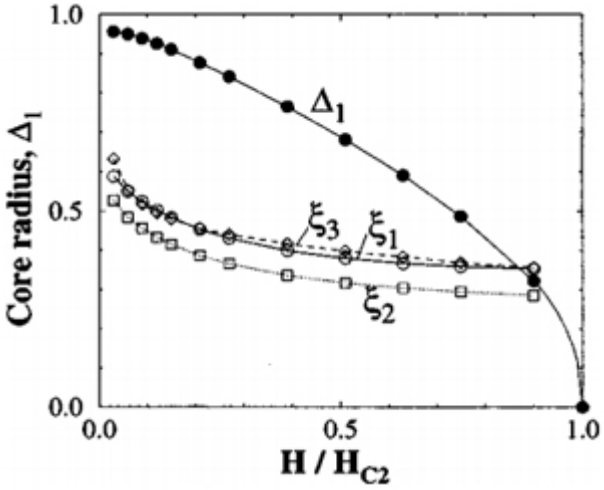


**Figure 5.20**: Field dependence of core radius $\xi_1$, $\xi_2$, and $\xi_3$ for the $s$-wave pairing. Maximum amplitude of the order parameter $\Delta_1$ is also plotted. The radius and $\Delta_1$ are, respectively, scaled by $\xi_0$ and $\Delta_0$ [Ichioka et al. (1999)].

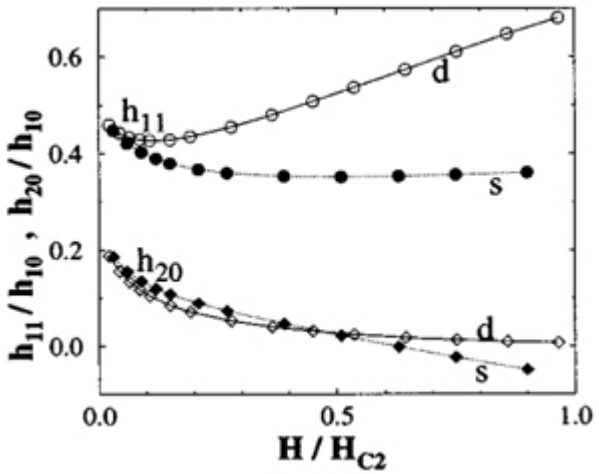


**Figure 5.21**: Field dependence of form factors $h_{1,1}/h_{1,0}$ and $h_{2,0}/h_{1,0}$ for the $d_{x^2-y^2}$- and $s$-wave pairings [Ichioka et al. (1999)].

$|\psi(\mathbf{r})|^2$ of an isolated vortex, Clem found for large $\kappa \gg 1$

$$B_z(G) = \frac{\Phi_0}{S}\frac{\mathrm{g}K_1(\mathrm{g})}{1+\lambda^2 G^2}, \quad \mathrm{g} = \sqrt{2}\xi(G^2+\lambda^{-2})^{\frac{1}{2}}. \tag{5.10}$$

Here $K_1(x) = -K_0'(x)$ is a modified Bessel function. The London solution can be recovered from Eq. (5.10) if the vortex shrinks to zero. The cutoff factor $\mathrm{g}K_1(\mathrm{g})$ in Eq. (5.10) may be approximated for all g values by $\exp(-\sqrt{2}\xi G)$ [Brandt (1992)]. The cutoff $\exp(-\xi^2 G^2/4)$ suggested by Brandt [Brandt (1972)] was derived from the GL solution near $B_{c2}$, and is not valid at low magnetic fields ($B \ll B_{c2}$). At intermediate fields the cutoff should interpolate between these two expressions.

Clem's approximate analytical theory of the dilute vortex lattice [Clem (1975)] was extended to larger fields and to anisotropic superconductors by Hao *et al* [Hao et al. (1991)] using the same type of variational approach. The resulting Fourier components for an isotropic superconductor may be written as

$$B_z(\mathbf{G}) = \frac{\Phi_0}{S}\frac{f_\infty K_1\left[\frac{\xi_v}{\lambda}(f_\infty^2+\lambda^2G^2)^{\frac{1}{2}}\right]}{(f_\infty^2+\lambda^2G^2)^{\frac{1}{2}}K_1\left(\frac{\xi_v}{\lambda}f_\infty\right)}, \tag{5.11}$$

where $\xi_v$ and $f_\infty$ are two variational parameters representing the effective core radius of a vortex and the depression of the order parameter due to the overlap of the vortex cores, respectively. For high-$\kappa$ case the two variational parameters have simple functional dependences on $b \equiv B/B_{c2}$ and $\kappa$ [Clem (1975); Hao et al. (1991)]:

$$f_\infty^2 = 1 - b^4, \tag{5.12}$$

$$\xi_v = \xi\left(\sqrt{2} - \frac{0.75}{\kappa}\right)(1+b^4)^{\frac{1}{2}}[1-2b(1-b)^2]^{\frac{1}{2}}. \tag{5.13}$$

In Eqs. (5.12) and (5.13) $\Phi_0/S = B = bB_{c2}$ is the mean induction, which for $2b\kappa^2 > 1$ may be equated to $B_{ext}$.

For $\kappa \gg 1$ the argument of $K_1$ in the denominator of Eq. (5.11) is much smaller than 1, thus one may use $K_1(x) \approx 1/x$. Since for high-$T_c$ superconductors and typical $B_{ext}$ values, $b$ is never larger than a few percents, the field dependence of $f_\infty$ and $\xi_v$ can be neglected, putting $f_\infty \approx 1$ and $\xi_v \approx \sqrt{2}\xi$. For the analysis of measurements performed on heavy fermion superconductors, the field dependence of $f_\infty(b)$ can thus be disregarded, usually $B_{ext} \leqslant 1$ T [Kleiman et al. (1992)], but this may not be true for $\xi_v(b)$. For instance, with $UPt_3$ at $B_{ext} = 1$ T one has $b \approx 0.4$ [Kleiman et al. (1992)] and therefore $\xi_v \approx 0.854 \cdot \sqrt{2}\xi$. The smallest nonzero reciprocal vector for an equilateral triangular lattice is $G_{10} = G_{min} = a_v^* = (2\pi/S)a_v$, thus $G_{min}^2 = (8\pi^2/\sqrt{3})(B/\Phi_0)$. This means that for the high-$T_c$ compounds at $B \simeq B_{ext} = 20$ mT one has $\Lambda G_{min}^2 \simeq 10 \gg 1$, if $\Lambda^{1/2} = \lambda = 1500$ Å is used. For $UPt_3$ $\lambda$ is even larger [Kleiman et al. (1992)]. Accounting for the large value of $\Lambda G_{min}^2 = (4\pi/\sqrt{3})b\kappa^2$ one may write

$$B_z(\mathbf{G}) = \frac{\Phi_0}{S}\frac{f_\infty^2}{\Lambda G^2}(\xi_v G)K_1(\xi_v G). \tag{5.14}$$

The conventional superconductor $CeRu_2$ has attracted some interest because of its complex phase diagram in the $(B_{ext}, T)$ plane. Notably, a reversible-irreversible line is observed. The form factor

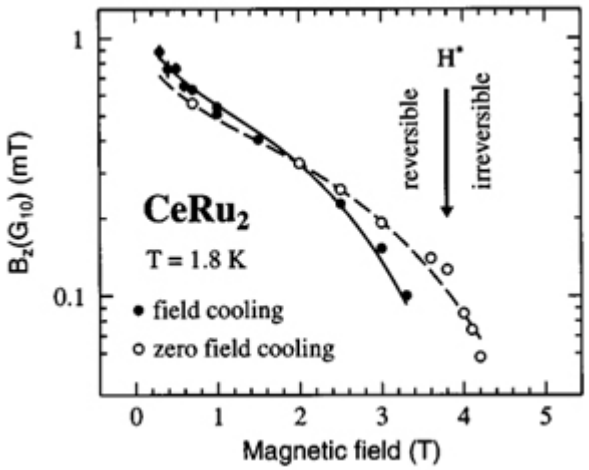


**Figure 5.22**: Form factor for the reflection [1,0] from the vortex lattice of $CeRu_2$ as a function of the applied field. The lines are fits to Eq. (5.15) [Yaouanc et al. (1997)].

$B_z(G)$ is easily obtained from the SANS cross section [de Gennes (1989)]. The $CeRu_2$ measurements of $B_z(G_{10})$ as a function of $B_{ext}$ are presented in Fig. 5.22 [Yaouanc et al. (1997)]. Because $\Lambda$ is scalar, one derives from Eq. (5.14)

$$B_z(G_{10}) = \frac{3^{\frac{1}{4}}}{2\pi\sqrt{2}} \frac{\sqrt{\Phi_0 B_{ext}} f_\infty^2 \xi_v}{\lambda^2} K_1 \left( \frac{2\pi\sqrt{2}}{3^{\frac{1}{4}}} \xi_v \sqrt{\frac{B_{ext}}{\Phi_0}} \right). \tag{5.15}$$

This expression depends only on the two parameters $\lambda$ and $\xi$. The fits yield for the data recorded either in the field cooling (FC) or zero-field cooling (ZFC) procedure, $\lambda = 1870$ Åand $\xi = 84$ Å and $\lambda = 2090$ Å and $\xi = 74$ Å, respectively. Taking the traditional point of view, the field cooling (FC) data reflect the equilibrium properties of the vortex lattice. From these data $\kappa = 22$ is larger than the previously estimated $\kappa = 14.5$ [Huxley et al. (1993)]. From the $\xi$ value one may compute $B_{c2} = \Phi_0/(2\pi\xi^2) = 4.7$ T. Magnetization measurements at 1.8 K give $B_{c2} = 5.3$ T. The values deduced from the FC neutron data are satisfactory in view of the well known difficulty to extract a reliable $\kappa$ value from magnetization measurements. The traditional Gaussian cutoff predicts $\ln[B_z(G_{10})] \propto B_{ext}$, i.e. a straight line in Fig. 5.22, which is not observable. The generalization of Eq. (5.14) to anisotropic penetration length tenzors reads for $\kappa \gg 1$

$$B_z(\mathbf{G}) = \frac{\Phi_0}{S}(1-b^4) \frac{uK_1(u)}{\Lambda_x G_y^2 + \Lambda_y G_x^2}. \tag{5.16}$$

Here, $uK_1(u)$ is an anisotropic cutoff factor with

$$u^2 = 2\left(\xi_x^2 G_x^2 + \xi_y^2 G_y^2\right)\left(1+b^4\right)\left[1-2b(1-b)^2\right], \tag{5.17}$$

$$uK_1(u) = 1 - \frac{u^2}{4}\ln\left(\frac{2.937}{u^2}\right) \quad \text{for } u \ll 1. \tag{5.18}$$

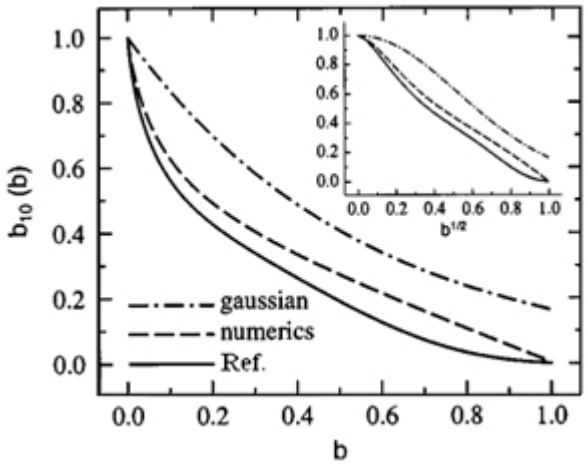


**Figure 5.23**: The universal functions of the largest reduced form factor, $b_{10}(b)$, defined in Eq. 5.21 [Yaouanc et al. (1997)].

For the computation of $B_z(\mathbf{G})$ the geometry of the vortex lattice needs to be specified. As shown for $B \gg B_{c1}$ [Kogan (1981)], the angle characterizing this lattice depends only on the penetration-length ratio

$$\tan\alpha = \sqrt{3}\frac{\lambda_x}{\lambda_y}. \tag{5.19}$$

Using Kogan's formula (5.19), the form factor factorizes, $B_z(G_{pq}) = B_0 b_{pq}(b)$, where

$$B_0 = \frac{1}{\pi^2}\left(\frac{3}{64}\right)^{\frac{1}{2}}\frac{\Phi_0}{\lambda_x\lambda_y} \tag{5.20}$$

and $b_{pq}(b)$ is a universal function,

$$b_{pq}(b) = \left(1-b^4\right)\frac{v_{pq}K_1(v_{pq})}{p^2-pq+q^2}, \tag{5.21}$$

$$v_{pq}(b) = \frac{2\sqrt{2\pi}}{3^{\frac{1}{4}}}b^{\frac{1}{2}}\left[1+b^4\right]^{\frac{1}{2}}\left[1-2b\left(1-b^2\right)^2\right]^{\frac{1}{2}}\left(p^2-pq+q^2\right)^{\frac{1}{2}}. \tag{5.22}$$

In Fig. 5.23 form factor $b_{10}(b)$ computed from the variational solution (5.21)-(5.22) [Yaouanc et al. (1997)], the Gaussian cutoff [Brandt (1972)], and the numerical solution of the GL equations [Brandt (1997)] are presented. Remarkably, the comparison between the variational and the numerical solutions show that for $b \leqslant 0.05$ the first three Fourier coefficients $B_z(G)$ deviate by less than $10\%$ and for $b \leqslant 0.01$ by less than $4\%$ [Yaouanc et al. (1997)].

For $s$-wave superconductors, Caroli *et al* [Caroli et al. (1964)] have shown that there are a series of bound states in a vortex. Later a detailed structure of the bound state wave function has been explored by Gygi and Schlüter [Gygi and Schlüter (1991)]. Scanning tunneling spectroscopy showed different core structures of the vortex in YBCO and Bi2212 [Maggio-Aprile et al. (1995); Renner

et al. (1998); Pan et al. (2000)]. Contrary to the theoretical expectation [Soininen et al. (1994); Schopohl and Maki (1995); Wang and MacDonald (1995)], a bound state with energy $E$, a fraction of $\Delta$, was observed.

To resolve these contradictions, Morita *et al* [Morita et al. (1997)] have abandoned the quasiclassical approximation used in earlier analysis [Schopohl and Maki (1995)] and proposed to study the bound states in terms of Bogoliubov-de Gennes equation [Caroli et al. (1964)]. Indeed, this approach appeared to give a correct description of the observation. However, later Franz and Tesănović claimed that there should be no bound states [Franz and Tesănović (1998)], which was confirmed in a series of papers [Yasui and Kita (1999); Takigawa et al. (1999)]. In Ref. [Kopnin (1998)] the quasiclassical equations were solved. To find quasiparticle quantum levels the semiclassic Bohr-Sommerfeld quantization rule was used. It was found that there are no localized states even for a single vortex ($B \to 0$) [Kopnin (1998)].

Levy *et al* [Levy et al. (2005)] have carried out a detailed study of an individual vortex behavior in Bi2212. The salient features of the spectrum close to the center is that one sees a large gap-like structure reflecting the pseudogap and two peaks placed at $\sim \pm 0.3\Delta_p$ suggesting the presence of one pair of localized states. When this vortex was imaged at the energy of the core state a square pattern oriented in the Cu-O bond direction was obtained at the center of the vortex. The Fourier transform of this pattern showed four spots with a period close to $4a_0$, in addition to the atomic lattice. Mounce *et al* [Mounce et al. (2011)] investigated vortex magnetism by developing a spatially resolved probe based on NMR spin-lattice-relaxation spectroscopy. With this approach a spin-density wave associated with the vortex core was found in $Bi_2Sr_2CaCu_2O_{8+y}$, similar to patterns in the local density of electronic states reported from scanning tunneling microscope experiments.

Since it has been found that the vortex-core spectra exhibit the pseudogap one might expect that the spatially ordered structure in the vortex cores has the same origin as the one observed in the pseudogap state. One important property of the spatial modulations in the pseudogap is the absence of dispersion of the $\mathbf{q}$ vectors, contrary to the modulations observed in the low-temperature superconducting state. Thus one criterion in comparing the vortex cores with the pseudogap is to check whether the observed order disperses or not [Ø. Fischer et al. (2007)]. This was also studied by Levy *et al* [Levy et al. (2005)], who plotted the intensity of the Fourier transform along the $(\pi, 0)$ direction for the different energies. The position of the local order was indeed found to be independent of energy, exactly as observed for the pseudogap. The period in this overdoped sample was $(4.3 \pm 0.3)a_0$, somewhat less than observed in the underdoped Bi2212 by Vershinin *et al* [Vershinin et al. (2004)], where the reported periods were $4.7a_0$ in the pseudogap above $T_c$. This difference could be due to variations either in doping or in temperature.

The relation to the localized states was also studied by Levy *et al* [Levy et al. (2005)]. They demonstrated that the intensity of the peaks corresponding to these states is maximal at the four spots reflecting the local order, whereas in between and outside these four spots the peaks at $\pm 0.3\Delta_p$ were absent. Since the spatial dependence of the peaks suggests that these two peaks reflect only one pair of localized states [Ø. Fischer et al. (2007)], the STS measures the square of the wave function of this state. Therefore, the four spots pattern in the center of the vortex may be understood as a plot of the wave function of the localized state. This pattern is very different from one obtained for a classical $s$-wave localized state as predicted by Caroli *et al* [Caroli et al. (1964)].

Sonier *et al* [Sonier et al. (2011)] tried to fit the transverse-field $\mu$SR spectra of $BaFe_{1.82}Co_{0.18}As_2$ single crystals to a theoretical muon-spin-polarization time dependence, $P(t)$, that had been successfully applied to a wide variety of type-II superconductors, and utilized in some of the experi-

ments on iron-arsenic superconductors [Williams et al. (2009, 2010)]. The spatial variation of the field, from which the magnetic field distribution is calculated, was modeled by the AGL theory (Eqs. (5.11)-(5.13)). Using penetration depth and coherence length as fitting parameters they obtained the ratio $\xi_h/\xi_{c2} = 0.38$, which is considerably less than the AGL prediction ($\sqrt{2}$). To explain this contradiction the AGL theory was modified by introduction of the field-induced antiferromagnetic order in the field distribution, similar to procedure used for description of the NMR in high-$T_c$ cuprates [Mounce et al. (2011)]. In this method $\xi_h/\xi_{c2} = 3.75$ was obtained being much higher than the AGL value. In contrast to cuprate superconductors where the AFM order near vortex core was clearly detected [Refs. 33-38 in **Paper 5**, Mounce et al. (2011)], AFM in Co-doped iron-pnictides was not found [Williams et al. (2010); Oh et al. (2011)].

In **Paper 5** we calculated in Eilenberger approach the cutoff parameter in dirty superconductors with high scattering rate, which is suitable for Co-doped iron-pnictides [Vorontsov et al. (2009)]. The obtained $\xi_h/\xi_{c2}$ ratio is comparable with that of Ref. [Sonier et al. (2011)] and depicted in Fig. 2 of **Paper 5**.

CHAPTER VI

# Conclusions

The core structure of the vortices is studied for $s_{++}$, $s^{\pm}$, and $d_{x^2-y^2}$ symmetries using Eilenberger approach and compared with the experimental data for iron-based superconductors, where pairing symmetry depends on crystal structure (nodal and nodeless superconducting gaps are possible in these materials). Such compounds as $K_xFe_{2-y}Se_2$, $KFe_2As_2$, LiFeAs, and $BaFe_{2-x}Co_xAs_2$ are discussed.

It is shown that Eilenberger equations can be reduced to the London model with only one parameter, $\xi_h(B,T,\Gamma)$. This length determines the form factor of the vortex lattice which is measured by $\mu$SR and SANS techniques. The value of the dominant form factor depends on impurity scattering by different ways in systems with various pairing symmetries. Comparison with the analytical Ginzburg-Landau theory developed by Hao *at al* [Hao et al. (1991)] is conducted. The Hao-Clem model is generally adopted in the analysis of the field distribution in the mixed state of type-II superconductors obtained from the experiments. It is discovered that the magnetic field dependence of $\xi_h/\xi_{c2}$ is nonuniversal for $s^{\pm}$ pairing; depending on the chosen set of parameters it can reside both below and above the AGL curve. Such behavior is quite different from that in an $s_{++}$ pairing symmetry, where intraband and interband scattering rates act in a similar way and $\xi_h/\xi_{c2}$ always decreases with impurity scattering. In $d$-wave superconductors, $\xi_h/\xi_{c2}$ always increases with the scattering rate $\Gamma$.

The vortex core size $\xi_2$ determined as a distance from the core center to the position of the vortex supercurrent maximum is calculated. According to the conducted research the normalized core radius, $\xi_2/\xi_{c2}$, increases with pair-breaking impurity scattering. For $s^{\pm}$ pairing the dependence $\xi_2/\xi_{c2}(B/B_{c2})$ has a minimum at low temperatures and small value of interband impurity scattering, evolving into monotonously decreasing function at strong $\Gamma_\pi$ rate and high temperatures. The intraband scattering decreases value of $\xi_2/\xi_{c2}$. Similar behavior was found for $d$-wave case at intermediate and high temperatures. The transformation from diminishing to growing of $\xi_2/\xi_{c2}(B/B_{c2})$ dependence with lowering of the temperature is obtained for $s_{++}$-wave symmetry. The effect of impurity scattering in the latter case is similar to that of intraband scattering for $s^{\pm}$ symmetry.

Our numerical approach extends the theory of electromagnetic coherence length in the Meissner state, $\xi_{El}$, [Lemberger et al. (1978)] to the mixed state. It is found that the ratio $F = \xi_h/\xi_{El}$ is weakly dependent on the relaxation time illustrating that both $\xi_h$ and $\xi_{El}$ have a similar dependence on $\tau$. This demonstrates that characteristic relaxation times by impurities are similar in the Meissner and mixed states only with slight renormalization by the magnetic field in the latter case. A

strong reduction of $\xi_h/\xi_{El}$ with decreasing temperature can be explained by the Kramer-Pesch effect [Nakai et al. (2006)]. At low temperatures the $\xi_{El}$ is constant and decreases slowly at high temperatures [Lemberger et al. (1978)]. The reason is that in the Meissner state the nonlocality is described only by extended states. In contrast, low temperature physics of the vortex state is connected with the nature of the current-carrying quantum states of the quasiparticles in the vortex core. It means that the $\xi_h(B,T,\tau)$ dependence can be approximately attributed to two contributions. First is connected to the core effects described by the $F(T)$ function and second is responsible for impurity scattering characterized by $\xi_{El}(\tau)$. The severe suppression of $\xi_h/\xi_{c2}$ with $\Gamma$ can explain the experiment results in many low-temperature superconductors ($V_3Si$, $NbSe_2$, and $LuNi_2B_2C$).

For $d_{x^2-y^2}$ pairing the nonlocal generalized London equation and its connection with the Eilenberger theory are also considered. Our calculations prove that the NGLE model with $h_{NGLE}(\mathbf{r})$ needs a properly determined cutoff parameter, i. e. the introduction of only nonlocal extended electronic states does not allow the avoidance of the problem of vortex core solving. The problem of the effective penetration depth in the vortex state for $d$-wave superconductors is discussed. In this case, the field dependence of $\lambda_{eff}$ is due to the extended quasiparticle states near the nodes of the superconducting gap. The flattening of $\lambda_{eff}(B)$ at low temperatures has been observed by $\mu$SR measurements [Amin et al. (2000)] consistent with our microscopical model.

# BIBLIOGRAPHY


Abrikosov, A. A., Gor'kov, L. P., 1960. Zh. Eksp. Teor. Fiz. 39, 1781.

Abrikosov, A. A., Gor'kov, L. P., Dzyaloshinski, I. E., 1963. *Methods of Quantum Field Theory in Statistical Physics* Dover Publications Inc., New York.

Agterberg, D. F., Barzykin, V., Gor'kov, L. P., 1999. Phys. Rev. B 60, 14868.

Amin, M. H. S., Franz, M., Affleck, I., 2000. Phys. Rev. Lett. 84, 5864.

Anderson, P. W., 1959. Phys. Rev. Lett. 3, 325.

Aronov, A. G., Sonin, E. B., 1973. JETP 36, 556.

Balatsky, A. V., Vekhter, I., Zhu, J.-X., 2006. Rev. Mod. Phys. 78, 373.

Bao, W., Qiu, Y., Huang, Q., Green, M. A., Zajdel, P., Fitzsimmons, M. R., Zhernenkov, M., Chang, S., Fang, M. H., Qian, B., Vehstedt, E. K., Yang, J., Pham, H. M., Spinu, L., Mao, Z. Q., 2009. Phys. Rev. Lett. 102, 247001.

Basov, D., Chubukov, A., 2011. Nature Physics 7, 241.

Berk, N. P., Schrieffer, J. R., 1966. Phys. Rev. Lett. 17, 433.

Betbeder-Matibet, S. S. O., Weiss, P. R., 1964. Phys. Rev. 136, A1500.

Borisenko, S. V., Zabolotnyy, V. B., Evtushinsky, D. V., Kim, T. K., Morozov, I. V., Yaresko, A. N., Kordyuk, A. A., Behr, G., Vasiliev, A., Follath, R., Büchner, B., 2010. Phys. Rev. Lett. 105, 067002.

Borisenko, S. V., Zabolotnyy, V. B., Kordyuk, A. A., Evtushinsky, D. V., Kim, T. K., Morozov, I. V., Follath, R., Büchner, B., 2012. Symmetry 4(1), 251.

Brandt, E. H., 1972. Phys. Status Solidi 51, 345.

Brandt, E. H., 1992. Physica C 195, 1.

Brandt, E. H., 1997. Phys. Rev. Lett. 78, 2208.

Bud'ko, S. L., Ni, N., Canfield, P. C., 2009. Phys. Rev. B 79, 220516(R).

Caroli, C., de Gennes, P. G., Matricon, J., 1964. Phys. Lett. 9, 307.

Chen, F., Zhou, B., Zhang, Y., Wei, J., Ou, H.-W., Zhao, J.-F., He, C., Ge, Q.-Q., Arita, M., Shimada, K., Namatame, H., Taniguchi, M., Lu, Z.-Y., Hu, J. P., Cui, X.-Y., Feng, D. L., 2010. Phys. Rev. B 81, 014526.

Chi, S., Grothe, S., Liang, R., Dosanjh, P., Hardy, W. N., Burke, S. A., Bonn, D. A., Pennec, Y., 2012. Phys. Rev. Lett. 109, 087002.

Chiao, M., Hill, R. W., Lupien, C., Popić, B., Gagnon, R., Taillefer, L., 1999. Phys. Rev. Lett. 82, 2943.

Chu, J.-H., Analytis, J., Kucharczyk, C., Fisher, I., 2009. Phys. Rev. B 79, 014506.

Chubukov, A. V., Vavilov, M. G., Vorontsov, A. B., 2009. Phys. Rev. B 80, 140515(R).

Clem, J. R., 1975. J. Low Temp. Phys. 18, 427.

Daghofer, M., Nicholson, A., Moreo, A., Dagotto, E., 2010. Phys. Rev. B 81, 014511.

Dahm, T., Hinkov, V., Borisenko, S. V., Kordyuk, A. A., Zabolotnyy, V. B., Fink, J., Büchner, B., Scalapino, D. J., Hanke, W., Keimer, B., 2009. Nat. Phys. 5, 217.

Das, T., Balatsky, A. V., 2011a. Phys. Rev. B 84, 014521.

Das, T., Balatsky, A. V., 2011b. Phys. Rev. B 84, 115117.

de Gennes, P. G., 1989. Superconductivity of Metals and Alloys (Addison-Wesley, New York).

Ding, H., P. Richard and, K. N., Sugawara, K., Arakane, T., Sekiba, Y., Takayama, A., Souma, S., Sato, T., Takahashi, T., Wang, Z., Dai, X., Fang, Z., Chen, G. F., Luo, J. L., Wang, N. L., 2008. Europhys. Lett. 83, 47001.

Dong, J. K., Zhou, S. Y., Guan, T. Y., Zhang, H., Dai, Y. F., Qiu, X., Wang, X. F., He, Y., Chen, X. H., Li, S. Y., 2010a. Phys. Rev. Lett. 104, 087005.

Dong, J. K., Zhou, S. Y., Guan, T. Y., Zhang, H., Dai, Y. F., Qiu, X., Wang, X. F., He, Y., Chen, X. H., Li, S. Y., 2010b. Phys. Rev. Lett. 104, 087005.

Eilenberger, G., 1968. Z. Physik 214, 195.

Fang, C., Wu, Y.-L., Thomale, R., Bernevig, B. A., Hu, J., 2011a. Phys. Rev. X 1, 011009.

Fang, C., Xu, B., Dai, P., Xiang, T., Hu, J., 2012. Phys. Rev. B 85, 134406.

Fang, M.-H., Wang, H. D., Dong, C. H., Li, Z. J., Feng, C. M., Chen, J., Yuan, H. Q., 2011b. Europhys. Lett. 94, 27009.

Fetter, A. L., Hohenberg, P. C., 1969. in Superconductivity, edited by R. D. Parks (Marcel Dekker Inc., New York), p. 891.

Fletcher, J. D., Serafin, A., Malone, L., Analytis, J. G., Chu, J.-H., Erickson, A. S., Fisher, I. R., Carrington, A., 2009. Phys. Rev. Lett. 102, 147001.

Franz, M., Affleck, I., Amin, M. H. S., 1997. Phys. Rev. Lett. 79, 1555.

Franz, M., Tesănović, Z., 1998. Phys. Rev. Lett. 80, 4763.

Franz, M., Tesănović, Z., 2000. Phys. Rev. Lett. 84, 554.

Friemel, G., Park, J. T., Maier, T. A., Tsurkan, V., Li, Y., Deisenhofer, J., von Nidda, H.-A. K., Loidl, A., Ivanov, A., Keimer, B., Inosov, D. S., 2012. Phys. Rev. B 85, 140511(R).

Fukazawa, H., Yamada, Y., Kondo, K., Saito, T., Kohori, Y., Kuga, K., Matsumoto, Y., Nakatsuji, S., Kito, H., Shirage, P. M., Kihou, K., Takeshita, N., Lee, C.-H., Iyo, A., Eisaki, H., 2009. J. Phys. Soc. Jpn. 78, 083712.

Galitskii, V. M., Larkin, A. I., 2002. Phys. Rev. B 66, 064526.

Ghosal, A., Randeria, M., Trivedi, N., 1998. Phys. Rev. Lett. 81, 3940.

Glatz, A., Koshelev, A. E., 2010. Phys. Rev. B 82, 012507.

Golubov, A. A., Dolgov, O., Boris, A. V., Charnukha, A., Sun, D. L., Lin, C. T., Shevchun, A. F., Korobenko, A. V., Trunin, M. R., Zverev, V. N., 2011. Pis'ma v ZhETF 94, 357.

Golubov, A. A., Hartmann, U., 1994. Phys. Rev. Lett. 72, 3602.

Gordon, R. T., Kim, H., Tanatar, M. A., Prozorov, R., Kogan, V. G., 2010. Phys. Rev. B 81, 180501(R).

Gordon, R. T., Martin, C., Kim, H., Ni, N., Tanatar, M. A., Schmalian, J., Mazin, I. I., Bud'ko, S. L., Canfield, P. C., Prozorov, R., 2009. Phys. Rev. B 79, 100506(R).

Gor'kov, L. P., 1959. Soviet Physics Journal of Experimental and Theoretical Physics 9, 1364.

Gor'kov, L. P., Kalugin, P. A., 1985. JETP Lett. 41, 253.

Gorkov, L. P., Schrieffer, J. R., 1998. Phys. Rev. Lett. 80, 3360.

Goswami, P., Nikolic, P., Si, Q., 2010. Europhys. Lett. 91, 37006.

Graf, M., Yip, S.-K., Rainer, J. S. D., 1996. Phys. Rev. B 53, 15147.

Graser, S., Maier, T. A., Hirschfeld, P. J., Scalapino, D. J., 2009a. New J. Phys. 11, 025016.

Graser, S., Maier, T. A., Hirschfeld, P. J., Scalapino, D. J., 2009b. New J. Phys. 11, 02501.

Guo, J., Jin, S., Wang, G., Wang, S., Zhu, K., Zhou, T., He, M., Chen, X., 2010. Phys. Rev. B 82, 180520(R).

Gygi, F., Schlüter, M., 1991. Phys. Rev. B 43, 76092.

Hao, Z., Clem, J. R., McElfresh, M. W., Civale, L., Malozemoff, A. P., Holtzberg, F., 1991. Phys. Rev. B 43, 2844.

Hashimoto, K., Serafin, A., Tonegawa, S., Katsumata, R., Okazaki, R., Saito, T., Fukazawa, H., Kohori, Y., Kihou, K., Lee, C. H., Iyo, A., Eisaki, H., Ikeda, H., Matsuda, Y., Carrington, A., Shibauchi, T., 2010. Phys. Rev. B 82, 014526.

Hedo, M., Inada, Y., Yamamoto, E., Haga, Y., Onuki, Y., Aoki, Y., Matsuda, T. D., Sato, H., Takahashi, S., 1998. J. Phys. Soc. Jpn 67, 33.

Hill, R. W., Lupien, C., Sutherland, M., Boaknin, E., Hawthorn, D. G., Proust, C., Ronning, F., Taillefer, L., Liang, R., Bonn, D. A., Hardy, W. N., 2004. Phys. Rev. Lett. 92, 027001.

Hirschfeld, P. J., Goldenfeld, N., 1993. Phys. Rev. B 48, 4219.

Hirschfeld, P. J., Korshunov, M. M., Mazin, I. I., 2011. Rep. Prog. Phys. 74, 124508.

Hirschfeld, P. J., Wölfle, P., Einzel, D., 1988. Phys. Rev. B 37, 83.

Hirschfeld, P. J., Wölfle, P., Vollhard, D., 1986. Sol. State Comm. 59, 111.

Huxley, A. D., Paulsen, C., Laborde, O., Tholence, J. L., Sanchez, D., Junod, A., Calemczuk, R., 1993. J. Phys.: Condens. Matter 5, 7709.

Ichioka, M., Hasegawa, A., Machida, K., 1999. Phys. Rev. B 59, 184.

Ichioka, M., Hayashi, N., Enomoto, N., Machida, K., 1996. Phys. Rev. B 53, 15316.

Ichioka, M., Hayashi, N., Machida, K., 1997. Phys. Rev. B 55, 6565.

Ikeda, H., Arita, R., Kunes, J., 2010. Phys. Rev. B 81, 054502.

Inosov, D. S., Park, J. T., Bourges, P., Sun, D. L., Sidis, Y., Schneidewind, A., Hradil, K., Haug, D., Lin, C. T., Keimer, B., Hinkov, V., 2010a. Nature Physics 6, 178.

Inosov, D. S., White, J. S., Evtushinsky, D. V., Morozov, I. V., Cameron, A., Stockert, U., Zabolotnyy, V. B., Kim, T. K., Kordyuk, A. A., Borisenko, S. V., Forgan, E. M., Klingeler, R., Park, J. T., Wurmehl, S., Vasiliev, A. N., Behr, G., Dewhurst, C. D., Hinkov, V., 2010b. Phys. Rev. Lett. 104, 187001.

Ishida, K., Nakai, Y., Hosono, H., 2009. J. Phys. Soc. Japan 78, 062001.

Jishi, R. A., Alyahyaei, H. M., 2010. Adv. Cond. Mat. Phys. 2010, 804343.

Kadono, R., Higemoto, W., Koda, A., Larkin, M. I., Luke, G. M., Savici, A. T., Uemura, Y. J., Kojima, K. M., Okamoto, T., Kakeshita, T., Uchida, S., Ito, T., Oka, K., Takigawa, M., Ichioka, M., Machida, K., 2004. Phys. Rev. B 69, 104523.

Kamihara, Y., Watanabe, T., Hirano, M., Hosono, H., 2008. J. Am. Chem. Soc. 130, 3296.

Kampf, A. P., Devereaux, T. P., 1997. Phys. Rev. B 56, 2360.

Kemper, A., Maier, T., Graser, S., Cheng, H.-P., Hirschfeld, P. J., Scalapino, D. J., 2010. New J. Phys. 12, 073030.

Khodas, M., Chubukov, A. V., 2012. Phys. Rev. Lett. 108, 247003.

Kirshenbaum, K., Saha, S. R., Ziemak, S., Drye, T., Paglione, J., 2012. Phys. Rev. B 86, 140505.

Kleiman, R. N., Broholm, C., Aeppli, G., Bucher, E., Stücheli, N., Bishop, D. J., Clausen, K. N., Mortensen, K., Pedersen, J. S., Howard, B., 1992. Phys. Rev. Lett. 69, 3120.

Kogan, V. G., 1981. Phys. Lett. A 85, 298.

Kogan, V. G., 2009. Phys. Rev. B 80, 214532.

Kontani, H., Onari, S., 2010. Phys. Rev. Lett. 104, 157001.

Kopnin, N. B., 1998. Phys. Rev. B 57, 11775.

Kopnin, N. B., Volovik, G. E., 1996. JETP Lett. 64, 641.

Kordyuk, A. A., Zabolotnyy, V. B., Evtushinsky, D. V., Kim, T. K., Morozov, I. V., Kulić, M. L., Follath, R., Behr, G., Büchner, B., Borisenko, S. V., 2011. Phys. Rev. B 83, 134513.

Kosztin, I., Leggett, A. J., 1997. Phys. Rev. Lett. 79, 135.

Krüger, F., Kumar, S., Zaanen, J., van den Brink, J., 2009. Phys. Rev. B 79, 054504.

Kübert, C., Hirschfeld, P. J., 1998. Phys. Rev. Lett. 80, 4963.

Kubo, K., 2007. Phys. Rev. B 75, 224509.

Kuroki, K., Onari, S., Arita, R., Usui, H., Tanaka, Y., Kontani, H., Aoki, H., 2008. Phys. Rev. Lett. 101, 087004.

Kuroki, K., Usui, H., Onari, S., Arita, R., Aoki, H., 2009. Phys. Rev. B 79, 224511.

Lankau, A., Koepernik, K., Borisenko, S., Zabolotnyy, V., Büchner, B., van den Brink, J., Eschrig, H., 2010. Phys. Rev. B 82, 184518.

Lemberger, T. R., Ginsberg, D. M., Rickayzen, G., 1978. Phys. Rev. B 18, 6057.

Levy, G., Kugler, M., Manuel, A. A., Ø. Fischer, Li, M., 2005. Phys. Rev. Lett. 95, 257005.

Li, W., Ding, H., Li, Z., Deng, P., Chang, K., He, K., Ji, S., Wang, L., Ma, X., Hu, J.-P., Chen, X., Xue, Q.-K., 2012. Phys. Rev. Lett. 109, 057003.

Liechtenstein, A. I., Mazin, I. I., Andersen, O. K., 1995. Phys. Rev. Lett. 74, 2303.

Lipscombe, O. J., Chen, G. F., Fang, C., Perring, T. G., Abernathy, D. L., Christianson, A. D., Egami, T., Wang, N. L., Hu, J. P., Dai, P. C., 2011. Phys. Rev. Lett. 106, 057004.

Lu, X., Fang, C., Tsai, W. F., Jiang, Y., Hu, J., 2012. Phys. Rev. B 85, 054505.

Lumsden, M. D., Christianson, A. D., 2010. J. Phys.: Cond. Mat. 22, 203203.

Luo, X. G., Tanatar, M. A., Reid, J.-P., Shakeripour, H., Doiron-Leyraud, N., Ni, N., Bud'ko, S. L., Canfield, P. C., Luo, H., Wang, Z., Wen, H.-H., Prozorov, R., Taillefer, L., 2009. Phys. Rev. B 80, 140503(R).

Lynn, J., Dai, P., 2009. Physica C 469, 469.

Ma, M., Lee, P. A., 1985. Phys. Rev. B 32, 5658.

Maggio-Aprile, I., Renner, C., Erb, A., Walker, E., Fischer, Ø., 1995. Phys. Rev. Lett. 75, 2754.

Maier, T. A., Graser, S., Hirschfeld, P. J., Scalapino, D. J., 2011. Phys. Rev. B 83, 100515(R).

Maier, T. A., Hirschfeld, P. J., Scalapino, D. J., 2012a. arXiv:1206.5235.

Maier, T. A., Hirschfeld, P. J., Scalapino, D. J., 2012b. Phys. Rev. B 86, 094514.

Maiti, S., Korshunov, M. M., Chubukov, A. V., 2012. Phys. Rev. B 85, 014511.

Maiti, S., Korshunov, M. M., Maier, T. A., Hirschfeld, P. J., Chubukov, A. V., 2011a. Phys. Rev. B 84, 224505.

Maiti, S., Korshunov, M. M., Maier, T. A., Hirshfeld, P. J., Chubukov, A. V., 2011b. Phys. Rev. Lett. 107, 147002.

Maki, K., 1969. in *Superconductivity*, edited by R. D. Parks (Marcel Dekker Inc., New York), p. 1035.

Mazin, I., Schmalian, J., 2009. Physica C 469, 614.

Mazin, I. I., 2011. Phys. Rev. B 84, 024529.

Mazin, I. I., Johannes, M. D., Boeri, L., Koepernik, K., Singh, D. J., 2008a. Phys. Rev. B 78, 085104.

Mazin, I. I., Singh, D. J., Johannes, M. D., Du, M. H., 2008b. Phys. Rev. Lett. 101, 057003.

Miao, H., Richard, P., Tanaka, Y., Nakayama, K., Qian, T., Umezawa, K., Sato, T., Xu, Y.-M., Shi, Y. B., Xu, N., Wang, X.-P., Zhang, P., Yang, H.-B., Xu, Z.-J., Wen, J. S., Gu, G.-D., Dai, X., Hu, J.-P., Takahashi, T., Ding, H., 2012. Phys. Rev. B 85, 094506.

Miyake, T., Nakamura, K., Arita, R., Imada, M., 2010. J. Phys. Soc. Jpn. 79, 044705.

Moler, K. A., Baar, D. J., Urbach, J. S., Liang, R., Hardy, W. N., Kapitulnik, A., 1994. Phys. Rev. Lett. 73, 2744.

Moradian, R., Annett, J. F., Gyorffy, B. L., Litak, G., 2001. Phys. Rev. B 63, 024501.

Morita, Y., Kohmoto, M., Maki, K., 1997. Phys. Rev. Lett. 78, 4841.

Mou, D., Liu, S., Jia, X., He, J., Peng, Y., Zhao, L., Yu, L., Liu, G., He, S., Dong, X., Zhang, J., Wang, H., Dong, C., Fang, M., Wang, X., Peng, Q., Wang, Z., Zhang, S., Yang, F., Xu, Z., Chen, C., Zhou, X. J., 2011. Phys. Rev. Lett. 106, 107001.

Mounce, A. M., Oh, S., Mukhopadhyay, S., Halperin, W. P., Reyes, A. P., Kuhns, P. L., Fujita, K., Ishikado, M., Uchida, S., 2011. Phys. Rev. Lett. 106, 057003.

Nakai, N., Miranović, P., Ichioka, M., Machida, K., 2006. Phys. Rev. B 73, 172501.

Nakajima, S., 1973. Prog. Theor. Phys. 50, 1101.

Nakamura, K., Arita, R., Ikeda, H., 2011. Phys. Rev. B 83, 144512.

Nakayama, K., Sato, T., Richard, P., Xu, Y.-M., Kawahara, T., Umezawa, K., Qian, T., Neupane, M., Chen, G. F., Ding, H., Takahashi, T., 2011. Phys. Rev. B 83, 020501 (R).

Ni, N., Tillman, M. E., Yan, J.-Q., Kracher, A., Hannahs, S. T., Bud'ko, S. L., Canfield, P. C., 2008. Phys. Rev. B 78, 214515.

Nohara, M., Isshiki, M., Takagi, H., Cava, R. J., 1997. J. Phys. Soc. Jpn 66, 1888.

Ø. Fischer, Kugler, M., Maggio-Aprile, I., Berthod, C., Renner, C., 2007. Rev. Mod. Phys. 79, 353.

Oh, S., Mounce, A. M., Mukhopadhyay, S., Halperin, W. P., Vorontsov, A. B., Bud'ko, S. L., Canfield, P. C., Furukawa, Y., Reyes, A. P., Kuhnsa, P. L., 2011. Phys. Rev. B 83, 214501.

Okazaki, K., Ota, Y., Kontani, Y., Malaeb, W., Ishida, Y., Shimojima, T., Kiss, T., Watanabe, S., Chen, C.-T., Kihou, K., Lee, C. H., Iyo, A., Eisaki, H., Saito, T., Fukazawa, H., Kohori, Y., Hashimoto, K., Shibauchi, T., Matsuda, Y., Ikeda, H., Miyahara, H., Arita, R., Chainani, A., Shin, S., 2012. Science 337, 1314.

Onari, S., Kontani, H., 2010. arXiv:1009.3882.

Osheroff, D. D., Richardson, R. C., Lee, D. M., 1972. Phys. Rev. Lett. 28, 885.

Pan, S. H., Hudson, E. W., Gupta, A. K., Ng, K. W., Eisaki, H., Uchida, S., Davis, J. C., 2000. Phys. Rev. Lett. 85, 1536.

Park, J. T., Friemel, G., Li, Y., Kim, J.-H., Tsurkan, V., Deisenhofer, J., von Nidda, H.-A. K., Loidl, A., Ivanov, A., Keimer, B., Inosov, D. S., 2011. Phys. Rev. Lett. 107, 177005.

Qian, T., Wang, X.-P., Jin, W.-C., Zhang, P., Richard, P., Xu, G., Dai, X., Fang, Z., Guo, J.-G., Chen, X.-L., Ding, H., 2011. Phys. Rev. Lett. 106, 187001.

Qureshi, N., Steffens, P., Drees, Y., Komarek, A. C., Lamago, D., Sidis, Y., Harnagea, L., Grafe, H.-J., Wurmeh, S., Büchner, B., Braden, M., 2012. Phys. Rev. Lett. 108, 117001.

Reid, J.-P., Tanatar, M. A., Juneau-Fecteau, A., R. T. Gordon, S. R. d. C., Doiron-Leyraud, N., Saito, T., Fukazawa, H., Kohori, Y., Kihou, K., Lee, C. H., Iyo, A., Eisaki, H., Prozorov, R., Taillefer, L., 2012. Phys. Rev. Lett. 109, 087001.

Renner, C., Bevaz, B., Kadowaki, K., Maggio-Aprile, I., Fischer, Ø., 1998. Phys. Rev. Lett. 80, 3606.

Saito, T., Onari, S., Kontani, H., 2010. Phys. Rev. B 82, 144510.

Saito, T., Onari, S., Kontani, H., 2011. Phys. Rev. B 83, 140512(R).

Sakakibara, H., Usui, H., Kuroki, K., Arita, R., Aoki, H., 2010. Phys. Rev. Lett. 105, 057003.

Sato, T., Nakayama, K., Sekiba, Y., Richard, P., Xu, Y.-M., Souma, S., Takahashi, T., Chen, G. F., Luo, J. L., Wang, N. L., Ding, H., 2009. Phys. Rev. Lett. 103, 047002.

Sawatzky, G. A., Elfimov, I. S., van den Brink, J., Zaanen, J., 2009. Europhys. Lett. 86, 17006.

Scalapino, D. J., Loh, E., Hirsch, J. E., 1986. Phys. Rev. B 34, 8190.

Schopohl, N., Maki, K., 1995. Phys. Rev. B 52, 490.

Seo, K., Bernevig, B. A., Hu, J., 2008. Phys. Rev. Lett. 101, 206404.

Shiba, H., 1968. Prog. Theor. Phys. 40, 435.

Sigrist, D. J., Ueda, K., 1991. Rev. Mod. Phys. 63, 239.

Skornyakov, S., Skorikov, N., Lukoyanov, A., Shorikov, A., Anisimov, V., 2010. Phys. Rev. B 81, 174522.

Soininen, P. I., Kallin, C., Berlinsky, A. J., 1994. Phys. Rev. B 50, 13883.

Sonier, J. E., 2007. Rep. Prog. Phys. 70, 1717.

Sonier, J. E., Huang, W., Kaiser, C. V., Cochrane, C., Pacradouni, V., Sabok-Sayr, S. A., Lumsden, M. D., Sales, B. C., McGuire, M. A., Sefat, A. S., Mandrus, D., 2011. Phys. Rev. Lett. 106, 127002.

Sonier, J. E., Kiefl, R. F., Brewer, J. H., Chakhalian, J., Dunsiger, S. R., MacFarlane, W. A., Miller, R. I., Wong, A., Luke, G. M., Brill, J. W., 1997. Phys. Rev. Lett. 79, 1742.

Suhl, H., Matthias, B. T., Walker, L. R., 1959. Phys. Rev. Lett. 3, 552.

Suzuki, K., Usui, H., Kuroki, K., 2011a. J. Phys. Soc. Jpn. 80, 013710.

Suzuki, K., Usui, H., Kuroki, K., 2011b. Phys. Rev. B 84, 144514.

Taillefer, L., Lussier, B., Gagnon, R., Behnia, K., Aubin, H., 1997. Phys. Rev. Lett. 79, 483.

Takigawa, M., Ichioka, M., Machida, K., 1999. Phys. Rev. Lett. 83, 3057.

Taylor, A. E., Pitcher, M. J., Ewings, R. A., Perring, T. G., Clarke, S. J., Boothroyd, A. T., 2011. Phys. Rev. B 83, 220514(R).

Terashima, T., Kimata, M., Kurita, N., Satsukawa, H., Harada, A., Hazama, K., Imai, M., Sato, A., Kihou, K., Lee, C.-H., Kito, H., Eisaki, H., Iyo, A., Saito, T., Fukazawa, H., Kohori, Y., Harima, H., Uji, S., 2010. J. Phys. Soc. Jpn. 79, 053702.

Thomale, R., Platt, C., Hanke, W., Bernevig, B. A., 2011a. Phys. Rev. Lett. 106, 187003.

Thomale, R., Platt, C., Hanke, W., Hu, J., Bernevig, B. A., 2011b. Phys. Rev. Lett. 107, 117001.

Um, Y. J., Park, J. T., Min, B. H., Song, Y. J., Kwon, Y. S., Keimer, B., Tacon, M. L., 2012. Phys. Rev. B 85, 012501.

Ummarino, G. A., Galasso, S., Daghero, D., Tortello, M., Gonnelli, R. S., Sanna, A., 2013. arXiv:1301.1542.

Vershinin, M., Misra, A., Ono, S., Abe, Y., Ando, Y., Yazdani, A., 2004. Science 303, 1995.

Volovik, G. E., 1993. JETP Lett. 58, 469.

Volovik, G. E., Gor'kov, L. P., 1985. Sov. Phys. JETP 61, 843.

Vorontsov, A. B., Vavilov, M. G., Chubukov, A. V., 2009. Phys. Rev. B 79, 140507(R).

Wang, A. F., Zhou, S. Y., Luo, X. G., Hong, X. C., Yan, Y. J., Ying, J. J., Cheng, P., Ye, G. J., Xiang, Z. J., Li, S. Y., Chen, X. H., 2012. arXiv:1206.2030.

Wang, F., Yang, F., Gao, M., Lu, Z.-Y., Xiang, T., Lee, D.-H., 2011a. Europhys. Lett. 93, 57003.

Wang, M., Fang, C., Yao, D.-X., Tan, G. T., Harriger, L. W., Song, Y., Netherton, T., Zhang, C. L., Wang, M., Stone, M. B., Tian, W., Hu, J. P., Dai, P. C., 2011b. Nat. Commun. 2, 580.

Wang, X.-P., Qian, T., Richard, P., Zhang, P., Dong, J., Wang, H.-D., Dong, C.-H., Fang, M.-H., Ding, H., 2011c. Europhys. Lett. 93, 57001.

Wang, Y., MacDonald, A. H., 1995. Phys. Rev. B 52, 3876.

Wilde, Y. D., Iavarone, M., Welp, U., Metlushko, V., Koshelev, A. E., Aranson, I., Crabtree, G. W., 1997. Phys. Rev. Lett. 78, 4273.

Wilke, R. T. H., Bud'ko, S. L., Canfield, P. C., Farmer, J., Hannahs, S. T., 2006. Phys. Rev. B 73, 134512.

Williams, T. J., Aczel, A. A., Baggio-Saitovitch, E., Bud'ko, S. L., Canfield, P. C., Carlo, J. P., Goko, T., Kageyama, H., Kitada, A., Munevar, J., Ni, N., Saha, S. R., Kirschenbaum, K., Paglione, J., Sanchez-Candela, D. R., Uemura, Y. J., Luke, G. M., 2010. Phys. Rev. B 82, 094512.

Williams, T. J., Aczel, A. A., Baggio-Saitovitch, E., Bud'ko, S. L., Canfield, P. C., Carlo, J. P., Goko, T., Munevar, J., Ni, N., Uemura, Y. J., Yu, W., , Luke, G. M., 2009. Phys. Rev. B 80, 094501.

Woolf, M. A., Reif, F., 1965. Phys. Rev. 137, A557.

Xu, M., Ge, Q. Q., Peng, R., Ye, Z. R., Jiang, J., Chen, F., Shen, X. P., Xie, B. P., Zhang, Y., Feng, D. L., 2012. Phys. Rev. B 85, 220504(R).

Yada, K., Kontani, H., 2008. Phys. Rev. B 77, 184521.

Yanagi, Y., Yamakawa, Y., Ōno, Y., 2010. Phys. Rev. B 81, 054518.

Yaouanc, A., Réotier, P. D., Brandt, E. H., 1997. Phys. Rev. B 55, 11107.

Yasui, K., Kita, T., 1999. Phys. Rev. Lett. 80, 4168.

Zaanen, J., 2009. Phys. Rev. B 80, 212502.

Zabolotnyy, V. B., Inosov, D. S., Evtushinsky, D. V., Koitzsch, A., Kordyuk, A. A., Sun, G. L., Park, J. T., Haug, D., Hinkov, V., Boris, A. V., Lin, C. T., Knupfer, M., Yaresko, A. N., Büchner, B., Varykhalov, A., Follath, R., Borisenko, S. V., 2009. Nature 457, 569.

Zeng, B., Mu, G., Luo, H. Q., Ziang, T., Mazin, I. I., Yang, H., Shan, L., Ren, C., Dai, P. C., Wen, H.-H., 2010. Nat. Commun. 1, 112.

Zhang, J., Sknepnek, R., Fernandes, R. M., Schmalian, J., 2009. Phys. Rev. B 79, 220502(R).

Zhang, X., Oh, Y. S., Liu, Y., Yan, L., Saha, S. R., Butch, N. P., Kirshenbaum, K., Kim, K. H., Paglione, J., Greene, R. L., Takeuchi, I., 2010. Phys. Rev. B 82, 020515 (R).

Zhang, Y., Yang, L. X., Xu, M., Ye, Z. R., Chen, F., He, C., Jiang, H. C. X. J., Xie, B. P., Ying, J. J., Wang, X. F., Chen, X. H., Hu, J. P., Matsunami, M., Kimura, S., Feng, D. L., 2011. Nat. Mater. 10, 273.

Zhao, J., Yao, D.-X., Li, S., Hong, T., Chen, Y., Chang, S., Ratcliff, W., Lynn, J. W., Mook, H. A., Chen, G. F., Luo, J. L., Wang, N. L., Carlson, E. W., Hu, J., Dai, P., 2008. Phys. Rev. Lett. 101, 167203.

Zhao, L., Mou, D., Liu, S., Jia, X., He, J., Peng, Y., Yu, L., Liu, X., Liu, G., He, S., Dong, X., Zhang, J., He, J. B., Wang, D. M., Chen, G. F., Guo, J. G., Chen, X. L., Wang, X., Peng, Q., Wang, Z., Zhang, S., Yang, F., Xu, Z., Chen, C., Zhou, X. J., 2011. Phys. Rev. B 83, 140508(R).

Zheng, G.-Q., Ozaki, H., Kitaoka, Y., Kuhns, P., Reyes, A. P., Moulton, W. G., 2002. Phys. Rev. Lett. 88, 077003.

Zhu, J.-X., Yu, R., Balatsky, A. V., Si, Q., 2011. Phys. Rev. Lett. 107, 167002.

# PART II: PUBLICATIONS

# PUBL. 1

**I. Zakharchuk, P. Belova, M. Safonchik, K. B. Traito and E. Lähderanta**, Vortex core size in unconventional superconductors, *Journal of applied physics*, **113**, 013906, 2013 DOI: 10.1063/1.4772670

JOURNAL OF APPLIED PHYSICS **113**, 013906 (2013)

# Vortex core size in unconventional superconductors

I. Zakharchuk,[1,2] P. Belova,[1,3,a)] M. Safonchik,[1,4] K. B. Traito,[1] and E. Lähderanta[1]
[1]*Lappeenranta University of Technology, P.O. Box 20, FI-53851 Lappeenranta, Finland*
[2]*Saint-Petersburg Electrotechnical University, Popov str. 5, RU-197376 St. Petersburg, Russia*
[3]*Petrozavodsk State University, Lenin str. 33, RU-185640 Petrozavodsk, Russia*
[4]*A. F. Ioffe Physico-Technical Institute, RU-194021 St. Petersburg, Russia*

(Received 31 October 2012; accepted 4 December 2012; published online 3 January 2013)

Influence of the order parameter symmetries on the cutoff parameter $\xi_h$ and vortex core size $\xi_2$ (the distance from the vortex center at which the current density reaches the maximum value) in the mixed state are investigated in the framework of Eilenberger theory for unconventional superconductors. The cutoff parameter determines the field distribution in the generalized London equation obtained as a projection of the quasiclassical theory. It is used for the fitting of the $\mu$SR and small-angle neutron scattering experimental data. Anisotropic $d_{x^2-y^2}$ and isotropic $s^{\pm}$-wave superconducting pairings are studied. These pairing symmetries can be realized in iron pnictide superconductors. Conventional $s_{++}$ pairing mediated electron-phonon interaction is also considered. Temperature, field, and impurity scattering dependences of $\xi_h/\xi_{c2}$ are obtained. It is found that normalized $\xi_2/\xi_{c2}(B/B_{c2})$ dependence is increasing with pair breaking impurity scattering (interband scattering for $s^{\pm}$-wave and intraband impurity scattering for $d$-wave superconductors). Here, $\xi_{c2}$ is the Ginzburg-Landau coherence length determined from the relation $B_{c2} = \Phi_0/2\pi\xi_{c2}^2$, where $B_{c2}$ is an upper critical field and $\Phi_0$ is a flux quantum. Two types of $\xi_2/\xi_{c2}(B/B_{c2})$ dependences are obtained for $s^{\pm}$ superconductors. It has minimum at low temperatures and small impurity scattering transforming in monotonously decreasing function at strong scattering and high temperatures. The second kind of this dependence was also found for $d$-wave superconductors at intermediate and high temperatures. In contrast, impurity scattering results in decreasing of $\xi_2/\xi_{c2}$ field dependence in $s_{++}$ superconductors. © *2013 American Institute of Physics*. [http://dx.doi.org/10.1063/1.4772670]

## I. INTRODUCTION

Since recently, there is a great interest to the magnetically mediated pairing in the strongly correlated electronic systems of unconventional superconductors. It can be realized in cuprates,[1] heavy fermions,[2] and iron pnictide superconductors.[3,4] Connection to the magnetism can explain the neutron magnetic resonance observed in the superconducting state in all above mentioned compounds.[5] In iron-based superconductors $s^{\pm}$, pairing is more preferable, but depending on the band structure $d$-wave symmetry can exist in electron pockets.[6,7] An example of simple transformation is doped $Ba_{1-x}K_xFe_2As_2$ compound. At optimal doping, this compound shows $s^{\pm}$ pairing symmetry. The $d$-wave pairing with strong hole doping is consistent with the observation of nodal quasiparticles[8] in the heavily hole doped superconductor $KFe_2As_2$ with $T_c = 3$ K. It was found that Co impurities rapidly suppress the superconductivity, with $T_c$ down to zero at only $x = 0.042$ in $K(Fe_{1-x}Co_x)_2As_2$. Such an effective suppression of $T_c$ by impurities is distinctly different from that observed in $Ba_{0.5}K_{0.5}Fe_2As_2$, but mimics that in $d$-wave cuprate and heavy-fermion superconductors. These results supported a $d$-wave superconducting state in $KFe_2As_2$.[9] Small-angle neutron scattering (SANS) investigation of flux lines lattice in super-clean $KFe_2As_2$ single crystals was done.[10] The results showed clear Bragg spots from a well ordered vortex lattice in a FeAs superconductor. With field parallel to the fourfold $c$-axis, nearly isotropic hexagonal packing of vortices was observed without vortex lattice symmetry transitions up to high fields, indicating rather small anisotropy of the superconducting properties around this axis. This observation is not consistent with gap nodes parallel to the $c$-axis implying more complex symmetry than $d$-wave pairing. Evidence of competing $s$- and $d$-wave pairing channels in iron-based superconductors was obtained by Raman scattering in $Ba_{0.6}K_{0.4}Fe_2As_2$.[11] Band dependent energy gaps along with excitonic Bardasis-Schrieffer modes characterizing, respectively, the dominant and subdominant pairing channel was observed.

Recent experiments on the alkali-intercalated iron selenides have raised questions about the symmetry of the superconducting phase. Random phase approximation calculations of the leading pairing eigenstate for a tightbinding 5-orbital Hubbard-Hund model of $AFe_2Se_2$ show that a $d$-wave ($B_{1g}$) state evolves into an extended $s^{\pm}$ ($A_{1g}$) state as the system is hole-doped. However, these two states are nearly degenerate over a range of doping.[12] Also, interpocket pairing and gap symmetry were investigated in Fe-based superconductors with only electron pockets. The pairing condensate in such systems contains not only intrapocket component but also interpocket component, made of fermions belonging to different electron pockets. The interplay between intrapocket and interpocket pairing was analyzed, depending on the ellipticity of electron pockets and

a)Electronic mail: polina.belova@lut.fi.

 

the strength of their hybridization. With increasing hybridization, the system undergoes a transition from a $d$-wave state to an $s^{\pm}$ state, in which the gap changes sign between hybridized pockets. This $s^{\pm}$ state has the full gap and at the same time supports spin resonance, in agreement with the data. Near the boundary between $d$ and $s^{\pm}$ states, a long-sought $s+id$ state which breaks time-reversal symmetry was found.[13]

A non-trivial orbital structure of the order parameter in $d$-wave symmetry, in particular, the presence of the gap nodes, leads to the effects of disorder in high-temperature superconductors being much richer than in conventional materials. For instance, in contrast to the $s$-wave case, the Anderson theorem does not work and non-magnetic impurities exhibit a strong pair breaking effect. Also, a finite concentration of disorder produces a non-zero density of quasiparticle states at zero energy, which results in a considerable modification of the thermodynamic and transport properties at low temperatures.[14]

The specific feature of iron pnictide is that they have multiband gap structure. In conventional 2-band superconductors with two different isotropic gaps, nonmagnetic impurities can either scatter quasiparticles between bands or within the same band. Interband processes will average the gaps and can thus lead to some initial $T_c$ suppression, after which $T_c$ will saturate until localization effects become important. Interband scattering is much more profound in a sign-changing 2-band system,[15] where nonmagnetic impurities with interband component of the scattering potential are pair breaking even if the gaps and densities of states are equal on both bands (symmetric model). In such a situation, $T_c$ will eventually be suppressed to zero at a finite critical concentration as in the theory of scattering by magnetic impurities in a 1-band $s$-wave system.[16] A given type of chemical impurity in a given host will be characterized crudely by an effective interband potential $\Gamma_0$ and an intraband potential $\Gamma_\pi$, and results for various quantities in the superconducting state will depend crucially on the size and relative strengths of these two quantities.[6]

In spite of success of $s^{\pm}$ model, there are some indications that a conventional $s$-wave state without sign reversal ($s_{++}$-wave state) is also a possible candidate for iron pnictides. It has been proposed that the moderate electron-phonon interaction due to Fe-ion oscillation can induce the critical orbital fluctuation, without being prohibited by the Coulomb interaction.[17]

By applying angle-resolved photoemission spectroscopy (ARPES) to LiFeAs, a clear fingerprint of the phonon spectrum in the fermionic self-energy was identified and estimation of the electron-phonon coupling strength was done, which appears to be sufficient to mediate the superconductivity. This result suggests that the superconductivity in pnictides could be based on the conventional phonon pairing enhanced by the van Hove singularity in the electronic density of states and by the strong electron-electron interaction.[18] Moreover, the momentum dependence of the superconducting energy gap rules out coupling through spin fluctuations and the sign change.[19] The ARPES results instead suggest that orbital fluctuations assisted by phonons[17,20] are the best explanation for superconductivity ($s_{++}$ pairing). Nevertheless, there is also other candidate for pairing symmetry in this compound. The functional-renormalization-group study shows that the pairing wave function is optimized in $s^{\pm}$ channel.[21] Model incorporating both $s_{++}$ and $s_{\pm}$ pairing couplings by using Bogoliubov de-Gennes equation was studied in Ref. 22. It was shown that the Zn-impurity strongly suppresses $s^{\pm}$ pairing and may induce a transition from $s^{\pm}$ to $s_{++}$-wave. This theory is consistent with various experiments on the impurity effect in the Zn-doping $SmFe_{1-x}Zn_xAsO_{0.9}F_{0.1}$.

Important information about the order parameter symmetry can be obtained from the investigation of the mixed state. The scanning tunneling microscopy (STM) experiments probe the spatial variation of the local density of states,[23] whereas $\mu$SR is sensitive to the spatial dependence of the local internal magnetic field $B(r)$.[24] Effects of anisotropic $s^{\pm}$-wave and isotropic $s_{++}$-wave pairings on the near-vortex local density of states in LiFeAs were studied,[25] by solving Bogoliubov-de Gennes equations both non-self-consistently and self-consistently. While the isotropic $s_{++}$-wave showed a square-like feature of roughly equal intensity, four "hot spots" developed in the case of an (anisotropic) $s^{\pm}$-wave gap. These results for the latter case qualitatively agree with recent experiments in Ref. 26. The vortex core size is determined from the $\mu$SR measurements by fitting them to a theoretical function for $B(r)$ that includes a cutoff function $F(\mathbf{G}, \xi_h)$, where $\mathbf{G}$ are the reciprocal lattice vectors and $\xi_h$ is the cutoff parameter. The functional form of $F(\mathbf{G}, \xi_h)$ depends on the spatial dependence of the superconducting order parameter $\Delta(r)$ in the core region.[27] Consequently, cutoff parameter $\xi_h$ is generally not the coherence length, but rather a measure of the vortex core size. A definition of the vortex core size is the radius $\xi_2$ at which the supercurrent density $|J(r)|$ calculated from $B(r)$ reaches a maximum. While this definition is robust with respect to the assumed model for $B(r)$, there is a contribution to the field dependence of $\xi_2$ that comes naturally from the overlap of the $J(r)$ profiles of neighboring vortices.[28] The radius $\xi_2$ is different from another characteristic length $\xi_1$ determining the initial slope of pairing potential. Here, we use the notation of the characteristic lengths from Ref. 29. The case of $s$-wave pairing was considered in Refs. 30 and 31.

The aim of our paper is to apply quasiclassical Eilenberger approach to the vortex state of unconventional superconductors considering $s^{\pm}$ and $d_{x^2-y^2}$-wave pairing symmetries as presumable states for the different levels of impurity scattering rates, to calculate the cutoff parameter, $\xi_h$,[32,33] vortex core size, $\xi_2$, and to compare results with $\mu$SR and SANS experimental data for iron pnictides.[34,35]

## II. VORTEX CORE SIZE

Following the microscopical Eilenberger theory, the cutoff parameter, $\xi_h$, can be found from the fitting of the calculated magnetic field distribution $h_E(\mathbf{r})$ to the Eilenberger-Hao-Clem (EHC) field distribution $h_{EHC}(\mathbf{r})$[32,33]

$$h_{EHC}(\mathbf{r}) = \frac{\Phi_0}{S}\sum_{\mathbf{G}}\frac{F(G)e^{i\mathbf{G}\mathbf{r}}}{1+\lambda^2 G^2}. \quad (1)$$

Here,

$$F(\mathbf{G}) = uK_1(u), \tag{2}$$

where $K_1(u)$ is modified Bessel function, $u = \xi_h G$, $S$ is the area of the vortex lattice unit cell, and $\lambda(T)$ is the penetration depth in the Meissner state. Because the magnetic field distribution is taken similar to the analytical solution of the Ginzburg-Landau model (AGL),[36] we will call this approach as EHC model and $\xi_h$ as AGL cutoff parameter.

While the fitting analysis of the $\mu$SR data is performed entirely in time domain, one can reconstruct $B(r)$ by Eq. (1) using the physical parameters deduced from the fitting analysis. The vortex core size defined by $J(\xi_2) = J_{max}$ (where $J_{max}$ denotes the maximum of $J(r)$) is considerably large than the magnetic cutoff parameter $\xi_h$. The result of a data analysis for various fields/temperatures indicates that $\xi_2$ is always proportional to $\xi_h$ at low fields.[37]

There are several characteristic lengths ($\xi_1$, $\xi_2$, $\xi_3$) describing the vortex core. In the AGL theory, the equality $\xi_h = \xi_1$ is suggested. Here, the order characteristic length $\xi_1$ is determined as $1/\xi_1 = (\partial|\Delta(r)|/\partial r)_{r=0}/|\Delta_{NN}|$, where $|\Delta_{NN}|$ is the maximum value of the order parameter along the nearest-neighbor direction which is the direction of taking the derivative. The length $\xi_1$ is directly connected with the length $\xi_3$ responsible for the density of states and STM measurements description.[29] The microscopical theory valid in the whole temperature range is the quasiclassical Eilenberger theory. The characteristic lengths $\xi_1$ and $\xi_2$ have been calculated.[29,38,39] The similarity $\xi_1(B) \approx \xi_2(B)$ was found for clean superconductors.[29] In this work, we are interested in current distribution in the mixed state and use the term core size for $\xi_2$ length like in Ref. 27.

In the analysis of the experimental data, $\lambda$ and $\xi_h$ are often considered as fitting parameters. Simultaneous experimental determination of $\lambda$ and $\xi_h$ without any restrictions is very problematic, regardless of the model used to describe the vortex state.[40] It has been suggested that $P(B)$ of flux-line lattice (FLL) can be explained using only one fitting parameter.[41] The magnetic-field penetration depth $\lambda(T)$ is assumed to be field independent and to have the same value as in the Meissner state. In this approach, all field dependent effects are taken into account in $\xi_h(B)$ dependence.

The London penetration depth can be measured with great precision and its variation with temperature depends sensitively on the gap structure. For $T = T_c/3$, a conventional isotropic $s$-wave gap $\Delta_0$ results in an exponential behavior, $\Delta\lambda(T) \propto \exp(-\Delta_0/T)$, which is preserved even with the addition of non-magnetic impurities. Unconventional pairing states, on the other hand, are susceptible to the presence of non-magnetic impurities.[42] In nodal $d$-wave superconductors, $\lambda(T)$ exhibits a power-law behavior, $\Delta\lambda(T) \propto T^n$, with the exponent $n$ increasing from $n = 1$ in the clean case to $n = 2$ in the dirty limit.[43] For the extended $s^{\pm}$ state, the opposite trend is expected: $\Delta\lambda(T)$ is exponential in the clean limit, changing with disorder to a power-law, with $n$ as low as 1.6.[42]

Experimentally, a power-law behavior with the exponent $2 \leq n < 3$ has been observed in most of the iron based superconductors. This characteristic exponent $n \sim 2$ can be explained in both dirty $d$-wave and dirty $s^{\pm}$ scenarios.[44] The disorder is always present in the iron-based superconductors where doping is needed to induce superconductivity. Irradiation with Pb ions was used to study the effect of disorder on the in-plane London penetration depth, $\lambda(T)$, in single crystals of $Ba(Fe_{1-x}T_x)_2As_2$ (T = Co, Ni). An increase of the irradiation dose resulted in a monotonic decrease of the superconducting transition temperature, $T_c$, without affecting much the transition width. In both Co and Ni doped systems, a power-law behavior was observed, $\Delta\lambda(T) \propto T^n$, with the exponent $n$ systematically decreasing with the increase of disorder. This observation was supported by the theoretical analysis, conclusively pointed to a nodeless $s^{\pm}$ state with pair breaking impurity scattering (interband) with strength being intermediate between Born and unitary limits.[45]

In $d_{x^2-y^2}$-wave superconductor, $\lambda(T)$ in Eq. (1) is given as[46]

$$\frac{\lambda_{L0}^2}{\lambda^2(T)} = 2\pi T \oint \frac{d\theta}{2\pi} \sum_{\omega_n>0} \frac{|\tilde{\Delta}(\theta)|^2}{(\tilde{\omega}_n^2 + |\tilde{\Delta}(\theta)|^2)^{3/2}}, \tag{3}$$

where

$$\tilde{\omega}_n = \omega_n + \Gamma \left\langle \frac{\tilde{\omega}_n}{\sqrt{\tilde{\omega}_n^2 + |\tilde{\Delta}(\vec{p}_f', \omega_n)|^2}} \right\rangle_{\vec{p}_f'}, \tag{4}$$

$$\tilde{\Delta}(\vec{p}_f; \omega_n) = \Delta(\vec{p}_f) + \Gamma \left\langle \frac{\tilde{\Delta}(\vec{p}_f', \omega_n)}{\sqrt{\tilde{\omega}_n^2 + |\tilde{\Delta}(\vec{p}_f', \omega_n)|^2}} \right\rangle_{\vec{p}_f'}, \tag{5}$$

$$\Delta(\vec{p}_f) = \int d\vec{p}_f' V(\vec{p}_f, \vec{p}_f') \pi T \times \sum_{\omega_n}^{|\omega_n|<\omega_c} \frac{\tilde{\Delta}(\vec{p}_f')}{\sqrt{\tilde{\omega}_n^2 + |\tilde{\Delta}(\vec{p}_f')|^2}}. \tag{6}$$

Because of the symmetry of $d_{x^2-y^2}$-wave pairing the impurity induced corrections for the pairing potential in Eq. (5) are zero and $\tilde{\Delta} = \Delta$. This is different from the $s^{\pm}$- and $s_{++}$ cases, where the corrections are not zero. Fig. 1(a) shows the calculated temperature dependence of the superfluid density $\rho_S(T)/\rho_{S0} = \lambda_{L0}^2/\lambda^2(T)$ with different values of impurity scattering $\Gamma$ for $d_{x^2-y^2}$-wave pairing symmetry. Flattening of this dependence with increasing $\Gamma$ is visible in accordance with previous results.[43] To study high the field regime, we need to calculate the upper critical field $B_{c2}(T)$. For $d_{x^2-y^2}$-wave, superconductors $B_{c2}(T)$ is given in Ref. 47. The temperature dependence of the upper critical field $B_{c2}$ with different values of impurity scattering $\Gamma$ for $d_{x^2-y^2}$-wave pairing symmetry is demonstrated in Fig. 1(b). Figs. 1(a) and 1(b) are similar to those in $s^{\pm}$-wave superconductors. $T_c$ is suppressed by impurity scattering resulting in the same expressions for $s^{\pm}$ and $d$-wave superconductors with replacing $\Gamma_\pi \to \Gamma/2$.

The penetration depth for $s^{\pm}$-wave superconductor was calculated in Ref. 42

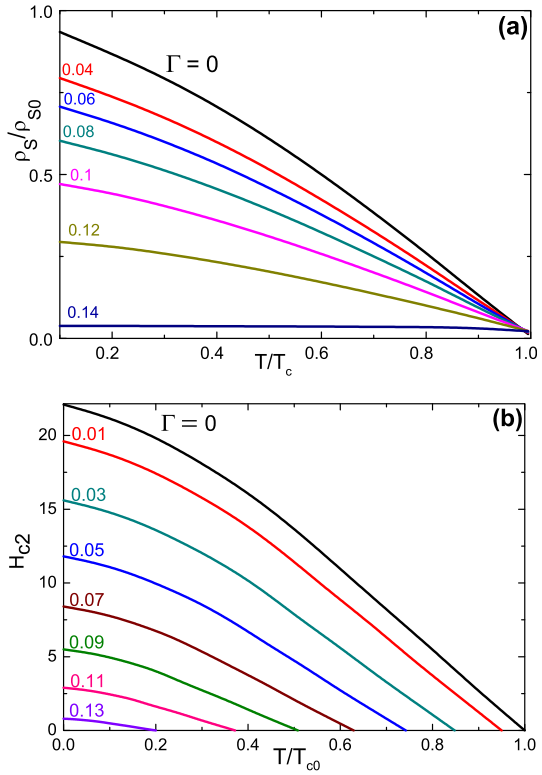


FIG. 1. (a) The temperature dependence of superfluid density $\rho_S(T)/\rho_{S0}$ with different values of impurity scattering $\Gamma$ for $d_{x^2-y^2}$-wave pairing symmetry. (b) The temperature dependence of the upper critical field $B_{c2}$ with different values of impurity scattering $\Gamma$ for $d_{x^2-y^2}$-wave pairing symmetry.

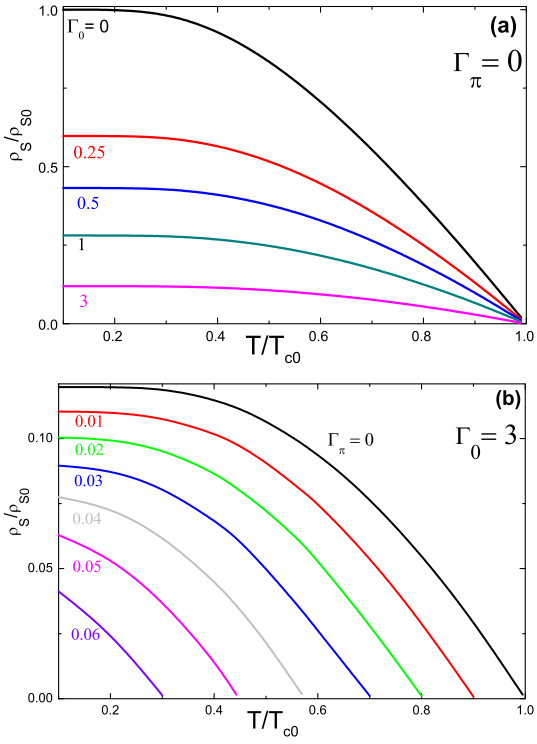


FIG. 2. The temperature dependence of superfluid density $\rho_S(T)/\rho_{S0}$ for $s^{\pm}$-wave superconductors at (a) interband scattering rate $\Gamma_\pi = 0$ with different values of intraband scattering $\Gamma_0$ and (b) intraband scattering rate $\Gamma_0 = 3$ with different values of interband scattering $\Gamma_\pi$.

$$\frac{\lambda_{L0}^2}{\lambda^2(T)} = 2\pi T \sum_{\omega_n>0} \frac{\bar{\Delta}_n^2}{\eta_n(\bar{\Delta}_n^2+\omega_n^2)^{3/2}}, \tag{7}$$

where $\lambda_{L0}$ is the London penetration depth at $T=0\,\mathrm{K}$ in the absence of the impurities and $\eta_n = 1 + 2\pi * (\Gamma_0 + \Gamma_\pi) \Big/ \left(\sqrt{\bar{\Delta}_n^2+\omega_n^2}\right)$. Here, $\Gamma_0 = \pi n_i N_F |u_0|^2$ and $\Gamma_\pi = \pi n_i N_F |u_\pi|^2$ are the intra- and interband impurity scattering rates, respectively ($u_{0,\pi}$ are impurity scattering amplitudes with correspondingly small, or close to $\pi = (\pi,\pi)$, momentum transfer). Fig. 2 shows the calculated temperature dependence of the superfluid density $\rho_S(T)/\rho_{S0} = \lambda_{L0}^2/\lambda^2(T)$, with different values of impurity scattering $\Gamma$ for $s^{\pm}$-wave pairing symmetry.

In Eq. (7), $\bar{\Delta}_n = \Delta(T) - 4\pi\Gamma_\pi\bar{\Delta}_n/\sqrt{\bar{\Delta}_n^2+\omega_n^2}$ for the $s^{\pm}$ pairing and $\bar{\Delta}_n = \Delta(T)$ for the $s_{++}$ pairing symmetry. The order parameter $\Delta(T)$ in Meissner state is determined by the selfconsistent equation

$$\Delta(T) = 2\pi T \sum_{0<\omega_n<\omega_c} \frac{V^{SC}\bar{\Delta}_n}{\sqrt{\bar{\Delta}_n^2+\omega_n^2}}. \tag{8}$$

## III. RESULTS FOR $d_{x^2-y^2}$-WAVE PAIRING SYMMETRY

To consider the mixed state of a $d$-wave superconductor, we take the center of the vortex as the origin and assume that the Fermi surface is isotropic and cylindrical. With the Riccati transformation of the Eilenberger equations, quasiclassical Green functions $f$ and $g$ can be parameterized via functions $a$ and $b$ (Ref. 39)

$$\bar{f} = \frac{2a}{1+ab}, \quad f^{\dagger} = \frac{2b}{1+ab}, \quad g = \frac{1-ab}{1+ab}, \tag{9}$$

satisfying the nonlinear Riccati equations. The Riccatti equations for $d_{x^2-y^2}$-wave superconductivity in Born impurity scattering are[48]

$$\mathbf{u}\cdot\nabla a = -a[2(\omega_n+G) + i\mathbf{u}\cdot\mathbf{A}_E] + \Delta - a^2\Delta^*, \tag{10}$$

$$\mathbf{u}\cdot\nabla b = b[2(\omega_n+G) + i\mathbf{u}\cdot\mathbf{A}_E] - \Delta^* + b^2\Delta, \tag{11}$$

where $G = 2\pi\langle g\rangle\Gamma$ and $\mathbf{u}$ is a unit vector of the Fermi velocity. In the new gauge, vector-potential $\mathbf{A}_E = \mathbf{A} - \nabla\Phi$ is proportional to the superfluid velocity. It diverges as $1/r$ at the vortex center. The FLL creates the anisotropy of the electron spectrum. Therefore, the impurity renormalization correction in Eqs. (10) and (11), averaged over the Fermi surface, can be reduced to averages over the polar angle $\theta$, i.e., $\langle\ldots\rangle = (1/2\pi)\int\ldots d\theta$.

To take into account the influence of screening, the vector potential $\mathbf{A_E}(\mathbf{r})$ in Eqs. (18) and (19) is obtained from the equation:

$$\nabla\times\nabla\times\mathbf{A_E} = \frac{4}{\kappa^2}\mathbf{J}, \tag{12}$$

where the supercurrent $\mathbf{J}(\mathbf{r})$ is given in terms of $g(\omega_n,\theta,\mathbf{r})$ by

$$\mathbf{J}(\mathbf{r}) = 2\pi T \sum_{\omega_n>0} \int_0^{2\pi} \frac{d\theta}{2\pi} \frac{\hat{\mathbf{k}}}{i} g(\omega_n, \theta, \mathbf{r}). \quad (13)$$

Here $\mathbf{A_E}$ and $\mathbf{J}$ are measured in units of $\Phi_0/2\pi\xi_0$ and $2ev_F N_0 T_c$, respectively. The spatial variation of the internal field $h_E(\mathbf{r})$ is determined through

$$\nabla \times \mathbf{A_E} = \mathbf{h_E}(\mathbf{r}). \quad (14)$$

The self-consistent condition for the pairing potential $\Delta(r)$ for $d$-wave pairing is

$$\Delta(\theta, \mathbf{r}) = V^{SC}_{d_{x^2-y^2}} 2\pi T \cos(2\theta) \times \sum_{\omega_n>0}^{\omega_c} \int_0^{2\pi} \frac{d\bar{\theta}}{2\pi} f(\omega_n, \bar{\theta}, \mathbf{r}) \cos(2\bar{\theta}), \quad (15)$$

where $V^{SC}_{d_{x^2-y^2}}$ is a coupling constant in the $d_{x^2-y^2}$ pairing channel and $\omega_c$ is the ultraviolet cutoff determining $T_{c0}$. Here, $\Gamma$ is impurity scattering rate. The obtained solution is fitted to Eq. (1) giving the value of cutoff parameter $\xi_h$ for $d_{x^2-y^2}$-wave pairing symmetry.

To study the obtained $\xi_h(B, T, \Gamma_0, \Gamma_\pi)$ dependences, it is convenient to use the normalization to the coherence length $\xi_{c2}$, determined from the upper critical field $B_{c2} = \Phi_0/2\pi\xi^2_{c2}$ (in our units $\xi_{c2} = 1/\sqrt{B_{c2}}$). For $d_{x^2-y^2}$-wave, $B_{c2}(T)$ is given as[47]

$$\ln\left(\frac{T}{T_c}\right) - \Psi\left(\frac{1}{2} + \frac{v}{2t_c}\right) + \Psi\left(\frac{1}{2} + \frac{v}{2t}\right) = \frac{3}{2} \int_0^\infty \frac{du}{shu} \int_0^1 dz (1 - z^2)[e^{-x}(1 - 2xc)^{-1}] e^{-\frac{v}{t}u}, \quad (16)$$

$$c\left[\ln\left(\frac{T}{T_c}\right) - \Psi\left(\frac{1}{2} + \frac{v}{2t_c}\right) + \Psi\left(\frac{1}{2} + \frac{v}{2t}\right)\right] = \frac{3}{2} \int_0^\infty \frac{du}{shu} x \int_0^1 dz |(1 - z^2) \times [e^{-x}(-x + c(1 - 4x + 2x^2)) - c] e^{-\frac{v}{t}u}, \quad (17)$$

where $v = 2\Gamma$, $t = T/T_{c0}$, $t_c = T_c/T_{c0}$ and $x = \rho u^2(1 - z^2)$, $\rho = B/(4\pi t)^2$. Fig. 1(b) depicts the temperature dependence of the upper critical field $B_{c2}$ with different values of impurity scattering $\Gamma$. Because of pair breaking effect of impurities the upper critical field decreases with increasing $\Gamma$. This is opposite to $s$-wave superconductors, where impurity scattering results in rise of $B_{c2}$.

Fig. 3 demonstrates the magnetic field dependence of cutoff parameter $\xi_h/\xi_{c2}$ at different temperatures $(T/T_{c0} = 0.2, 0.3, 0.4, 0.5, 0.7, 0.8)$ for $d_{x^2-y^2}$ pairing with $\Gamma = 0.01$. Kramer-Pesch effect obtained for single vortex[49] remains also for vortex lattice in $d_{x^2-y^2}$-wave superconductors. Field and temperature dependences of $\xi_h/\xi_{c2}$ are similar to those in $s$-wave superconductors:[50] $\xi_h/\xi_{c2}(B/B_{c2})$ dependence has minimum at high temperatures and shows monotonously increasing behavior at low temperatures.

Figs. 4 and 5 show the impurity scattering $\Gamma$ dependences of $\xi_h/\xi_{c2}$ for $d_{x^2-y^2}$ pairing at different temperatures and different fields, respectively. In contrast to $s$-wave superconductors[30,31] the pair breaking effect in $d$-wave symmetry gives rise to growth of $\xi_h/\xi_{c2}$.

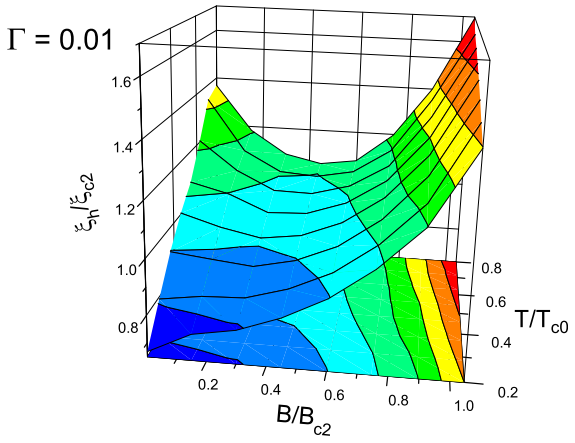


FIG. 3. Three dimensional magnetic field dependence of the cutoff parameter $\xi_h/\xi_{c2}$ with different temperatures for $d_{x^2-y^2}$ pairing symmetry with $\Gamma = 0.01$.

Fig. 6 presents the magnetic field dependence of $\xi_2/\xi_{c2}$ with different impurity scattering rates $\Gamma$ at $T/T_{c0} = 0.5$ (main panel) and $T/T_{c0} = 0.9$ (inset) for $d_{x^2-y^2}$ pairing symmetry. A similar increasing in field dependence of the vortex core size has been found in the framework of Bogoliubov-de Gennes equations for clean superconductors.[27] Our consideration includes effects of impurity. It shows that the core size increases with $\Gamma$ similar to the cutoff parameter behavior (Fig. 5). Monotonously decreasing behavior of $\xi_2/\xi_{c2}(B/B_{c2})$ is often observed experimentally in different superconductor compounds.[24,41]

## IV. RESULTS FOR $s^{\pm}$-WAVE PAIRING SYMMETRY

In Born approximation for impurity scattering in $s^{\pm}$-wave superconductivity, we have

$$\mathbf{u} \cdot \nabla a = -a[2(\omega_n + G) + i\mathbf{u} \cdot \mathbf{A}_E] + (\Delta + F) - a^2(\Delta^* + F^*), \quad (18)$$

$$\mathbf{u} \cdot \nabla b = b[2(\omega_n + G) + i\mathbf{u} \cdot \mathbf{A}_E] - (\Delta^* + F^*) + b^2(\Delta + F), \quad (19)$$

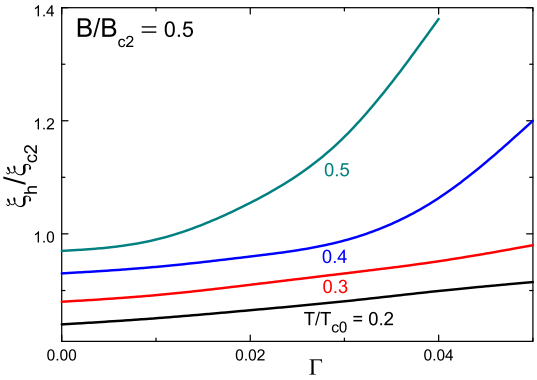


FIG. 4. The magnetic field dependence of the cutoff parameter $\xi_h/\xi_{c2}$ with different impurity scattering rates $\Gamma$ and temperatures $T/T_{c0}$ at $B/B_{c2} = 0.5$ for $d_{x^2-y^2}$ pairing symmetry.

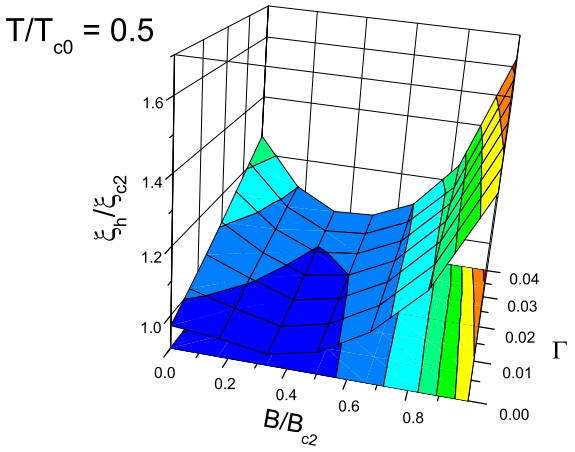


FIG. 5. The three dimensional magnetic field dependence of the cutoff parameter $\xi_h/\xi_{c2}$ with different impurity scattering rates $\Gamma$ with $T/T_{c0} = 0.5$ for $d_{x^2-y^2}$ pairing symmetry.

where $\omega_n = \pi T(2n+1)$, $G = 2\pi\langle g\rangle(\Gamma_0 + \Gamma_\pi) \equiv 2\pi\langle g\rangle\Gamma^*$, $F = 2\pi\langle f\rangle(\Gamma_0 - \Gamma_\pi)$ for $s^{\pm}$ pairing symmetry and $F = 2\pi\langle f\rangle\Gamma^*$ for the $s_{++}$ pairing symmetry.

The self-consistent condition for the pairing potential $\Delta(\mathbf{r})$ in the vortex state is given by

$$\Delta(\mathbf{r}) = V^{SC}2\pi T\sum_{\omega_n>0}\int_0^{2\pi}\frac{d\theta}{2\pi}f(\omega_n,\theta,\mathbf{r}), \qquad (20)$$

where $V^{SC}$ is the coupling constant.[33]

Using the similarity to the model of spin-flip superconductors, $B_{c2}(T)$ for two-dimensional $s^{\pm}$ pairing can be determined from the equations:[51]

$$\ln\left(\frac{T_{c0}}{T}\right) = 2\pi T\sum_{n\geq 0}[\omega_n^{-1} - 2D_1(\omega_n, B_{c2})], \qquad (21)$$

where

$$D_1(\omega_n, B_{c2}) = J(\omega_n, B_{c2}) \times [1 - 2(\Gamma_0 - \Gamma_\pi)J(\omega_n, B_{c2})]^{-1}, \qquad (22)$$

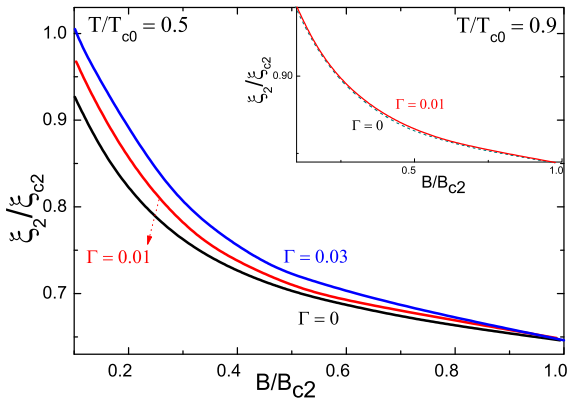


FIG. 6. The magnetic field dependence of $\xi_2/\xi_{c2}$ with different impurity scattering rates $\Gamma$ at $T/T_{c0} = 0.5$ (main panel) and $T/T_{c0} = 0.9$ (inset) for $d_{x^2-y^2}$ pairing symmetry.

$$J(\omega_n, B_{c2}) = \left(\frac{4}{\pi B_{c2}}\right)^{1/2} \times \int_0^{\infty} dy\exp(-y)\arctan\left[\frac{(B_{c2}y)^{1/2}}{\alpha}\right], \qquad (23)$$

where $\alpha = 2(\omega_n + \Gamma_0 + \Gamma_\pi)$.

Dashed line in Fig. 7(a) demonstrates the result of AGL theory for $\xi_v$ (Ref. 36)

$$\xi_v = \xi_{c2}\left(\sqrt{2} - \frac{0.75}{\kappa_{GL}}\right)(1+b^4)^{1/2}[1-2b(1-b)^2]^{1/2}. \qquad (24)$$

Here, we use the notation of the AGL theory for the cutoff parameter ($\xi_v$) and $b = B/B_{c2}$. This dependence with $\xi_{c2}$ as a fitting parameter is often used for the description of the experimental $\mu$SR results.[24,28] As can be seen from Fig. 7(a), the magnetic field dependence of $\xi_h/\xi_{c2}$ is nonuniversal because it depends not only on $B/B_{c2}$ (as in the AGL theory, dashed line in Fig. 7(a)), but also on interband and intraband impurity scattering parameters. In the cases where $\Gamma_0 = \Gamma_\pi = 0$, the results are the same for $s^{\pm}$ and $s_{++}$ pairing symmetries. We indicated that this curve is "clean" one. In

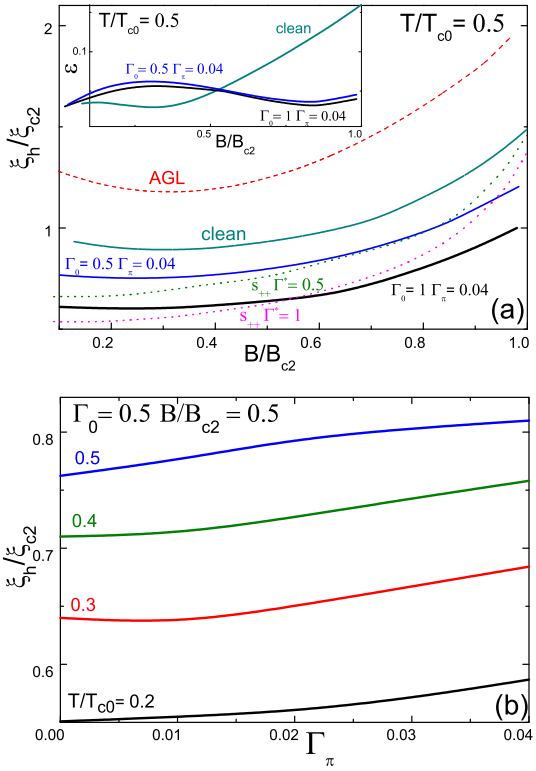


FIG. 7. (a) The magnetic field dependence of $\xi_h/\xi_{c2}$ for superconductors with impurity scattering. The solid lines represent our solution of Eilenberger equations at $T/T_{c0} = 0.5$ for "clean" case ($\Gamma_0 = \Gamma_\pi = 0$) and $s^{\pm}$ model ($\Gamma_0 = 0.5$, $\Gamma_\pi = 0.04$ and $\Gamma_0 = 1$, $\Gamma_\pi = 0.04$). The dotted lines show result for $s_{++}$ model ($\Gamma^* = 0.5$ and $\Gamma^* = 1$). Dashed line demonstrates the result of the AGL theory for $\xi_v$ from Eq. (24). The inset shows the magnetic field dependence of mean square deviation of the $h_{EHC}$ distribution from the Eilenberger distribution normalized by the variance of the Eilenberger distribution, $\varepsilon$, for $T/T_{c0} = 0.5$ at $\Gamma_0 = \Gamma_\pi = 0$ ("clean"); $\Gamma_0 = 0.5$, $\Gamma_\pi = 0.04$ and $\Gamma_0 = 1$, $\Gamma_\pi = 0.04$. (b) The interband scattering $\Gamma_\pi$ dependence of $\xi_h/\xi_{c2}$ at different temperatures $T/T_{c0}$ (intraband scattering $\Gamma_0 = 0.5$ and $B/B_{c2} = 0.5$) for the $s^{\pm}$ pairing.

this figure, the case $\Gamma_0 \gg \Gamma_\pi$ is considered and the value of $\xi_h$ is reduced considerably in comparison with the clean case. One can compare the observed behavior with that in $s_{++}$ pairing model. In $s_{++}$ pairing symmetry, the intraband and interband scattering rates act in a similar way and $\xi_h/\xi_{c2}$ decreases always with impurity scattering. In contrast, in $s^{\pm}$ model $\xi_h/\xi_{c2}(B/B_{c2})$ dependences show different forms of behavior with $\Gamma_\pi$. Here, $\xi_h/\xi_{c2}$ increases with $\Gamma_\pi$ at $B/B_{c2} < 0.8$ and decreases at higher fields, i.e., the curves become more flattened. A crossing point appears in the dependences $\xi_h/\xi_{c2}(B/B_{c2})$ for $s^{\pm}$ and $s_{++}$ pairing. We also calculated the magnetic field dependence of mean square deviation of $h_{EHC}$ distribution of the magnetic field from the Eilenberger distribution normalized by the variance of the Eilenberger distribution $\varepsilon = \sqrt{\overline{(h_E - h_{EHC})^2}/\overline{(h_E - B)^2}}$, where $\overline{\cdots}$ is the average over a unit vortex cell. The inset to Fig. 7(a) demonstrates $\varepsilon(B)$ dependence for $T/T_{c0} = 0.5$ at $\Gamma_0 = 0$, $\Gamma_\pi = 0$; $\Gamma_0 = 0.5$, $\Gamma_\pi = 0.04$ and $\Gamma_0 = 1$, $\Gamma_\pi = 0.04$. From this figure, it can be seen that the accuracy of effective London model is deteriorating as the magnetic field increases; however, in superconductors with impurity scattering the accuracy is below 6% even when it is close to the second critical field (the inset to Fig. 7(a)).

In Fig. 7(b), the interband scattering $\Gamma_\pi$ dependences of $\xi_h$ are presented in low fields for the $s^{\pm}$ pairing at different temperatures $T$. As can be seen, $\xi_h/\xi_{c2}$ increases with the interband scattering rate $\Gamma_\pi$. Strong decreasing of $\xi_h/\xi_{c2}$ with a decrease in the temperature can be explained by the Kramer-Pesch effect.[52] Recently, the image of the vortices in a wide field range from 0.1 T to 11 T by mapping the tunneling conductance at the Fermi energy in LiFeAs compound was obtained.[26] It was found that the vortex radius shrinked with decreasing temperature and became smaller than the coherence length estimated from the upper critical field. This effect was considered as a direct evidence of the Kramer-Pesch effect expected in a clean superconductor.[26] It should be noted that the normalization constant $\xi_{c2}$ increases with $\Gamma_\pi$ because $\Gamma_\pi$ suppress $T_c$ similar to superconductors with spin-flip scattering (violation of the Anderson theorem). Thus, rising of $\xi_h/\xi_{c2}$ implies more strong growth of $\xi_h$ than $\xi_{c2}$ (from GL theory one would expect $\xi_h/\xi_{c2} = \text{Const}$). Qualitatively, it can be explained by the strong temperature dependence of $\xi_h(B, T/T_c)$, which is connected to the Kramer-Pesch effect.[52] Increasing $\Gamma_\pi$ results in suppression of $T_c$, i.e., effective increasing of $T$ and $\xi_h(T/T_c)$. The $\xi_{c2}(T/T_c)$ does not have such a strong $T_c$ dependence, thus, leading to the increase of $\xi_h/\xi_{c2}$ ratio with $\Gamma_\pi$. The small value of the cutoff parameter ($\xi_h/\xi_{c2} \sim 0.4$ at $T/T_c = 0.18$) was observed in iron pnictide $BaFe_{1.82}Co_{0.18}As$,[34] which is comparable with our theoretical prediction, Fig. 7(b). In Ref. 34, the magnetic field distribution shape of the sample was explained by effects of field-induced magnetic order and vortex-lattice disorder. Our consideration shows the importance of impurity scattering even in the triangular lattice giving another possible explanation of the experimental results.

We also study the case of weak intraband scattering. This case can be realized in stoichiometrical pnictides such as LiFeAs. The symmetry of the order parameter in this compound is under discussion now. A combined density-functional theory and functional-renormalization-group method was introduced[21] which took into account orbital-dependent interaction parameters to derive the effective low-energy theory of weakly to intermediately correlated Fermi systems. The competing fluctuations were investigated and the superconducting order parameter was found to be of the $s^{\pm}$ type, driven by collinear antiferromagnetic fluctuations.[21] In contrast, the conventional phonon pairing enhanced by the van Hove singularity in the electronic density of states and by the strong electron-electron interaction was suggested.[18] The high value $\xi_h(B \to 0, T = 0) = 9.8\,\text{nm}$ was obtained in SANS measurements in LiFeAs (Ref. 35) in comparison with $\xi_{c2}(T = 0) \approx 4.6\,\text{nm}$,[53] i.e., $\xi_h/\xi_{c2} \approx 2.1$. For the simplicity, we considered the same scattering parameters $\Gamma_0 = \Gamma_\pi = \Gamma$. The inset to Fig. 8 presents the $\xi_h/\xi_{c2}$ field dependence at $\Gamma_0 = \Gamma_\pi = \Gamma = 0, 0.05, 0.06, 0.065$ and $T/T_{c0} = 0.15$. The dotted line shows the result for $s_{++}$ model ($\Gamma^* = 0.5$). As can be seen from this picture, the shape of curve does not change considerably, but the absolute values of $\xi_h/\xi_{c2}$ depend crucially on it. At low values of $\Gamma$, $\xi_h/\xi_{c2}$ resides below the AGL curve and moves above it at high $\Gamma$ (for gapless superconductivity case $\Gamma > 0.064$). Such behavior is quite different from that in $s_{++}$ pairing symmetry where intraband and interband scattering rates act in similar way and $\xi_h/\xi_{c2}$ decreases always with impurity scattering. The obtained $\xi_h(B \to 0)/\xi_{c2} = 1.8$ in the $s^{\pm}$ model is much more near to the experimental results[35] than in the $s_{++}$ model, where strong reduction of $\xi_h$ is visible. But this requires too high value of $\Gamma_\pi > 0.064$, so sample would be in the gapless state in this case. This contradicts to the observed value of gap by the ARPES measurements.[35]

Pair breaking effects can improve the comparison between theory and experiments, but they are not enough to resolve the contradiction. We believe that inclusion of the field-induced antiferromagnetic (AFM) fluctuations can improve the model. Field-induced magnetism has been investigated in cuprate superconductors, particularly following neutron studies of $La_{2-x}Sr_xCuO_4$,[54] the results of which

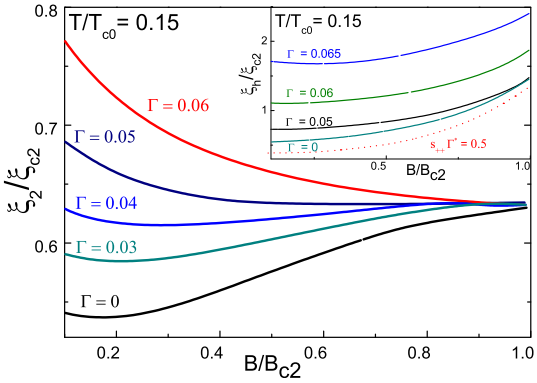


FIG. 8. The magnetic field dependence of $\xi_2/\xi_{c2}$ with the same values of intraband $\Gamma_0$ and interband $\Gamma_\pi$ scattering rate $\Gamma$ ($\Gamma = 0, 0.03, 0.04, 0.05, 0.06$) at $T/T_{c0} = 0.15$ for $s^{\pm}$ pairing symmetry. The inset shows magnetic field dependence of the cutoff parameter at $T/T_{c0} = 0.15$ with the same values of intraband $\Gamma_0$ and interband $\Gamma_\pi$ scattering rate $\Gamma$ ($\Gamma = 0$ for "clean" case and $\Gamma = 0.05, 0.06, 0.065$ for the $s^{\pm}$ pairing). Dotted line shows result for $s_{++}$ model ($\Gamma^* = 0.5$).

have been interpreted as microscopic phase coexistence of spin density wave and superconducting states, driven by coupling of the two order parameters.[55] Such effect has been observed in same samples of LiFeAs.[56] Enhanced value of the $\xi_h$ in undoped cuprates with increasing of AFM has been observed by $\mu$SR measurements in La-based[37] and Y-based[57] high $T_c$ cuprates. A model calculation based on Bogoliubov-de Gennes theory, where both the $d$-wave superconductivity and the spatially modulated AFM spin correlations are simultaneously considered by incorporating a pairing interaction to the standard Hubbard model for two-dimensional square lattice.[58] It has been shown that an expansion of the vortex cores with decreasing hole doping can result from a strengthening of AFM correlations competing with superconductivity.[37] In the framework of our model, it means that the local increasing of $\Gamma_\pi$ is induced by AFM fluctuations inside the vortex core. In this case, the $\xi_h$ (determined by $\mu$SR or SANS measurements) is connected with $\Gamma_\pi^{core}$ and the value of gap (determined by ARPES) is dependent on $\Gamma_\pi^{balk}$, where $\Gamma_\pi^{core} > \Gamma_\pi^{bulk}$ resulting from AFM. Taking into account, two different nodeless gaps found by scanning tunneling spectroscopy[59] can also improve the theory and experiments matching.

The difference between pairing symmetries reveals itself in impurity scattering dependence of $\xi_h/\xi_{c2}$. In $s_{++}$ symmetry, $\xi_h/\xi_{c2}$ always decreases with impurity scattering rate $\Gamma$ (Fig. 7(a)), in $s^{\pm}$ symmetry its behavior depends on the field range and relative values of intraband and interband impurity scattering rates: it can be a decreasing function of $\Gamma_\pi$ (Ref. 60) or an increasing function of $\Gamma_\pi$ (Fig. 7(b)). In $d$-wave superconductors $\xi_h/\xi_{c2}$ always increases with $\Gamma$ (Fig. 4) similar to the case of $s^{\pm}$ symmetry with $\Gamma_0 = \Gamma_\pi$ (inset to Fig. 8). This can be understood from the comparison of the Ricatti equations of the $s^{\pm}$ and $d$-wave pairing. In both cases, the renormalization factor $F = 0$ due to a cancelation of the intraband and interband impurity scattering rates in $s^{\pm}$ pairing or symmetry reason $\langle f \rangle = 0$ for $d$-wave pairing.

Fig. 8 shows the magnetic field dependence of $\xi_2/\xi_{c2}$ with different impurity scattering rates $\Gamma$ with $T/T_{c0} = 0.15$ for $s^{\pm}$ pairing symmetry. It can be seen from this figure that the normalized vortex core size increases monotonously with growth of impurity scattering rate. The shape of $\xi_2/\xi_{c2}(B/B_{c2})$ curve also changes: curves with minimum at small $\Gamma$ transform to the monstrously decreasing field dependent function at high $\Gamma$, i.e., crossover from $d\xi_2/dB > 0$ to $d\xi_2/dB < 0$ behavior at $B = B_{c2}$ occurs. Different shapes of core size field dependence were observed in reversible magnetization experiments.[41] The dependence $\xi_2/\xi_{c2}(B/B_{c2})$ at $\Gamma = 0.06$ looks similar to that obtained from the Usadel equation for dirty $s$-wave superconductors.[61] The impurity transformation of the shape $\xi_2/\xi_{c2}$ is like order parameter coherence length found from numerical solution of Eilenberger equations[39] for $s$-wave superconductors (Fig. 10 in Ref. 41). The value of half-width-at-half-maximum (HWHM) of tunneling-conductance vortex images of LiFeAs $\sim$2.5 at $T \to 0$,[26] i.e., HWHM/$\xi_{c2} \approx 0.54$ comparable to our results $\xi_2/\xi_{c2}$. We note here that the value of HWHM is similar to value $\xi_2$ (Ref. 61) in Fig. 8.

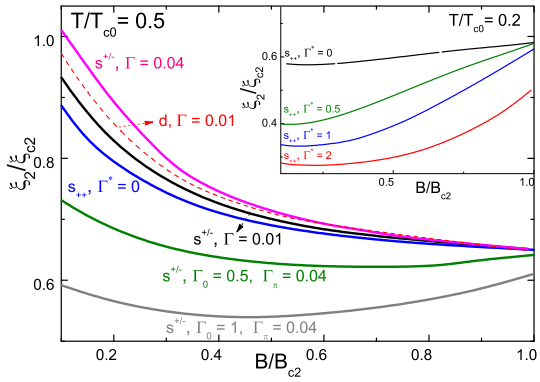


FIG. 9. The magnetic field dependence of $\xi_2/\xi_{c2}$ with different impurity scattering rates $\Gamma$ with $T/T_{c0} = 0.5$ for $s_{++}$ model ($\Gamma^* = 0$), for $s^{\pm}$ pairing symmetry ($\Gamma_0 = \Gamma_\pi = \Gamma = 0.01, 0.04$, $\Gamma_0 = 0.5$, $\Gamma_\pi = 0.04$ and $\Gamma_0 = 1$, $\Gamma_\pi = 0.04$) and $d$-wave pairing symmetry ($\Gamma = 0.01$). The inset shows magnetic field dependence of $\xi_2/\xi_{c2}$ at $T/T_{c0} = 0.2$ with different impurity scattering rates ($\Gamma = 0, 0.5, 1, 2$) for $s_{++}$ symmetry.

Fig. 9 depicts the magnetic field dependence of $\xi_2/\xi_{c2}$ with different impurity scattering rates $\Gamma$ at $T/T_{c0} = 0.5$ for $s_{++}$ model ($\Gamma^* = 0$), for $s^{\pm}$ pairing symmetry ($\Gamma_0 = \Gamma_\pi = \Gamma = 0.01, 0.04$, $\Gamma_0 = 0.5$, $\Gamma_\pi = 0.04$, and $\Gamma_0 = 1$, $\Gamma_\pi = 0.04$) and $d$-wave pairing symmetry ($\Gamma = 0.01$). It can be seen from Fig. 9 that all considered pairing symmetries result in similar monotonously decreasing $\xi_2/\xi_{c2}(B/B_{c2})$ dependence at weak impurity scattering rates and intermediate temperatures. The difference between $s^{\pm}$ and $d$-wave pairing can be obtained by introducing impurities. Intraband impurity scattering for $s^{\pm}$ pairing symmetry results in strong decreasing $\xi_2/\xi_{c2}$ value while in $d$-wave superconductors it increases with impurity scattering. The inset shows magnetic field dependence of $\xi_2/\xi_{c2}$ at $T/T_{c0} = 0.2$ with different impurity scattering rates ($\Gamma = 0, 0.5, 1, 2$) for $s_{++}$ symmetry. Here, $\xi_2/\xi_{c2}$ decreases with impurity scattering for $s_{++}$ symmetry. To differentiate $s_{++}$ and $s^{\pm}$ symmetries, the impurities creating interband scattering are needed (inset to Fig. 8).

Core size field dependences were investigated in low- and high-temperature superconductors with different pairing symmetries at low temperatures in $\mu$SR experiments.[28] Main attention there was paid to low field region ($B/B_{c2} \ll 1$) of $\xi_2/\xi_{c2}(B/B_{c2})$. First, these dependences show rapid decreasing at low fields turning into a plateau, where $\xi_2/\xi_{c2} < 1$. The initial diminution of $\xi_2/\xi_{c2}$ can be explained by the field suppression of the proximity induced small gap in multiband superconductors (e.g., chain band in $YBa_2Cu_3O_{7-\delta}$, Ref. 27). In this paper, we present the results for $\xi_2/\xi_{c2}$ from intermediate to high fields ($0.1 \le B/B_{c2} \le 1$) and we neglect the effect of smallest gap on $\xi_2/\xi_{c2}(B/B_{c2})$ which is important at low fields. Thus, we can only compare calculated values of vortex core size at $B/B_{c2} \sim 0.1$ with those at plateau in experimental data.[28] As can be seen from Figs. 8 and 9 that $\xi_2/\xi_{c2}$ is in order of 0.5 at these fields in clean superconductors in reasonable agreement with experiments.[28]

## V. CONCLUSIONS

Eilenberger equations have been solved for superconductors with isotropic $s^{\pm}$, $s_{++}$ and anisotropic $d_{x^2-y^2}$ pairing

symmetries in the mixed state. These symmetries are proposed for the pairing state of the iron based superconductors. For example, the pairing symmetry transformation has been found in $Ba_{1-x}K_xFe_2As_2$ compound. At optimal doping, this compound shows $s^{\pm}$ pairing symmetry. The $d$-wave pairing with strong hole doping is consistent with the observation of nodal quasiparticles in the heavily hole doped superconductor $KFe_2As_2$ with $T_c = 3\,K$. Pairing symmetry transformation is also suggested in ternary selenide. A clear fingerprint of the phonon spectrum in the fermionic self-energy was identified in LiFeAs and estimation of the electron-phonon coupling strength was done, which appears to be sufficient to mediate the $s_{++}$-wave superconductivity. However, it was shown that collinear antiferromagnetic fluctuations are also important resulting in $s^{\pm}$ pairing symmetry. It is found that Eilenberger equations can be reduced to London model with only one parameter, $\xi_h(B)$. This length determines the form factor of FLL, which can be obtained in $\mu$SR and SANS experiments. It is found that normalized value of $\xi_h/\xi_{c2}$ decreases with temperature due to Kramer-Pesch effect. In clean superconductors, the shape of $\xi_h/\xi_{c2}(B)$ for $d$-wave is similar to that in $s$-wave symmetry. Magnetic field dependence of $\xi_h/\xi_{c2}$ is nonuniversal for $s^{\pm}$ pairing, depending on the chosen parameter set it can reside both below and above AGL curve. Such behavior is quite different from that in $s_{++}$ pairing symmetry where intraband and interband scattering rates act in similar way and $\xi_h/\xi_{c2}$ decreases always with impurity scattering. Detailed investigation of $\xi_h(B)$ dependence in the whole field range in LiFeAs is desirable. In $d$-wave superconductors, $\xi_h/\xi_{c2}$ always increases with the scattering rate $\Gamma$.

The vortex core size $\xi_2$ determined as a distance, where current has its maximum is also calculated. In unconventional superconductors, $\xi_2/\xi_{c2}$ increases with pair breaking impurity scattering. Two types of $\xi_2/\xi_{c2}(B/B_{c2})$ dependence are obtained for $s^{\pm}$ superconductors. It has minimum at low temperatures with small value of interband impurity scattering, transforming in monotonously decreasing function at strong interband scattering and high temperatures. The intraband scattering results in decreasing of $\xi_2/\xi_{c2}$ value. The second kind of this dependence was also found for $d$-wave superconductors at intermediate and high temperatures. The transformation from diminishing to growing of $\xi_2/\xi_{c2}(B/B_{c2})$ dependence with lowering of the temperature is obtained for $s_{++}$-wave symmetry. The effect of impurity scattering in this case is similar to that of intraband scattering for $s^{\pm}$ symmetry.

This work was supported by the Finnish Cultural Foundation (Etelä-Karjalan rahasto).

[1]C. C. Tsuei and J. R. Kirtley, Rev. Mod. Phys. **72**, 969 (2000).
[2]C. Pfleiderer, Rev. Mod. Phys. **81**, 1551 (2009).
[3]G. R. Stewart, Rev. Mod. Phys. **83**, 1589 (2011).
[4]J. Hu and H. Ding, Sci. Rep. **2**, 381 (2012).
[5]S. Hüfner, M. A. Hossain, A. Damascelli, and G. A. Sawatzky, Rep. Prog. Phys. **71**, 062501 (2008).
[6]P. J. Hirschfeld, M. M. Korshunov, and I. I. Mazin, Rep. Prog. Phys. **74**, 124508 (2011).
[7]S. Maiti, M. M. Korshunov, T. A. Maier, P. J. Hirschfeld, and A. V. Chubukov, Phys. Rev. B **84**, 224505 (2011).
[8]J. K. Dong, S. Y. Zhou, T. Y. Guan, H. Zhang, Y. F. Dai, X. Qiu, X. F. Wang, Y. He, X. H. Chen, and S. Y. Li, Phys. Rev. Lett. **104**, 087005 (2010).
[9]A. F. Wang, S. Y. Zhou, X. G. Luo, X. C. Hong, Y. J. Yan, J. J. Ying, P. Cheng, G. J. Ye, Z. J. Xiang, S. Y. Li, and X. H. Chen, e-print: arXiv:1206.2030.
[10]H. Kawano-Furukawa, C. J. Bowell, J. S. White, R. W. Heslop, A. S. Cameron, E. M. Forgan, K. Kihou, C. H. Lee, A. Iyo, H. Eisaki, T. Saito, and H. Fukazawa, Phys. Rev. B **84**, 024507 (2011).
[11]F. Kretzschmar, B. Muschler, T. Bohm, A. Baum, R. Hackl, H.-H. Wen, V. Tsurkan, J. Deisenhofer, and A. Loidl, e-print: arXiv:1208.5006.
[12]T. Maier, P. Hirschfeld, and D. Scalapino, e-print: arXiv:1206.5235.
[13]M. Khodas and A. V. Chubukov, Phys. Rev. Lett. **108**, 247003 (2012).
[14]K. Samokhin and M. Walker, Phys. Rev. B **64**, 024507 (2001).
[15]A. Golubov and I. Mazin, Phys. Rev. B **55**, 15146 (1997).
[16]A. Abrikosov and L. P. Gorkov, Sov. Phys. JETP **12**, 1243 (1961).
[17]H. Kontani and S. Onari, Phys. Rev. Lett. **104**, 157001 (2010).
[18]A. A. Kordyuk, V. B. Zabolotnyy, D. V. Evtushinsky, T. K. Kim, I. V. Morozov, M. L. Kulić, R. Follath, G. Behr, B. Büchner, and S. V. Borisenko, Phys. Rev. B **83**, 134513 (2011).
[19]S. V. Borisenko, V. B. Zabolotnyy, A. A. Kordyuk, D. V. Evtushinsky, T. K. Kim, I. V. Morozov, R. Follath, and B. Büchner, Symmetry **4**(1), 251 (2012).
[20]Y. Yanagi, Y. Yamakawa, and Y. Ōno, Phys. Rev. B **81**, 054518 (2010).
[21]C. Platt, R. Thomale, and W. Hanke, Phys. Rev. B **84**, 235121 (2011).
[22]Z.-J. Yao, W.-Q. Chen, Y.-K. Li, G.-H. Cao, H.-M. Jiang, Q.-E. Wang, Z.-A. Xu, and F.-C. Zhang, e-print: arXiv:1209.0709.
[23]O. Fischer, M. Kugler, I. Maggio-Aprile, C. Berthod, and C. Renner, Rev. Mod. Phys. **79**, 353 (2007).
[24]J. E. Sonier, Rep. Prog. Phys. **70**, 1717 (2007).
[25]K. Lee, M. H. Fischer, and E.-A. Kim, e-print: arXiv:1209.0788.
[26]T. Hanaguri, K. Kitagawa, K. Matsubayashi, Y. Mazaki, Y. Uwatoko, and H. Takagi, Phys. Rev. B **85**, 214505 (2012).
[27]W. A. Atkinson and J. E. Sonier, Phys. Rev. B **77**, 024514 (2008).
[28]J. E. Sonier, J. Phys.: Condens. Matter **16**, S4499 (2004).
[29]M. Ichioka, A. Hasegawa, and K. Machida, Phys. Rev. B **59**, 184 (1999).
[30]P. Belova, K. B. Traito, and E. Lähderanta, J. Appl. Phys. **110**, 033911 (2011).
[31]P. Belova, I. Zakharchuk,M. Safonchik, K. B. Traito, and E. Lähderanta, Physica C **426**, 1 (2012).
[32]R. Laiho, M. Safonchik, and K. B. Traito, Phys. Rev. B **76**, 140501(R) (2007).
[33]R. Laiho, M. Safonchik, and K. B. Traito, Phys. Rev. B **78**, 064521 (2008).
[34]J. E. Sonier, W. Huang, C. V. Kaiser, C. Cochrane, V. Pacradouni, S. A. Sabok-Sayr, M. D. Lumsden, B. C. Sales, M. A. McGuire, A. S. Sefat, and D. Mandrus, Phys. Rev. Lett. **106**, 127002 (2011).
[35]D. S. Inosov, J. S. White, D. V. Evtushinsky, I. V. Morozov, A. Cameron, U. Stockert, V. B. Zabolotnyy, T. K. Kim, A. A. Kordyuk, S. V. Borisenko, E. M. Forgan, R. Klingeler, J. T. Park, S. Wurmehl, A. N. Vasiliev, G. Behr, C. D. Dewhurst, and V. Hinkov, Phys. Rev. Lett. **104**, 187001 (2010).
[36]Z. Hao, J. R. Clem, M. W. McElfresh, L. Civale, A. P. Malozemoff, and F. Holtzberg, Phys. Rev. B **43**, 2844 (1991).
[37]R. Kadono, W. Higemoto, A. Koda, M. I. Larkin, G. M. Luke, A. T. Savici, Y. J. Uemura, K. M. Kojima, T. Okamoto, T. Kakeshita, S. Uchida, T. Ito, K. Oka, M. Takigawa, M. Ichioka, and K. Machida, Phys. Rev. B **69**, 104523 (2004).
[38]N. Nakai, P. Miranović, M. Ichioka, and K. Machida, Phys. Rev. B **73**, 172501 (2006).
[39]P. Miranović, M. Ichioka, and K. Machida, Phys. Rev. B **70**, 104510 (2004).
[40]A. Maisuradze, R. Khasanov, A. Shengelaya, and H. Keller, J. Phys.: Condens. Matter **21**, S075701 (2009).
[41]V. G. Kogan, R. Prozorov, S. L. Bud'ko, P. C. Canfield, J. R. Thompson, J. Karpinski, N. D. Zhigadlo, and P. Miranović, Phys. Rev. B **74**, 184521 (2006).
[42]A. B. Vorontsov, M. G. Vavilov, and A. V. Chubukov, Phys. Rev. B **79**, 140507(R) (2009).
[43]P. J. Hirschfeld and N. Goldenfeld, Phys. Rev. B **48**, 4219 (1993).
[44]R. Prozorov and V. G. Kogan, Rep. Prog. Phys. **74**, 124505 (2011).
[45]H. Kim, R. T. Gordon, M. A. Tanatar, J. Hua, U. Welp, W. K. Kwok, N. Ni, S. L. Bud'ko, P. C. Canfield, A. B. Vorontsov, and R. Prozorov, Phys. Rev. B **82**, 060518 (2010).

[46]D. Xu, S. K. Yip, and J. A. Sauls, Phys. Rev. B **51**, 16233 (1995).
[47]G. Yin and K. Maki, Physica B **194**, 2025 (1994).
[48]A. Zare, A. Markowsky, T. Dahm, and N. Schopohl, Phys. Rev. B **78**, 104524 (2008).
[49]M. Ichioka, N. Hayashi, N. Enomoto, and K. Machida, Phys. Rev. B **53**, 15316 (1996).
[50]R. Laiho, M. Safonchik, and K. B. Traito, Phys. Rev. B **75**, 174524 (2007).
[51]Y. N. Ovchinnikov and V. Z. Kresin, Phys. Rev. B **52**, 3075 (1995).
[52]L. Kramer and W. Pesch, Z. Phys. **269**, 59 (1974).
[53]N. Kurita, K. Kitagawa, K. Matsubayashi, A. Kismarahardja, E. Choi, J. S. Brooks, Y. Uwatoko, S. Uji, and T. Terashima, J. Phys. Soc. Jpn. **80**, 013706 (2011).
[54]B. Lake, H. M. Rønnow, N. B. Christensen, G. Aeppli, K. Lefmann, D. F. McMorrow, P. Vorderwisch, P. Smeibidl, N. Mangkorntong, T. Sasagawa, M. Nohara, H. Takagi, and T. E. Mason, Nature (London) **415**, 299 (2002).
[55]Y. Zhang, E. Demler, and S. Sachdev, Phys. Rev. B **66**, 094501 (2002).
[56]F. L. Pratt, P. J. Baker, S. J. Blundell, T. Lancaster, H. J. Lewtas, P. Adamson, M. J. Pitcher, D. R. Parker, and S. J. Clarke, Phys. Rev. B **79**, 052508 (2009).
[57]J. E. Sonier, S. A. Sabok-Sayr, F. D. Callaghan, C. V. Kaiser, V. Pacradouni, J. H. Brewer, S. L. Stubbs, W. N. Hardy, D. A. Bonn, R. Liang, and W. A. Atkinson, Phys. Rev. B **76**, 134518 (2007).
[58]M. Takigawa, M. Ichioka, and K. Machida, Phys. Rev. Lett. **90**, 047001 (2003).
[59]S. Chi, S. Grothe, R. Liang, P. Dosanjh, W. N. Hardy, S. A. Burke, D. A. Bonn, and Y. Pennec, Phys. Rev. Lett. **109**, 087002 (2012).
[60]P. Belova, M. Safonchik, K. B. Traito, and E. Lähderanta, Phys. Rev. B **83**, 104518 (2011).
[61]J. E. Sonier, R. F. Kiefl, J. H. Brewer, J. Chakhalian, S. R. Dunsiger, W. A. MacFarlane, R. I. Miller, A. Wong, G. M. Luke, and J. W. Brill, Phys. Rev. Lett. **79**, 1742 (1997).

# PUBL. 2

**I. Zakharchuk, P. Belova, K. B. Traito and E. Lähderanta**, Eilenberger approach to the vortex state in iron pnictide superconductors, *Supercondutors - Materials, Properties and Applications*, Alexander Gabovich (ed.), chapter 9, ISBN 979-953-307-798-6, InTech, 2012 DOI: 10.5772/48571

Chapter 9

# Eilenberger Approach to the Vortex State in Iron Pnictide Superconductors

I. Zakharchuk, P. Belova, K. B. Traito and E. Lähderanta

Additional information is available at the end of the chapter

http://dx.doi.org/10.5772/48571

## 1. Introduction

The SC gap, which characterizes the energy cost for breaking a Cooper pair, is an important quantity when clarifying the SC mechanism. The gap size and its momentum dependence reflect the strength and anisotropy of the pairing interactions, respectively. Some experiment executed by Li *et al*. [1] in response to a suggestion by Klemm [2] tested the phase of the wave function in $Bi_2Sr_2CaCu_2O_8$ and revived the *s*-wave viewpoint [3, 4]], which, although championed by Dynes's group [4], had been out of favor even for $Bi_2Sr_2CaCu_2O_8$, although not disproven. This experiment once more created uncertainty over whether the superconducting pairs are consistent with *s*-wave or *d*-wave superconductivity (Van Harlingen [5], Ginsberg [6], Tsuei and Kirtley [7]).

The discovery of Fe-based superconductors [8] generated intensive debate on the superconducting (SC) mechanism. Motivated by high-$T_c$ values up to 56 K [9], the possibility of unconventional superconductivity has been intensively discussed. A plausible candidate is the SC pairing mediated by antiferromagnetic (AFM) interactions. Two different approaches, based on the itinerant spin fluctuations promoted by Fermi-surface (FS) nesting [10, 11], and the local AFM exchange couplings [12], predict the so-called $s^{\pm}$-wave pairing state, in which the gap shows a *s*-wave symmetry that changes sign between different FSs. Owing to the multiorbital nature and the characteristic crystal symmetry of Fe-based superconductors, $s_{++}$-wave pairing without sign reversal originating from novel orbital fluctuations has also been proposed [13, 14]. The unconventional nature of the superconductivity is supported by experimental observations such as strongly FS-dependent anomalously large SC gaps [15–17] and the possible sign change in the gap function [18, 19] on moderately doped $BaFe_2As_2$, NdFeAsO and $FeTe_{1-x}Se_x$. However, a resonance like peak structure, observed by neutron scattering measurements [18], is reproduced by considering the strong correlation effect via quasiparticle damping, without the necessity of sign reversal in the SC gap [20]. Although the $s^{\pm}$-wave state is expected to be very fragile as regards impurities due to the interband scattering [21], the superconducting state is remarkably robust regarding impurities and $\alpha$-particle irradiation [22].

There is growing evidence that the superconducting gap structure is not universal in the iron-based superconductors [23, 24]. In certain materials, such as optimally doped $BaKFe_2As_2$ and $BaFeCo_2As_2$, strong evidence for a fully gapped superconducting state has been observed from several low-energy quasiparticle excitation probes, including magnetic penetration depth [25, 26], and thermal conductivity measurements [27]. In contrast, significant excitations at low temperatures due to nodes in the energy gap have been detected in several Fe-pnictide superconductors. These include LaFePO ($T_c = 6$ K) [28, 29], $BaFe_2AsP_2$ ($T_c = 31$ K) [30–32], and $KFe_2As_2$ ($T_c = 4$ K) [33, 34].

At a very early stage, it was realized that electron and hole doping can have qualitatively different effects in the pnictides [35]. Hole doping should increase the propensity to a nodeless ($s^{\pm}$) SC phase. The qualitative picture applies to both the "122" as the "1111" compounds: As the Fermi level is lowered, the $M$ $h$ pocket becomes more relevant and the $M \leftrightarrow X$ scattering adds to the $(\pi, 0)/(0, \pi)$ scattering from $\Gamma$ to $X$. As such, the anisotropy-driving scattering, such as interelectron pocket scattering, becomes less relevant and yields a nodeless, less anisotropic, and more stable $s^{\pm}$ [36]. This picture is qualitatively confirmed by experiments. While thermoelectric, transport, and specific heat measurements have been performed for $K_xBa_{1-x}Fe_2As_2$ from $x = 0$ to the strongly hole-doped case $x = 1$ [37, 38], more detailed studies have previously focused on the optimally doped case $x = 0.4$ with $T_c = 37$ K, where all measurements such as penetration depth and thermal conductivity find indication for a moderately anisotropic nodeless gap [39, 40]. Similarly, angle-resolved photoemission spectroscopy (ARPES) on doped $BaFe_2As_2$ reveals a nodeless SC gap [16, 41].

The experimental findings for the SC phase in $KFe_2As_2$ were surprising. Thermal conductivity [33], penetration depth [34], and NMR [42] provide a clear indication of nodal SC. The critical temperature for $KFe_2As_2$ is $\sim 3$ K, an order of magnitude less than the optimally doped samples. ARPES measurements [43] show that the $e$ pockets have nearly disappeared, while the $h$ pockets at the folded $\Gamma$ point are large and have a linear dimension close to $\pi/a$. A detailed picture of how the SC phase evolves under hole doping in $K_xBa_{1-x}Fe_2As_2$ was found and that the nodal phase observed for $x = 1$ is of the (extended) $d$-wave type [44]. The functional renormalization group was used to investigate how the SC form factor evolves under doping from the nodeless anisotropic $s^{\pm}$ in the moderately hole-doped regime to a $d$-wave in the strongly hole-doped regime, where the $e$ pockets are assumed to be gapped out. The $d$-wave SC minimizes the on-pocket hole interaction energy. It was found that the critical divergence scale to be of an order of magnitude lower than for the optimally doped $s^{\pm}$ scenario, which is consistent with experimental evidence [44].

The synthesis of another iron superconductor immediately attracted much attention for several reasons [9, 45]. LiFeAs is one of the few superconductors which does not require additional charge carriers and is characterized by $T_c$ approaching the boiling point of hydrogen. Similar to $AeFe_2As_2$ ( Ae = Ba, Sr, Ca "122") and LnOFeAs ("1111") parent compounds, LiFeAs ($T_c = 18$ K) consists of nearly identical $(Fe_2As_2)^{2-}$ structural units and all three are isoelectronic, though the former do not superconduct. The band structure calculations unanimously yield the same shapes for the FS, as well as very similar densities of states, and low energy electronic dispersions [46, 47]. Moreover the calculations even find in LiFeAs an energetically favorable magnetic solution which exactly corresponds to the famous stripelike antiferromagnetic order in "122" and "1111" systems [46, 48]. The experiments, however, show a rather different situation. The structural transition peculiar to "122" and "1111" families is remarkably absent in LiFeAs and is not observed under an applied pressure

of up to 20 GPa [49]. Resistivity and susceptibility as well as $\mu$-spin rotation experiments show no evidence of magnetic transition [50, 51]. Only a weak magnetic background [51] and field induced magnetism in the doped compound have been detected [50]. What was identified was a notable absence of the Fermi surface nesting, a strong renormalization of the conduction bands by a factor of 3, a high density of states at the Fermi level caused by a van Hove singularity, and no evidence of either a static or a fluctuating order; although superconductivity with in-plane isotropic energy gaps have been found implying the $s_{++}$ pairing state [52]. However, a gap anisotropy along the Fermi surface up to $\sim$ 30% was observed in Ref. [53]. Thus, the type of the superconducting gap symmetry in LiFeAs is still an open question.

The aim of our paper is to apply quasiclassical Eilenberger approach to the vortex state considering $s^{\pm}$, $s_{++}$ and $d_{x^2-y^2}$-wave pairing symmetries as presumable states for the different levels of impurity scattering rates $\Gamma^*$, to calculate the cutoff parameter $\xi_h$ [54, 55] and to compare results with experimental data for iron pnictides. As described in Ref. [56], $\xi_h$ is important for the description of the muon spin rotation ($\mu$SR) experiments and can be directly measured.

The London model used for the analysis of the experimental data does not account for the spatial dependence of the superconducting order parameter and it fails down at distances of the order of coherence length from the vortex core center, *i.e.*, $B(r)$ logarithmically diverges as $r \to 0$. To correct this, the **G** sum in the expression for the vortex lattice free energy can be truncated by multiplying each term by a cutoff function $F(G)$. Here, **G** is a reciprocal vortex lattice vector. In this method the sum is cut off at high $G_{max} \approx 2\pi/\xi_h$, where $\xi_h$ is the cutoff parameter. The characteristic length $\xi_h$ accommodates a number of inherent uncertainties of the London approach; the question was discussed originally by de Gennes group [57] and discussed in some detail in Ref. [58]. It is important to stress that the appropriate form of $F(G)$ depends on the precise spatial dependence of the order parameter in the the vortex core region, and this, in general, depends on the temperature and the magnetic field.

A smooth Gaussian cutoff factor $F(G) = exp(-\alpha G^2\xi^2)$ was phenomenologically suggested. Here, $\xi$ is the Gizburg-Landau coherence length. If there is no dependence of the superconducting coherence length on temperature and magnetic field, then changes in the spatial dependence of the order parameter around a vortex correspond to changes in $\alpha$. By solving the Ginzburg-Landau (GL) equations, Brandt determined that $\alpha = 1/2$ at fields near $B_{c2}$ [59], and arbitarily determined it to be $\alpha \approx 2$ at fields immediately above $B_{c1}$ [60]. For an isolated vortex in an isotropic extreme (the GL parameter $\kappa_{GL} \gg 1$) $s$-wave superconductor, $\alpha$ was obtained by numerical calculation of GL equations. It was found that $\alpha$ decreases smoothly from $\alpha = 1$ at $B_{c1}$ to $\alpha \approx 0.2$ at $B_{c2}$ [61]. The analytical GL expression was obtained by [62] for isotropic superconductors at low inductions $B \ll B_{c2}$. Using a Lorentzian trial function for the order parameter of an isolated vortex, Clem found for large $\kappa_{GL} \gg 1$ that $F(G)$ is proportional to the modified Bessel function. In Ref. [63], the Clem model [62] was extended to larger magnetic fields up to $B_{c2}$ through the linear superposition of the field profiles of individual vortices. In this model, the Clem trial function [62] is multiplied by a second variational parameter $f_\infty$ to account for the suppression of the order parameter due to the overlapping of vortex cores. This model gave the method for calculating the magnetization of type-II superconductors in the full range $B_{c1} < B < B_{c2}$. Their analytical formula is in a good agreement with the well-known Abrikosov high-field result and considerably corrects the results obtained with an exponential cutoff function at

low fields [64]. This approximation was widely used for the analysis of the experimental data on magnetization of type-II superconductors (see references 27-29 in Ref. [65]). The improved approximate Ginzburg-Landau solution for the regular flux-line lattice using circular cell method was obtained in Ref. [65]. This solution gives better correlation with the numerical solution of GL equations.

The Ginzburg-Landau theory, strictly speaking, is only valid near $T_c$ but it is often used in the whole temperature range taking the cutoff parameter $\xi_h$ and penetration depth $\lambda$ as a fitting parameters. Recently, an effective London model with the effective cutoff parameter $\xi_h(B)$ as a fitting parameter was obtained for clean [54] and dirty [55] superconductors, using self-consistent solution of quasiclassical nonlinear Eilenberger equations. In this approach, $\lambda$ is not a fitting parameter but calculated from the microscopical theory of the Meissner state. As was shown in Ref. [66], the reduction of the amount of the fitting parameters to one, considerably simplifies the fitting procedure. In this method, the cutoff parameter obtained from the Ginzburg-Landau model was extended over the whole field and temperature ranges. In this case, the effects of the bound states in the vortex cores lead to the Kramer-Pesch effect [67], i.e. delocalization between the vortices [68, 69], nonlocal electrodynamic [58] and nonlinear effects [70] being self-consistently included.

Following the microscopical Eilenberger theory, $\xi_h$ can be found from the fitting of the calculated magnetic field distribution $h_E(\mathbf{r})$ to the Eilenberger - Hao-Clem (EHC) field distribution $h_{EHC}(\mathbf{r})$ [54, 55]

$$h_{EHC}(\mathbf{r}) = \frac{\Phi_0}{S}\sum_{\mathbf{G}}\frac{F(G)e^{i\mathbf{G}\mathbf{r}}}{1+\lambda^2 G^2}, \tag{1}$$

where

$$F(\mathbf{G}) = uK_1(u), \tag{2}$$

where $K_1(u)$ is modified Bessel function, $u = \xi_h G$ and $S$ is the area of the vortex lattice unit cell. It is important to note that $\xi_h$ in Eq. (1) is obtained from solving the Eilenberger equations and does not coincide with the variational parameter $\xi_v$ of the analytical Ginzburg-Landau (AGL) model.

In **chapter 2** and **3** we solve the Eilenberger equations for $s^{\pm}$, $s_{++}$ and $d_{x^2-y^2}$-wave pairing symmetries, fit the solution to Eq. (1) and find the cutoff parameter $\xi_h$. In this approach all nonlinear and nonlocal effects connected with vortex core and extended quasiclassical states are described by one effective cutoff parameter $\xi_h$. The nonlocal generalized London equation with separated quasiclassical states was also developed as regards the description of the mixed state in high-$T_c$ superconductors such as $YBa_2Cu_3O_{7-\delta}$ compounds (the Amin-Franz-Affleck (AFA) model) [70, 71]. In this case, fourfold anisotropy arises from $d$-wave pairing. This theory was applied to the investigation of the flux line lattice (FLL) structures [72] and effective penetration depth measured by $\mu$SR experiments [73]. This approach will be considered in **chapter 4**.

## 2. The cutoff parameter for the field distribution in the mixed states of $s^{\pm}$- and $s_{++}$-wave pairing symmetries

In this chapter, we consider the model of the iron pnictides, where the Fermi surface is approximated by two cylindrical pockets centered at Γ (hole) and M (electron) points of the

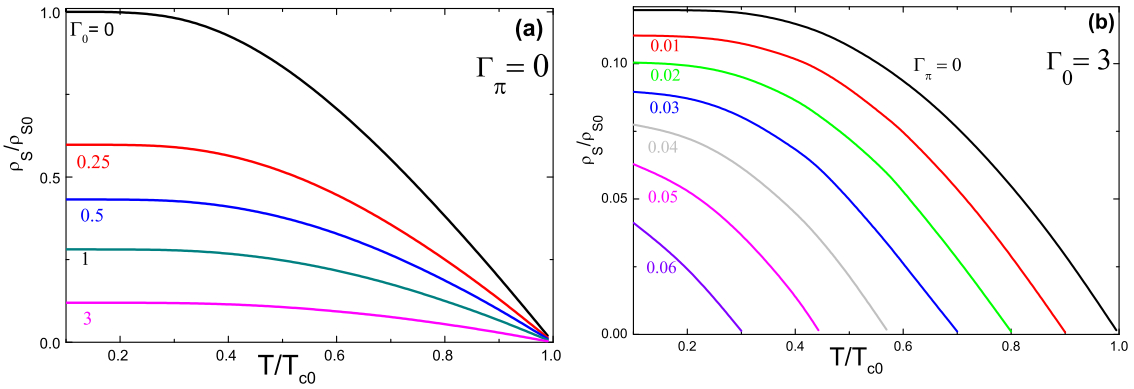


**Figure 1.** (Color online) The temperature dependence of superfluid density $\rho_S(T)/\rho_{S0}$ at (a) interband scattering rate $\Gamma_\pi = 0$ with different values of intraband scattering $\Gamma_0$ and (b) intraband scattering rate $\Gamma_0 = 3$ with different values of interband scattering $\Gamma_\pi$.

Fermi surface, i.e. a two dimensional limit of the five-band model [74]. In Eq. (1) $\lambda(T)$ is the penetration depth in the Meissner state. In this model $\lambda(T)$ is given as

$$\frac{\lambda_{L0}^2}{\lambda^2(T)} = 2\pi T \sum_{\omega_n>0} \frac{\bar{\Delta}_n^2}{\eta_n(\bar{\Delta}_n^2+\omega_n^2)^{3/2}}, \tag{3}$$

where $\lambda_{L0} = (c^2/4\pi e^2 v_F^2 N_0)^{1/2}$ is the London penetration depth at $T = 0$ including the Fermi velocity $v_F$ and the density of states $N_0$ at the Fermi surface and $\eta_n = 1 + 2\pi(\Gamma_0+\Gamma_\pi)/(\sqrt{\bar{\Delta}_n^2+\omega_n^2})$. Here, $\Gamma_0 = \pi n_i N_F |u_0|^2$ and $\Gamma_\pi = \pi n_i N_F |u_\pi|^2$ are the intra- and interband impurity scattering rates, respectively ($u_{0,\pi}$ are impurity scattering amplitudes with correspondingly small, or close to $\pi = (\pi,\pi)$, momentum transfer). In this work, we investigate the field distribution in the vortex lattice by systematically changing the impurity concentration in the Born approximation, and analyzing the field dependence of the cutoff parameter. In particular, we consider two limits: small $\Gamma^* \ll 1$ (referred to as the "stoichiometric" case) and relatively high $\Gamma^* \geq 1$ ("nonstoichiometric" case). Here, $\Gamma^*$ is measured in the units of $2\pi T_{c0}$. We consider $\Gamma^*$ as intraband scattering $\Gamma_0$ with constant interband scattering $\Gamma_\pi = 0$.

In Eq. (3), $\bar{\Delta}_n = \Delta(T) - 4\pi\Gamma_\pi\bar{\Delta}_n/\sqrt{\bar{\Delta}_n^2+\omega_n^2}$ for the $s^\pm$ pairing and $\bar{\Delta}_n = \Delta(T)$ for the $s_{++}$ pairing symmetry. The order parameter $\Delta(T)$ in Meissner state is determined by the self-consistent equation

$$\Delta(T) = 2\pi T \sum_{0<\omega_n<\omega_c} \frac{V^{SC}\bar{\Delta}_n}{\sqrt{\bar{\Delta}_n^2+\omega_n^2}}. \tag{4}$$

Experimentally, $\lambda(T)$ can be obtained by radio-frequency measurements [75] and magnetization measurements of nanoparticles [76]. Fig. 1 shows the calculated temperature dependence of the superfluid density $\rho_S(T)/\rho_{S0} = \lambda_{L0}^2/\lambda^2(T)$, with different values of impurity scattering $\Gamma$ for $s^\pm$-wave pairing symmetry. With the Riccati transformation of the Eilenberger equations, quasiclassical Green functions $f$ and $g$ can be parameterized via functions $a$ and $b$ [77]

$$\bar{f} = \frac{2a}{1+ab}, \quad f^\dagger = \frac{2b}{1+ab}, \quad g = \frac{1-ab}{1+ab}, \tag{5}$$

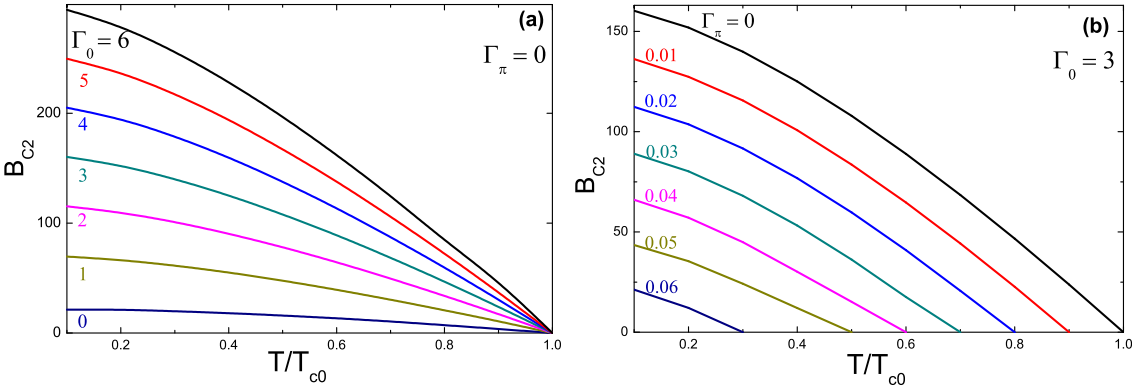


**Figure 2.** (Color online) (a) The temperature dependence of the upper critical field $B_{c2}$ at interband scattering $\Gamma_\pi = 0$ with different values of intraband scattering values $\Gamma_0$. (b) The calculated temperature dependence of $B_{c2}$ at intraband scattering rate $\Gamma_0 = 3$ with different values of interband scattering $\Gamma_\pi$.

satisfying the nonlinear Riccati equations. In Born approximation for impurity scattering we have

$$\mathbf{u}\cdot\nabla a = -a\left[2(\omega_n + G) + i\mathbf{u}\cdot\mathbf{A}_s\right] + (\Delta + F) - a^2(\Delta^* + F^*), \tag{6}$$

$$\mathbf{u}\cdot\nabla b = b\left[2(\omega_n + G) + i\mathbf{u}\cdot\mathbf{A}_s\right] - (\Delta^* + F^*) + b^2(\Delta + F), \tag{7}$$

where $\omega_n = \pi T(2n+1)$, $G = 2\pi\langle g\rangle(\Gamma_0 + \Gamma_\pi) \equiv 2\pi\langle g\rangle\Gamma^*$, $F = 2\pi\langle f\rangle(\Gamma_0 - \Gamma_\pi)$ for $s^{\pm}$ pairing symmetry and $F = 2\pi\langle f\rangle\Gamma^*$ for the $s_{++}$ pairing symmetry. Here, $\mathbf{u}$ is a unit vector of the Fermi velocity. In the new gauge vector-potential $\mathbf{A}_s = \mathbf{A} - \nabla\phi$ is proportional to the superfluid velocity. It diverges as $1/r$ at the vortex center (index $s$ is put to denote its singular nature). The FLL creates the anisotropy of the electron spectrum. Therefore, the impurity renormalization correction in Eqs. (6) and (7), averaged over the Fermi surface, can be reduced to averages over the polar angle $\theta$, i.e. $\langle\ldots\rangle = (1/2\pi)\int\ldots d\theta$.

To take into account the influence of screening the vector potential $\mathbf{A}(\mathbf{r})$ in Eqs. (6) and (7) is obtained from the equation

$$\nabla\times\nabla\times\mathbf{A}_\mathbf{E} = \frac{4}{\kappa^2}\mathbf{J}, \tag{8}$$

where the supercurrent $\mathbf{J}(\mathbf{r})$ is given in terms of $g(\omega_n,\theta,\mathbf{r})$ by

$$\mathbf{J}(\mathbf{r}) = 2\pi T\sum_{\omega_n>0}\int_0^{2\pi}\frac{d\theta}{2\pi}\frac{\hat{\mathbf{k}}}{i}g(\omega_n,\theta,\mathbf{r}). \tag{9}$$

Here $\mathbf{A}$ and $\mathbf{J}$ are measured in units of $\Phi_0/2\pi\xi_0$ and $2ev_FN_0T_c$, respectively. The spatial variation of the internal field $h(\mathbf{r})$ is determined through

$$\nabla\times\mathbf{A} = \mathbf{h}(\mathbf{r}), \tag{10}$$

where $\mathbf{h}$ is measured in units of $\Phi_0/2\pi\xi_0^2$.

The self-consistent condition for the pairing potential $\Delta(\mathbf{r})$ in the vortex state is given by

$$\Delta(\mathbf{r}) = V^{SC} 2\pi T \sum_{\omega_n>0}^{\omega_c} \int_0^{2\pi} \frac{d\theta}{2\pi} f(\omega_n, \theta, \mathbf{r}), \tag{11}$$

where $V^{SC}$ is the coupling constant and $\omega_c$ is the ultraviolet cutoff determining $T_{c0}$ [55]. Consistently throughout our paper energy, temperature, and length are measured in units of $T_{c0}$ and the coherence length $\xi_0 = v_F/T_{c0}$, where $v_F$ is the Fermi velocity. The magnetic field $\mathbf{h}$ is given in units of $\Phi_0/2\pi\xi_0^2$. The impurity scattering rates are in units of $2\pi T_{c0}$. In calculations the ratio $\kappa = \lambda_{L0}/\xi_0 = 10$ is used. It corresponds to $\kappa_{GL} = 43.3$ [77].

To obtain the quasiclassical Green function, the Riccati equations [Eq. (6, 7)] are solved by the Fast Fourier Transform (FFT) method for triangular FLL [55]. This method is reasonable for the dense FLL, discussed in this paper. In the high field the pinning effects are weak and they are not considered in our paper. To study the high field regime we needed to calculate the upper critical field $B_{c2}(T)$. This was found from using the similarity of the considered model to the model of spin-flip superconductors from the equations [78]

$$\ln(\frac{T_{c0}}{T}) = 2\pi T \sum_{n\geq 0} [\omega_n^{-1} - 2D_1(\omega_n, B_{c2})], \tag{12}$$

where

$$D_1(\omega_n, B_{c2}) = J(\omega_n, B_{c2}) \times [1 - 2(\Gamma_0 - \Gamma_\pi) J(\omega_n, B_{c2})]^{-1}, \tag{13}$$

$$J(\omega_n, B_{c2}) = (\frac{4}{\pi B_{c2}})^{1/2} \times \int_0^\infty dy \exp(-y) \arctan[\frac{(B_{c2}y)^{1/2}}{\alpha}], \tag{14}$$

where $\alpha = 2(\omega_n + \Gamma_0 + \Gamma_\pi)$.

Fig. 2 shows $B_{c2}(T)$ dependences at (a) $\Gamma_\pi = 0$, $\Gamma_0 = 0, 1, 2, 3, 4, 5, 6$ and (b) $\Gamma_0 = 3$, $\Gamma_\pi = 0.01, 0.02, 0.03, 0.04, 0.05, 0.06$ calculated from Eqs. (12-14). In Fig. 2 the different influence of the intraband and interband scattering on $B_{c2}(T)$ dependence can be seen. The $B_{c2}(T)$ curve increases with $\Gamma_0$ ($\xi_{c2}$ decreases with $\Gamma_0$), but $\Gamma_\pi$ results in decreasing $B_{c2}(T)$ (increasing of $\xi_{c2}$).

Fig. 3 (a) shows magnetic field dependence $\xi_h(B)$ in reduced units at $T/T_{c0} = 0.5$ for the $s^\pm$ pairing with $\Gamma_0 = 3$, $\Gamma_\pi = 0.02$ and $\Gamma_0 = 0.5$, $\Gamma_\pi = 0.03$ and "clean" case (solid lines) and for the $s_{++}$ pairing with $\Gamma^*$= 0.5 and $\Gamma^* = 3$ (dotted lines). The dashed line shows the analytical solution of the AGL theory [63]

$$\xi_v = \xi_{c2}(\sqrt{2} - \frac{0.75}{\kappa_{GL}})(1 + b^4)^{1/2}[1 - 2b(1-b)^2]^{1/2}. \tag{15}$$

This dependence with $\xi_{c2}$ as a fitting parameter is often used for the description of the experimental $\mu$SR results [56, 79]. As can be seen from Fig. 3 (a), the magnetic field dependence of $\xi_h/\xi_{c2}$ is nonuniversal because it depends not only on $B/B_{c2}$ (as in the AGL theory, dashed line in Fig. 3 (a)), but also on interband and intraband impurity scattering parameters. In the cases where $\Gamma_0 = \Gamma_\pi = 0$, the results are the same for $s^\pm$ and $s_{++}$ pairing symmetries. We indicated that this curve is "clean" one. In this figure, the case $\Gamma_0 \gg \Gamma_\pi$ is considered

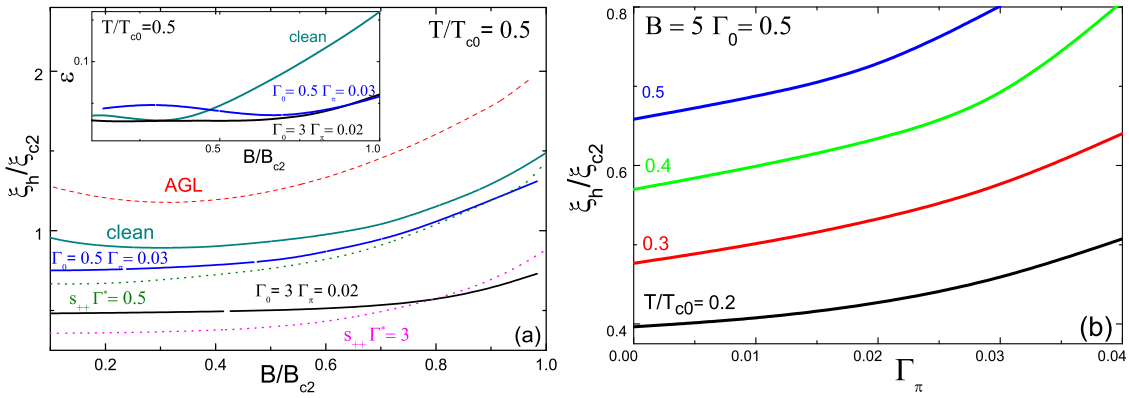


**Figure 3.** (Color online) (a) The magnetic field dependence of $\xi_h/\xi_{c2}$ for superconductors with impurity scattering. The solid lines represent our solution of Eilenberger equations at $T/T_{c0} = 0.5$ for "clean" case ($\Gamma_0 = \Gamma_\pi = 0$) and $s^{\pm}$ model ($\Gamma_0 = 0.5$, $\Gamma_\pi = 0.03$ and $\Gamma_0 = 3$, $\Gamma_\pi = 0.02$). The dotted lines show result for $s_{++}$ model ($\Gamma^* = 0.5$ and $\Gamma^* = 3$). Dashed line demonstrates the result of the AGL theory for $\xi_v$ from Eq. 15. The inset shows the magnetic field dependence of mean square deviation of the $h_{EHC}$ distribution from the Eilenberger distribution normalized by the variance of the Eilenberger distribution, $\varepsilon$, for $T/T_{c0} = 0.5$ at $\Gamma_0 = \Gamma_\pi = 0$ ("clean"); $\Gamma_0 = 3$, $\Gamma_\pi = 0.02$ and $\Gamma_0 = 0.5$, $\Gamma_\pi = 0.03$. (b) The interband scattering $\Gamma_\pi$ dependence of $\xi_h/\xi_{c2}$ at different temperatures $T/T_{c0}$ (intraband scattering $\Gamma_0 = 0.5$ and $B = 5$) for the $s^{\pm}$ pairing.

and the value of $\xi_h$ is reduced considerably in comparison with the clean case. One can compare the observed behavior with that in $s_{++}$ pairing model. In $s_{++}$ pairing symmetry the intraband and interband scattering rates act in a similar way and $\xi_h/\xi_{c2}$ decreases always with impurity scattering. In contrast, in $s^{\pm}$ model $\xi_h/\xi_{c2}(B/B_{c2})$ dependences show different forms of behavior with $\Gamma_\pi$. Here, $\xi_h/\xi_{c2}$ increases with $\Gamma_\pi$ at $B/B_{c2} < 0.8$ and decreases at higher fields, i.e. the curves become more flattened. A crossing point appears in the dependences $\xi_h/\xi_{c2}(B/B_{c2})$ for $s^{\pm}$ and $s_{++}$ pairing. We also calculated the magnetic field dependence of mean square deviation of $h_{EHC}$ distribution of the magnetic field from the Eilenberger distribution normalized by the variance of the Eilenberger distribution $\varepsilon = \sqrt{\overline{(h_E - h_{EHC})^2}/\overline{(h_E - B)^2}}$, where $\overline{\cdots}$ is the average over a unit vortex cell. The inset to Fig. 3 (a) demonstrates $\varepsilon(B)$ dependence for $T/T_{c0} = 0.5$ at $\Gamma_0 = 0$, $\Gamma_\pi = 0$; $\Gamma_0 = 3$, $\Gamma_\pi = 0.02$ and $\Gamma_0 = 0.5$, $\Gamma_\pi = 0.03$. From this figure, it can be seen that the accuracy of effective London model is deteriorating as the magnetic field increases; however, in superconductors with impurity scattering the accuracy is below 6% even when it is close to the second critical field (the inset to Fig. 3 (a)).

In Fig. 3 (b), the interband scattering $\Gamma_\pi$ dependences of $\xi_h$ are presented in low fields for the $s^{\pm}$ pairing at different temperatures $T$. As can be seen $\xi_h/\xi_{c2}$ increases with the interband scattering rate $\Gamma_\pi$. Strong decreasing of $\xi_h/\xi_{c2}$ with a decrease in the temperature can be explained by the Kramer-Pesch effect [67]. It should be noted that the normalization constant $\xi_{c2}$ increases with $\Gamma_\pi$ because $\Gamma_\pi$ suppress $T_c$ similar to superconductors with spin-flip scattering (violation of the Anderson theorem). Thus, the rising $\xi_h/\xi_{c2}$ implies more strong growth of $\xi_h$ than $\xi_{c2}$ (from GL theory one can expect $\xi_h/\xi_{c2} = Const$). Qualitatively, it can be explained by the strong temperature dependence of $\xi_h(B, T/T_c)$, which is connected to the Kramer-Pesch effect [67]. Increasing $\Gamma_\pi$ results in suppression of $T_c$, i.e. effective increasing of $T$ and $\xi_h(T/T_c)$. $\xi_{c2}(T/T_c)$ has not such a strong $T_c$ dependence, thus leading to the increasing of the ratio $\xi_h/\xi_{c2}$ with $\Gamma_\pi$.

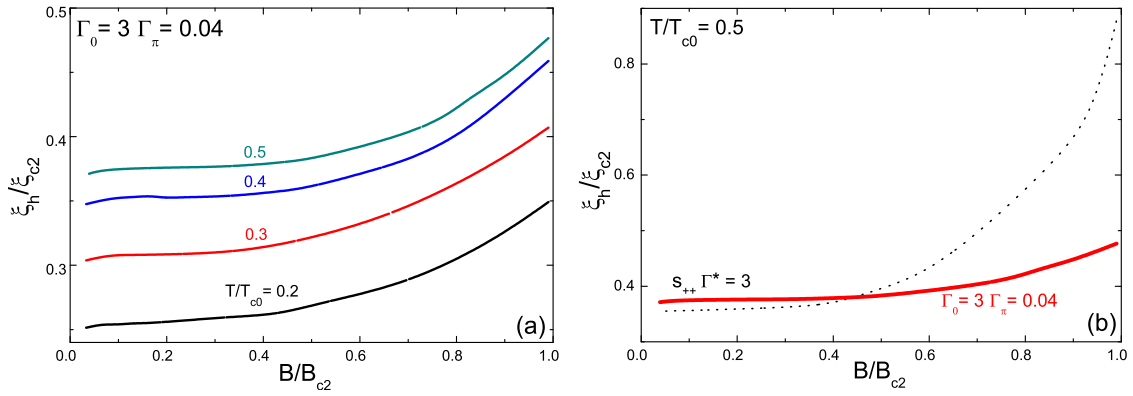


**Figure 4.** (Color online) (a) The magnetic field dependence of cutoff parameter $\xi_h/\xi_{c2}$ at different temperatures ($T/T_{c0} = 0.2, 0.3, 0.4, 0.5$) for $s^{\pm}$ pairing with $\Gamma_0 = 3$, $\Gamma_\pi = 0.04$. (b) The magnetic field dependence of $\xi_h/\xi_{c2}$ for $s^{\pm}$ model ($\Gamma_0 = 3$, $\Gamma_\pi = 0.04$, solid line) and $s_{++}$ model ($\Gamma^* = 3$, dotted line) at $T/T_{c0} = 0.5$.

The superfluid density in iron pnictides often shows a power law dependence with theexponent, which is approximately equal to two at low temperatures [39, 74]. This law was explained by $s^{\pm}$ model with parameters $\Gamma_0 = 3$ and $\Gamma_\pi = 0.04 - 0.06$. Fig. 4 (a) shows $\xi_h/\xi_{c2}(B/B_{c2})$ dependence with $\Gamma_0 = 3$ and $\Gamma_\pi = 0.04$ at different temperatures. All curves demonstrate rising behavior with values much less than one in the whole field range, i.e. they are under the AGL curve of $\xi_v$. The small value of the cutoff parameter was observed in iron pnictide $BaFe_{1.82}Co_{0.18}As$, where $\xi_h/\xi_{c2}(\sim 0.4) < 1$ [80]. Fig. 4 (b) shows $\xi_h/\xi_{c2}(B/B_{c2})$ for $\Gamma_0 = 3$, $\Gamma_\pi = 0.04$ ($s^{\pm}$ pairing) and $\Gamma^* = 3$ ($s_{++}$ pairing). It can be seen from the graph that $\xi_h/\xi_{c2}$ is strongly suppressed in $s^{\pm}$ pairing with comparison to the $s_{++}$ pairing. This can be explained by the fact that in superconductors, without interband pair breaking, the increase in high field is connected with the field-dependent pair breaking, as the upper critical field is approached. The physics of unconventional superconductors depends on impurity pair breaking and introducing characteristic field $B^*$ in the field dependence by the substitution $B/B_{c2} \to (B + B^*(\Gamma_\pi))/B_{c2}(\Gamma_\pi)$. The crossing point between $s^{\pm}$ and $s_{++}$ curves depends on $\Gamma_\pi$ and it shifts to the lower field in comparison with case $\Gamma_\pi = 0.02$ shown in Fig. 3 (a).

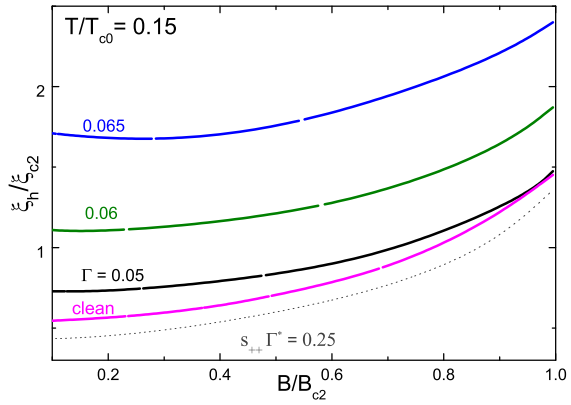


**Figure 5.** (Color online) The magnetic field dependence of the cutoff parameter at $T/T_{c0} = 0.15$ with the same values of intraband $\Gamma_0$ and interband $\Gamma_\pi$ scattering rate $\Gamma$ ($\Gamma = 0$ for "clean" case and $\Gamma = 0.05, 0.06, 0.065$ for the $s^{\pm}$ pairing). Dotted line shows result for $s_{++}$ model ($\Gamma^* = 0.25$).

The case of weak intraband scattering was also studied. This case can be realized in stoichiometrical pnictides such as LiFeAs. Fig. 5 presents the magnetic field dependence of $\xi_h/\xi_{c2}$ with scattering parameters $\Gamma_0 = \Gamma_\pi = \Gamma$ equal to 0, 0.05, 0.06 and 0.065 at $T/T_{c0} = 0.15$. The dotted line shows the result for $s_{++}$ model ($\Gamma^* = 0.25$). The $\xi_h(B)$ dependence shifts upward from the "clean" curve and has a higher values in $s^{\pm}$ model. In contrast, the $\xi_h/\xi_{c2}$ curve shifts downward with impurity scattering in $s_{++}$ model. The high values of $\xi_h$ observed in $\mu$SR measurements in LiFeAs [81] supports the $s^{\pm}$ pairing.

## 3. The cutoff parameter in the mixed state of $d_{x^2-y^2}$-wave pairing symmetry

A nontrivial orbital structure of the order parameter, in particular the presence of the gap nodes, leads to an effect in which the disorder is much richer in $d_{x^2-y^2}$-wave superconductors than in conventional materials. For instance, in contrast to the $s$-wave case, the Anderson theorem does not work, and nonmagnetic impurities exhibit a strong pair-breaking effect. In addition, a finite concentration of disorder produces a nonzero density of quasiparticle states at zero energy, which results in a considerable modification of the thermodynamic and transport properties at low temperatures. For a pure superconductor in a $d$-wave-like state at temperatures $T$ well below the critical temperature $T_c$, the deviation $\Delta\lambda$ of the penetration depth from its zero-temperature value $\lambda(0)$ is proportional to $T$. When the concentration $n_i$ of strongly scattering impurities is nonzero, $\Delta\lambda \propto T^n$, where $n = 2$ for $T < T^* \ll T_c$ and $n = 1$ for $T^* < T \ll T_c$ [24]. Unlike $s$-wave superconductor, impurity scattering suppresses both the transition temperature $T_c$ and the upper critical field $H_{c2}(T)$ [82].

The presence of the nodes in the superconducting gap can also result in unusual properties of the vortex state in $d_{x^2-y^2}$-wave superconductors. At intermediate fields $H_{c1} < H \ll H_{c2}$, properties of the flux lattice are determined primarily by the superfluid response of the condensate, i.e., by the relation between the supercurrent $\vec{j}$ and the superfluid velocity $\vec{v}_s$. In conventional isotropic strong type-II superconductors, this relation is to a good approximation that of simple proportionality,

$$\vec{j} = -e\rho_s\vec{v}_s, \tag{16}$$

where $\rho_s$ is a superfluid density. More generally, however, this relation can be both nonlocal and nonlinear. The concept of nonlocal response dates is a return to the ideas of Pippard [83] and is related to the fact that the current response must be averaged over the finite size of the Cooper pair given by the coherence length $\xi_0$. In strongly type-II materials the magnetic field varies on a length scale given by the London penetration depth $\lambda_0$, which is much larger than $\xi_0$ and, therefore, nonlocality is typically unimportant unless there exist strong anisotropies in the electronic band structure [84]. Nonlinear corrections arise from the change of quasiparticle population due to superflow which, to the leading order, modifies the excitation spectrum by a quasiclassical Doppler shift [85]

$$\varepsilon_k = E_k + \vec{v}_f\vec{v}_s, \tag{17}$$

where $E_k = \sqrt{\epsilon_k^2 + \Delta_k^2}$ is the BCS energy. Once again, in clean, fully gapped conventional superconductors, this effect is typically negligible except when the current approaches the pair breaking value. In the mixed state, this happens only in the close vicinity of the vortex cores that occupy a small fraction of the total sample volume at fields well below $H_{c2}$. The situation changes dramatically when the order parameter has nodes, such as in $d_{x^2-y^2}$ superconductors.

Nonlocal corrections to Eq. (16) become important for the response of electrons with momenta on the Fermi surface close to the gap nodes, even in strongly type-II materials. This can be understood by realizing that the coherence length, being inversely proportional to the gap [85], becomes very large close to the node and formally diverges at the nodal point. Thus, quite generally, there exists a locus of points on the Fermi surface where $\xi \gg \lambda_0$ and the response becomes highly nonlocal. This effect was first discussed in Refs. [72, 86] in the mixed state. Similarly, the nonlinear corrections become important in a $d$-wave superconductors. Eq. (17) indicates that finite areas of gapless excitations appear near the node for arbitrarily small $v_s$.

Low temperature physics of the vortex state in $s$-wave superconductors is connected with the nature of the current-carrying quantum states of the quasiparticles in the vortex core (formed due to particle-hole coherence and Andreev reflection [87]). The current distribution can be decomposed in terms of bound states and extended states contributions [88]. Close to the vortex core, the current density arises mainly from the occupation of the bound states. The effect of extended states becomes important only at distances larger than the coherence length. The bound states and the extended states contributions to the current density have opposite signs. The current density originating from the bound states is paramagnetic, whereas extended states contribute a diamagnetic term. At distances larger than the penetration depth, the paramagnetic and diamagnetic parts essentially cancel out each other, resulting in exponential decay of the total current density. The vortex core structure in the $d$-wave superconductors can be more complicated because there are important contributions coming from core states, which extend far from the vortex core into the nodal directions and significantly effect the density of states at low energy [89]. The possibility of the bound states forming in the vortex core of $d$-wave superconductors was widely discussed in terms of the Bogoliubov-de Gennes equation. For example, Franz and Teŝanoviĉ claimed that there should be no bound states [90]. However, a considerable number of bound states were found in Ref.[91] which were localized around the vortex core. Extended states, which are rather uniform, for $|E| < \Delta$ where $E$ is the quasiparticle energy and $\Delta$ is the asymptotic value of the order parameter, were also found far away from the vortex. In the problem of the bound states, the conservation of the angular momentum around the vortex is important. In spite of the strict conservation of the angular momentum it is broken due to the fourfold symmetry of $\Delta(k)$, however, the angular momentum is still conserved by modulo 4, and this is adequate to guarantee the presence of bound states.

Taking into account all these effects, the applicability of EHC theory regarding the description of the vortex state in $d_{x^2-y^2}$-wave superconductors is not evident *apriori*. In this chapter, we numerically solve the quasiclassical Eilenberger equations for the mixed state of a $d_{x^2-y^2}$-wave superconductor for the pairing potential $\Delta(\theta, \mathbf{r}) = \Delta(\mathbf{r}) \cos(2\theta)$, where $\theta$ is the angle between the $\mathbf{k}$ vector and the $a$ axis (or $x$ axis). We check the applicability of Eq. (1) and find the cutoff parameter $\xi_h$. The anisotropic extension of Eq. (1) to Amin-Franz-Affleck will be discussed in chapter 4.

To consider the mixed state of a $d$-wave superconductor we take the center of the vortex as the origin and assume that the Fermi surface is isotropic and cylindrical. The Riccatti equations for $d_{x^2-y^2}$-wave superconductivity are [92]

$$\mathbf{u} \cdot \nabla a = -a\left[2(\omega_n + G) + i\mathbf{u} \cdot \mathbf{A}_s\right] + \Delta - a^2\Delta^*, \tag{18}$$

$$\mathbf{u} \cdot \nabla b = b\left[2(\omega_n + G) + i\mathbf{u} \cdot \mathbf{A}_s\right] - \Delta^* + b^2\Delta, \tag{19}$$

where $G = 2\pi \langle g \rangle \Gamma$ with $d$-wave pairing potential $\Delta(r)$

$$\Delta(\theta, \mathbf{r}) = V^{SC}_{d_{x^2-y^2}} 2\pi T \cos(2\theta) \sum_{\omega_n>0}^{\omega_c} \int_0^{2\pi} \frac{d\bar{\theta}}{2\pi} f(\omega_n, \bar{\theta}, \mathbf{r}) cos(2\bar{\theta}), \tag{20}$$

where $V^{SC}_{d_{x^2-y^2}}$ is a coupling constant in the $d_{x^2-y^2}$ pairing channel. The obtained solution is fitted to Eq. (1) giving the value of cutoff parameter $\xi_h$ for $d_{x^2-y^2}$-wave pairing symmetry.

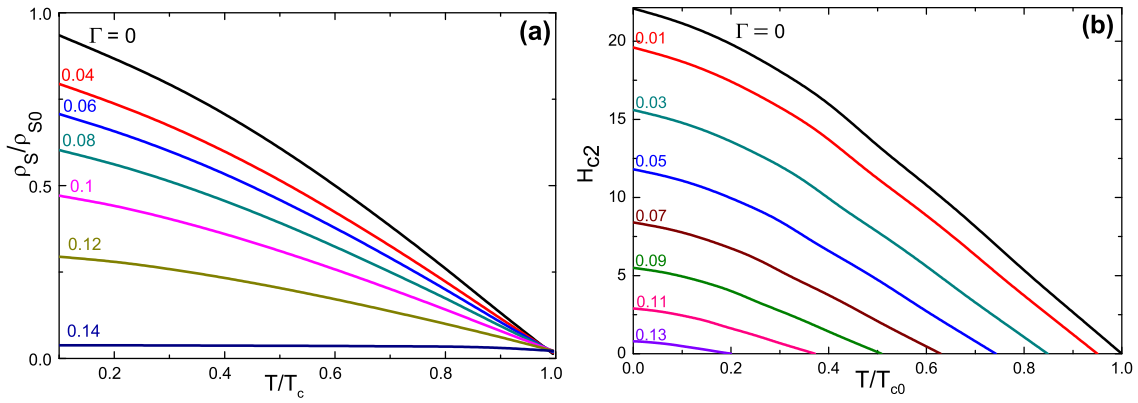


**Figure 6.** (Color online) (a) The temperature dependence of superfluid density $\rho_S(T)/\rho_{S0}$ with different values of impurity scattering $\Gamma$. (b) The temperature dependence of the upper critical field $B_{c2}$ with different values of impurity scattering $\Gamma$.

In $d_{x^2-y^2}$-wave superconductor $\lambda(T)$ in Eq. (1) is given as [85]

$$\frac{\lambda^2_{L0}}{\lambda^2(T)} = 2\pi T \oint \frac{d\theta}{2\pi} \sum_{\omega_n>0} \frac{|\tilde{\Delta}(\theta)|^2}{(\tilde{\omega}_n^2 + |\tilde{\Delta}(\theta)|^2)^{3/2}}, \tag{21}$$

where

$$\tilde{\omega}_n = \omega_n + \Gamma \langle \frac{\tilde{\omega}_n}{\sqrt{\tilde{\omega}_n^2 + |\tilde{\Delta}(\vec{p}_f^{\,\prime}; \omega_n)|^2}} \rangle_{\vec{p}_f^{\,\prime}}, \tag{22}$$

$$\tilde{\Delta}(\vec{p}_f; \omega_n) = \Delta(\vec{p}_f) + \Gamma \langle \frac{\tilde{\Delta}(\vec{p}_f^{\,\prime}; \omega_n)}{\sqrt{\tilde{\omega}_n^2 + |\tilde{\Delta}(\vec{p}_f^{\,\prime}; \omega_n)|^2}} \rangle_{\vec{p}_f^{\,\prime}}, \tag{23}$$

$$\Delta(\vec{p}_f) = \int d\vec{p}_f^{\,\prime} V(\vec{p}_f, \vec{p}_f^{\,\prime}) \pi T \sum_{\omega_n}^{|\omega_n|<\omega_c} \frac{\tilde{\Delta}(\vec{p}_f^{\,\prime})}{\sqrt{\tilde{\omega}_n^2 + |\tilde{\Delta}(\vec{p}_f^{\,\prime})|^2}}. \tag{24}$$

Because of the symmetry of $d_{x^2-y^2}$-wave pairing the impurity induced corrections for the pairing potential in Eq. (23) are zero and $\tilde{\Delta} = \Delta$. This is different from the $s^{\pm}$- and $s_{++}$ cases, where the corrections are not zero. Fig. 6 (a) shows the calculated temperature dependence of the superfluid density $\rho_S(T)/\rho_{S0} = \lambda^2_{L0}/\lambda^2(T)$ with different values of impurity scattering $\Gamma$ for $d_{x^2-y^2}$-wave pairing symmetry.

To study high the field regime we need to calculate the upper critical field $B_{c2}(T)$. For $d_{x^2-y^2}$-wave $B_{c2}(T)$ is given as [82]

$$\ln(\frac{T}{T_c}) - \Psi(\frac{1}{2} + \frac{v}{2t_c}) + \Psi(\frac{1}{2} + \frac{v}{2t}) = \frac{3}{2} \int_0^{\infty} \frac{du}{shu} \int_0^1 dz(1-z^2)[e^{-x}(1-2xc)^{-1}]e^{-\frac{v}{t}u}, \tag{25}$$

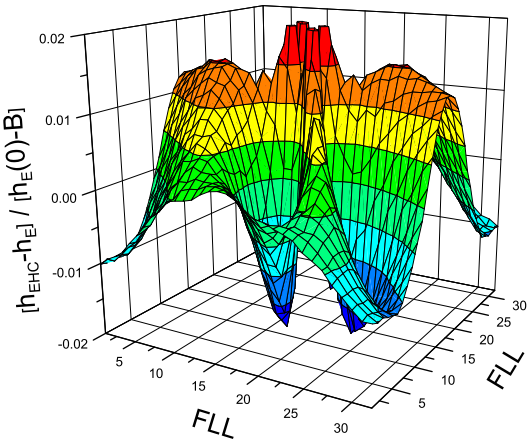


**Figure 7.** (Color online) Normalized differences between the fields calculated with the London model and the Eilenberger equation for $d_{x^2-y^2}$-wave pairing with $\Gamma = 0.03$, $B/B_{c2} = 0.1$ and $T/T_{c0} = 0.3$.

$$c[\ln(\frac{T}{T_c}) - \Psi(\frac{1}{2} + \frac{v}{2t_c}) + \Psi(\frac{1}{2} + \frac{v}{2t})] =$$

$$= \frac{3}{2}\int_0^\infty \frac{du}{shu} x \int_0^1 dz|(1-z^2)[e^{-x}(-x + c(1-4x+2x^2)) - c]e^{-\frac{v}{t}u}, \qquad (26)$$

where $v = 2\Gamma$, $t = T/T_{c0}$, $t_c = T_c/T_{c0}$ and $x = \rho u^2(1-z^2)$, $\rho = B/(4\pi t)^2$. Fig. 6 (b) depicts the temperature dependence of the upper critical field $B_{c2}$ with different values of impurity scattering $\Gamma$. Figs. 6 (a) and (b) are similar to those in $s^{\pm}$-wave superconductors. $T_c$ is suppressed by impurity scattering resulting in the same expressions for $s^{\pm}$ and $d$-wave superconductors with replacing $\Gamma_\pi \to \Gamma/2$.

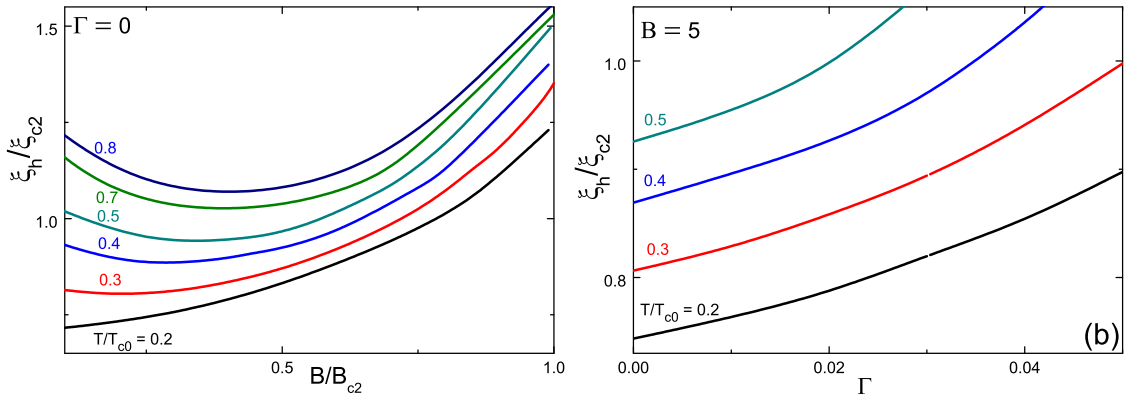


**Figure 8.** (Color online) (a) The magnetic field dependence of the cutoff parameter $\xi_h/\xi_{c2}$ with different temperatures ($T/T_{c0} = 0.2, 0.3, 0.4, 0.5, 0.7, 0.8$) for $d_{x^2-y^2}$ pairing with $\Gamma = 0$. (b) The impurity scattering $\Gamma$ dependence of $\xi_h/\xi_{c2}$ at different temperatures for $d_{x^2-y^2}$ pairing with $B = 5$.

Fig. 7 shows the normalized differences between the fields calculated with the London model and the Eilenberger equations for $d_{x^2-y^2}$-wave pairing symmetry for the values of $\Gamma = 0.03$, $B/B_{c2} = 0.1$ and $T/T_{c0} = 0.3$. The accuracy of the fitting is better than 2%.

Fig. 8 (a) demonstrates the magnetic field dependence of cutoff parameter $\xi_h/\xi_{c2}$ at different temperatures ($T/T_{c0} = 0.2, 0.3, 0.4, 0.5, 0.7, 0.8$) for $d_{x^2-y^2}$ pairing with $\Gamma = 0$. Fig. 8 (b) shows the impurity scattering $\Gamma$ dependence of $\xi_h/\xi_{c2}$ at different temperatures for $d_{x^2-y^2}$

pairing with $B = 5$. For clean superconductors (Fig. 8 (a)) $\xi_h/\xi_{c2}$ has a minimum in its field dependence similar to usual $s$-wave superconductors [93]. However, this ratio decreases with temperature due to Kramer-Pesch effect. It was demonstrated theoretically and experimentally that the low energy density of states $N(E)$ is described by the same singular $V$-shape form $N(E) = N_0(H) + \alpha|E| + O(E^2)$ for all clean superconductors in a vortex state, irrespective of the underlying gap structure [94]. This explains the similarity in the behavior between $s$- and $d$-wave pairing symmetries.

The difference between pairing symmetries reveals itself in impurity scattering dependence $\xi_h/\xi_{c2}$. In $s_{++}$ symmetry $\xi_h/\xi_{c2}$ always decreases with impurity scattering rate $\Gamma$ (Fig. 3 (a)), in $s^{\pm}$ symmetry its behavior depends on the field range and relative values of intraband and interband impurity scattering rates: it can be a decreasing function of $\Gamma_\pi$ (Fig. 4 (b)) or an increasing function of $\Gamma_\pi$ (Fig. 3 (b)). In $d$-wave superconductors $\xi_h/\xi_{c2}$ always increases with $\Gamma$ (Fig. 8 (b)) similar to the case of $s^{\pm}$ symmetry with $\Gamma_0 = \Gamma_\pi$ ( Fig. 5). This can be understood from the comparison of the Ricatti equations of the $s^{\pm}$ and $d$-wave pairing. In both cases the renormalization factor $F = 0$ due to a cancelation of the intraband and interband impurity scattering rates in $s^{\pm}$ pairing or symmetry reason $\langle f \rangle = 0$ for $d$-wave pairing.

## 4. The quasiclassical approach to the Amin-Franz-Affleck model and the effective penetration depth in the mixed state in $d_{x^2-y^2}$-wave pairing symmetry

In this chapter, we construct a model where the nonlinear corrections arising from the Doppler energy shift of the quasiparticle states by the supercurrent [85] and effects of the vortex core states are described by an effective cutoff function. Nonlocal effects of the extended quasiparticle states are included in our model explicitly, i. e. instead of $\lambda(T)$ in Eq. (1) we use an analytically obtained anisotropic electromagnetic response tensor [70, 72, 73]. Because the nonlocal effects are assumed to be effective in clean superconductors we limit our consideration to the case $\Gamma = 0$.

For a better comparison with the nonlocal generalized London equation (NGLE) and the AGL theory we used another normalization of the cutoff parameter in Eq. (1), $u = k_1\sqrt{2}\xi_{BCS}G$. This form of $F(G)$ correctly describes the high temperature regime. We compare our results with those obtained from the NGLE theory in a wide field and temperature range considering $k_1$ as the fitting parameter.

The magnetic field distribution in the mixed state in the NGLE approximation is given by [72]

$$h_{NGLE}(\mathbf{r}) = \frac{\Phi_0}{S}\sum_{\mathbf{G}}\frac{F(G)e^{i\mathbf{G}\mathbf{r}}}{1 + L_{ij}(\mathbf{G})G_iG_j}, \tag{27}$$

where

$$L_{ij}(\mathbf{G}) = \frac{Q_{ij}(\mathbf{G})}{\det\hat{\mathbf{Q}}(\mathbf{G})}. \tag{28}$$

The anisotropic electromagnetic response tensor is defined by

$$Q_{ij}(\mathbf{G}) = \frac{4\pi T}{\lambda_{L0}^2}\sum_{\omega_n>0}\int_0^{2\pi}\frac{d\theta}{2\pi}\frac{\Delta(\theta)^2\hat{v}_{Fi}\hat{v}_{Fj}}{\sqrt{\omega_n^2 + |\Delta(\theta)^2|}(\omega_n^2 + |\Delta(\theta)^2| + \gamma_{\mathbf{G}}^2)}, \tag{29}$$

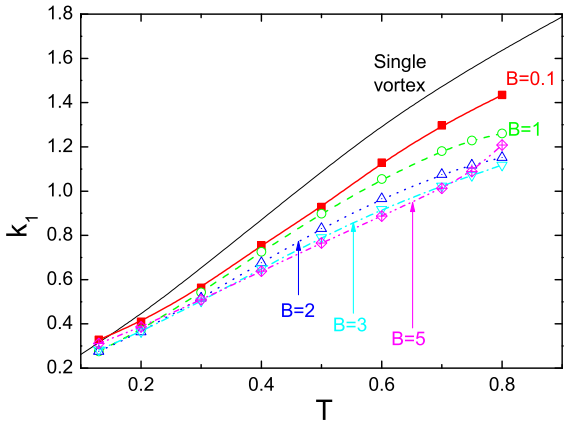


**Figure 9.** (Color online) The temperature dependence of the coefficient $k_1$ in the NGLE model obtained at $\kappa = 10$ and $B = 0.1, 1, 2, 3, 5$ from a fitting made with the solution of the Eilenberger equations.

where $\gamma_{\mathbf{G}} = \mathbf{v}_F \cdot \mathbf{G}/2$. In Eq. (29) the term with $\gamma_{\mathbf{G}}$ describes the nonlocal correction to the London equation. Putting $\gamma_{\mathbf{G}} = 0$ we obtain the London result $L_{ij}(\mathbf{G}) = \lambda(T)^2\delta_{ij}$. We use the same shape of the cutoff function as in Eq. (1) but the values of the cutoff parameters are different because of fitting them to the various field distributions. In presentation of $h_{NGLE}$ the anisotropy effects of the Eilenberger theory remain.

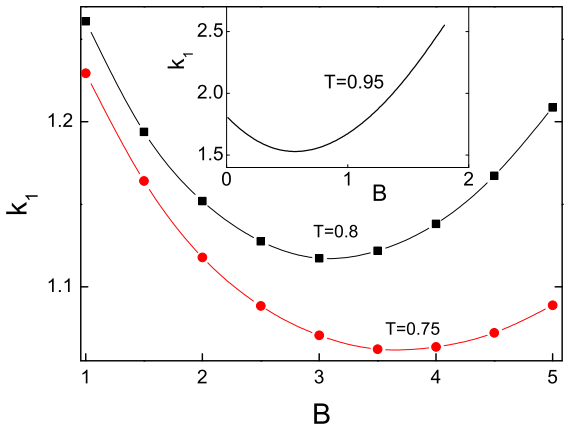


**Figure 10.** (Color online) Field dependence of $k_1$ at $T = 0.75$ and 0.8 obtained from the fitting to the Eilenberger equations. The inset shows $k_1(B)$ calculated from the Hao-Clem theory at $T = 0.95$.

Fig. 9 shows the $k_1(T)$ dependence in the NGLE model obtained at $\kappa = 10$ and $B = 0.1, 1, 2, 3, 5$ from the fitting to the solution of the Eilenberger equations. As can be seen from Fig. 9 the coefficient $k_1$ is strongly reduced at low temperatures. This is a reminiscent of the Kramer-Pesch result for $s$-wave superconductors (shrinking of the vortex core with decreasing temperature) [95]. It is also found that $k_1$ is a decreasing function of $B$. This can be explained by reduction of the vortex core size by the field [68]. The topmost curve in Fig. 9 gives the values of $k_1$ calculated for a single vortex [96]. At high temperatures the Ginzburg-Landau theory can be applied. Using the values of the parameters of this theory for $d$-wave superconductors [97] $\xi_{GL} = \xi_{BCS}\pi/\sqrt{3}$ is obtained. A variational approach of the Ginzburg-Landau equations for the single vortex [62] gives $k_1 = \pi/\sqrt{3} \approx 1.81$ is in reasonable agreement with the high temperature limit of $k_1$ for a single vortex in Fig. 9. Another interesting observation is the nonmonotonic behavior of $k_1(B)$ in low fields at high

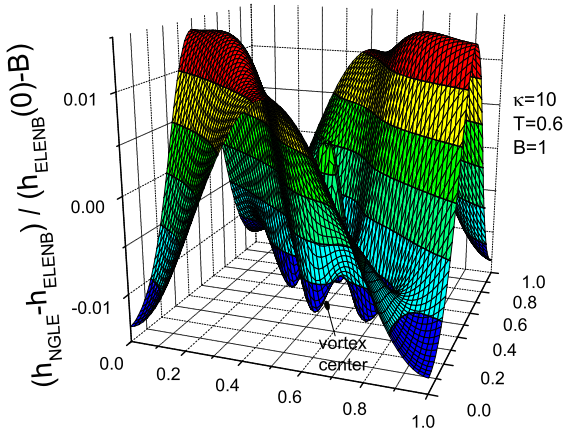


**Figure 11.** (Color online) Normalized differences between the fields calculated with the London model (NGLE) and the Eilenberger equation (ELENB) for $B = 1$ and $T = 0.6$. The scales of lengths are those of the flux line lattice unit vectors.

temperatures. Fig. 10 depicts the field dependence of $k_1$ at $T = 0.75$ and 0.8 showing a minimum which moves to lower fields with increasing of the temperature. This result agrees qualitatively with the Hao-Clem theory [63] which also predicts a minimum in the $k_1(B)$ dependence. This is demonstrated in the inset to Fig. 10, where $k_1(B)$ is shown at $T = 0.95$.

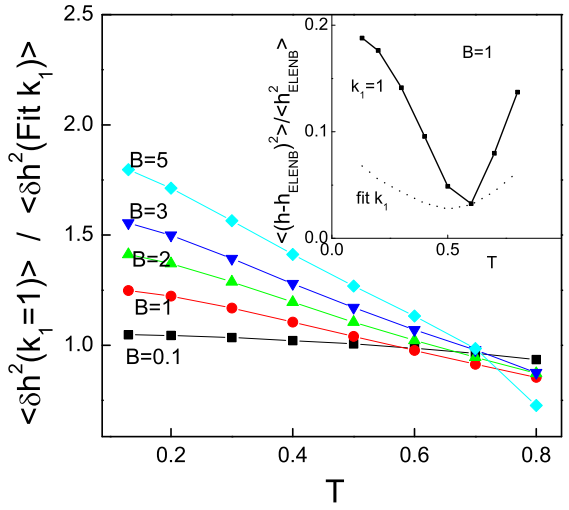


**Figure 12.** (Color online) Temperature dependence of the ratio of the second moment of the magnetic field distributions obtained from the NGLE model with the fixed and fitted parameter $k_1$ (see the text below). The inset shows the mean-square deviation of the magnetic field distribution from the origin for parameter $k_1$ set to unity (solid line) and fitted (dotted line).

The quality of the fitting can be seen from Fig. 11 where the normalized difference between the fields calculated in the NGLE model and the Eilenberger equations at $B = 1$, $T = 0.6$ and $\kappa = 10$ is shown. The accuracy of the fitting is about 1 percent. Thus, there is only a little improvement in the Eilenberger equations fitting to NGLE theory in comparison with local London theory (Eq. (1)). The similarity of the field and temperature dependences of the cutoff parameter in these theories are shown in Fig. 9 and Fig. 10.

To show the influence of the magnetic field and temperature on $k_1$ dependence, we calculate the values of $\langle \delta h^2_{NGLE} \rangle$ using the field distribution obtained in the Eq. 27. Fig. 12 shows

the temperature dependence of the ratio $\langle \delta h^2_{NGLE} \rangle$ with the cutoff parameter obtained from the solution of the Eilenberger equations to that with $k_1 = 1$. From the data presented in Fig. 12, it can be sen that this ratio deviates considerably from unity when the temperature is lowered, which points to the importance of the proper determination of the value for the cutoff parameter. For the magnetic field distribution, obtained from solving the NGLE, we also calculate the mean-square deviation of this distribution from the origin (the Eilenberger equations solution). The inset demonstrates this deviation for fixed and fitted parameter $k_1$.

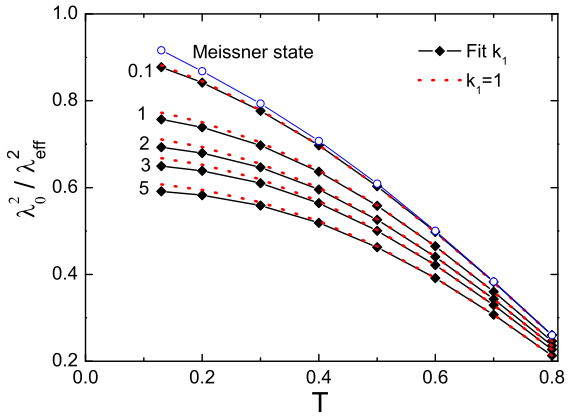


**Figure 13.** (Color online) The ratio of $\lambda_0$ to $\lambda_{eff}$ calculated from the NGLE equation with $k_1 = 1$ and $k_1$ from Fig. 9.

This consideration proves that the nonlocal generalized London model with $h_{NGLE}(\mathbf{r})$ distribution also needs the properly determined cutoff parameter $k_1$, *i.e.* introducing only nonlocal extended electronic states does not allow the avoidance of the problem of vortex core solving.

In the analysis of the experimental $\mu$SR and SANS data the field dependent penetration depth $\lambda_{eff}(B)$ is often introduced [56]. It has physical sense even if it is not dependent on the core effects, *i.e.* it should be an invariant of the cutoff parameter. One such way of doing this was suggested in the AFA model [70, 73]:

$$\frac{\lambda_{eff}}{\lambda} = \left(\frac{|\delta h_0^2|}{|\delta h^2_{NGLE}|}\right)^{1/4}. \tag{30}$$

Here, $|\delta h_0^2|$ is the variance of the magnetic field $h_0(\mathbf{r})$ obtained by applying the ordinary London model with the same average field $B$ and $\lambda$ and with the same cutoff parameter as in the field distribution $h_{NGLE}(\mathbf{r})$.

In Fig. 13 establishes the temperature dependence of the ratio $\lambda_0^2/\lambda_{eff}^2$ calculated from the $h_{NGLE}$ distribution with $k_1 = 1$ and with Fit $k_1$ from the solution of Eilenberger equations for the different field value. The obtained $\lambda_{eff}(B)$ dependences are quite similar in these cases. The low-field result ($B/B_0 = 0.1$) for $\lambda_{eff}$ is close to $\lambda(T)$ in the Meissner state. This demonstrates that $\lambda_{eff}$ is determined by a large scale of the order of FLL period and is not very sensitive to details of the microscopical core structure and the cutoff parameter [98]. The AFA model was originally developed in order to explain the structural transition in FLL in $d$-wave superconductors where anisotropy and nonlocal effects arise from nodes in the gap at the Fermi surface and the appearance there of the long extending electronic states [72].

The obtained anisotropy of superconducting current around the single vortex in AFA theory agrees reasonably with that found from the Eilenberger equations [96]. Extending electronic states also results in the observed field dependent flattening of $\lambda_{eff}(B)$ at low temperatures [73]. Thus, our microscopical consideration justifies the phenomenological AFA model and the separation between localized and extended states appears to be quite reasonable.

## 5. Conclusions

The core structure of the vortices is studied for $s^{\pm}$, $d_{x^2-y^2}$ symmetries (connected with interband and intraband antiferromagnetic spin fluctuation mechanism, respectively) and $s_{++}$ symmetry (mediated by moderate electron-phonon interaction due to Fe-ion oscillation and the critical orbital fluctuation) using Eilenberger approach and compared with the experimental data for iron pnictides. It is assumed [99] that the nodeless $s^{\pm}$ pairing state is realized in all optimally-doped iron pnictides, while nodes in the gap are observed in the over-doped $KFe_2As_2$ compound, implying a $d_{x^2-y^2}$-wave pairing state, there are also other points of view [10, 13]. The stoichiometrical LiFeAs, without antifferomagmetic ordering, is considered as a candidate for the implementation of the $s_{++}$ symmetry. Different impurity scattering rate dependences of cutoff parameter $\xi_h$ are found for $s^{\pm}$ and $s_{++}$ cases. In the nonstoichiometric case, when intraband impurity scattering ($\Gamma_0$) is much larger than the interband impurity scattering rate ($\Gamma_\pi$) the $\xi_h/\xi_{c2}$ ratio is less in $s^{\pm}$ symmetry. When $\Gamma_0 \approx \Gamma_\pi$ (stoichiometric case) opposite tendencies are found, in $s^{\pm}$ symmetry the $\xi_h/\xi_{c2}$ rises above the "clean" case curve ($\Gamma_0 = \Gamma_\pi = 0$) while it decreases below the curve in the $s_{++}$ case. In $d$-wave superconductors $\xi_h/\xi_{c2}$ always increases with $\Gamma$. For $d_{x^2-y^2}$ pairing the nonlocal generalized London equation and its connection with the Eilenberger theory are also considered. The problem of the effective penetration depth in the vortex state for $d$-wave superconductors is discussed. In this case, the field dependence of $\lambda_{eff}$ is connected with the extended quasiclassical state near the nodes of the superconducting gap.

## Author details

I. Zakharchuk, P. Belova, K. B. Traito and E. Lähderanta
*Lappeenranta University of Technology, Finland*

## 6. References

[1] Q. Li, Y. N. Tsay, M. Suenaga, R. A. Klemm, G. D. Gu, and N. Koshizuka. *Phys. Rev. Lett.*, 83:4160, 1999.
[2] R. A. Klemm. *Int. J. Mod. Phys. B*, 12:2920, 1983.
[3] D. R. Harshman, W. J. Kossler, X. Wan, A. T. Fiory, A. J. Greer, D. R. Noakes, C. E. Stronach, E. Koster, and J. D. Dow. *Phys. Rev. B*, 69:174505, 2004.
[4] A. G. Sun, D. A. Cajewski, M. B. Maple, and R. C. Dynes. *Phys. Rev. Lett.*, 72:2267, 1994.
[5] D. A. Wollmann, D. J. Van Harlingen, J. Giapintzakis, and D. M. Ginsberg. *Phys. Rev. Lett.*, 74:797, 1995.
[6] J. P. Rice, N. Rigakis, D. M. Ginsberg, and J. M. Mochel. *Phys. Rev. B*, 46:11050, 1992.
[7] C. C. Tsuei, J. R. Kirtley, C. C. Chi, L. S. Yu-Jahnes, A. Gupta, T. Shaw, J. Z. Sun, and M. B. Ketchen. *Phys. Rev. Lett.*, 73:593, 1994.
[8] Y. Kamihara, T. Watanabe, M. Hirano, and H. Hosono. *J. Am. Chem. Soc.*, 130:3296, 2008.

[9] X.C. Wang, Q.Q. Liu, Y.X. Lv, W.B. Gao, L.X. Yang, R.C. Yu, F.Y. Li, and C.Q. Jin. *Solid State Commun.*, 148:538, 2008.
[10] I. I. Mazin, D. J. Singh, M. D. Johannes, and M. H. Du. *Phys. Rev. Lett.*, 101:057003, 2008.
[11] K. Kuroki, S. Onari, R. Arita, H. Usui, Y. Tanaka, H. Kontani, and H. Aoki. *Phys. Rev. Lett.*, 101:087004, 2008.
[12] K. Seo, B. A. Bernevig, and J. Hu. *Phys. Rev. Lett.*, 101:206404, 2008.
[13] H. Kontani and S. Onari. *Phys. Rev. Lett.*, 104:157001, 2010.
[14] Y. Yanagi, Y. Yamakawa, and Y. Ōno. *Phys. Rev. B*, 81:054518, 2010.
[15] H. Ding, K. Nakayama P. Richard and, K. Sugawara, T. Arakane, Y. Sekiba, A. Takayama, S. Souma, T. Sato, T. Takahashi, Z. Wang, X. Dai, Z. Fang, G. F. Chen, J. L. Luo, and N. L. Wang. *Europhys. Lett.*, 83:47001, 2008.
[16] L. Wray, D. Qian, D. Hsieh, Y. Xia, L. Li, J. G. Checkelsky, A. Pasupathy, K.K. Gomes, C.V. Parker, A.V. Fedorov, G. F. Chen, J. L. Luo, A. Yazdani, N. P. Ong, N. L. Wang, and M. Z. Hasan. *Phys. Rev. B*, 78:184508, 2008.
[17] Z. H. Liu, P. Richard, K. Nakayama, G.-F. Chen, S. Dong, J. B. He, D. M. Wang, T.-L. Xia, K. Umezawa, T. Kawahara, S. Souma, T. Sato, T. Takahashi, T. Qian, Y. Huang, N. Xu, Y. Shi, H. Ding, and S. C. Wang. *Phys. Rev. B*, 84:064519, 2011.
[18] A. D. Christianson, E. A. Goremychkin, R. Osborn, S. Rosenkranz, M. D. Lumsden, C. D. Malliakas, I. S. Todorov, H. Claus, D. Y. Chung, M. G. Kanatzidis, R. I. Bewley, and T. Guidi. *Nature (London)*, 456:930, 2008.
[19] T. Hanaguri, S. Niitaka, K. Kuroki, and H. Takagi. *Science*, 328:474, 2010.
[20] S. Onari, H. Kontani, and M. Sato. *Phys. Rev. B*, 81:060504(R), 2010.
[21] S. Onari and H. Kontani. *Phys. Rev. Lett.*, 103:177001, 2009.
[22] C. Tarantini, M. Putti, A. Gurevich, Y. Shen, R. K. Singh, J. M. Rowell, N. Newman, D. C. Larbalestier, P. Cheng, Y.Jia, and H.-H. Wen. *Phys. Rev. Lett.*, 104:087002, 2010.
[23] G. R. Stewart. *Rep. Prog. Phys.*, 83:1589, 2011.
[24] P. J. Hirschfeld and N. Goldenfeld. *Phys. Rev. B*, 48:4219, 1993.
[25] K. Hashimoto, T. Shibauchi, S. Kasahara, K. Ikada, S. Tonegawa, T. Kato, R. Okazaki, C. J. van der Beek, M. Konczykowski, H. Takeya, K. Hirata, T. Terashima, and Y. Matsuda. *Phys. Rev. Lett.*, 102:207001, 2009.
[26] L. Luan, T. M. Lippman, C. W. Hicks, J. A. Bert, O. M. Auslaender, J.-H. Chu, J. G. Analytis, I. R. Fisher, and K. A. Moler. *Phys. Rev. Lett.*, 106:067001, 2011.
[27] M. A. Tanatar, J.-Ph. Reid, H. Shakeripour, X. G. Luo, N. Doiron-Leyraud, N. Ni, S. L. Bud'ko, P. C. Canfield, R. Prozorov, and L. Taillefer. *Phys. Rev. Lett.*, 104:067002, 2010.
[28] J. D. Fletcher, A. Serafin, L. Malone, J. G. Analytis, J.-H. Chu, A. S. Erickson, I. R. Fisher, and A. Carrington. *Phys. Rev. Lett.*, 102:147001, 2009.
[29] C. W. Hicks, T. M. Lippman, M. E. Huber, J. G. Analytis, J.-H. Chu, A. S. Erickson, I. R. Fisher, and K. A. Moler. *Phys. Rev. Lett.*, 103:127003, 2009.
[30] K. Hashimoto, M. Yamashita, S. Kasahara, Y. Senshu, N. Nakata, S. Tonegawa, K. Ikada, A. Serafin, A. Carrington, T. Terashima, H. Ikeda, T. Shibauchi, and Y. Matsuda. *Phys. Rev. B*, 81:220501(R), 2010.
[31] Y. Nakai, T. Iye, S. Kitagawa, K. Ishida, S. Kasahara, T. Shibauchi, Y. Matsuda, and T. Terashima. *Phys. Rev. B*, 81:020503(R), 2010.
[32] M. Yamashita, Y. Senshu, T. Shibauchi, S. Kasahara, K. Hashimoto, D. Watanabe, H. Ikeda, T. Terashima, I. Vekhter, A. B. Vorontsov, and Y. Matsuda. *Phys. Rev. B*, 84:060507(R), 2011.

[33] J. K. Dong, S. Y. Zhou, T. Y. Guan, H. Zhang, Y. F. Dai, X. Qiu, X. F. Wang, Y. He, X. H. Chen, and S. Y. Li. *Phys. Rev. Lett.*, 104:087005, 2010.
[34] K. Hashimoto, A. Serafin, S. Tonegawa, R. Katsumata, R. Okazaki, T. Saito, H. Fukazawa, Y. Kohori, K. Kihou, C. H. Lee, A. Iyo, H. Eisaki, H. Ikeda, Y. Matsuda, A. Carrington, and T. Shibauchi. *Phys. Rev. B*, 82:014526, 2010.
[35] G. Xu, H. Zhang, X. Dai, and Z. Fang. *Europhys. Lett.*, 84:67015, 2008.
[36] R. Thomale, C. Platt, W. Hanke, and B. A. Bernevig. *Phys. Rev. Lett.*, 106:187003, 2011.
[37] Y. J. Yan, X. F. Wang, R. H. Liu, H. Chen, Y. L. Xie, J. J. Ying, and X. H. Chen. *Phys. Rev. B*, 81:235107, 2010.
[38] N. Ni, S. L. Bud'ko, A. Kreyssig, S. Nandi, G. E. Rustan, A. I. Goldman, S. Gupta, J. D. Corbett, A. Kracher, and P. C. Canfield. *Phys. Rev. B*, 78:014507, 2008.
[39] C. Martin, R. T. Gordon, M. A. Tanatar, H. Kim, N. Ni, S. L. Bud'ko, P. C. Canfield, H. Luo, H. H. Wen, Z. Wang, A. B. Vorontsov, V. G. Kogan, and R. Prozorov. *Phys. Rev. B*, 80:020501(R), 2009.
[40] M. Rotter, M. Tegel, and D. Johrendt. *Phys. Rev. Lett.*, 101:107006, 2008.
[41] Y. Zhang, L. X. Yang, F. Chen, B. Zhou, X. F. Wang, X. H. Chen, M. Arita, K. Shimada, H. Namatame, M. Taniguchi, J. P. Hu, B. P. Xie, and D. L. Feng. *Phys. Rev. Lett.*, 105:117003, 2010.
[42] S.W. Zhang, L. Ma, Y. D. Hou, J. Zhang, T.-L. Xia, G. F. Chen, J. P. Hu, G. M. Luke, and W. Yu. *Phys. Rev. B*, 81:012503, 2010.
[43] T. Sato, K. Nakayama, Y. Sekiba, P. Richard, Y.-M. Xu, S. Souma, T. Takahashi, G. F. Chen, J. L. Luo, N. L. Wang, and H. Ding. *Phys. Rev. Lett.*, 103:047002, 2009.
[44] R. Thomale, C. Platt, W. Hanke, J. Hu, and B. A. Bernevig. *Phys. Rev. Lett.*, 107:117001, 2011.
[45] J. H. Tapp, Z. J. Tang, B. Lv, K. Sasmal, B. Lorenz, P. C. W. Chu, and A. M. Guloy. *Phys. Rev. B*, 78:060505(R), 2008.
[46] D. J. Singh. *Phys. Rev. B*, 78:094511, 2008.
[47] I. A. Nekrasov, Z.V. Pchelkina, and M.V. Sadovskii. *JETP Lett.*, 88:543, 2008.
[48] R. A. Jishi and H. M. Alyahyaei. *Adv. Condens. Matter Phys.*, 2010:1, 2010.
[49] S. J. Zhang, X. C. Wang, R. Sammynaiken, J. S. Tse, L. X. Yang, Z. Li, Q. Q. Liu, S. Desgreniers, Y. Yao, H. Z. Liu, and C. Q. Jin. *Phys. Rev. B*, 80:014506, 2009.
[50] F. L. Pratt, P. J. Baker, S. J. Blundell, T. Lancaster, H. J. Lewtas, P. Adamson, M. J. Pitcher, D. R. Parker, and S. J. Clarke. *Phys. Rev. B*, 79:052508, 2009.
[51] C.W. Chu, F. Chen, M. Gooch, A.M. Guloy, B. Lorenz, B. Lv, K. Sasmal, Z.J. Tang, J.H. Tapp, and Y.Y. Xue. *Physica C*, 469:326, 2009.
[52] S. V. Borisenko, V. B. Zabolotnyy, D. V. Evtushinsky, T. K. Kim, I. V. Morozov, A. N. Yaresko, A. A. Kordyuk, G. Behr, A. Vasiliev, R. Follath, and B. Büchner. *Phys. Rev. Lett.*, 105:067002, 2010.
[53] K. Umezawa, Y. Li, H. Miao, K. Nakayama, Z.-H. Liu, P. Richard, T. Sato, J. B. He, D.-M. Wang, G. F. Chen, H. Ding, T. Takahashi, and S.-C. Wang. *Phys. Rev. Lett.*, 108:037002, 2012.
[54] R. Laiho, M. Safonchik, and K. B. Traito. *Phys. Rev. B*, 76:140501(R), 2007.
[55] R. Laiho, M. Safonchik, and K. B. Traito. *Phys. Rev. B*, 78:064521, 2008.
[56] J. E. Sonier. *Rep. Prog. Phys.*, 70:1717, 2007.
[57] P. deGennes. *Superconductivity of Metals and Alloys*, pages Addison–Wesley, New York, 1989.

[58] V. G. Kogan, A. Gurevich, J. H. Cho, D. C. Johnston, M. Xu, J. R. Thompson, and A. Martynovich. *Phys. Rev. B*, 54:12386, 1996.
[59] E. H. Brandt. *Phys. Rev. B*, 37:2349(R), 1988.
[60] E. H. Brandt. *Physica C*, 195:1, 1992.
[61] I. G. de Oliveira and A. M. Thompson. *Phys. Rev. B*, 57:7477, 1998.
[62] J. R. Clem. *J. Low Temp. Phys*, 18:427, 1975.
[63] Z. Hao, J. R. Clem, M. W. McElfresh, L. Civale, A. P. Malozemoff, and F. Holtzberg. *Phys. Rev. B*, 43:2844, 1991.
[64] A. Yaouanc, P. Dalmas de Reotier, and E. H. Brandt. *Phys. Rev. B*, 55:11107, 1997.
[65] W. V. Pogosov, K. I. Kugel, A. L. Rakhmanov, and E. H. Brandt. *Phys. Rev. B*, 64:064517, 2001.
[66] A. Maisuradze, R. Khasanov, A. Shengelaya, and H. Keller. *J. Phys.: Condens. Matter*, 21:S075701, 2009.
[67] L. Kramer and W. Pesch. *Z. Phys.*, 269:59, 1974.
[68] M. Ichioka, A. Hasegawa, and K. Machida. *Phys. Rev. B*, 59:8902, 1999.
[69] M. Ichioka, A. Hasegawa, and K. Machida. *Phys. Rev. B*, 59:184, 1999.
[70] M. H. S. Amin, I. Affleck, and M. Franz. *Phys. Rev. B*, 58:5848, 1998.
[71] I. Affleck, M. Franz, and M. H. Sharifzadeh Amin. *Phys. Rev. B*, 55, 1997.
[72] M. Franz, I. Affleck, and M. H. S. Amin. *Phys. Rev. Lett.*, 79:1555, 1997.
[73] M. H. S. Amin, M. Franz, and I. Affleck. *Phys. Rev. Lett.*, 84:5864, 2000.
[74] A. B. Vorontsov, M. G. Vavilov, and A. V. Chubukov. *Phys. Rev. B*, 79:140507(R), 2009.
[75] W. A. Huttema, J. S. Bobowski, P. J. Turner, R.Liang, W. N. Hardy, D. A. Bonn, and D. M. Broun. *Phys. Rev. B*, 80:104509, 2009.
[76] V. G. Fleisher, Yu. P. Stepanov, K. B. Traito, E. Lähderanta, and R. Laiho. *Physica C*, 264:295, 1996.
[77] P. Miranović, M. Ichioka, and K. Machida. *Phys. Rev. B*, 70:104510, 2004.
[78] Y. N. Ovchinnikov and V. Z. Kresin. *Phys. Rev. B*, 52:3075, 1995.
[79] J. E. Sonier. *J. Phys.: Condens. Matter*, 16:S4499, 2004.
[80] J. E. Sonier, W. Huang, C. V. Kaiser, C. Cochrane, V. Pacradouni, S. A. Sabok-Sayr, M. D. Lumsden, B. C. Sales, M. A. McGuire, A. S. Sefat, and D. Mandrus. *Phys. Rev. Lett.*, 106:127002, 2011.
[81] D. S. Inosov, J. S. White, D. V. Evtushinsky, I. V. Morozov, A. Cameron, U. Stockert, V. B. Zabolotnyy, T. K. Kim, A. A. Kordyuk, S. V. Borisenko, E. M. Forgan, R. Klingeler, J. T. Park, S. Wurmehl, A. N. Vasiliev, G. Behr, C. D. Dewhurst, and V. Hinkov. *Phys. Rev. Lett.*, 104:187001, 2010.
[82] G. Yin and K. Maki. *Physica B*, 194-196:2025, 1994.
[83] A. B. Pippard. *Proc. R. Soc. London A*, 216:547, 1953.
[84] V. G. Kogan, M. Bullock, B. Harmon, P. Miranovic̀, Lj. Dobrosavljevic̀-Grujic̀, P. L. Gammel, and D. J. Bishop. *Phys. Rev. B*, 55:8693 (R), 1997.
[85] D. Xu, S. K. Yip, and J. A. Sauls. *Phys. Rev. B*, 51:16233, 1995.
[86] I. Kosztin and A. J. Leggett. *Phys. Rev. Lett.*, 79:135, 1997.
[87] D. Rainer, J. A. Sauls, and D. Waxman. *Phys. Rev. B*, 54:10094, 1996.
[88] F. Gygi and M. Schluter. *Phys. Rev. B*, 41:822, 1990.
[89] T. Dahm, S. Graser, C. Iniotakis, and N. Schopohl. *Phys. Rev. B*, 66:144515, 2002.
[90] M. Franz and Z. Tesȃnovic̑. *Phys. Rev. Lett.*, 80:4763, 1998.
[91] M. Kato and K. Maki. *Physica B*, 284:739, 2000.
[92] A. Zare, A. Markowsky, T. Dahm, and N. Schopohl. *Phys. Rev. B*, 78:104524, 2008.

[93] P. Belova, K. B. Traito, and E. Lähderanta. *J. Appl. Phys.*, 110:033911, 2011.
[94] N. Nakai, P. Miranovic, M. Ichioka, H. F. Hess, K. Uchiyama, H. Nishimori, S. Kaneko, N. Nishida, and K. Machida. *Phys. Rev. Lett.*, 97:147001, 2006.
[95] L. Kramer and W. Pesch. *J. Low Temp. Phys.*, 15:367, 1974.
[96] R. Laiho, E. Lähderanta, M. Safonchik, and K. B. Traito. *Phys. Rev. B*, 71:024521, 2005.
[97] Y. Ren, J.-H. Xu, and C. S. Ting. *Phys. Rev. Lett.*, 74:3680, 1995.
[98] R. Laiho, M. Safonchik, and K. B. Traito. *Phys. Rev. B*, 73:024507, 2006.
[99] D. C. Johnston. *Advances in Physics*, 59:803, 2010.

# PUBL. 3

**P. Belova, I. Zakharchuk, K. B. Traito and E. Lähderanta**, Impact of the order parameter symmetries on the vortex core structure in iron-based superconductors, *Modern Physics Letters B*, **26**, 1230013, 2012 DOI: 10.1142/S021798491230013X

Brief Review

Modern Physics Letters B
Vol. 26, No. 21 (2012) 1230013 (25 pages)

DOI: 10.1142/S021798491230013X

World Scientific
www.worldscientific.com

# IMPACT OF THE ORDER PARAMETER SYMMETRIES ON THE VORTEX CORE STRUCTURE IN IRON-BASED SUPERCONDUCTORS

POLINA BELOVA*,†,§, IVAN ZAKHARCHUK*,‡, KONSTANTIN BORISOVICH TRAITO* and ERKKI LÄHDERANTA*

*Department of Technomathematics and Technical Physics,
Lappeenranta University of Technology, P. O. Box 20, FI-53851, Lappeenranta, Finland
†Petrozavodsk State University, Lenin Str. 33, RU-185640, Petrozavodsk, Russia
‡Saint-Petersburg Electrotechnical University,
Popov Str. 5, RU-197376, St. Petersburg, Russia
§Polina.Belova@lut.fi

Received 6 June 2012
Accepted 6 June 2012
Published 13 July 2012

Effects of the order parameter symmetries on the cutoff parameter $\xi_h$ (determining the magnetic field distribution) in the mixed state are investigated in the framework of quasiclassical Eilenberger theory for isotropic $s^{\pm}$, $s_{++}$ and anisotropic $d_{x^2-y^2}$-wave superconducting pairings. These symmetries are proposed for the pairing state of the Fe-pnictides. In $s^{\pm}$ pairing symmetry, the gap function has opposite sign at the electron and hole pockets of the Fermi surface, it is connected with interband antiferromagnetic spin fluctuations. In $s_{++}$ pairing symmetry, the gap function has the same sign at the Fermi surface, it is mediated by moderate electron–phonon interaction due to Fe-ion oscillation and the critical orbital fluctuation. The $d_{x^2-y^2}$ pairing symmetry can rise from intraband antiferromagnetic spin fluctuation in strongly hole overdoped iron pnictide $KFe_2As_2$ and ternary chalcogenides. The $s^{\pm}$ pairing symmetry results in different effects of intraband ($\Gamma_0$) and interband ($\Gamma_\pi$) impurity scattering on $\xi_h$. It is found that $\xi_h/\xi_{c2}$ value decreases with $\Gamma_0$ leading to the values much less than those predicted by the analytical Ginzburg–Landau (AGL) theory for high $\Gamma_0$. At very high $\Gamma_0$, the interband scattering suppresses $\xi_h/\xi_{c2}$ considerably below one in the whole field range making it flat for both $s^{\pm}$ and $s_{++}$ pairing symmetries. Scaling of the cutoff parameter with the electromagnetic coherence length shows the importance of the nonlocal effects in mixed state. The small values of $\xi_h/\xi_{c2}$ were observed in $\mu$SR measurements of Co-doped $BaFe_2As_2$. If $\Gamma_0$ and $\Gamma_\pi$ are small and equal than the $\xi_h/\xi_{c2}(B/B_{c2})$ dependence for $s^{\pm}$ symmetry behaves like that of the AGL model and shows a minimum with value much more than that obtained for $s_{++}$ superconductors. With high $\Gamma_\pi$, the $\xi_h/\xi_{c2}(B/B_{c2})$ dependence resides above the AGL curve for $s^{\pm}$ pairing symmetry, as observed in SANS measurements of stoichiometrical LiFeAs compound. In $d$-wave superconductors, $\xi_h/\xi_{c2}$ always increases with $\Gamma$ similar to the $s^{\pm}$ symmetry case with $\Gamma_0 = \Gamma_\pi$.

*Keywords*: Eilenberger; pnictides; Kramer–Pesch.

## 1. Introduction

Since the discovery of superconductivity of iron pnictides with high transition temperature near to high-$T_c$ cuprates,[1] the structure of the superconducting (SC) gap of these novel materials has been studied very intensively. While the cuprates and conventional phonon-mediated superconductors are characterized by distinct $d$-wave and $s$-wave pairing symmetries with nodal and nodeless gap distributions, respectively, the superconducting gap distributions in iron-based superconductors are rather diversified.[2] While nodeless gap distributions have been directly observed in $SmFeAsO_{1-x}F_x$,[3] $Ba_{1-x}K_xFe_2As_2$,[4–6] optimally-doped $BaFe_{2-x}Co_xAs_2$,[7,8] LiFeAs[9] and $K_xFe_{2-y}Se_2$,[10] the signatures of nodal superconducting gap have been reported in LaOFeP,[11] LiFeP,[9] $KFe_2As_2$ (Ref. 12) and $BaFe_2(As_{1-x}P_x)_2$.[13]

The current theoretical opinion on the SC order parameter has converged on a nodeless $s^{\pm}$ order parameter that changes sign between the electron ($e$) and hole ($h$) pockets. This order parameter comes out of both the strong- and the weak-coupling pictures of the iron-based superconductors[14–16] and owes its origin to the pnictide Fermi surface (FS) topology of $h$ pockets at the $\Gamma$ and $e$ pockets at the $X$ $(0,\pi)/(\pi,0)$, point of the unfolded Brillouin zone. The dominant scattering contributions originate from $h$ pocket scattering at $\Gamma$ to $e$ pockets at $X$, yielding the $s^{\pm}$ SC order parameter for the doped case and the collinear antiferromagnetic phase in the undoped case. Detailed nesting properties of the pockets, the multi-orbital character of the FS, and the presence or absence of a third $h$ pocket at $M$ $(\pi,\pi)$ in the unfolded Brillouin zone complicate this picture. For the "1111" compounds, it was shown that the absence of the $M$ $h$ pocket (whose Fermi level can be significantly tuned by the pnictogen height through replacing As by P[17]) can modify the SC order parameter anisotropy from a nodeless to a nodal $s^{\pm}$ phase, which gives the correct material trend for As-P substitution in other pnictide families.[18–20]

With small exceptions, the anisotropic extended $s$-wave scenario (and its extension to the nodal $s^{\pm}$) was consistent with experimental findings for most of the pnictide compounds with moderate doping. This spin-wave fluctuation mechanism due to the nesting of the Fermi surface results in the peak in the inelastic neutron scattering.[21] In $s^{\pm}$ superconductors, the interband impurity scattering $\Gamma_\pi$ mixes hole and electron states with opposite values of the order parameter $\pm\Delta$ and by reason of this should be pair breaking and behave in the same way as a magnetic impurity in a conventional $s$-wave superconductor.[22] The temperature dependences of nuclear magnetic resonance and Knight shift can be fitted by a "dirty" $s^{\pm}$ model.[15,23] Using $s^{\pm}$ model for superconducting gap, good explanation of experimental results on penetration depth in electron-doped and hole-doped $BaFe_2As_2$ pnictides was obtained.[22,24] There are other experimental indications on unusual superconductivity in Fe-based superconductors (FeSCs). The measurements of negative isotopic effect in pnictides also indicate on $s^{\pm}$ symmetry[25,26]

and contradict with usual electron–phonon mechanism of superconductivity. By applying a magnetic field to break the time-reversal symmetry, the relative sign of the SC gap can be determined from the magnetic-field dependence of quasiparticle impurity scattering amplitudes. The results of scanning tunneling microscopy[27] indicate that the sign is reversed between the hole and the electron Fermi-surface pockets ($s^{\pm}$-wave), favoring the unconventional pairing mechanism associated with spin fluctuations. The $s^{\pm}$ pairing can explain the half-integer flux quantum transitions in composite niobium-iron pnictide SC loops.[28,29] Directional point-contact Andreev-reflection measurements in $Ba(Fe_{1-x}Co_x)_2As_2$ single crystals bring unambiguous evidence for spin-fluctuation-mediated $s^{\pm}$ mechanism of superconductivity in these compounds.[30]

Detailed angle-resolved photoemission spectroscopy (ARPES) measurement results on overdoped (OD) $Ba_{1-x}K_xFe_2As_2$ were reported and compared with the results on underdoped (UD) and optimally-doped (OPD) compounds.[31] The opening of multiple nodeless SC gaps in the OD sample was observed, similarly to the results in UD and OPD samples. This result suggests the universality of the pairing symmetry over a wide doping range ($0.25 \leq x \leq 0.7$). It was found that the FS-dependent gaps can be fitted by a single gap function, $\Delta(k) = \Delta_1 \cos k_x \cos k_y + \Delta_2(\cos k_x + \cos k_y)/2$ (anisotropic $A_1g$ gap symmetry), consistently with short-range pairing with the $s^{\pm}$-wave symmetry. The anisotropy order parameter determined by the second term in this expression was found to be small in these compounds, i.e. $\Delta_2 \ll \Delta_1$.[31] Weak anisotropy of the order parameter has also been found in $FeTe_{0.55}Se_{0.45}$ (Fe-chalcogenide), where the gap function is fitted by expression $\Delta_2 \cos k_x \cos k_y - \Delta_3(\cos 2k_x + \cos 2k_y)/2$, where $\Delta_3 \ll \Delta_2$.[32] Generally, the magnitude of the anisotropic component in the $A_1g$ state depends on the values of the interaction parameters and, hence, is material-dependent. Thus, possibilities range from isotropic $\Delta_e$, to a gap with deep minima on the electronic FS along $\Gamma - M$ line, to a state with a pair of "accidental" nodes near this line.[18–20,33,34] This anisotropy results in the oscillations of the specific heat and thermal transport under rotated magnetic field.[35,36]

The symmetry and the structure of the gap in Fe-based superconductors obtained in the random phase approximation (RPA) by decomposing the pairing interaction into *s*- and *d*-wave components and into contributions from scattering between different Fermi surfaces were studied in Ref. 34. It has been shown that each interaction is well approximated by the lowest angular harmonics and use this simplification to analyze the origin of the attraction in $s^{\pm}$, $d_{x^2-y^2}$ channels and the competition between *s*- and *d*-wave solutions. It has been found that the mechanism of the pairing in FeSCs with hole and electron FSs is different from the one at strong hole or electron doping, when only one type of FS remains. At small/moderate dopings, the pairing is driven by inter-pocket electron-hole interaction, no matter how small hole or electron FSs are. In hole-doped FeSCs, the leading instability is extended *s*-wave ($A_1g$ gap symmetry), while in electron-doped FeSCs, *s*- and $d_{x^2-y^2}$-wave ($B_1g$) channels are strong competitors, and which of the

two wins depends on the model parameters. With large electron and hole dopings, $d$-wave is the leading instability, although the $s$-wave channel remains attractive. At strong electron doping, the origin of the pairing is a direct $d$-wave attraction between electron pockets. At strong hole doping, however, the reason for the $d$-wave pairing is a $d$-wave attraction within the $(\pi, \pi)$ pocket and between the two hole pockets at (0, 0). The effects of nearest-neighbor, next-nearest-neighbor Heisenberg terms on the symmetry and the binding energy of two electrons added to the undoped state of the two-orbital Hubbard model were studied using Lanczos techniques on small clusters.[37] Quasinodal $A_1g$ bound states are stabilized for physical values of $J_H/U$ in the intermediate or large $U$ region, in agreement with RPA results.[34] The results also indicate that a competing $B_2g$ state may become stable in physically relevant regimes of $U/|t_1|$. In addition, the pairing susceptibility presents low-lying excitations with $B_2g$, $A_1g$ and $B_1g$ symmetries. Thus, pairing correlations with any of these symmetries could be stabilized by small modifications in the model parameters, in agreement with Refs. 20 and 38. This suggests that similar sensitivity to small details may occur among different compounds of the pnictide family. The $d$-wave pairing with strong hole doping is consistent with the observation of nodal quasiparticles[12] in the heavily hole doped superconductor $KFe_2As_2$ with $T_c = 3$ K. Superconductivity at heavy electron doping at a rather high $T_c \sim 30$ K has been recently discovered in $A_xFe_{2-y}Se_2$ (A = K, Cs, Rb), which only have electron FSs, according to recent ARPES studies.[39] ARPES measurements[12] and NMR studies[40] in $K_xFe_{2-y}Se_2$ point on the presence of the gap. Quasinodal $d_{x^2-y^2}$ state[2] and incipient $s^{\pm}$ pairing states[41] were suggested. For the incipient $s^{\pm}$ ternary iron chalcogenide $K_2Fe_4Se_5$, the pairing mechanism remains essentially the same as in the iron pnictides, although the hole pocket is below the Fermi energy of the electron doping side.

In spite of success of $s^{\pm}$ model, there are some indications that a conventional $s$-wave state without sign reversal ($s_{++}$-wave state)[42] is also a possible candidate for iron pnictides. It has been proposed that the moderate electron–phonon interaction due to Fe-ion oscillation can induce the critical orbital fluctuation, without being prohibited by the Coulomb interaction. For example, "resonance-like" peak structure observed by neutron scattering measurements[21] is reproduced by considering the strong correlation effect via quasiparticle damping, without the necessity of sign reversal in the SC gap.[43] The superconducting gap in many iron pnictides is band dependent, as shown by the penetration depth measurements,[44–46] temperature dependence of anisotropy parameter[44] and the ARPES studies.[47] The superfluid density, $\rho_s$, has been studied as a function of pressure by means of muon-spin rotation ($\mu$SR) in the $FeSe_{1-x}$.[46] The analysis of $\rho_s(T)$ within the two-gap scheme reveals that the effect on both, the $T_c$ and $\rho_s(0)$, is entirely determined by the band where the large superconducting gap develops, while the band with the small gap becomes practically unaffected. Using two-gap $s_{++}$-wave model for two-band superconductors,[48] the excellent fitting has been obtained with weak interband coupling constant for the low-temperature superconductors $V_3Si$. The pressure dependence

of $T_c$ is explained by the increase of Debye frequency, i.e. the usual electron–phonon mechanism. Additionally, the $s^{\pm}$-wave state is expected to be very fragile against impurities due to the interband scattering,[49] the superconducting state is remarkably robust against impurities (see discussion in Ref. 49) and $\alpha$-particle irradiation.[50] In the same time $s_{++}$ gap is much more steady with impurity scattering[49] consistently with the experiments. Even if spin fluctuation mechanism dominates in clean superconductors, impurities can induce transition between $s^{\pm}$ and $s_{++}$ symmetries.[42] The ARPES studies reported that the SC gap size is almost identical among the observed three hole-like FSs on $Ba_{1-x}K_xFe_2As_2$ and $BaFe_2As_{2-x}P_x$,[51] leading to an interpretation based on the $s_{++}$-wave pairing due to orbital fluctuations.

To study the effects of impurities on superconductivity, stoichiometrical iron pnictides such as LiFeAs ("111" pnictide) are preferable because the level of impurities can be regulated by doping from clean single crystals up to dirty superconductors. Electronic structure of LiFeAs is quasi-two-dimensional[52] and supports superconductivity in the absence of any notable Fermi surface nesting or static magnetism.[53,54] However, the presence of the field-induced magnetic state[55] in this pnictide suggests the importance of the antiferromagnetic (AF) fluctuations. The absence of the FS nesting ,which is important for the $s^{\pm}$ pairing, makes the study of the order parameter symmetry in LiFeAs especially interesting. Moreover, compared to other pnictide families, LiFeAs has much shallower hole pockets around the center of the Brillouin zone.[54] It has been pointed out that the flat top of these pockets implies a large density of states,[54] which are expected to promote ferromagnetic fluctuations. Investigating magnetic and pairing instabilities in the RPA it has been found that antiferromagnetic order is absent. Instead almost ferromagnetic fluctuations were observed which drive an instability toward spin-triplet $p$-wave superconductivity.[56] Nevertheless, using the functional-renormalization-group method the superconducting order parameter was found to be of the $s^{\pm}$ type, driven by collinear antiferromagnetic fluctuations. They eventually exceed the ferromagnetic fluctuations stemming from the small hole pocket at the $\Gamma$ point, as the system flows to low energies.[57] The high-resolution angle-resolved photoemission spectroscopy on Fe-based superconductor LiFeAs ($T_c = 18$ K) was performed in Ref. 58. While the simple $s^{\pm}$-wave gap function of $\cos k_x \cos k_y$ can describe the overall FS dependence of the SC gap, a moderate gap anisotropy is observed along the outer hole and inner electron FSs, suggesting the complicity of pairing interactions in this material, possibly due to the mixture with another pairing symmetry. The measuring of the quasiparticle interference (QPI) by scanning tunneling spectroscopy indicates that the superconducting pairing mechanism in LiFeAs is based on an unusual pairing symmetry such as a chiral $p$-wave (which provides optimal agreement between the experimental data and QPI simulations) or a more complex order parameter (e.g., $s + id$-wave symmetry).[59] By applying ARPES to LiFeAs, a clear fingerprint of the phonon spectrum in the fermionic self-energy was identified and estimation of the electron–phonon coupling strength was done, which appears

to be sufficient to mediate the superconductivity. This result suggests that the superconductivity in pnictides could be based on the conventional phonon pairing enhanced by the van Hove singularity in the electronic density of states and by the strong electron-electron interaction.[60] Moreover, the momentum dependence of the superconducting energy gap rules out coupling through spin fluctuations and the sign change.[61] The ARPES results instead suggest that orbital fluctuations assisted by phonons[42,62] are the best explanation for superconductivity ($s_{++}$ pairing).

Investigations of the mixed state allow to obtain the information about short range correlations of the coherence length order.[63,64] The aim of our paper is to study effects of interband and intraband impurity scattering on field distribution of the mixed state comparing them with the prediction of the $s^{\pm}$ and $s_{++}$ models. The effects of anisotropy and nodes in the superconducting order parameter are studied in the framework of $d_{x^2-y^2}$ pairing symmetry.

## 2. Model

First, we solve the quasiclassical self-consistent Eilenberger equations for triangular flux line lattice (FLL) for $s^{\pm}$ and $s_{++}$-wave pairing symmetries. We approximate the Fermi surface by two equivalent cylindrical pockets centered at $\Gamma$ (hole) and $M$ (electron) points of the Fermi surface, i.e. two-dimensional limit of five-band model is considered. Two band approximation is often used in the numerical calculations.[37,65,66] Such model allows to consider a pair breaking effects which are inhering for the iron-based SCs.[67] We consider the case with $B\|\hat{c}$ (where the current flows in $ab$ plane) and neglect $z$ dependence of superconducting gap, which can be important for iron pnictides having nodes in this direction, e.g. $BaFe_2(As_{1-x}P_x)_2$ (Ref. 13) and overdoped $Ba(Fe,Co)_2As_2$.[68] Doping-induced vertical line nodes in the superconducting gap appears in strongly underdoped[69] and overdoped[12] $Ba_{1-x}K_xFe_2As_2$. Our model can be used for more isotropic superconductors as optimally-doped $BaFe_{2-x}Co_xAs_2$,[8] $Ba_{1-x}K_xFe_2As_2$,[31] $FeTe_{0.55}Se_{0.45}$ (Ref. 32) and LiFeAs.[53,54] With the Riccati transformation of the Eilenberger equations quasiclassical Green functions $f$ and $g$ can be parameterized via functions $a$ and $b$[70,71]

$$\bar{f} = \frac{2a}{1+ab}, \quad f^{\dagger} = \frac{2b}{1+ab}, \quad g = \frac{1-ab}{1+ab}, \tag{1}$$

satisfying the nonlinear Riccati equations. In Born approximation for impurity scattering, we have

$$\mathbf{u}\cdot\nabla a = -a[2(\omega_n + G) + i\mathbf{u}\cdot\mathbf{A}_E] + (\Delta + F) - a^2(\Delta^* + F^*), \tag{2}$$

$$\mathbf{u}\cdot\nabla b = b[2(\omega_n + G) + i\mathbf{u}\cdot\mathbf{A}_E] - (\Delta^* + F^*) + b^2(\Delta + F), \tag{3}$$

where $\omega_n = \pi T(2n+1)$, $G = 2\pi\langle g\rangle(\Gamma_0 + \Gamma_\pi) \equiv 2\pi\langle g\rangle\Gamma^*$, $F = 2\pi\langle f\rangle(\Gamma_0 - \Gamma_\pi)$ for $s^{\pm}$ pairing symmetry and $F = 2\pi\langle f\rangle\Gamma^*$ for the $s_{++}$ pairing symmetry. $\Gamma_0 = \pi n_i N_F |u_0|^2$ and $\Gamma_\pi = \pi n_i N_F |u_\pi|^2$ are the intra- and interband impurity scattering

rates, respectively ($u_{0,\pi}$ are impurity scattering amplitudes with correspondingly small, or close to $\pi = (\pi, \pi)$, momentum transfer) and $\mathbf{u}$ is a unit vector of the Fermi velocity. In the new gauge vector-potential $\mathbf{A}_E = \mathbf{A} - \nabla\Phi$ is proportional to the superfluid velocity. It diverges as $1/r$ at the vortex center. The FLL creates the anisotropy of the electron spectrum. Therefore, the impurity renormalization corrections in Eqs. (2) and (3) averaged over Fermi surface can be reduced to averages over the polar angle $\theta$, $\langle\cdots\rangle = (1/2\pi)\int\cdots d\theta$. Since the $f$ function has opposite signs in two bands, $\Gamma_\pi$ has the opposite effect on normal and anomalous self-energies.

To take into account the influence of screening, the vector potential $\mathbf{A_E}(\mathbf{r})$ in Eqs. (2) and (3) is obtained from the equation

$$\nabla \times \nabla \times \mathbf{A_E} = \frac{4}{\kappa^2}\mathbf{J}\,, \tag{4}$$

where the supercurrent $\mathbf{J}(\mathbf{r})$ is given in terms of $g(\omega_n, \theta, \mathbf{r})$ by

$$\mathbf{J}(\mathbf{r}) = 2\pi T \sum_{\omega_n>0} \int_0^{2\pi} \frac{d\theta}{2\pi} \frac{\hat{\mathbf{k}}}{i} g(\omega_n, \theta, \mathbf{r})\,. \tag{5}$$

Here $\mathbf{A_E}$ and $\mathbf{J}$ are measured in units of $\Phi_0/2\pi\xi_0$ and $2ev_F N_0 T_c$, respectively. The spatial variation of the internal field $h_E(\mathbf{r})$ is determined through

$$\nabla \times \mathbf{A_E} = \mathbf{h_E}(\mathbf{r})\,. \tag{6}$$

The self-consistent condition for the pairing potential $\Delta(\mathbf{r})$ is given by

$$\Delta(\mathbf{r}) = V^{\mathrm{SC}} 2\pi T \sum_{\omega_n>0} \int_0^{2\pi} \frac{d\theta}{2\pi} f(\omega_n, \theta, \mathbf{r})\,, \tag{7}$$

where $V^{\mathrm{SC}}$ is the $s^{\pm}$ coupling constant and $\omega_c$ is the ultraviolet cutoff.

The coupling constant $V^{\mathrm{SC}}$ can be obtained from the expression

$$\frac{1}{V^{\mathrm{SC}}} = \ln\frac{T}{T_{c0}} + 2\pi T \sum_{0<\omega_n<\omega_c} \frac{1}{|\omega_n|}\,. \tag{8}$$

All over the paper, the energy, the temperature and the length are measured in units of $T_{c0}$ and the coherence length $\xi_0 = v_F/T_{c0}$, where $v_F$ is the Fermi velocity. The magnetic field $\mathbf{h}$ is given in units of $\Phi_0/2\pi\xi_0^2$. In equations, impurities are in a units of $T_{c0}$, but in the plots impurities are in a units of $2\pi T_{c0}$. In computations, the ratio $\kappa = \lambda_{L0}/\xi_0 = 10$ is used.

To obtain the quasiclassical Green function, the Riccati equations (2) and (3) are solved by the Fast Fourier Transform (FFT) method. Unlike the square vortex lattice studied in Ref. 72, we consider a triangular vortex lattice, for which the wave vector mesh is transformed from square to hexagonal shape.[73]

Iterations of the coefficients $a$ in the Fourier space are made using the relation

$$a(\mathbf{Q}) = \frac{\left[\Delta + F - (\Delta^* + F^*)a^2 - i\mathbf{u}\mathbf{A_E}\right]_{FT}}{i\mathbf{u}\mathbf{Q} + 2(\omega_n + G)}\,, \tag{9}$$

which makes possible to solve the Riccati equations simultaneously for a full set of reciprocal vectors $\mathbf{Q}$ in the mesh, greatly increasing the calculation speed. The shifts to next iteration have to be damped[72] by a value depending on the Matsubara frequency, $\omega_n$ and the wave vector direction $\mathbf{u}$ forming the $\mathrm{Damp}_{nu}$ matrix. Every value in this matrix is optimized dynamically before the first and after every 50th iteration. The improved damping reads

$$a'_{\mathrm{new}} = \frac{a_{\mathrm{new}} + a_{\mathrm{old}}\,\mathrm{Damp}_{nu}}{1 + \mathrm{Damp}_{nu}}, \qquad 0 \leq \mathrm{Damp}_{nu} < \infty\,, \tag{10}$$

where $a_{\mathrm{new}}$ calculated by Eq. (9) is substituted by $a'_{\mathrm{new}}$ taking into account the matrix from previous iteration, $a_{\mathrm{old}}$ and the appropriate damping $\mathrm{Damp}_{nu}$. Considering the low temperature range, even improved damping fails to start the iteration process. In this case, the solutions obtained at a higher temperature are used as initial values of $a$ in Eq. (9) and then the temperature is gradually decreased by factor 0.85.

To obtain the magnetic field distribution from a known vector potential distribution, the field $\mathbf{h}_E(\mathbf{r}) = \nabla \times \mathbf{A}_E(\mathbf{r})$ is calculated simultaneously for all $\mathbf{r}$ in the mesh using FFT. While transforming the real vector $\mathbf{A}_E = A_{Ex}\mathbf{e}_x + A_{Ey}\mathbf{e}_y$ to a complex number $A_E = A_{Ex} + iA_{Ey}$, we use the equation

$$\mathrm{FFT}^{-1}[(q_x - iq_y)\mathrm{FFT}(A_{Ex} + iA_{Ey})] = (\nabla \times \mathbf{A}_E) \cdot \mathbf{e}_z - i\nabla \cdot \mathbf{A}_E\,, \tag{11}$$

where FFT and $\mathrm{FFT}^{-1}$ denote direct and reverse two-dimensional Fast Fourier Transforms and $q_x$ and $q_y$ are the coordinates of the corresponding wave vector $\mathbf{q}_{ij} = q_x(i)\mathbf{e}_x + q_y(j)\mathbf{e}_y$ over all matrix cells.

The investigation of experimental results of field distribution in mixed state of type II-superconductors is usually done[63,64] in the framework of the Hao–Clem theory (analytical solution of the Ginzburg–Landau theory, AGL[74,75]). Strictly speaking, the Ginzburg–Landau theory is valid only near $T_c$ but it is often used in the whole temperature range taking the cutoff parameter $\xi$ and penetration depth $\lambda$ as a fitting parameters in Eq. (12). Recently, an effective London model with the effective cutoff parameter $\xi_h(B)$ as a fitting parameter was obtained for clean[76] and dirty[77] superconductors using self-consistent solution of quasiclassical nonlinear Eilenberger equations. To emphasize the differences between calculated cutoff parameter and variational parameter of the AGL, we changed the notations $\xi_v \to \xi_h$. In this approach, the cutoff parameter obtained from the Ginzburg–Landau model is extended over the whole field and temperature ranges. In this case, the effects of bound states in the vortex cores leading to Kramer–Pesch effect,[78] their delocalization between the vortices[79,80] and nonlocal electrodynamics[81] are self-consistently included. In this model, the magnetic field distribution is given[77]

$$h_{\mathrm{EHC}}(\mathbf{r}) = \frac{\Phi_0}{S}\sum_{\mathbf{G}} \frac{F(G)e^{i\mathbf{G}\mathbf{r}}}{1 + \lambda^2 G^2}\,, \tag{12}$$

where $F(\mathbf{G}) = uK_1(u)$, $K_1(u)$ is the modified Bessel function, $u = \xi_h G$, $\mathbf{G}$ is a reciprocal lattice vector and $S$ is the area of the vortex lattice unit cell, the $\xi_h$

is a cutoff parameter. Because the magnetic field distribution is taken similar to the GL model, we will call this approach as Eilenberger–Hao–Clem (EHC) model. Here, penetration depth $\lambda$ is not a fitting parameter but is calculated from the microscopical theory of the Meissner state and $\xi_h$ is calculated from Eilenberger theory of the mixed state.

After solving the Eilenberger equations, the obtained magnetic field distribution $h_E(\mathbf{r})$ is fitted to the London field distribution $h_{\rm EHC}(\mathbf{r})$ [Eq. (12)] with $\lambda(T)$ calculated from isotropic $s^{\pm}$ model[22]

$$\frac{\lambda_{L0}^2}{\lambda^2(T)} = 2\pi T \sum_{\omega_n>0} \frac{\bar{\Delta}_n^2}{\eta_n(\bar{\Delta}_n^2+\omega_n^2)^{3/2}}\,, \tag{13}$$

where

$$\eta_n = 1 + 2\pi \frac{\Gamma_0+\Gamma_\pi}{\sqrt{\bar{\Delta}_n^2+\omega_n^2}}\,, \tag{14}$$

$$\bar{\Delta}_n = \Delta(T) - 4\pi\Gamma_\pi \frac{\bar{\Delta}_n}{\sqrt{\bar{\Delta}_n^2+\omega_n^2}}\,, \tag{15}$$

$\lambda_{L0}$ is the London penetration depth at $T = 0$ K in the absence of the impurities. The order parameter $\Delta(T)$ is determined by the self-consistency equation

$$\Delta(T) = 2\pi T \sum_{0<\omega_n<\omega_c} \frac{V^{\rm SC}\bar{\Delta}_n}{\sqrt{\bar{\Delta}_n^2+\omega_n^2}}\,. \tag{16}$$

The penetration depth $\lambda(T)$ scales as $1/\sqrt{\rho_S(T)}$, where $\rho_S(T)$ is the superfluid density, $\rho_{S0}$ is the superfluid density at $T = 0$ in the absence of impurities. Without interband scattering ($\Gamma_\pi = 0$), we have $T_c = T_{c0}$, where $T_{c0}$ is BCS transition temperature in clean superconductors. In the case of interband scattering ($\Gamma_\pi \neq 0$), the transition temperature obeys[22] $\ln(T_c/T_{c0}) = \Psi(1/2) - \Psi(1/2 + 2\zeta T_{c0}/T_c)$, where $\Psi(x)$ is the di-Gamma function and $\zeta = \Gamma_\pi/2\pi T_{c0}$. This is similar to the $s$-wave superconductors with the magnetic impurities showing spin-flip processes.[82] The critical temperature $T_c$ decreases with $\zeta$ and vanishes at $\zeta_{cr} = e^{-\gamma}/8 \approx 0.07$ ($\Gamma_\pi/\Delta_0 = 1/4$). For $0.064 < \zeta < \zeta_{cr}$, $\bar{\Delta}(T,\omega) \propto i\omega$ for small $\omega$, including $T = 0$, and thus even $T = 0$ zero-energy density of states becomes finite and gapless superconductivity arises. (At the onset, at $\zeta = 0.064$, $T_c \approx 0.22T_{c0}$ and $\Delta(0) = 0.46\Delta_0$). At $\zeta < 0.064$ the $T$ dependence of $\rho_s(T)$ remains exponential at low $T$, $\rho_s(T) \propto e^{-\bar{\Delta}(\omega=0)/T}$ with $\bar{\Delta}(\omega = 0) = \Delta_0[1 - (\zeta/\zeta_{cr})^{2/3}]^{3/2}$, but at the onset of gapless superconductivity, when $\bar{\Delta}(\omega) \propto (-i\omega)^{2/3}$ the $\rho_s(T) \propto T^{5/3}$. Finally, in the gapless regime $0.064 < \zeta < \zeta_{cr}$, it was found that $\rho_s(T) \propto T^2$ at low $T$. As has been shown by Hashimoto *et al.*,[6] $\lambda(T)$ in hole-doped $Ba_{1-x}K_xFe_2As_2$ depends critically on impurity scattering. It has power shape dependence with exponent approximately equal two in dirty superconductors and exponential shape in clean superconductors. The excellent fitting of power-law dependences of $\rho_S(T)$ in doped $BaFe_2As_2$ pnictides was obtained with parameters $\Gamma_0/2\pi T_{c0} = 3$, $\Gamma_\pi/2\pi T_{c0} = 0.04 - 0.06$.[22,24]

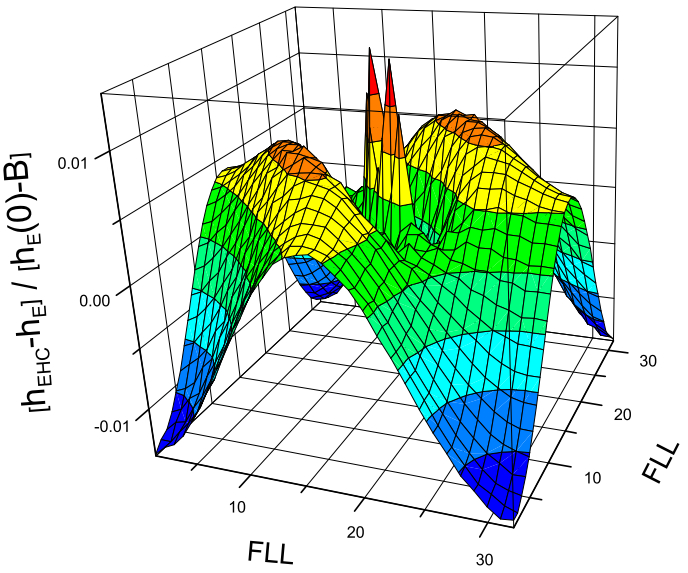


Fig. 1. (Color online) Normalized differences between the fields $h_{\rm EHC}$ and $h_E$ calculated with the generalized London model and with the Eilenberger equation, respectively, for $B/B_0 = 1$, $T/T_{c0} = 0.5$ and $\Gamma^* = 0.25$ ($s_{++}$ model). The scales of the lengths are those of the flux line lattice unit vectors.

To study the obtained $\xi_h(B, T, \Gamma_0, \Gamma_\pi)$ dependences, it is convenient to use the normalization to the coherence length $\xi_{c2}$, determined from the upper critical field $B_{c2} = \Phi_0/2\pi\xi_{c2}^2$ (in our units $\xi_{c2} = 1/\sqrt{B_{c2}}$). Using the similarity to the model of spin-flip superconductors $B_{c2}(T)$ for two-dimensional $s^{\pm}$ pairing can be determined from the equations[83]

$$\ln\left(\frac{T_{c0}}{T}\right) = 2\pi T \sum_{n\geq 0} [\omega_n^{-1} - 2D_1(\omega_n, B_{c2})]\,, \tag{17}$$

where

$$D_1(\omega_n, B_{c2}) = J(\omega_n, B_{c2})[1 - 2(\Gamma_0 - \Gamma_\pi)J(\omega_n, B_{c2})]^{-1}\,, \tag{18}$$

$$J(\omega_n, B_{c2}) = \left(\frac{4}{\pi B_{c2}}\right)^{1/2} \int_0^\infty dy \exp(-y) \arctan\left[\frac{(B_{c2}y)^{1/2}}{\alpha}\right], \tag{19}$$

where $\alpha = 2(\omega_n + \Gamma_0 + \Gamma_\pi)$.

After solving the Eilenberger equations, the obtained magnetic field distribution $h_E(\mathbf{r})$ is fitted to the London field distribution $h_{\rm EHC}(\mathbf{r})$ finding the fitting parameter $\xi_h$. The normalized difference between these fields corresponding to $B/B_0 = 1$, $T/T_{c0} = 0.5$ and $\Gamma^* = 0.25$ is shown in Fig. 1. The accuracy of the fitting exceeds 1%.

We also numerically solve the quasiclassical Eilenberger equations for the mixed state of a $d_{x^2-y^2}$-wave superconductor for the pairing potential $\Delta(\theta, \mathbf{r}) = \Delta(\mathbf{r})\cos(2\theta)$, where $\theta$ is the angle between the $\mathbf{k}$ vector and the $a$-axis (or $x$-axis). We check the applicability of Eq. (12) and find the cutoff parameter $\xi_h$. The results for the $d_{x^2-y^2}$ symmetry can be relevant for $KFe_2As_2$ (Ref. 12) and electron-doped $K_xFe_{2-y}Se_2$ (Ref. 34) compounds.

To consider the mixed state of a $d$-wave superconductor, we take the center of the vortex as the origin and assume that the Fermi surface is isotropic and cylindrical. The Riccatti equations for $d_{x^2-y^2}$-wave superconductivity are[84]

$$\mathbf{u}\cdot\nabla a = -a[2(\omega_n + G) + i\mathbf{u}\cdot\mathbf{A}_E] + \Delta - a^2\Delta^*\,, \tag{20}$$

$$\mathbf{u}\cdot\nabla b = b[2(\omega_n + G) + i\mathbf{u}\cdot\mathbf{A}_E] - \Delta^* + b^2\Delta\,, \tag{21}$$

where $G = 2\pi\langle g\rangle\Gamma$ ($\Gamma$ is impurity scattering rate) with $d$-wave pairing potential $\Delta(r)$

$$\Delta(\theta,\mathbf{r}) = V^{\rm SC}_{d_{x^2-y^2}}\, 2\pi T\cos(2\theta)\sum_{\omega_n>0}^{\omega_c}\int_0^{2\pi}\frac{d\bar{\theta}}{2\pi}f(\omega_n,\bar{\theta},\mathbf{r})\cos(2\bar{\theta})\,, \tag{22}$$

where $V^{\rm SC}_{d_{x^2-y^2}}$ is a coupling constant in the $d_{x^2-y^2}$ pairing channel. The obtained solution is fitted to Eq. (12) giving the value of cutoff parameter $\xi_h$ for $d_{x^2-y^2}$-wave pairing symmetry. For $d_{x^2-y^2}$-wave superconductor $\lambda(T)$ in Eq. (12) was calculated in Ref. 85.

## 3. Effects of Interband and Intraband Impurity Scattering on the Cutoff Parameter

Figure 2 demonstrates the calculated magnetic field and temperature dependence of $\xi_h/\xi_{c2}$ for clean $s$-wave superconductors ($\Gamma_0 = \Gamma_\pi = 0$). Strong decreasing of the cutoff parameter with decreasing of temperature is clearly observed. It is connected with the Kramer–Pesch effect.[86] The most interesting feature of the obtained results is the nonmonotonous field dependence of $\xi_h$. The clear minimum of $\xi_h/\xi_{c2}(B/B_{c2})$ at high temperatures becomes weaker at low temperatures. A minimum was found also in the order parameter coherence length: $1/\xi_\Delta = (\partial|\Delta(r)|/\partial r)_{r=0}/|\Delta_{NN}|$,

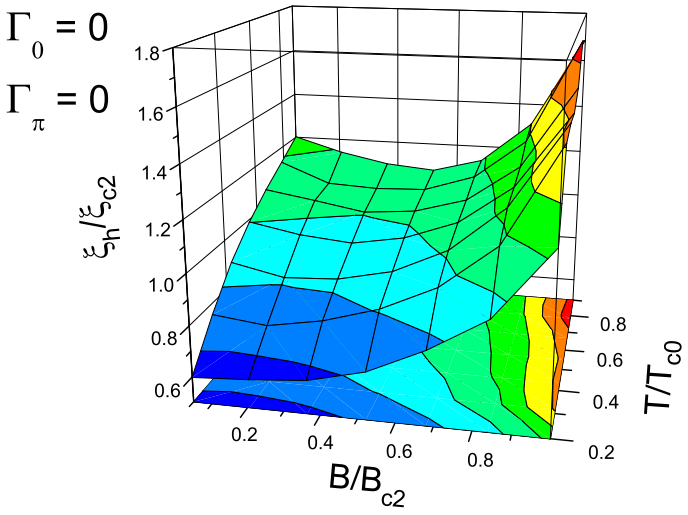


Fig. 2. (Color online) The magnetic field and temperature dependences of the cutoff parameter $\xi_h/\xi_{c2}$ for clean $s$-wave superconductors ($\Gamma_0 = \Gamma_\pi = 0$).

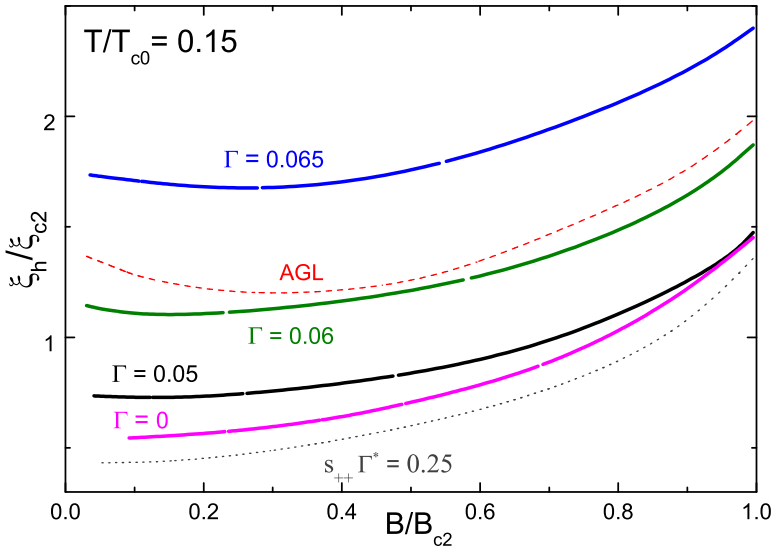


Fig. 3. (Color online) The magnetic field dependence of $\xi_h/\xi_{c2}$ at $T/T_{c0} = 0.15$ with the same values of intraband $\Gamma_0$ and interband $\Gamma_\pi$ scattering $\Gamma$ ($\Gamma = 0, 0.05, 0.06, 0.065$). Dotted lines show the magnetic field dependence of $\xi_h/\xi_{c2}$ for $s_{++}$ model ($\Gamma^* = 0.25$). Dashed line demonstrates the result of the AGL theory for $\xi_v$ from Eq. (23).

where $|\Delta_{NN}|$ is the maximum value of the order parameter along the nearest-neighbor direction which is also the direction of taking the derivative.[87] This reflects an interconnection between the cutoff parameter $\xi_h(B)$ and the order parameter distribution. The characteristic lengths of the vortex core were discussed in Refs. 88 and 89.

First, we study the case of weak intraband scattering. This case can be realized in stoichiometrical pnictides such as LiFeAs. Figure 3 presents the $\xi_h/\xi_{c2}$ magnetic field dependence at $\Gamma_0 = \Gamma_\pi = \Gamma = 0, 0.05, 0.06, 0.065$ and $T/T_{c0} = 0.15$. Dashed line demonstrates the result of the AGL theory for $\xi_v$ (Ref. 74)

$$\xi_v = \xi_{c2}\left(\sqrt{2} - \frac{0.75}{\kappa_{GL}}\right)(1 + b^4)^{1/2}[1 - 2b(1 - b)^2]^{1/2}\,. \tag{23}$$

This dependence with $\xi_v$ as a fitting parameter is often used for the description of the $\mu$SR experimental results.[64] As can be seen from this picture, the shape of the curve does not change considerably, but the absolute values of $\xi_h/\xi_{c2}$ depend crucially on it. At low $\Gamma$ values, $\xi_h/\xi_{c2}$ resides below the AGL curve and moves above at high $\Gamma$, opposite to the case of the strong intraband scattering considered in Fig. 4. Such behavior is quite different from that in $s_{++}$ pairing symmetry where intraband and interband scattering rates act in similar way and $\xi_h/\xi_{c2}$ decreases always with impurity scattering. It should be noted that the normalization constant $\xi_{c2}$ increases with $\Gamma_\pi$, because $\Gamma_\pi$ suppresses $T_c$ similar to superconductors with spin-flip scattering (violation of the Anderson theorem). Thus, the growing $\xi_h/\xi_{c2}$ implies more strong growth of $\xi_h$ than $\xi_{c2}$ (from GL theory one can expect $\xi_h/\xi_{c2} =$ const.). Qualitatively, it can be explained by the strong temperature dependence of $\xi_h(T/T_c)$ connected with the Kramer–Pesch effect.[78] Increasing $\Gamma_\pi$ results in

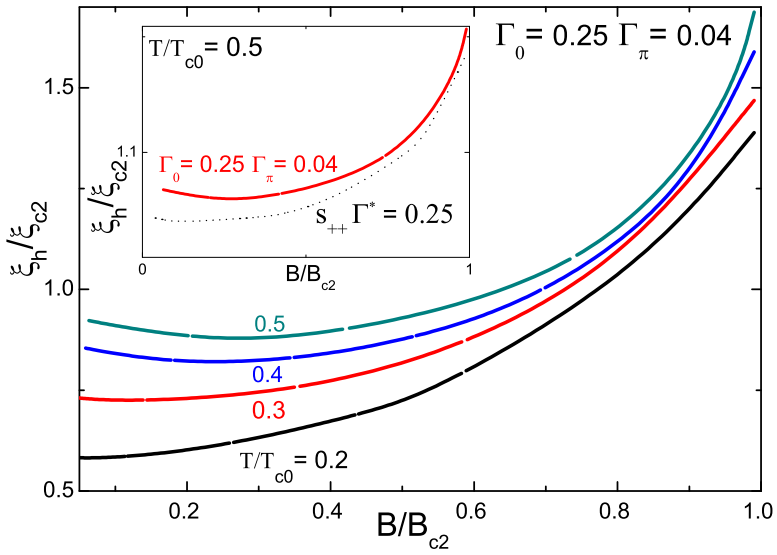


Fig. 4. (Color online) The magnetic field dependence of cutoff parameter $\xi_h$ with different temperatures for $\Gamma_0 = 0.25$ and $\Gamma_\pi = 0.04$. The inset shows the magnetic field dependence $\xi_h/\xi_{c2}$ for $s^{\pm}$ model ($\Gamma_0 = 0.25, \Gamma_\pi = 0.04$) and $s_{++}$ model ($\Gamma_* = 0.25$, dot line) at $T/T_{c0} = 0.5$.

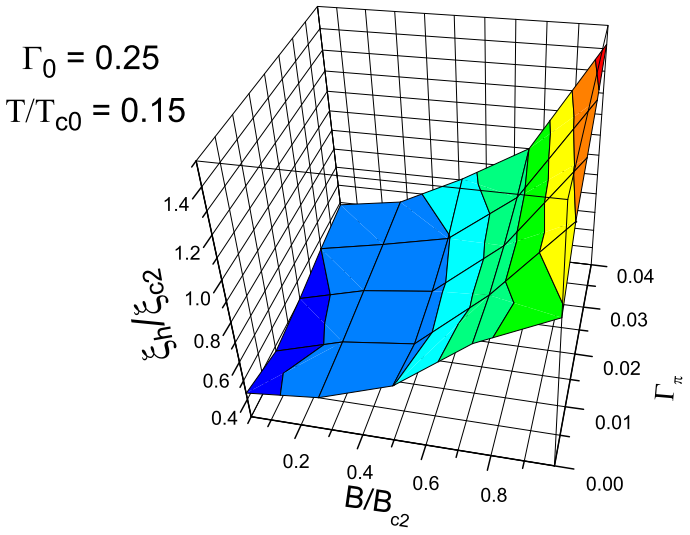


Fig. 5. (Color online) The magnetic field and interband impurity scattering dependences of cutoff parameter $\xi_h/\xi_{c2}$ at $T/T_{c0} = 0.15$ and $\Gamma_0 = 0.25$ for $s^{\pm}$ model.

suppression of $T_c$, i.e. effective increasing of $T$ and $\xi_h(T/T_c)$. The $\xi_{c2}(T/T_c)$ has not so strong $T_c$ dependence leading to the increasing of the ratio $\xi_h/\xi_{c2}$ with $\Gamma_\pi$. The values $\xi_h/\xi_{c2} > 1$ were found in small angular neutron scattering (SANS) investigation of LiFeAs.[53]

Figures 4 and 5 present magnetic field dependences of $\xi_h/\xi_{c2}$ with $\Gamma_0 = 0.25$ at different temperatures and scattering rates $\Gamma_\pi$, respectively. Similar to clean superconductors (Fig. 2), the Kramer–Pesch effect is also visible at small scattering in Fig. 4. General raise of $\xi_h/\xi_{c2}$ with interband impurity scattering can be observed in Fig. 5. Figure 6 shows magnetic field dependences of $\xi_h/\xi_{c2}$ for $s^{\pm}$ model with

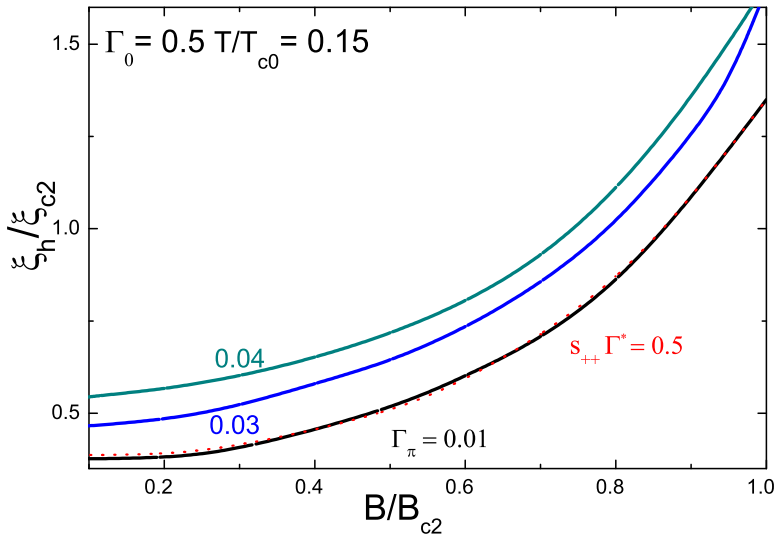


Fig. 6. (Color online) The magnetic field dependence of $\xi_h/\xi_{c2}$ for $s^{\pm}$ model with different interband impurity scattering rates for $\Gamma_0 = 0.5$, $T/T_{c0} = 0.15$ and $s_{++}$ model ($\Gamma^* = 0.5$, dotted line).

$\Gamma_0 = 0.5$, $T/T_{c0} = 0.15$ at different interband impurity scattering rates and for $s_{++}$ model ($\Gamma^* = 0.5$, dotted line). Increasing of $\xi_h/\xi_{c2}$ with $\Gamma_\pi$ for $s^{\pm}$ relatively to $s_{++}$ pairing (inset of Fig. 4, Figs. 5 and 6) conserves at moderate level of intraband scattering. The small value of ratio $\xi_h/\xi_{c2} \sim 0.4$ which is comparable with our theoretical prediction, Fig. 6, has been obtained in $\mu$SR investigation of Co-doped $BaFe_2As_2$.[90] In Ref. 90, the magnetic field distribution shape of the sample was explained by effects of field-induced magnetic order and vortex-lattice disorder. Our consideration shows the importance of impurity scattering even in the triangular lattice giving another possible explanation of the experimental results.

We also consider the case of strong intraband scattering. Figure 7 shows $\xi_h/\xi_{c2}(B/B_{c2})$ dependence at different temperatures with the parameters $\Gamma_0 = 3$ and $\Gamma_\pi = 0.05$. All curves demonstrate growing behavior with values much less than one in the whole field range, i.e. they are under the AGL curve of $\xi_v$. The physical meaning of this result is discussed in next section. The inset of Fig. 7 shows $\xi_h/\xi_{c2}(B/B_{c2})$ for $\Gamma_0 = 3$, $\Gamma_\pi = 0.05$ ($s^{\pm}$ pairing) and $\Gamma^* = 3$ ($s_{++}$ pairing). It can be seen from the inset that $\xi_h/\xi_{c2}$ is strongly suppressed in $s^{\pm}$ pairing with comparison to the $s_{++}$ pairing specially at high field range. This can be explained by the fact that in superconductors without interband pair breaking, the increasing in high field is connected to the field-dependent pair breaking when approaching the upper critical field. This type of the behavior is cut off by the impurity pair breaking, slowing the growth of $\xi_h$. The low field rise in the $s_{++}$ pairing is connecting to the "dirty" limit transition described by Usadel equations.[71,91]

The results for clean $s$- and $d$-wave superconductors at different temperatures are presented in Fig. 8. The shapes of the $\xi_h/\xi_0$ dependences on $B/B_0$ are similar in

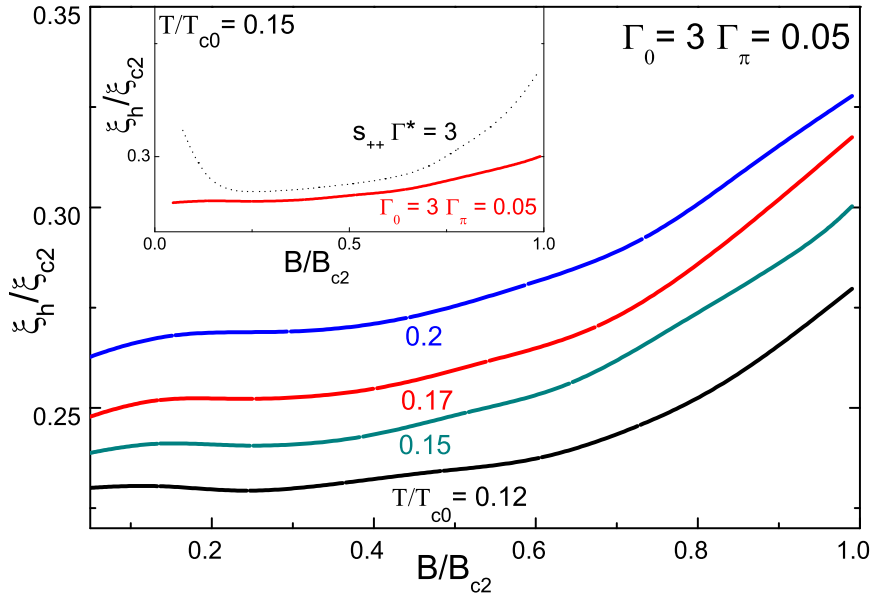


Fig. 7. (Color online) The magnetic field dependence of $\xi_h/\xi_{c2}$ with different temperatures for $\Gamma_0 = 3$ and $\Gamma_\pi = 0.05$ for $s^{\pm}$ model. The inset shows the magnetic field dependence $\xi_h/\xi_{c2}$ for $s^{\pm}$ model ($\Gamma_0 = 3, \Gamma_\pi = 0.05$) and $s_{++}$ model ($\Gamma^* = 3$, dotted line) at $T/T_{c0} = 0.15$.

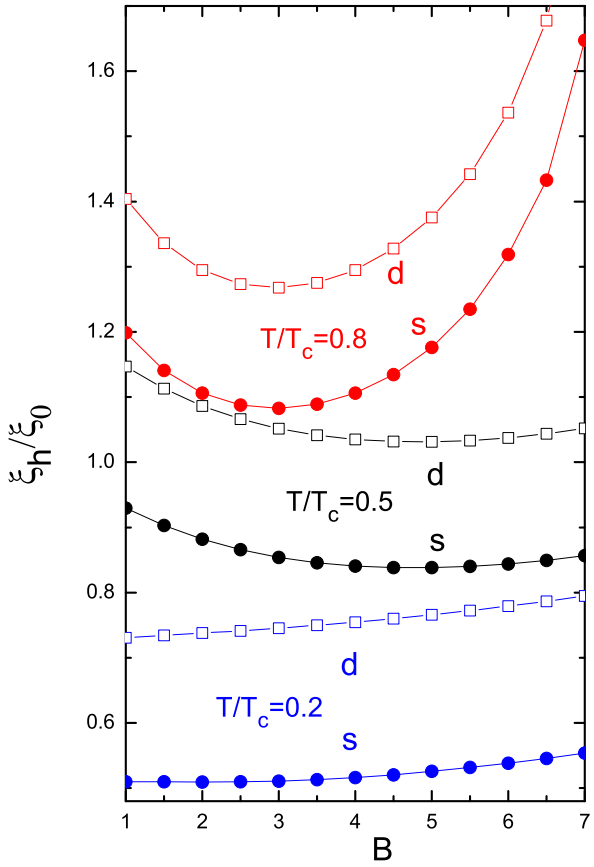


Fig. 8. (Color online) Magnetic field dependences ($B/B_0$) of the normalized cutoff parameter $\xi_h/\xi_0$ for $s$- and $d$-wave superconductors at different temperatures.

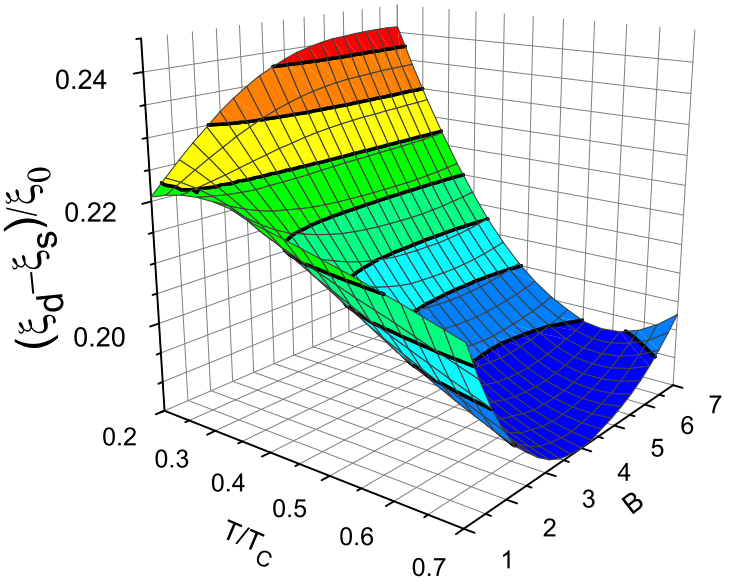


Fig. 9. (Color online) Magnetic field ($B/B_0$) and temperature ($T/T_{c0}$) dependences of the difference between the cutoff parameters for $s$- ($\xi_s$) and $d$-wave ($\xi_d$) superconductors.

these two cases and differ only by a numerical value. Figure 9 demonstrates that the difference between the cutoff parameters for $s$- ($\xi_s$) and $d$-wave ($\xi_d$) superconductors has field and temperature dependence less than 10%. This can be explained by the V-shape of the low energy density of the states $N(E) = N_0(H) + \alpha|E|$ for all clean superconductors in the vortex state, irrespective of the underlying gap structure. The V-shape has been obtained by microscopic calculations for isotropic gap as well as for the line and the point-node gaps.[92,93] The singular density of states with V-shape is universally independent of the underlying original gap structure.

The difference between pairing symmetries reveals itself in impurity scattering dependence of $\xi_h/\xi_{c2}$. In $s_{++}$ symmetry, $\xi_h/\xi_{c2}$ always decreases with impurity scattering rate $\Gamma$ (Figs. 3–7), in $s^{\pm}$ symmetry its behavior depends on the field range and relative values of intraband and interband impurity scattering rates: It can be a decreasing function of $\Gamma_\pi$ (the inset of Fig. 7) or an increasing function of $\Gamma_\pi$ (Fig. 3).[94] In $d$-wave superconductors, $\xi_h/\xi_{c2}$ always increases with $\Gamma$ (Fig. 10) similar to the case of $s^{\pm}$ symmetry with $\Gamma_0 = \Gamma_\pi$ (Fig. 3). This can be understood from the comparison of the Ricatti equations of the $s^{\pm}$ and $d$-wave pairing. In both cases, the renormalization factor $F = 0$ due to a cancelation of the intraband and interband impurity scattering rates in $s^{\pm}$ pairing or symmetry reason $\langle f \rangle = 0$ for $d$-wave pairing.

## 4. Scaling of the Cutoff Parameter with the Electromagnetic Coherence Length

For the description of the electromagnetic properties of superconductors, three characteristics lengths are important: London penetration depth, $\lambda$, Ginzburg–Landau coherence length, $\xi_{c2}$ and the electromagnetic coherence length, $\xi_{El}$, connected with

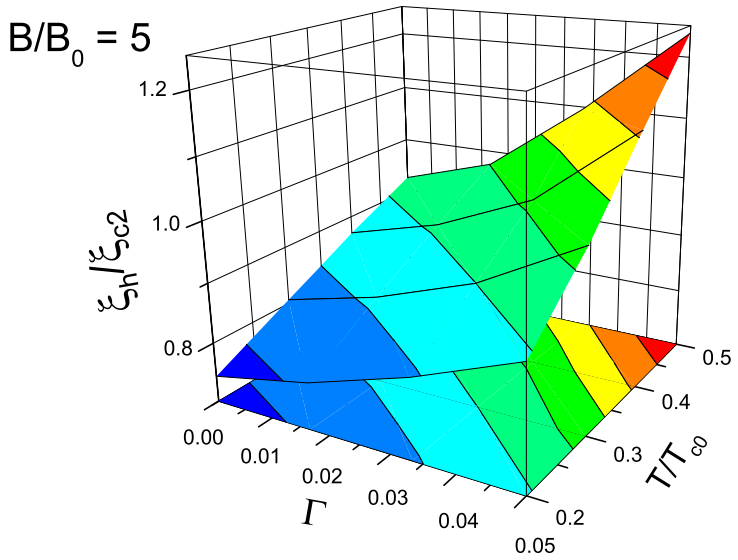


Fig. 10. (Color online) Three-dimensional plot of $\xi_h/\xi_{c2}(\Gamma, T/T_{c0})$ at $B/B_0 = 5$ for $d_{x^2-y^2}$-wave superconductors.

nonlocal effects.[95] The ratio between $\lambda$ and $\xi_{c2}$ determines the type of superconductivity (I or II-type). The nonlocal effects are usually important for the I-type superconductors. Because the screening current changes rapidly in the vortex core area, nonlocal effects can be important there also, so both $\xi_{c2}$ and $\xi_{El}$ should be taken into account for proper description of the magnetic properties. We note that they have different behavior in the "dirty" limit: $\xi_{c2} \sim \sqrt{\tau}$ and $\xi_{El} \sim \tau$, where $\tau$ is impurity scattering relaxation time ($2\pi\Gamma = 1/\tau$ in our units).[96,97] In previous section, we have found that $\xi_h/\xi_{c2}$ depends on $\Gamma$ appreciably. This strong dependence implies the importance of the nonlocal effects. The aim of this section is to study the nonlocal properties of the mixed state investigating the $\xi_h/\xi_{El}$ ratio in the case of $s$-wave superconductors with the impurity scattering relaxation time $\tau$. Such consideration can help to understand the physical sense of the small $\xi_h/\xi_{c2}$ ratio shown in Fig. 7.

Figure 11 illustrates the behavior of $\xi_h(\tau)$ in a wide range of $\tau$ up to moderate scattering, where $\tau$ is comparable with characteristic time $\tau_0$ (to be defined below) at $B/B_0 = 5$ and $T/T_{c0} = 0.2$, 0.5 and 0.8. At small $\tau$, a sharp increase of $\xi_h(\tau)$ with increasing $\tau$ is evident. It resembles the prediction for $\xi_{El}$ in dirty superconductors with uniform order parameter, where $\xi \propto \tau$.[97] In the clean limit, we have $\tau \gg 1$ and asymptotically $\xi_h(\tau) - \xi_h(\infty) \propto 1/\tau$. The value of $\xi_h(5)$ is near the limit for clean superconductors $\xi_h(\infty)$, shown in Fig. 11 by the dotted lines.

Our numerical approach extends the theory of electromagnetic coherence length in the Meissner state[97] to the mixed state. The electromagnetic length $\xi_{El}$ is defined by the relation[95]

$$\lim_{q\to\infty} qK(q,T)/K(0,T) = 3\pi/4\xi_{El}\,, \tag{24}$$

where $K(q,T)$ can be calculated in terms of single-particle Green's functions. It

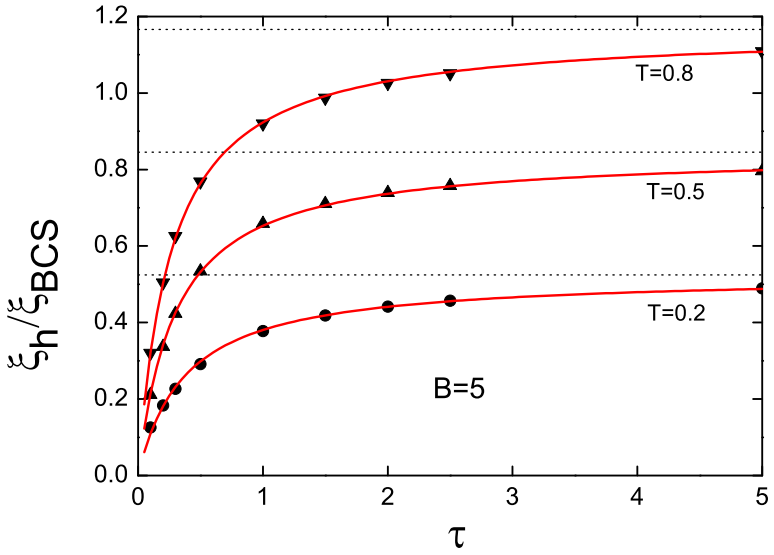


Fig. 11. (Color online) The dependence of $\xi_h$ on impurity scattering at $B/B_0 = 5$ and $T/T_{c0} = 0.2, 0.5, 0.8$. The solid lines represent fitting according to Eq. (28), the dotted lines denote the pure limit ($\tau = \infty$).

governs the connection between the current and the vector potential in the Meissner state

$$\mathbf{j}(\mathbf{q}, T) = -\frac{c}{4\pi} K(\mathbf{q}, T)\mathbf{A}(\mathbf{q})\,. \tag{25}$$

In the framework of the BCS theory, we have

$$\xi_{El}/\xi_{\rm BCS} = \frac{\pi\Delta}{2} \sum_{n\geq 0} \frac{1}{\tilde{\Delta}_n (1+u_n^2)^{3/2}} \Bigg/ \sum_{n\geq 0} \frac{1}{1+u_n^2}\,, \tag{26}$$

$$\tilde{\Delta}_n = \Delta + \frac{1}{\tau\sqrt{u_n^2+1}}\,, \tag{27}$$

where $u_n = w_n/\Delta$ and the scattering time $\tau$ is given in units of $1/(2T_c)$. Figure 12 shows the ratio $\xi_h/\xi_{El}$ at $B/B_0 = 1$ (a) and $B/B_0 = 4$ (b) at different relaxation times $\tau = 0.2, 0.5, 1.5$ and 5.0.

As can be seen from Fig. 12, the $\xi_h/\xi_{El} \equiv F$ ratio is weakly dependent on the relaxation time illustrating that both $\xi_h$ and $\xi_{El}$ have a similar dependence on $\tau$. This demonstrates that characteristic relaxation times by impurities are similar in the Meissner and in the mixed state only with slight renormalization by the magnetic field in the last case. A strong decrease in $\xi_h/\xi_{El}$ with decreasing temperature is clearly visible in Fig. 13, which can be explained by the Kramer–Pesch effect.[98] The $\xi_{El}$ is not dependent from $T$ at low temperatures and decreases slowly at high temperatures.[97] The reason for this is that in the Meissner state the nonlocality is described only by extended states. In contrast, low temperature physics of the vortex state is connected with the nature of the current-currying quantum states of the quasiparticles in the vortex core (formed due to particle-holed coherence and

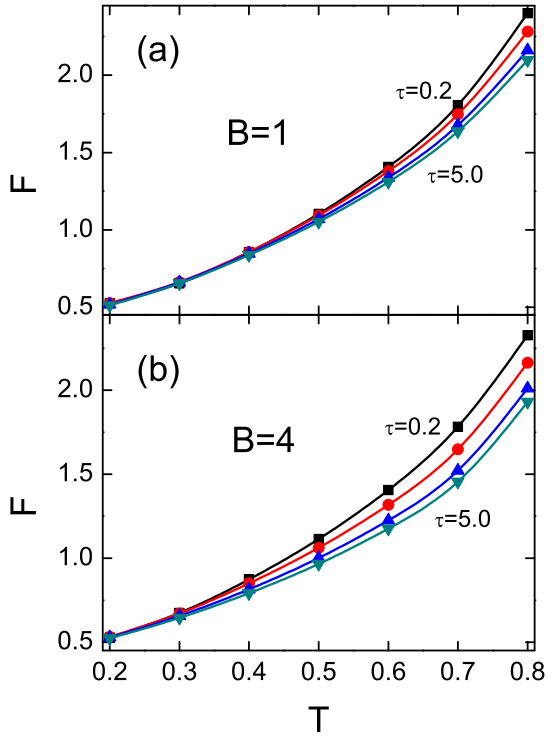


Fig. 12. (Color online) Temperature dependence of $F \equiv \xi_h/\xi_{El}$ ratio at $B/B_0 = 1$ (a) and $B/B_0 = 4$ (b). From top to bottom the relaxation times $\tau$ are $0.2, 0.5, 1.5$ and $5.0$ in both plots.

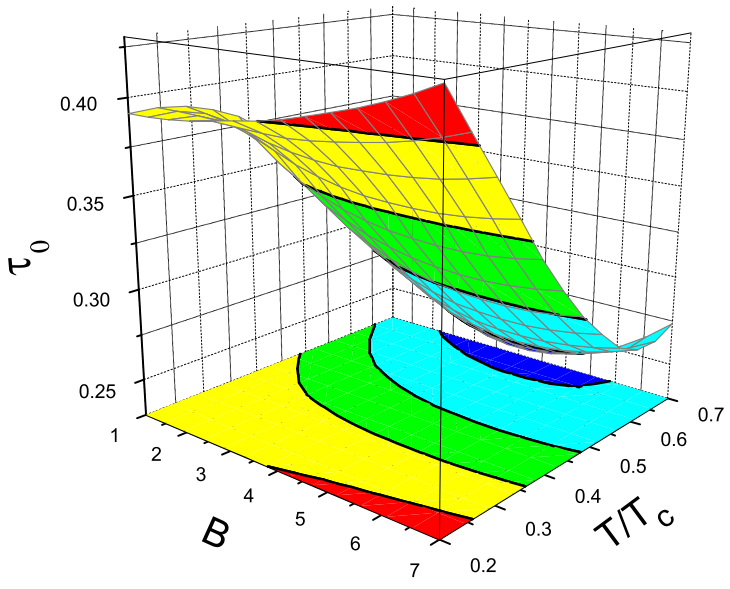


Fig. 13. (Color online) Three-dimensional plot of characteristic relaxation time $\tau_0(B/B_0, T/T_{c0})$.

Andreev reflection[99]). The current distribution can be decomposed in terms of bound states and extended states contributions.[100] Close to the vortex core, the current density arises mainly from the occupation of the bound states resulting in a new characteristic scale in the mixed state. It means that the $\xi_h(B, T, \tau)$

Table 1. The parameters $\xi_{\rm pure}$ and $\tau_0$ used for fitting Eq. (28) at $B/B_0 = 5$ and $T/T_{c0} = 0.2, 0.5$ and 0.8.

| $T/T_{c0}$ | 0.2 | 0.5 | 0.8 |
|---|---|---|---|
| $\xi_{\rm pure}/\xi_{\rm BCS}$ | 0.525 | 0.845 | 1.167 |
| $\tau_0$ $(2k_BT_c/\hbar)$ | 0.379 | 0.294 | 0.264 |

dependence can be approximately attributed to two contributions: one is connected with core effects described by the $F(T)$ function (see Fig. 12) and the other is responsible for impurity scattering characterized by $\xi_{El}(\tau)$.

For comparison with experiments, an analytical relation is needed. This approach was successfully used for description of the electromagnetic coherence length in the Meissner state.[97] To describe the mixed state, we fit $\xi_h(\tau)$ in the considered range of impurity concentration by the function

$$\xi_h(B,T,\tau) = \frac{\xi_{\rm pure}(B,T)}{1+\frac{\tau_0(B,T)}{\tau}}\,, \tag{28}$$

where $\xi_{\rm pure}(B,T)$ is the effective coherence length in clean superconductors.[101] The chosen $\xi_h(\tau)$ interpolation formula Eq. (28) has the same behavior as $\xi_{El}$ in the limits of $\tau \to 0$ $\xi_h \propto \tau$ and at $\tau \to \infty$ $\xi_h \to \xi_{\rm pure}$. The characteristic relaxation time $\tau_0(B,T)$ is given at temperatures $T/T_{c0} = 0.2, 0.5, 0.8$ and $B/B_0 = 5$ in Table 1. As can be seen from Fig. 11, one fitting parameter represents excellently the numerically calculated impurity dependence of $\xi_h(\tau)$ which has a similar shape as in the Meissner state[95] but with different temperature dependence of the fitting coefficients: in the Meissner state all parameters are decreasing functions of temperature but in our case $\tau_0(T)$ is a decreasing and $\xi_{\rm pure}(T)$ an increasing function, resulting from core effects.

Figure 13 demonstrates the $\tau_0(B,T)$ surface where decreasing of $\tau_0$ with temperature holds out in a wide magnetic field range. As can be seen from Fig. 12 the function $F$ depends mainly on temperature. This means that characteristic relaxation time is similar in the Meissner and in the mixed states.

## 5. Conclusion

Eilenberger equations have been solved for superconductors with isotropic $s^{\pm}$, $s_{++}$ and anisotropic $d_{x^2-y^2}$ pairing symmetries in the mixed state. These symmetries are proposed for the pairing state of the Fe-pnictides. It is found that these equations can be reduced to London model with only one parameter, $\xi_h(B)$. This length determines the form factor of FLL. It is found that normalized value of $\xi_h/\xi_{c2}$ decreases with temperature due to Kramer–Pesch effect. In clean superconductors, the shape of $\xi_h/\xi_{c2}(B)$ for $d$-wave is similar to that in $s$-wave symmetry. The resemblance of the shape of $\xi_h(B,T)$ between $s$- and $d$-wave superconductors is connected with

the V-shaped density of states in the mixed state in both cases. Different impurity scattering dependences of the cutoff parameter $\xi_h(B)$ are obtained for $s$- and $d$-wave superconductors. It is found that magnetic field dependence of $\xi_h/\xi_{c2}$ is nonuniversal for $s^{\pm}$ pairing, depending on the chosen parameter set it can reside both below and above AGL curve. Such behavior is quite different from that in $s_{++}$ pairing symmetry where intraband and interband scattering rates act in similar way and $\xi_h/\xi_{c2}$ decreases always with impurity scattering. It is found that intraband scattering ($\Gamma_0$) suppresses $\xi_h/\xi_{c2}$ leading to values much less than unit at high $\Gamma_0$. The effects of interband impurity scattering ($\Gamma_\pi$) depend on the value of $\Gamma_0$ for $s^{\pm}$ pairing: at small $\Gamma_0$, $\xi_h/\xi_{c2}$ increases with $\Gamma_\pi$, but at high $\Gamma_0$ it decreases with $\Gamma_\pi$. The effects of interband impurity scattering at moderate $\Gamma_0$ depends on the field range resulting in increasing of $\xi_h/\xi_{c2}$ at low fields, but suppressing it at high fields. In $d$-wave superconductors $\xi_h/\xi_{c2}$ always increases with the scattering rate $\Gamma$. Our results of $\xi_h/\xi_{c2}(B/B_{c2})$ calculations can be used for the analysis of the $\mu$SR and SANS experiments both for doped $BaFe_2As_2$ compound, where $\Gamma_0 \sim 1 \gg \Gamma_\pi$ and stoichiometrical LiFeAs, where $\Gamma_0, \Gamma_\pi \ll 1$. In the first case, $\xi_h/\xi_{c2}(B/B_{c2})$ dependences demonstrate growing behavior defined by $\Gamma_0$ with values much less than one in the whole field range, i.e. they are considerably lower the AGL curve of $\xi_v$, while in the second case, it can reside above AGL curve. Scaling of the cutoff parameter with the electromagnetic coherence length in the Meissner state is discussed. The prediction for $\xi_h/\xi_{c2}$ field dependences can be tested in $\mu$SR and SANS measurements.

## References


1. Y. Kamihara, T. Watanabe, M. Hirano and H. Hosono, *J. Am. Chem. Soc.* **130** (2008) 3296.
2. P. J. Hirschfeld, M. M. Korshunov and I. I. Mazin, *Rep. Prog. Phys.* **74** (2011) 124508.
3. D. Daghero, M. Tortello, R. S. Gonnelli, V. A. Stepanov, N. D. Zhigadlo and J. Karpinski, *Phys. Rev. B* **80** (2009) 060502(R).
4. X. G. Luo, M. A. Tanatar, J. P. Reid, H. Shakeripour, N. Doiron-Leyraud, N. Ni, S. L. Bud'ko, P. C. Canfield, H. Luo, Z. Wang, H. H. Wen, R. Prozorov and L. Taillefer, *Phys. Rev. B* **80** (2009) 140503(R).
5. H. Ding, P. Richard, K. N. Richard, K. Sugawara, T. Arakane, Y. Sekiba, A. Takayama, S. Souma, T. Sato, T. Takahashi, Z. Wang, X. Dai, Z. Fang, G. F. Chen, J. L. Luo and N. L. Wang, *Europhys. Lett.* **83** (2008) 47001.
6. K. Hashimoto, T. Shibauchi, S. Kasahara, K. Ikada, S. Tonegawa, T. Kato, R. Okazaki, C. J. van der Beek, M. Konczykowski, H. Takeya, K. Hirata, T. Terashima and Y. Matsuda, *Phys. Rev. Lett.* **102** (2009) 207001.
7. M. A. Tanatar, J. P. Reid, H. Shakeripour, X. G. Luo, N. Doiron-Leyraud, N. Ni, S. L. Bud'ko, P. C. Canfield, R. Prozorov and L. Taillefer, *Phys. Rev. Lett.* **104** (2010) 067002.
8. L. Luan, T. M. Lippman, C. W. Hicks, J. A. Bert, O. M. Auslaender, J. H. Chu, J. G. Analytis, I. R. Fisher and K. A. Moler, *Phys. Rev. Lett.* **106** (2011) 067001.

9. K. Hashimoto, S. Kasahara, R. Katsumata, Y. Mizukami, M. Yamashita, H. Ikeda, T. Terashima, A. Carrington, Y. Matsuda and T. Shibauchi, *Phys. Rev. Lett.* **108** (2011) 047003.
10. Y. Zhang, L. X. Yang, M. Xu, Z. R. Ye, F. Chen, C. He, H. C. Xu, J. Jiang, B. P. Xie, J. J. Ying, X. F. Wang, X. H. Chen, J. P. Hu, M. Matsunami, S. Kimuraz and D. L. Feng, *Nat. Mater.* **10** (2011) 273.
11. J. D. Fletcher, A. Serafin, L. Malone, J. G. Analytis, J. H. Chu, A. S. Erickson, I. R. Fisher and A. Carrington, *Phys. Rev. Lett.* **102** (2009) 147001.
12. J. K. Dong, S. Y. Zhou, T. Y. Guan, H. Zhang, Y. F. Dai, X. Qiu, X. F. Wang, Y. He, X. H. Chen and S. Y. Li, *Phys. Rev. Lett.* **104** (2010) 087005.
13. Y. Zhang, Z. R. Ye, Q. Q. Ge, F. Chen, J. Jiang, M. Xu, B. P. Xie and D. L. Feng, *Nat. Phys.* **8** (2012) 371.
14. I. I. Mazin, D. J. Singh, M. D. Johannes and M. H. Du, *Phys. Rev. Lett.* **101** (2008) 057003.
15. A. V. Chubukov, D. V. Efremov and I. Eremin, *Phys. Rev. B* **78** (2008) 134512.
16. K. Kuroki, S. Onari, R. Arita, H. Usui, Y. Tanaka, H. Kontani and H. Aoki, *Phys. Rev. Lett.* **101** (087004) 2008.
17. K. Hashimoto, S. Kasahara, R. Katsumata, Y. Mizukami, M. Yamashita, H. Ikeda, T. Terashima, A. Carrington, Y. Matsuda and T. Shibauchi, *Phys. Rev. Lett.* **108** (2012) 047003.
18. T. A. Maier, S. Graser, D. J. Scalapino and P. J. Hirschfeld, *Phys. Rev. B* **79** (2009) 224510.
19. K. Kuroki, H. Usui, S. Onari, R. Arita and H. Aoki, *Phys. Rev. B* **79** (2009) 224511.
20. R. Thomale, C. Platt, W. Hanke and B. A. Bernevig, *Phys. Rev. Lett.* **106** (2011) 187003.
21. A. D. Christianson, E. A. Goremychkin, R. Osborn, S. Rosenkranz, M. D. Lumsden, C. D. Malliakas, I. S. Todorov, H. Claus, D. Y. Chung, M. G. Kanatzidis, R. I. Bewley and T. Guidi, *Nature (London)* **456** (2008) 930.
22. A. B. Vorontsov, M. G. Vavilov and A. V. Chubukov, *Phys. Rev. B* **79** (2009) 140507(R).
23. D. Parker, O. V. Dolgov, M. M. Korshunov, A. A. Golubov and I. I. Mazin, *Phys. Rev. B* **78** (2008) 134524.
24. C. Martin, R. T. Gordon, M. A. Tanatar, H. Kim, N. Ni, S. L. Bud'ko, P. C. Canfield, H. Luo, H.-H. Wen, Z. Wang, A. B. Vorontsov, V. G. Kogan and R. Prozorov, *Phys. Rev. B* **80** (2009) 020501(R).
25. H. Y. Choi, J. H. Yun, Y. Bang and H. C. Lee, *Phys. Rev. B* **80** (2009) 052505.
26. P. M. Shirage, K. Kihou, K. Miyazawa, C. H. Lee, H. Kito, H. Eisaki, T. Yanagisawa, Y. Tanaka and A. Iyo, *Phys. Rev. Lett.* **103** (2009) 257003.
27. T. Hanaguri, S. Niitaka, K. Kuroki and H. Takagi, *Science* **328** (2010) 474.
28. C. T. Chen, C. C. Tsuei, M. B. Ketchen, Z. A. Ren and Z. X. Zhao, *Nat. Phys.* **6** (2010) 260.
29. E. Berg, N. H. Lindner and T. Pereg-Barnea, *Phys. Rev. Lett.* **106** (2011) 147003.
30. M. Tortello, D. Daghero, G. A. Ummarino, V. A. Stepanov, J. Jiang, J. D. Weiss, E. E. Hellstrom and R. S. Gonnelli, *Phys. Rev. Lett.* **105** (2010) 237002.
31. K. Nakayama, T. Sato, P. Richard, Y. M. Xu, T. Kawahara, K. Umezawa, T. Qian, M. Neupane, G. F. Chen, H. Ding and T. Takahashi, *Phys. Rev. B* **83** (2011) 020501(R).
32. H. Miao, P. Richard, Y. Tanaka, K. Nakayama, T. Qian, K. Umezawa, T. Sato, Y. M. Xu, Y. B. Shi, N. Xu, X. P. Wang, P. Zhang, H. B. Yang, Z. J. Xu, J. S. Wen, G. D. Gu, X. Dai, J. P. Hu, T. Takahashi and H. Ding, *Phys. Rev. B* **85** (2012) 094506.

33. A. V. Chubukov, M. G. Vavilov and A. B. Vorontsov, *Phys. Rev. B* **80** (2009) 140515(R).
34. S. Maiti, M. M. Korshunov, T. A. Maier, P. J. Hirschfeld and A. V. Chubukov, *Phys. Rev. Lett.* **107** (2011) 147002.
35. A. B. Vorontsov and I. Vekhter, *Phys. Rev. Lett.* **105** (2010) 187004.
36. M. Yamashita, Y. Senshu, T. Shibauchi, S. Kasahara, K. Hashimoto, D. Watanabe, H. Ikeda, T. Terashima, I. Vekhter, A. B. Vorontsov and Y. Matsuda, *Phys. Rev. B* **84** (2011) 060507(R).
37. A. Nicholson, W. Ge, X. Zhang, J. Riera, M. Daghofer, A. M. Oles, G. B. Martins, A. Moreo and E. Dagotto, *Phys. Rev. Lett.* **106** (2011) 127002.
38. R. Thomale, C. Platt, W. Hanke, J. Hu and B. A. Bernevig, *Phys. Rev. Lett.* **107** (2011) 117001.
39. T. Qian, X. P. Wang, W. C. Jin, P. Zhang, P. Richard, G. Xu, X. Dai, Z. Fang, J. G. Guo, X. L. Chen and H. Ding, *Phys. Rev. Lett.* **106** (2011) 187001.
40. W. Yu, L. Ma, J. B. He, D. M. Wang, T. L. Xia, G. F. Chen and W. Bao, *Phys. Rev. Lett.* **106** (2011) 197001.
41. Y. Z. You, F. Yang, S. P. Kou and Z. Y. Weng, *Phys. Rev. Lett.* **107** (2011) 167001.
42. H. Kontani and S. Onari, *Phys. Rev. Lett.* **104** (2010) 157001.
43. S. Onari, H. Kontani and M. Sato, *Phys. Rev. B* **81** (2010) 060504(R).
44. R. Khasanov, D. V. Evtushinsky, A. Amato, H. Klauss, H. Luetkens, C. Niedermayer, B. Buchner, G. L. Sun, C. T. Lin, J. T. Park, D. S. Inosov and V. Hinkov, *Phys. Rev. Lett.* **102** (2009) 187005.
45. R. Khasanov, A. Maisuradze, H. Maeter, A. Kwadrin, H. Luetkens, A. Amato, W. Schnelle, H. Rosner, A. Leithe-Jasper and H. Klauss, *Phys. Rev. B* **103** (2009) 067010.
46. R. Khasanov, M. Bendele, A. Amato, K. Conder, H. Keller, H. H. Klauss, H. Luetkens and E. Pomjakushina, *Phys. Rev. Lett.* **104** (2010) 087004.
47. D. V. Evtushinsky, D. S. Inosov, V. B. Zabolotnyy, M. S. Viazovska, R. Khasanov, A. Amato, H. H. Klauss, H. Luetkens, C. Niedermayer, G. L. Sun, V. Hinkov, C. T. Lin, A. Varykhalov, A. Koitzsch, M. Knupfer, B. Buchner, A. A. Kordyuk and S. V. Borisenko, *New J. Phys.* **11** (2009) 055069.
48. V. G. Kogan, C. Martin and R. Prozorov, *Phys. Rev. B* **80** (2009) 014507.
49. S. Onari and H. Kontani, *Phys. Rev. Lett.* **103** (2009) 177001.
50. C. Tarantini, M. Putti, A. Gurevich, Y. Shen, R. K. Singh, J. M. Rowell, N. Newman, D. C. Larbalestier, P. Cheng, Y. Jia and H. H. Wen, *Phys. Rev. Lett.* **104** (2010) 087002.
51. T. Shimojima, F. Sakaguchi, K. Ishizaka, Y. Ishida, T. Kiss, M. Okawa, T. Togashi, C. T. Chen, S. Watanabe, M. Arita, K. Shimada, H. Namatame, M. Taniguchi, K. Ohgushi, S. Kasahara, T. Terashima, T. Shibauchi, Y. Matsuda, A. Chainani and S. Shin, *Science* **332** (2011) 564.
52. D. J. Singh, *Phys. Rev. B* **78** (2008) 094511.
53. D. S. Inosov, J. S. White, D. V. Evtushinsky, I. V. Morozov, A. Cameron, U. Stockert, V. B. Zabolotnyy, T. K. Kim, A. A. Kordyuk, S. V. Borisenko, E. M. Forgan, R. Klingeler, J. T. Park, S. Wurmehl, A. N. Vasiliev, G. Behr, C. D. Dewhurst and V. Hinkov, *Phys. Rev. Lett.* **104** (2010) 187001.
54. S. Borisenko, V. B. Zabolotnyy, D. Evtushinsky, T. K. Kim, I. Morozov, A. N. Yaresko, A. A. Kordyuk, G. Behr, A. Vasiliev, R. Follath and B. Büchner, *Phys. Rev. Lett.* **105** (2010) 067002.
55. F. L. Pratt, P. J. Baker, S. J. Blundell, T. Lancaster, H. J. Lewtas, P. Adamson, M. J. Pitcher, D. R. Parker and S. J. Clarke, *Phys. Rev. B* **79** (2009) 052508.

56. P. M. R. Brydon, M. Daghofer, C. Timm and J. Brink, *Phys. Rev. B* **83** (2011) 060501(R).
57. C. Platt, R. Thomale and W. Hanke, *Phys. Rev. B* **84** (2011) 235121.
58. K. Umezawa, Y. Li, H. Miao, K. Nakayama, Z. H. Liu, P. Richard, T. Sato, J. B. He, D. M. Wang, G. F. Chen, H. Ding, T. Takahashi and S. C. Wang, *Phys. Rev. Lett.* **108** (2012) 037002.
59. T. Hänke, S. Sykora, R. Schlegel, D. Baumann, L. Harnagea, S. Wurmehl, M. Daghofer, B. Büchner, J. Brink and C. Hess, *Phys. Rev. Lett.* **108** (2012) 127001.
60. A. A. Kordyuk, V. B. Zabolotnyy, D. V. Evtushinsky, T. K. Kim, I. V. Morozov, M. L. Kulić, R. Follath, G. Behr, B. Büchner and S. V. Borisenko, *Phys. Rev. B* **83** (2011) 134513.
61. S. V. Borisenko, V. B. Zabolotnyy, A. A. Kordyuk, D. V. Evtushinsky, T. K. Kim, I. V. Morozov, R. Follath and B. Büchner, *Symmetry* **4**(1) (2012) 251.
62. Y. Yanagi, Y. Yamakawa and Y. Ōno, *Phys. Rev. B* **81** (2010) 054518.
63. J. E. Sonier, *J. Phys.: Condens. Matter* **16** (2004) S4499.
64. J. E. Sonier, *Rep. Prog. Phys.* **70** (2007) 1717.
65. H. M. Jiang, J. X. Li and Z. D. Wang, *Phys. Rev. B* **80** (2009) 134505.
66. Y. Gao, H. X. Huang, C. Chen, C. S. Ting and W. P. Su, *Phys. Rev. Lett.* **106** (2011) 027004.
67. R. T. Gordon, H. Kim, M. A. Tanatar, R. Prozorov and V. G. Kogan, *Phys. Rev. B* **81** (2010) 180501(R).
68. J. P. Reid, M. A. Tanatar, X. G. Luo, H. Shakeripour, N. Doiron-Leyraud, N. Ni, S. L. Bud'ko, P. C. Canfield, R. Prozorov and L. Taillefer, *Phys. Rev. B* **82** (2010) 064501.
69. J. P. Reid, M. A. Tanatar, X. G. Luo, H. Shakeripour, S. R. de Cotrett, N. Doiron-Leyraud, J. Chang, B. Shen, H. H. Wen, H. Kim, R. Prozorov and L. Taillefer, arXiv:1105.2232.
70. N. Schopohl and K. Maki, *Phys. Rev. B* **52** (1995) 490–493.
71. P. Miranović, M. Ichioka and K. Machida, *Phys. Rev. B* **70** (2004) 104510.
72. P. Miranović and K. Machida, *Phys. Rev. B* **67** (2003) 092506.
73. M. Safonchik, Ph.D. thesis (Turku University, 2007).
74. Z. Hao, J. R. Clem, M. W. McElfresh, L. Civale, A. P. Malozemoff and F. Holtzberg, *Phys. Rev. B* **43** (1991) 2844.
75. A. Yaouanc, P. D. de Reotier and E. H. Brandt, *Phys. Rev. B* **55** (1997) 11107.
76. R. Laiho, M. Safonchik and K. B. Traito, *Phys. Rev. B* **76** (2007) 140501(R).
77. R. Laiho, M. Safonchik and K. B. Traito, *Phys. Rev. B* **78** (2008) 064521.
78. L. Kramer and W. Pesch, *Z. Phys.* **269** (1974) 59.
79. M. Ichioka, A. Hasegawa and K. Machida, *Phys. Rev. B* **59** (1999) 8902.
80. M. Ichioka, A. Hasegawa and K. Machida, *Phys. Rev. B* **59** (1999) 184.
81. V. G. Kogan, A. Gurevich, J. H. Cho, D. C. Johnston, M. Xu, J. R. Thompson and A. Martynovich, *Phys. Rev. B* **54** (1996) 12386.
82. A. A. Abrikosov and L. P. Gor'kov, *Zh. Eksp. Teor. Fiz.* **39** (1961) 1781.
83. Y. N. Ovchinnikov and V. Z. Kresin, *Phys. Rev. B* **52** (1995) 3075.
84. A. Zare, A. Markowsky, T. Dahm and N. Schopohl, *Phys. Rev. B* **78** (2008) 104524.
85. D. Xu, S. K. Yip and J. A. Sauls, *Phys. Rev. B* **51** (1995) 16233.
86. L. Kramer and W. Pesch, *Z. Phys.* **269** (1974) 59.
87. P. Miranović, M. Ichioka and K. Machida, *Phys. Rev. B* **70** (2004) 104510.
88. P. Belova, K. B. Traito and E. Lähderanta, *J. Appl. Phys.* **110** (2011) 033911.
89. P. Belova, I. Zakharchuk, M. Safonchik, K. B. Traito and E. Lähderanta, *Physica C* **426** (2012) 1.

90. J. E. Sonier, W. Huang, C. V. Kaiser, C. Cochrane, V. Pacradouni, S. A. Sabok-Sayr, M. D. Lumsden, B. C. Sales, M. A. McGuire, A. S. Sefat and D. Mandrus, *Phys. Rev. Lett.* **106** (2011) 127002.
91. J. E. Sonier, R. F. Kiefl, J. H. Brewer, J. Chakhalian, S. R. Dunsiger, W. A. MacFarlane, R. I. Miller, A. Wong, G. M. Luke and J. W. Brill, *Phys. Rev. Lett.* **79** (1997) 1742.
92. N. Nakai, P. Miranović, M. Ichioka and K. Machida, *Phys. Rev. B* **73** (2006) 172501.
93. N. Nakai, P. Miranović, M. Ichioka, H. F. Hess, K. Uchiyama, H. Nishimori, S. Kaneko, N. Nishida and K. Machida, *Phys. Rev. Lett.* **97** (2006) 147001.
94. P. Belova, M. Safonchik, K. B. Traito and E. Lähderanta, *Phys. Rev. B* **83** (2011) 104518.
95. M. Tinkham, *Introduction to Superconductivity* (McGraw-Hill, New York, 1975).
96. P. G. de Gennes, *Superconductivity of Metals and Alloys* (Addison-Wesley, Redwood City, CA, 1989).
97. T. R. Lemberger, D. M. Ginsberg and G. Rickayzen, *Phys. Rev. B* **18** (1978) 6057.
98. N. Nakai, P. Miranović, M. Ichioka and K. Machida, *Phys. Rev. B* **73** (2006) 172501.
99. A. Gumann, S. Graser, T. Dahm and N. Schopohl, *Phys. Rev. B* **73** (2006) 104506.
100. F. Gygi and M. Schlüter, *Phys. Rev. B* **41** (1990) 822.
101. R. Laiho, M. Safonchik and K. B. Traito, *Phys. Rev. B* **76** (2007) 140501(R).

# PUBL. 4

**P. Belova, I. Zakharchuk, K. B. Traito and E. Lähderanta**, Cutoff parameter versus Ginzburg-Landau coherence length in the mixed state of high-$\kappa$ superconductors with impurities: quasiclassical approach, *Journal of Physics: Conference Series*, **400**, 022007, 2012 DOI: 10.1088/1742-6596/400/2/022007

Journal of Physics: Conference Series **400** (2012) 022007 doi:10.1088/1742-6596/400/2/022007

# Cutoff parameter versus Ginzburg-Landau coherence length in the mixed state of high-$\kappa$ superconductors with impurities: quasiclassical approach

**P. Belova[1,2], I. Zakharchuk[1,3], K. B. Traito[1], E. Lähderanta[1]**

[1] Lappeenranta University of Technology, P.O.Box 20, FI-53851, Lappeenranta, Finland
[2] Petrozavodsk State University, Lenin str. 33, RU-185640, Petrozavodsk, Russia
[3] Saint-Petersburg Electrotechnical University, Popov str. 5, RU-197376, St.Petersburg, Russia

E-mail: Polina.Belova@lut.fi

**Abstract.** The influence of the impurities on the ratio of the cutoff parameter, $\xi_h$, and the Ginzburg-Landau coherence length, $\xi_{c2}$, in the mixed state of high-$\kappa$ $s$-wave superconductors is investigated in framework of the quasiclassical nonlocal Eilenberger theory. Quasiparticle scattering by impurities and lowering of the temperature reduce the value of $\xi_h$ to values much less than $\xi_{c2}$. This is different from the prediction of the local Ginzburg-Landau theory where $\xi_h$ is scaled by $\xi_{c2}$. Detailed comparison with the behavior of the order parameter coherence length $\xi_1$ is done. It is found that impurities influence by different way on $\xi_h$ and $\xi_1$. The curve $\xi_h/\xi_{c2}(B/B_{c2})$ shifts downward with increasing of impurity scattering rate while $\xi_1/\xi_{c2}(B/B_{c2})$ curve shifts upward in this case.

The detailed properties of the vortex structure, such as its field dependence, attract much attention both in the conventional $s$-wave superconductors and in high-$T_c$ superconductors. Several important means to probe the vortex structure are available experimentally in various superconductors (see review in Ref. [1]). The vortex core size is determined from the $\mu$SR measurements by fitting it into a theoretical function for $B(r)$ that includes a cutoff function $F(\mathbf{G}, \xi_h)$, where $\mathbf{G}$ refers to the reciprocal lattice vectors. The parameter $\xi_h$ is the cutoff $\mathbf{G}_{max}$ of the sum over the reciprocal lattice. This takes away the divergence of the sum over the $\mathbf{G}$ in the expression for the field distribution in the London approach. The cutoff cannot be improved within the London theory; to this end, one should use a theory which is able to handle the core structure properly. The functional form of $F(\mathbf{G}, \xi_h)$ depends on the spatial dependence of the superconducting order parameter $\Delta(r)$ in the core region. Cutoff function $F(\mathbf{G}, \xi_h)$ was obtained in the variational approach of the Ginzburg-Landau (GL) equations [2] (the Hao-Clem theory (HC), the analytical GL theory (AGL)) and the field dependence of $\xi_h$ was calculated ($\xi_v$ in a notation of the AGL theory). In this model, $\xi_h/\xi_{c2}$ is a universal function of $B/B_{c2}$. Here, $\xi_{c2}$ is determined from the relation $B_{c2} = \Phi_0/2\pi\xi_{c2}^2$, where $B_{c2}$ is an upper critical field and $\Phi_0$ is a flux quantum. Analyzed with this method, $\mu$SR experimental results in $V_3Si$, $Nb_3Sn$, $NbSe_2$, $YNi_2BC$ and $LuNi_2B_2C$ in intermediate magnetic fields and low temperatures showed that $\xi_h/\xi_{c2} \ll 1$ [1], which needs explanations. In the AGL theory, the equality $\xi_h = \xi_1$ is suggested. Here, the order characteristic length $\xi_1$ is determined as $1/\xi_1 = (\partial|\Delta(r)|/\partial r)_{r=0}/|\Delta_{NN}|$, where $|\Delta_{NN}|$ is the maximum value of the order parameter along the nearest-neighbor direction which is the direction of taking the derivative.

The microscopical theory valid in the whole temperature range is the quasiclassical Eilenberger theory. The cutoff parameter can be found from the fitting of the calculated magnetic field distribution obtained from the Eilenberger equations to the Hao-Clem type field distribution [3]

$$h_{EHC}(\mathbf{r}) = \frac{\Phi_0}{S}\sum_{\mathbf{G}}\frac{F(G)e^{i\mathbf{Gr}}}{1+\lambda^2 G^2}, \tag{1}$$

where $F(\mathbf{G}) = uK_1(u)$, $K_1(u)$ is the modified Bessel function, $u = \xi_h G$ and $S$ is the area of the vortex lattice unit cell. In Eq. (1), $\lambda(T)$ is calculated from microscopical theory and renormalized by nonmagnetic impurity scattering.

We solve the quasiclassical self-consistent Eilenberger equations for triangular FLL and $s$-wave pairing symmetry. Quasiclassical Green functions $f$ and $g$ can be parameterized with the Riccati transformation of the Eilenberger equations via functions $a$ and $b$ [4]

$$\bar{f} = \frac{2a}{1+ab}, \quad f^{\dagger} = \frac{2b}{1+ab}, \quad g = \frac{1-ab}{1+ab}, \tag{2}$$

satisfying the nonlinear Riccati equations. In Born approximation for the nonmagnetic impurity scattering we have

$$\mathbf{n}\cdot\nabla a = -a[2(\omega_n + G) + i\mathbf{n}\cdot\mathbf{A}] + (\Delta + F) - a^2(\Delta^* + F^*), \tag{3}$$

$$\mathbf{n}\cdot\nabla b = b\,[2(\omega_n + G) + i\mathbf{n}\cdot\mathbf{A}] - (\Delta^* + F^*) + b^2(\Delta + F), \tag{4}$$

where $\omega_n = \pi T(2n+1)$, $F = 2\pi\,\langle f\rangle\cdot\Gamma$ and $G = 2\pi\,\langle g\rangle\cdot\Gamma$. Here, $\Gamma = \pi n_i N_F|u|^2$ is the impurity scattering rate ($u$ is impurity scattering amplitude) and $\mathbf{n}$ is a unit vector of the Fermi velocity. The impurity renormalization correction in Eqs. (3) and (4) are averaged over Fermi surface and can be reduced to averages over the polar angle $\theta$, i.e. $\langle\ldots\rangle = (1/2\pi)\int\ldots d\theta$. To take into account the influence of screening, the vector potential $\mathbf{A}(\mathbf{r})$ in Eqs. (3) and (4) is obtained from the equation $\nabla\times\nabla\times\mathbf{A_E} = \frac{4}{\kappa^2}\mathbf{J}$, where the supercurrent $\mathbf{J}(\mathbf{r})$ is given in terms of $g(\omega_n,\theta,\mathbf{r})$ by

$$\mathbf{J}(\mathbf{r}) = 2\pi T\sum_{\omega_n>0}^{\omega_c}\int_0^{2\pi}\frac{d\theta}{2\pi}\frac{\hat{\mathbf{k}}}{i}g(\omega_n,\theta,\mathbf{r}). \tag{5}$$

Here $\mathbf{A}$ and $\mathbf{J}$ are measured in units of $\phi_0/2\pi\xi_0$ and $2ev_F N_0 T_c$, respectively. The self-consistent condition for the pairing potential $\Delta(\mathbf{r})$ is given by

$$\Delta(\mathbf{r}) = V^{SC}2\pi T\sum_{\omega_n>0}^{\omega_c}\int_0^{2\pi}\frac{d\theta}{2\pi}f(\omega_n,\theta,\mathbf{r}), \tag{6}$$

where $V^{SC}$ is the superconducting coupling constant and $\omega_c$ is the ultraviolet cutoff frequency determining $T_{c0}$ [3]. All over our paper, the energy, the temperature, and the length are measured in units of $T_{c0}$ and the characteristic length $\xi_0 = v_F/T_{c0} = \xi_{BCS}\pi\Delta_0/T_{c0}$. Here $\xi_{BCS} = v_F/\pi\Delta_0$, where $v_F$ is the Fermi velocity and $\Delta_0$ is temperature dependent uniform gap. The magnetic field $\mathbf{h}$ is given in units of $\phi_0/2\pi\xi_0^2$. The impurity scattering rates are in units of $2\pi T_{c0}$. In computations the ratio $\kappa = \lambda_{L0}/\xi_0 = 10$ is used. It corresponds to $\kappa_{GL} = 43.3$ [4]. The Riccati equations are solved by the Fast Fourier Transform (FFT) method [3, 5].

A strong decrease in $\xi_h/\xi_{c2}$ with a decreasing temperature is clearly visible in Fig. 1 at $\Gamma = 0.5$. This can be explained by the Kramer-Pesch effect [6]. This effect was observed in the $\mu$SR investigation of the $NbSe_2$ single crystal [1]. The change of the shape of the $\xi_h(B)$ curve in different fields with an increasing scattering rate $\Gamma$ is shown in detail in Fig. 2 at $T/T_{c0} = 0.5$.

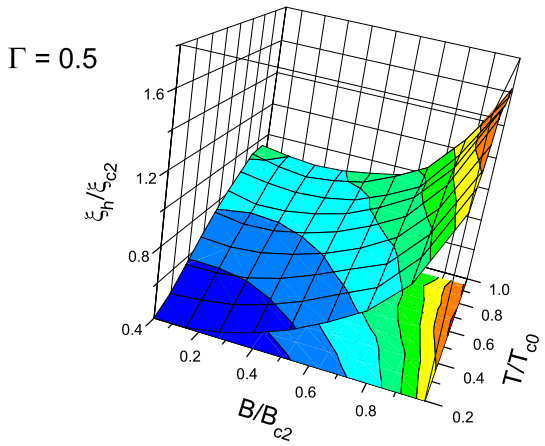


**Figure 1.** The magnetic field dependence of $\xi_h/\xi_{c2}$ at different temperatures with impurity scattering values $\Gamma = 0.5$.

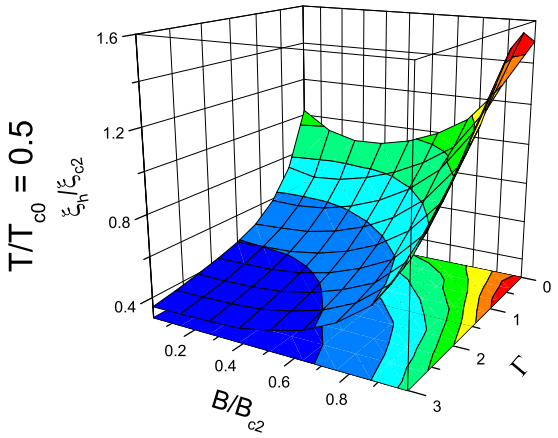


**Figure 2.** The magnetic field dependence of $\xi_h/\xi_{c2}$ with different impurity scattering values $\Gamma$ at the temperature $T/T_{c0} = 0.5$.

Strong suppression of the $\xi_h/\xi_{c2}$ to values much lower than 1 at an increasing $\Gamma$ is also visible from this figure. This is different from the prediction of the local Usadel theory where $\xi_h$ is scaled by $\xi_{c2}$ and the ratio $\xi_h/\xi_{c2}$ is not dependent on impurity scattering [7, 8]. It means that the nonlocal effects are important for the description of the vortex core even in the "dirty" limit. This is the main result of our paper. The low $\xi_h/\xi_{c2}$ values obtained are consistent with the experimental observation in some high-$\kappa$ low-$T_c$ superconductors.

In Figs. 1 and 2, the normalization constant $\xi_{c2}$ depends on the impurity scattering rate $\Gamma$. It is well known that at a high $\Gamma$, the $\xi_{c2} \sim \sqrt{1/\Gamma} \sim \sqrt{l}$, where $l$ is the mean-free path. Therefore, the decreasing of the ratio $\xi_h/\xi_{c2}$ with $\Gamma$ implies a strong dependence of $\xi_h$ on $l$. It is found that $\xi_h$ in dirty superconductors can be scaled with the relaxation time $\tau$, $\xi_h(B,T,\tau) = \xi_{pure}(B,T)/(1 + \frac{\tau_0(B,T)}{\tau})$, where $\xi_{pure}(B,T)$ is the effective coherence length in clean superconductors [3] and $\tau_0$ is a characteristic relaxation time. This results in $\xi_h \sim l$ dependence at a high $\Gamma$ similar to the behavior of the nonlocality radius resulting in the decrease of $\xi_h/\xi_{c2}$ versus $B/B_{c2}$ at a high $\Gamma$, as shown in Fig. 2.

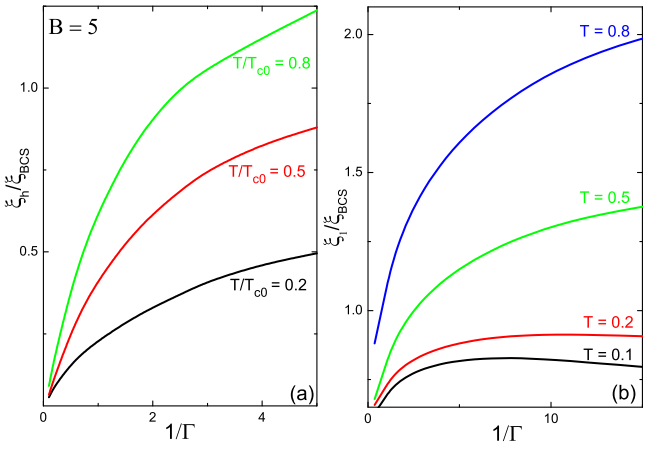


**Figure 3.** (a) The magnetic field dependence of $\xi_h/\xi_{BCS}$ at $B = 5$ at different temperatures. (b) The magnetic field dependence of $\xi_1/\xi_{BCS}$ at different temperatures from Ref. [9].

Such a rapid decrease of $\xi_h$ can be compared with the behavior of the another characteristic length $\xi_1$. It has been found that at low temperatures impurity scattering suppresses Kramer-

Pesch effect in $\xi_1(T)$ dependence, resulting in the nonmonotonous behavior of $\xi_1(\Gamma)$. This can be seen from Fig. 3, where the normalization constant $\xi_{BCS}$ is used ($\xi_{BCS}$ is not dependent on $\Gamma$). It is apparent that $\xi_h$ monotonously decreases with $1/\Gamma$ (Fig. 3 (a)) in contrast to the nonmonotonous behavior of $\xi_1$ for a single vortex obtained from Ref. [9] (Fig. 3 (b)). The different behavior of $\xi_h$ and $\xi_1$ is also visible when using the $\Gamma$-dependent normalization constant $\xi_{c2}$. This is shown in Fig. 4, which presents the curves $\xi_h/\xi_{c2}(B/B_{c2})$ at $T/T_{c0} = 0.15$ (Fig. 4 (a)) and $\xi_1/\xi_{c2}(B/B_{c2})$ at $T/T_{c0} = 0.1$ (Fig. 4 (b)) obtained from Ref. [4] at different scattering rates. The curve $\xi_h/\xi_{c2}(B/B_{c2})$ shifts downward with an increasing impurity scattering rate, while the $\xi_1/\xi_{c2}(B/B_{c2})$ curve shifts upward in this case. The high scattering limit for $\xi_1(B)$ dependence (Fig. 4 (b)) looks similar to Usadel theory prediction [7]. However, the different behavior of $\xi_h(B)$ at a high $\Gamma$ (Fig. 4 (a)) means that the local limit [8] is achieved more slowly for $\xi_h$ than for $\xi_1$ or it is not achieved at all. The high scattering limit of the Eilenberger theory for $\xi_1$ was investigated in Ref. [9] for the single vortex problem , and in addition, the "dirty" limit was not observed clearly.

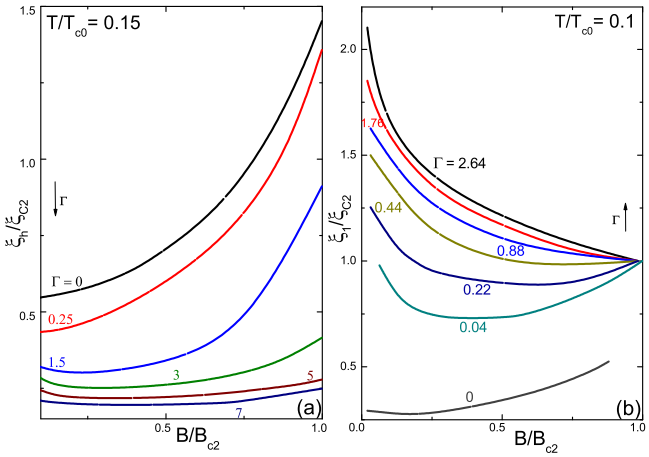


**Figure 4.** (a) The magnetic field dependence of $\xi_h/\xi_{c2}$ at $T/T_{c0} = 0.15$ at different impurity scattering rates $\Gamma$. (b) The magnetic field dependence of $\xi_1/\xi_{c2}$ at $T/T_{c0} = 0.1$ at different impurity scattering rates $\Gamma$ from Ref. [4].

To conclude, the field distribution of the mixed state in dirty $s$-wave superconductors in a wide temperature and field range is investigated in the framework of the nonlocal Eilenberger theory. The normalized magnetic field dependences of the cutoff parameter $\xi_h/\xi_{c2}(B/B_{c2})$ responsible for the line shape of the $\mu$SR resonance are obtained. It is found that this dependence is nonuniversal and depends on the impurity scattering rate $\Gamma$ and the temperature. At high enough values of $\Gamma/2\pi T_{c0} \geq 0.5$, the dependence plateaus in the intermediate field range and the low temperatures, and $\xi_h(B)/\xi_{c2}$ is of the order of 0.25. The strong suppression of $\xi_h/\xi_{c2}$ with $\Gamma$ can explain the experimental results in many low-temperature superconductors ($V_3Si$, $NbSe_2$ and $LuNi_2B_2C$).

This work was supported by Finnish Cultural Foundation.

## References

[1] Sonier J E 2007 *Rep. Prog. Phys.* **70** 1717
[2] Hao Z, Clem J R, McElfresh M W, Civale L, Malozemoff A P and Holtzberg F 1991 *Phys. Rev. B* **43** 2844
[3] Laiho R, Safonchik M and Traito K B 2008 *Phys. Rev. B* **78** 064521
[4] Miranović P, Ichioka M and Machida K 2004 *Phys. Rev. B* **70** 104510
[5] Belova P, Traito K B and Lähderanta E 2011 *J. Appl. Phys.* **110** 033911
[6] Nakai N, Miranović P, Ichioka M and Machida K 2006 *Phys. Rev. B* **73** 172501
[7] Golubov A A and Hartmann U 1994 *Phys. Rev. Lett.* **72** 3602
[8] Sonier J E, Kiefl R F, Brewer J H, Chakhalian J, Dunsiger S R, MacFarlane W A, Miller R I, Wong A, Luke G M and Brill J W 1997 *Phys. Rev. Lett.* **79** 1742
[9] Hayashi N, Kato Y and Sigrist M 1995 *J. Low Temp. Phys.* **139** 79

# PUBL. 5

**P. Belova, I. Zakharchuk, M. Safonchik, K. B. Traito and E. Lähderanta**, Vortex lattice form factor in stoichiometric and nonstoichiometric iron pnictide superconductors, *Physica C*, submitted.

# Vortex lattice form factor in stoichiometric and nonstoichiometric iron pnictide superconductors

P. Belova[a,b,*], I. Zakharchuk[a,c], M. Safonchik[a,d], K. B. Traito[a], E. Lähderanta[a]

[a] *Lappeenranta University of Technology, P.O. Box 20, FI-53851, Lappeenranta, Finland*
[b] *Petrozavodsk State University, Lenin str. 33, RU-185640, Petrozavodsk, Russia*
[c] *Saint-Petersburg Electrotechnical University, Popov str. 5, RU-197376, St.Petersburg, Russia*
[d] *A. F. Ioffe Physico-Technical Institute, St. Petersburg, 194021, Russia*

**Abstract**

The vortex lattice form factor and the cutoff parameter $\xi_h$ in stoichiometric and nonstoichiometric iron pnictides are calculated using the Eilenberger approach. It is generally accepted that the nodeless $s^{\pm}$ pairing state is realized in majority of over-doped iron pnictides (e.g. $BaFe_{1.82}Co_{0.18}As$), while nodes in a gap are observed in the over-doped $KFe_2As_2$ compound, implying a $d_{x^2-y^2}$-wave pairing state. The stoichiometrical LiFeAs without antifferomagnetic ordering is considered as a candidate for the implementation of the $s_{++}$ symmetry. Different impurity scattering rate dependences of the cutoff parameter $\xi_h$ are found determining the form factor for $s^{\pm}$ and $s_{++}$ cases. The $s^{\pm}$ pairing symmetry results in different effects of intraband ($\Gamma_0$) and interband ($\Gamma_\pi$) impurity scattering on $\xi_h$. It is found that $\xi_h/\xi_{c2}$ decreases with the $\Gamma_0$ leading to values much less than those predicted by the analytical Ginzburg-Landau (AGL) theory for a high $\Gamma_0$, where $\xi_{c2} = 1/\sqrt{B_{c2}}$ in our units. At a very high $\Gamma_0$, the interband scattering suppresses $\xi_h/\xi_{c2}$ considerably less than the one in the whole field range making it flat. If $\Gamma_0$ and $\Gamma_\pi$ are small and equal, then the $\xi_h/\xi_{c2}(B/B_{c2})$ dependence behaves like that of the AGL model and shows a minimum value much higher than that obtained for $s_{++}$ superconductors. With a high $\Gamma_\pi$ the dependence of $\xi_h/\xi_{c2}(B/B_{c2})$ resides above the AGL curve. Such behavior is quite different from that in the $s_{++}$ pairing symmetry where intraband and interband scattering rates act in a similar way and $\xi_h/\xi_{c2}$ decreases monotonously with impurity scattering and resides below the AGL curve. In $d$-wave superconductors, $\xi_h/\xi_{c2}$ always increases with the scattering rate $\Gamma$. Our results can explain the small angle neutron scattering (SANS) and muon spin rotation ($\mu$SR) experimental data.

*Keywords:* quasiclassic, mixed state, Eilenberger, Kramer-Pesch.

## 1. Introduction

Muon spin rotation ($\mu$SR) [1] and small angle neutron scattering (SANS) [2] are powerful local microscopic tools for characterizing the magnetic properties of materials, in superconducting or other states. In the presence of a vortex lattice (VL), the spatial variation in the magnetic field distribution results in a dephasing of the muon spin polarization and a relaxation of the precession signal. The Fourier transform of the spin-polarization function essentially reveals the field distribution which exhibits a characteristic Abrikosov line shape. The line shape (or equivalently the relaxation function in the time domain) determined by the form factor depends on the lattice geometry, magnetic field penetration depth $\lambda$, cutoff parameter $\xi_h$, and the amount of lattice disorder which can be important in nonstoichiometric iron pnictides (such as $BaFe_{1.82}Co_{0.18}As$) [3].

SANS measurements are able to observe the structure of the flux line lattice in stoichiometrical iron pnictides such as LiFeAs [2] and $KFe_2As_2$ [4]. For all fields, the fitted peak position agrees within the experimental error with the expected radius of the diffraction ring $q_\triangle = 4\pi/a_\triangle\sqrt{3}$, calculated for a perfect triangular VL with the lattice parameter $a_\triangle = \sqrt{2\Phi_0/B\sqrt{3}}$, where $\Phi_0$ is the magnetic

*Corresponding author
*Email address:* Polina.Belova@lut.fi (P. Belova )

flux quantum. The integrated intensity $I$ corresponding to 1/6 of the diffraction ring (one Bragg spot of a triangular vortex lattice), obtained from the rocking curve, is proportional to the modulus squared of the VL form factor $F(q,T)$ [2], i.e. the Fourier transform of the 2D magnetic flux modulation within the sample. The good quality of stoichiometric LiFeAs single crystals was confirmed with recent observation of the Kramer-Pesch effect by scanning tunneling microscopy [5].

While the cuprates and conventional phonon-mediated superconductors are characterized by distinct $d$-wave and $s$-wave pairing symmetries with nodal and nodeless gap distributions, respectively, the superconducting gap distributions in iron-based superconductors are rather diversified [6]. For the hole-doped $Ba_{1-x}K_xFe_2As_2$ (Ba122) system, the angle-resolved photoemission spectroscopy (ARPES) experiment revealed multiple nodeless gaps at doping $0.25 < x < 0.7$ [7], which was confirmed by bulk thermal conductivity measurements [8]. The order parameter is fully gapped but changes signs between different Fermi sheets [6, 9]. This situation is referred to as the extended $s^{\pm}$ symmetry. Using an $s^{\pm}$ model for the superconducting gap, a good explanation of experimental results on the penetration depth in Co-doped and K-doped $BaFe_2As_2$ pnictides has been obtained [10]. In this model, the Fermi surface is approximated by two cylindrical pockets centered at $\Gamma$ (hole) and M (electron) points of the Fermi surface, i.e. a two-dimensional limit for a five-band model is proposed. However, further increasing doping to the end member $KFe_2As_2$ only with hole pockets [11], the nodal superconducting gap was found by thermal conductivity [12] and penetration depth [13]. It is now under debate whether this is a $d$-wave gap with symmetry-imposed nodes [14] or an $s$-wave gap with accidental nodes [9, 15].

Unexpected doping effects of Co impurities are found in $K(Fe_{1-x}Co_x)_2As_2$. Firstly, Co doping suppresses superconductivity quickly, and at $x = 0.042$ no superconductivity can be observed down to 50 mK. The critical impurity scattering rate requested to suppress $T_c$ to zero is far smaller than that in $Ba_{0.5}K_{0.5}Fe_2As_2$, suggesting a very different pairing symmetry from the $s$-wave. Secondly, a universal heat conduction is observed for $x = 0$ and 0.034, despite that the scattering rate increases by 70 times. These results all point to a $d$-wave superconducting state in $KFe_2As_2$, not an accidental nodal $s$-wave [16].

To study the effects of impurities on superconductivity, stoichiometrical iron pnictides such as LiFeAs ('111' pnictide) are preferable because the level of impurities can be regulated by doping from clean single crystals up to dirty superconductors. The electronic structure of LiFeAs is quasi-two-dimensional and supports superconductivity in the absence of any notable Fermi surface nesting or static magnetism [2]. Nevertheless, using the functional-renormalization-group method the superconducting order parameter was found to be of the $s^{\pm}$ type, driven by collinear antiferromagnetic fluctuations [17]. While the simple $s^{\pm}$-wave gap function of $\cos k_x \cos k_y$ can describe the overall FS dependence of the SC gap, a moderate gap anisotropy is observed along the outer hole and inner electron FSs, suggesting the complicity of pairing interactions in this material, possibly due to the mixture with another pairing symmetry [18]. By applying ARPES to LiFeAs, a clear fingerprint of the phonon spectrum in the fermionic self-energy was identified and the electron-phonon coupling strength was estimated, which appears to be sufficient to mediate the superconductivity. This result suggests that the superconductivity in pnictides could be based on the conventional phonon pairing enhanced by the van Hove singularity in the electronic density of states and by the strong electron-electron interaction [19]. Moreover, the momentum dependence of the superconducting energy gap rules out coupling through spin fluctuations and the sign change [20]. The ARPES results instead suggest that orbital fluctuations assisted by phonons [21] are the best explanation for superconductivity ($s_{++}$ pairing).

The aim of our paper is to apply the quasiclassical Eilenberger approach to the vortex state of iron pnictides, taking into account different possible pairing symmetries ($s^{\pm}$, $s_{++}$ and $d_{x^2-y^2}$-wave).

## 2. Model

Following to the microscopical Eilenberger theory, the cutoff parameter $\xi_h$ can be found from the fitting of the calculated magnetic field distribution $h_E(\mathbf{r})$ to the Eilenberger - Hao-Clem field distribution $h_{EHC}(\mathbf{r})$ [22]

$$h_{EHC}(\mathbf{r}) = \frac{\Phi_0}{S} \sum_{\mathbf{G}} \frac{F(G) e^{i\mathbf{G}\mathbf{r}}}{1 + \lambda^2 G^2}, \qquad (1)$$

where $F(\mathbf{G}) = uK_1(u)$, $K_1(u)$ is the modified Bessel function of the second kind, $u = \xi_h G$ and

$S$ is the area of the vortex lattice unit cell. It is important to note that $\xi_h$ in (1) is obtained from solving the Eilenberger equations and does not coincide with the variational parameter $\xi_v$ (analytical Ginzburg-Landau (AGL) model [23]). Using the GL type of the field distribution does not mean a direct connection to the GL theory. It can be taken as a reasonable starting point of the investigation similarly to the empirical approach to the problem [1]. Because we use the same shape of the cutoff function as in Ref. [23], we will call the obtained field distribution the Eilenberger - Hao-Clem field distribution $h_{EHC}(\mathbf{r})$. In Equation (1), $\lambda(T)$ is the penetration depth in the Meissner state. For $s^{\pm}$ and $s_{++}$ pairing symmetries, the penetration depth is calculated in [10] and for the $d$-wave pairing symmetry in Ref. [24]. The form factor $h_{m,n}$ ($m$ and $n$ are integers) is the Fourier component of $h_{EHC}(\mathbf{r})$ (normalized to $B$).

With the Riccati transformation of the Eilenberger equations, quasiclassical Green functions $f$ and $g$ can be parameterized via functions $a$ and $b$ [25]

$$\bar{f} = \frac{2a}{1+ab}, \quad f^{\dagger} = \frac{2b}{1+ab}, \quad g = \frac{1-ab}{1+ab}, \qquad (2)$$

satisfying the nonlinear Riccati equations. In a Born approximation for impurity scattering, we have

$$\begin{aligned} \mathbf{u}\cdot\nabla a &= -a\,[2(\omega_n + G) + i\mathbf{u}\cdot\mathbf{A}] \\ &+ (\Delta + F) - a^2(\Delta^* + F^*), \end{aligned} \qquad (3)$$

$$\begin{aligned} \mathbf{u}\cdot\nabla b &= b\,[2(\omega_n + G) + i\mathbf{u}\cdot\mathbf{A}] \\ &- (\Delta^* + F^*) + b^2(\Delta + F), \end{aligned} \qquad (4)$$

where $\omega_n = \pi T(2n+1)$, $G = 2\pi \langle g \rangle(\Gamma_0 + \Gamma_\pi) \equiv 2\pi \langle g \rangle \Gamma^*$, $F = 2\pi \langle f \rangle(\Gamma_0 - \Gamma_\pi)$ for the $s^{\pm}$ pairing symmetry and $F = 2\pi \langle f \rangle \Gamma^*$ for the $s_{++}$ pairing symmetry. $\Gamma_0 = \pi n_i N_F |u_0|^2$ and $\Gamma_\pi = \pi n_i N_F |u_\pi|^2$ are the intra- and interband impurity scattering rates, respectively ($u_{0,\pi}$ are impurity scattering amplitudes with correspondingly small, or close to $\pi = (\pi, \pi)$, momentum transfer) and $\mathbf{u}$ is a unit vector of the Fermi velocity. In the new gauge, vector-potential $\mathbf{A_E} = \mathbf{A} - \nabla\phi$ is proportional to the superfluid velocity. It diverges as $1/r$ at the vortex center. The flux line lattice (FLL) creates the anisotropy of the electron spectrum. Therefore, the impurity renormalization corrections in Eqs. (3) and (4) averaged over the Fermi surface can be reduced to averages over the polar angle $\theta$,

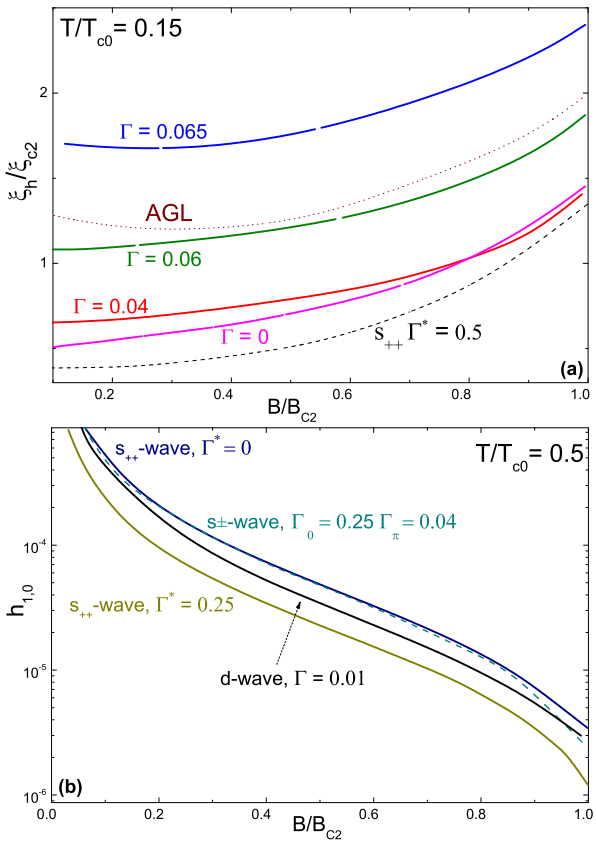


Figure 1: (Color online) (a) The magnetic field dependence of $\xi_h/\xi_{c2}$ at $T/T_{c0} = 0.15$ with the same values of intraband $\Gamma_0$ and interband $\Gamma_\pi$ scattering $\Gamma$ ($\Gamma = 0, 0.04, 0.06, 0.065$) for the $s^{\pm}$-wave symmetry. The dashed line shows the magnetic field dependence of $\xi_h/\xi_{c2}$ for the $s_{++}$ model ($\Gamma^* = 0.5$). The dotted line demonstrates the result of the AGL theory for $\xi_v$ from Eq. (6). (b) The field dependence of the dominant form factor $h_{1,0}$ for the $s^{\pm}$ ($\Gamma_0 = 0.25, \Gamma_\pi = 0.04$, dashed line), $s_{++}$ ($\Gamma^* = 0, 0.25$) and $d_{x^2-y^2}$ ($\Gamma = 0.01$) models.

$\langle \ldots \rangle = (1/2\pi)\int \ldots d\theta$. Since the $f$ function has opposite signs in two bands, $\Gamma_\pi$ has the opposite effect on normal and anomalous self-energies. Due to symmetry, $F = 0$ for $d$-wave pairing. To take into account the influence of screening the vector potential $\mathbf{A}(\mathbf{r})$ in Eqs. (3) and (4) is obtained from the equation $\nabla \times \nabla \times \mathbf{A_E} = \frac{4}{\kappa^2}\mathbf{J}$, where the supercurrent $\mathbf{J}(\mathbf{r})$ is given in terms of $g(\omega_n, \theta, \mathbf{r})$ by

$$\mathbf{J}(\mathbf{r}) = 2\pi T \sum_{\omega_n > 0} \int_0^{2\pi} \frac{d\theta}{2\pi} \frac{\hat{\mathbf{k}}}{i} g(\omega_n, \theta, \mathbf{r}). \qquad (5)$$

Here, $\mathbf{A_E}$ and $\mathbf{J}$ are measured in units of $\Phi_0/2\pi\xi_0$ and $2ev_F N_0 T_c$, respectively. The spatial variation of the internal field $h_E(\mathbf{r})$ is determined through $\nabla \times \mathbf{A_E} = \mathbf{h_E}(\mathbf{r})$. The self-consistent condition for

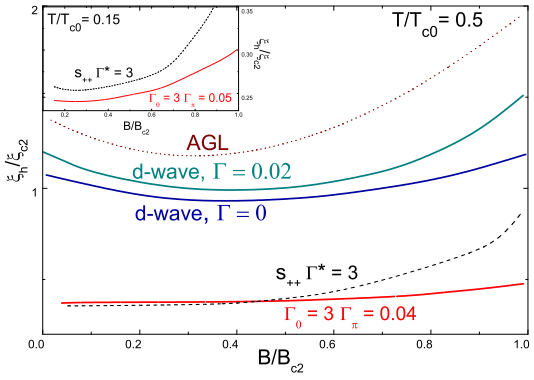


Figure 2: (Color online) The magnetic field dependence $\xi_h/\xi_{c2}$ for $s^{\pm}$ model ($\Gamma_0 = 3, \Gamma_\pi = 0.04$), $s_{++}$ model ($\Gamma^* = 3$, dashed line) and $d_{x^2-y^2}$-wave model ($\Gamma = 0$ and 0.02) at $T/T_{c0} = 0.5$. The dotted line demonstrates the result of the AGL theory for $\xi_v$ from Eq. (6). The inset shows the magnetic field dependence $\xi_h/\xi_{c2}$ for $s^{\pm}$ model ($\Gamma_0 = 3, \Gamma_\pi = 0.05$) and $s_{++}$ model ($\Gamma^* = 3$, dotted line) at $T/T_{c0} = 0.15$.

the pairing potential $\Delta(\mathbf{r})$ is given in Ref. [22]. In this paper, the energy, the temperature, and the length are measured in units of $T_{c0}$ and the coherence length $\xi_0 = v_F/T_{c0}$, where $v_F$ is the Fermi velocity. The magnetic field $\mathbf{h}$ is given in units of $\Phi_0/2\pi\xi_0^2$. In the equations, impurities are in units of $T_{c0}$, but in the plots impurities are in units of $2\pi T_{c0}$. In computations, the ratio $\kappa = \lambda_{L0}/\xi_0 = 10$ is used.

## 3. Results

First, we study the case of weak scattering. This case can be realized in stoichiometrical pnictides such as LiFeAs and $KFe_2As_2$. Fig. 1 (a) presents the $\xi_h/\xi_{c2}$ magnetic field dependence at $\Gamma_0 = \Gamma_\pi = \Gamma = 0, 0.04, 0.06, 0.065$ and $T/T_{c0} = 0.15$. The dashed line shows the magnetic field dependence of $\xi_h/\xi_{c2}$ for the $s_{++}$ model ($\Gamma^* = 0.5$). The dotted line demonstrates the result of the AGL theory for $\xi_v$ [23]

$$\xi_v = \xi_{c2}(\sqrt{2} - \frac{0.75}{\kappa_{GL}})(1+b^4)^{1/2} \times \\ \times[1-2b(1-b)^2]^{1/2}. \quad (6)$$

This dependence with $\xi_v$ as a fitting parameter is often used for the description of the $\mu$SR experimental results [1]. As can be seen from this picture, the shape of the curve does not change considerably, but the absolute values of $\xi_h/\xi_{c2}$ depend crucially on it. At low $\Gamma$ values, $\xi_h/\xi_{c2}$ resides below the AGL curve and moves above it at a high $\Gamma$. $KFe_2As_2$ compound is considered as a candidate for realization of $d$-wave symmetry [16]. Fig. 2 (a) shows that in $d$-wave superconductors, $\xi_h/\xi_{c2}$ increases with $\Gamma$ similarly to the case of the $s^{\pm}$ symmetry with $\Gamma_0 = \Gamma_\pi$ (Fig. 1 (a)). This can be understood from the comparison of the Ricatti equations of the $s^{\pm}$ and $d$-wave pairings. In both cases, the renormalization factor $F = 0$ due to a cancelation of the intraband and interband impurity scattering rates in $s^{\pm}$ pairing or symmetry reason, $\langle f \rangle = 0$ for $d$-wave pairing.

The field dependence of the dominant form factor $h_{1,0}$ was calculated in [26] for the clean $s$- and $d_{x^2-y^2}$-wave pairings. The two pairing cases showed a similar dependence on the applied field. Fig. 1 (b) shows the magnetic field dependence of the dominant form factor $h_{1,0}$ for the $s^{\pm}$ ($\Gamma_0 = 0.25, \Gamma_\pi = 0.04$, dashed line), $s_{++}$ ($\Gamma^* = 0, 0.25$) and $d_{x^2-y^2}$ ($\Gamma = 0.01$) models. The obtained field dependences show behaviour suchlike in [26]. Nevertheless, absolute values are different and depend on impurity scattering, decreasing in the $s_{++}$-wave pairing. By introducing interband scattering in the $s^{\pm}$ symmetry, the value of the dominant form factor $h_{1,0}$ increases.

The obtained $\xi_h(B \to 0)/\xi_{c2} = 1.75$ in the $s^{\pm}$ model is much nearer to the experimental results [2] than in the $s_{++}$ model, where strong reduction of $\xi_h$ is visible. However, this requires an excessively high value of $\Gamma_\pi > 0.064$, and therefore, the sample would be in the gapless state in this case. This is in contradiction to the observed value of the gap according to the ARPES measurements [2]. Thus, the experimental results give the anomalously high value of $\xi_h/\xi_{c2}$ for LiFeAs. Pair breaking effects can improve the comparison between theory and experiments, but it is not enough to resolve the contradiction. It has been shown that an expansion of the vortex cores cuprate superconductors can result from a strengthening of antiferromagnetic (AF) correlations competing with superconductivity [27]. AF fluctuations have also been observed in LiFeAs [28]. In the framework of our model, it means that the local increase of $\Gamma_\pi$ is induced by AF fluctuations inside the vortex core. In this case, the $\xi_h$ (determined by $\mu$SR or SANS measurements) is connected with $\Gamma_\pi^{core}$ and the value of the gap (determined by ARPES) is dependent on $\Gamma_\pi^{bulk}$, where $\Gamma_\pi^{core} > \Gamma_\pi^{bulk}$ resulting from AF. The investigation of the microwave surface impedance of LiFeAs sin-

gle crystals under finite magnetic fields implies that the mean free path inside the vortex core is much shorter than that outside, and is close to the core radius [29]. The increase of the orbital fluctuations in the vortex core in the $s_{++}$ model [21] may also be important.

Next, we consider the case of strong scattering. This case can be realized in nonstoichiometrical pnictides such as Co- or K-doped $BaFe_2As_2$. The superfluidity density in pnictides often shows the power shape dependence with the exponent approximately equals two at low temperatures. This law was explained by the $s^{\pm}$ model with the parameters $\Gamma_0 = 3$ and $\Gamma_\pi = 0.04 - 0.06$ [10]. In spite of the success of the $s^{\pm}$ model, there are some indications that a conventional $s$-wave state without sign reversal ($s_{++}$-wave state) is also a possible candidate for iron pnictides [21]. Fig. 2 shows $\xi_h/\xi_{c2}(B/B_{c2})$ for the $s^{\pm}$ model ($\Gamma_0 = 3, \Gamma_\pi = 0.04$), the $s_{++}$ model ($\Gamma^* = 3$, dashed line) at $T/T_{c0} = 0.5$, the dotted line demonstrates the result of the AGL theory for $\xi_v$ from Eq. (6). The inset to Fig. 2 presents $\xi_h/\xi_{c2}(B/B_{c2})$ dependences for the $s^{\pm}$ model ($\Gamma_0 = 3, \Gamma_\pi = 0.05$) and the $s_{++}$ model ($\Gamma^* = 3$, dotted line) at $T/T_{c0} = 0.15$. It can be seen that $\xi_h/\xi_{c2}$ is strongly suppressed in $s^{\pm}$ pairing in comparison to the $s_{++}$ pairing specially at high field range. This can be explained by the fact that in superconductors without interband pair breaking, the increase in the high field range is connected to the field-dependent pair breaking when approaching the upper critical field. This type of behavior is cut off by the impurity pair breaking, slowing the growth of $\xi_h$. The low field rise of $\xi_h/\xi_{c2}$ in the $s_{++}$ pairing correlates with the nonmonotonous field dependence of the order parameter coherence length in the 'dirty' limit and low temperatures [25]. The small value of the ratio $\xi_h/\xi_{c2} \sim 0.4$ which is comparable with our theoretical prediction, Fig. 2, has been obtained in a $\mu$SR investigation of a Co-doped $BaFe_2As_2$ [3]. In Ref. [3], the magnetic field distribution shape of the sample was explained by effects of a field-induced magnetic order. Magnetic susceptibility measurements show a sharp superconducting transition and complete diamagnetic screening, and energy dispersive x-ray spectroscopy measurements on different parts of the crystal indicate a uniform Co composition [3]. Therefore, the effects of disorder in the vortex lattice cannot be so strong. Our consideration shows the importance of impurity scattering even in the triangular lattice giving another possible explanation for the experimental results. However, fits assuming magnetic order exhibit a linear temperature dependence well below $T_c$, which is suggestive of gap nodes [3]. Nevertheless, London penetration depth measurements in the Meissner state do not agree with these results [30].

Many experiments have reported observations of field-induced magnetic order in the high-$T_c$ superconductors. It has been noted that the periodicity of the charge ordering observed in STM [31] could be consistent with inelastic neutron-scattering experiments on optimally doped $La_{2-x}Sr_xCuO_4$ ($x = 0.163$) that show a field-induced signal in the low-frequency spin-fluctuation spectrum, near the $(\pi, \pi)$ point in reciprocal space [32]. More local measurements using spatially resolved NMR also provide strong evidence for the presence of antiferromagnetic order in the vortex cores of near-optimally doped $YBa_2Cu_3O_{7-\delta}$ [33] and $Tl_2Ba_2CuO_{6+\delta}$ [34]. Muon-spin resonance measurements of the magnetic field distribution of underdoped $YBa_2Cu_3O_{6.5}$ reveal a structure in the high-field tail that is not seen in optimally doped $YBa_2Cu_3O_{6.95}$ and is consistent with static antiferromagnetism [35]. Elastic neutron-scattering has shown a strong enhancement of incommensurate static antiferromagnetism in an applied magnetic field in underdoped $La_{2-x}Sr_xCuO_4$ with $x = 0.10$ [36] and with $x = 0.12$ [37]. The antiferromagnetism is observed to have a very long correlation length $> 400$ Å showing that AFM and superconductivity coexist in the bulk [36]. Similar results are seen in elastic neutron scattering experiments on $La_2CuO_{4+y}$ [38]. The picture that emerges from these various measurements is that static or dynamic antiferromagnetic order is induced, or at least strongly enhanced, by an applied magnetic field. This antiferromagnetic order appears to be nucleated at the vortex cores, and extends into the bulk of the superconductor with a correlation length that is much longer than the superconducting coherence length.

The fractional shift within the superconducting state was found in $Ba(Fe_{1-x}Co_x)_2As_2$ [39]. The shift was largest for the samples with the highest $T_c$ and highest superfluid density $n_s/m* \propto 1/\lambda^2$. Previous $\mu$SR studies of the electron-doped cuprate superconductor $Pr_{2-x}Ce_xCuO_4$ also exhibited a positive frequency shift below $T_c$, which was interpreted as evidence of field-induced magnetism [40]. In that case, the absolute shift decreased with increasing field (not just the fractional shift), indicating that the induced fields were perpendicular to the applied

field. The fact that the absolute shift is roughly field-independent indicates that the induced moments must be parallel to the applied field and have a ferromagnetic character (antiferromagnetic fields would split the precession line, rather than shift it).

## 4. Conclusion

Eilenberger equations have been solved for superconductors with isotropic $s^{\pm}$, $s_{++}$ and anisotropic $d_{x^2-y^2}$ pairing symmetries in the mixed state. These symmetries are proposed for the pairing state of the Fe-pnictides. It is found that Eilenberger equations can be reduced to the London model with only one parameter, $\xi_h(B)$. This length determines the form factor of the FLL. Thr value of thedominant form factor depends on impurity scattering by different ways in various pairing symmetries. The normalized value of $\xi_h/\xi_{c2}$ decreases with temperature due to the Kramer-Pesch effect, which was recently observed in the LiFeAs compound by scanning tunneling microscopy [5]. It is found that the magnetic field dependence of $\xi_h/\xi_{c2}$ is nonuniversal for $s^{\pm}$ pairing; depending on the chosen parameter set it can reside both below and above the AGL curve. Such behavior is quite different from that in an $s_{++}$ pairing symmetry where intraband and interband scattering rates act in a similar way and $\xi_h/\xi_{c2}$ always decreases with impurity scattering. In $d$-wave superconductors, $\xi_h/\xi_{c2}$ always increases with the scattering rate $\Gamma$.

This work was supported by the Finnish Cultural Foundation.

## References


[1] J. E. Sonier Rep. Prog. Phys. 70 (2007) 1717.

[2] D. S. Inosov, J. S. White, D. V. Evtushinsky, I. V. Morozov, A. Cameron, U. Stockert, V. B. Zabolotnyy, T. K. Kim, A. A. Kordyuk, S. V. Borisenko, E. M. Forgan, R. Klingeler, J. T. Park, S. Wurmehl, A. N. Vasiliev, G. Behr, C. D. Dewhurst, V. Hinkov, Phys. Rev. Lett. 104 (2010) 187001.

[3] J. E. Sonier, W. Huang, C. V. Kaiser, C. Cochrane, V. Pacradouni, S. A. Sabok-Sayr, M. D. Lumsden, B. C. Sales, M. A. McGuire, A. S. Sefat, D. Mandrus, Phys. Rev. Lett. 106 (2011) 127002.

[4] H. Kawano-Furukawa, C. J. Bowell, J. S White, R. Heslop, A. Cameron, E. Forgan, K. Kihou, C. H. Lee, A. Iyo, H. Eisaki, T. Saito, H. Fukazawa, Y. Kohori, R. Cubitt, C. D. Dewhurst, J. L. Gavilano, M. Zolliker, arXiv:1005.4468v2 (2010).

[5] T. Hanaguri, K. Kitagawa, K. Matsubayashi, Y. Mazaki, Y. Uwatoko, H. Takagi, Phys. Rev. B 85 (2012) 214505.

[6] P. J. Hirschfeld, M. M. Korshunov, I. I. Mazin, Rep. Prog. Phys. 74 (2011) 124508.

[7] K. Nakayama, T. Sato, P. Richard, Y. M. Xu, T. Kawahara, K. Umezawa, T. Qian, M. Neupane, G. F. Chen, H. Ding, T. Takahashi, Phys. Rev. B 83 (2011) 020501(R).

[8] X. G. Luo, M. A. Tanatar, J. P. Reid, H. Shakeripour, N. Doiron-Leyraud, N. Ni, S. L. Bud'ko, P. C. Canfield, H. Luo, Z. Wang, H. H. Wen, R. Prozorov, L. Taillefer, Phys. Rev. B 80 (2009) 140503(R).

[9] S. Maiti, M. M. Korshunov, T. A. Maier, P. J. Hirschfeld, A. V. Chubukov, Phys. Rev. B 84 (2011) 224505.

[10] A. B. Vorontsov, M. G. Vavilov, A. V. Chubukov, Phys. Rev. B 79 (2009) 140507(R).

[11] T. Sato, K. Nakayama, Y. Sekiba, P. Richard, Y. M. Xu, S. Souma, T. Takahashi, G. F. Chen, J. L. Luo, N. L. Wang, H. Ding, Phys. Rev. Lett. 103 (2009) 047002.

[12] J. K. Dong, S. Y. Zhou, T. Y. Guan, H. Zhang, Y. F. Dai, Qiu X, X. F. Wang, Y. He, X. H. Chen, S. Y. Li, Phys. Rev. Lett. 104 (2010) 087005.

[13] K. Hashimoto, A. Serafin, S. Tonegawa, R. Katsumata, R. Okazaki, T. Saito, H. Fukazawa, Y. Kohori, K. Kihou, C. H. Lee, A. Iyo, H. Eisaki, H. Ikeda, Y. Matsuda, A. Carringto, T. Shibauchi, Phys. Rev. B 82 (2010) 014526.

[14] R. Thomale, C. Platt, W. Hanke, J. Hu, B. A. Bernevig, Phys. Rev. Lett. 107 (2011) 117001.

[15] K. Suzuki, H. Usui, K. Kuroki, Phys. Rev. B 84 (2011) 144514.

[16] A. F. Wang, S. Y. Zhou, X. G. Luo, X. C. Hong, Y. J. Yan, J. J. Ying, P. Cheng, G. J. Ye, Z. J. Xiang, S. Y. Li, X. H. Chen, arXiv:1206.2030v1 (2012).

[17] C. Platt, R. Thomale, W. Hanke, Phys. Rev. B 84 (2011) 235121.

[18] K. Umezawa, Y. Li, H. Miao, K. Nakayama, Z. H. Liu, P. Richard, T. Sato, He J B, D. M. Wang, G. F. Chen, H. Ding, T. Takahashi, S. C. Wang, Phys. Rev. Lett. 108 (2012) 037002.

[19] A. A. Kordyuk, V. B. Zabolotnyy, D. V. Evtushinsky, T. K. Kim, I. V. Morozov, M. L. Kulié, R. Follath, G. Behr, B. Büchner, S. V. Borisenko, Phys. Rev. B 83 (2011)134513.

[20] S. V. Borisenko, V. B. Zabolotnyy, A. A. Kordyuk, D. V. Evtushinsky, T. K. Kim, I. V. Morozov, R. Follath, B. Büchner, Symmetry 4(1) (2012) 251.

[21] H. Kontani, S. Onari, Phys. Rev. Lett. 104 (2010) 157001.

[22] P. Belova, I. Zakharchuk, M. Safonchik, K. B. Traito, E. Lähderanta, Mod. Phys. Lett. B 26 (2012) 1230013.

[23] Z. Hao, J. R. Clem, M. W. McElfresh, L. Civale, A. P. Malozemoff, F. Holtzberg, Phys. Rev. B 43 (1991) 2844.

[24] D. Xu, S. K. Yip, J. A. Sauls, Phys. Rev. B 51 (1995) 16233.

[25] P. Miranović, M. Ichioka, K. Machida, Phys. Rev. B 70 (2004) 104510.

[26] M. Ichioka, A. Hasegawa, K. Machida, Phys. Rev. B 59 (1999) 8902.

[27] R. Kadono, W. Higemoto, A. Koda, M. I. Larkin, G. M. Luke, A. T. Savici, Y. J. Uemura, K. M. Kojima, T. Okamoto, T. Kakeshita, S. Uchida, T. Ito, K. Oka, M. Takigawa, M. Ichioka, K. Machida, Phys. Rev. B 69 (2004) 104523.

[28] F. L. Pratt, P. J. Baker, S. J. Blundell, T. Lancaster, H. J. Lewtas, P. Adamson, M. J. Pitcher, D. R. Parker,

S. J. Clarke, Phys. Rev. B 79 (2009) 052508.
[29] T. Okada, H. Takahashi, Y. Imai, K. Kitagawa, K. Matsubayashi, Y. Uwatoko, A. Maeda, arXiv:1110.6575v2 (2012).
[30] R. Prozorov, V. G. Kogan, Rep. Prog. Phys. 74 (2011) 124505.
[31] J. E. Hoffman, E. W. Hudson, K. M. Lang, V. Madhavan, H. Eisaki, S. Uchida, J. C. Davis, Science 295 (2002) 466.
[32] B. Lake, G. Aeppli, K. N. Clausen, D. F. McMorrow, K. Lefmann, N. E. Hussey, N. Mangkorntong, M. Nohara, H. Takagi, T. E. Mason, Science 291 (2001) 1759.
[33] V. F. Mitrović, E. E. Sigmund, W. P. Halperin, A. P. Reyes, P. Kuhns, W. G. Moulton Phys. Rev. B 67 (2003) 220503(R).
[34] K. Kakuyanagi, K. Kumagai, Y. Matsuda, M. Hasegawa, Phys. Rev. Lett. 90 (2003) 197003.
[35] R. I. Miller, R. F. Kiefl, J. H. Brewer, J. E. Sonier, J. Chakhalian, S. Dunsiger, G. D. Morris, A. N. Price, D. A. Bonn, W. H. Hardy, Phys. Rev. Lett. 88 (2002) 137002.
[36] B. Lake, H. M. Ronnow, N. B. Christensen, G. Aeppli, K. Lefmann, McMorrow D F, P. Vorderwisch, P. Smeibidl, P. Mangkorntong, T. Sasagawa, Nature 415 (2002) 299.
[37] S. Katano, M. Sato, K. Yamada, T. Suzuki, T. Fukase, Phys. Rev. B 62 (2000) 14677(R).
[38] B. Khaykovich, Y. S. Lee, Erwin R, S. H. Lee, Wakimoto S, K. J. Thomas, M. A. Kastner, R. J. Birgeneau, Phys. Rev. B 66 (2002) 014528.
[39] T. J. Williams, A. A. Aczel, E. Baggio-Saitovitch, S. L. Bud'ko, P. C. Canfield, J. P. Carlo, T. Goko, H. Kageyama, A. Kitado, J. Munevar, N. Ni, S. R. Saha, K. Kirschenbaum, J. Paglione, D. R. Sanchez-Candela, Y. J. Uemura, G. M. Luke, Phys. Rev. B 82 (2010) 094512.
[40] J. E. Sonier, K. F. Poon, G. M. Luke, P. Kyriakou, R. I. Miller, R. Liang, C. R. Wiebe, P. Fournier, R. L. Greene, Phys. Rev. Lett. 91 (2003) 147002.

**ACTA UNIVERSITATIS LAPPEENRANTAENSIS**

**478.** LÄTTILÄ, LAURI. Improving transportation and warehousing efficiency with simulation based decision support systems. 2012. Diss.

**479.** OYOMNO, WERE. Usable privacy preservation in mobile electronic personality. 2012. Diss.

**480.** LINNALA, MIKKO. Simulation and optimization tools in paper machine concept design. 2012. Diss.

**481.** KORPIJÄRVI, JUHA. Aging based maintenance and reinvestment scheduling of electric distribution network. 2012. Diss.

**482.** KORHONEN, JUHAMATTI. Active inverter output filtering methods. 2012. Diss.

**483.** KLODOWSKI, ADAM. Flexible multibody approach in bone strain estimation during physical activity: quantifying osteogenic potential. 2012. Diss.

**484.** VUORENMAA, MARKKU. Osaamisen johtaminen pk-yrityksen kansainvälisen kasvun elinkaarella. 2012. Diss.

**485.** RAUTIAINEN, MARITA. Dynamic ownership in family business systems – a portfolio business approach. 2012. Diss.

**486.** LILIUS, REIJO. THE FINNISH IT INDUSTRIES IN TRANSITION Defining and measuring the Finnish software product and IT services industries by applying theoretical frameworks . 2012. Diss.

**487.** TUOMINEN, PASI. The purpose of consumer co-operation: implications for the management and governance of co-operatives. 2012. Diss.

**488.** SAARI, ESA. Suurnopeus-turbokoneroottoreiden termodynaaminen ja mekaaninen mallinnus sekä rakenneanalyysi. 2012. Diss.

**489.** PAANANEN, MIKKO. On innovative search: the use of internal and external sources of innovation among Finnish innovators. 2012. Diss.

**490.** BELOVA, POLINA. Quasiclassical approach to the vortex state in iron-based superconductors. 2012. Diss.

**491.** HIETANEN, IIRO. Design and characterization of large area position sensitive radiation detectors. 2012. Diss.

**492.** PÄSSILÄ, ANNE. A reflexive model of research-based theatre Processing innovation of the cross-road of theatre, reflection and practice-based innovation activities. 2012. Diss.

**493.** RIIPINEN, TOMI. Modeling and control of the power conversion unit in a solid oxide fuel cell environment. 2012. Diss.

**494.** RANTALAINEN, TUOMAS. Simulation of structural stress history based on dynamic analysis. 2012. Diss.

**495.** SALMIMIES, RIINA. Acidic dissolution of iron oxides and regeneration of a ceramic filter medium. 2012. Diss.

**496.** VAUTERIN, JOHANNA JULIA. The demand for global student talent: Capitalizing on the value of university-industry collaboration. 2012. Diss.

**497.** RILLA, MARKO. Design of salient pole PM synchronous machines for a vehicle traction application. 2012. Diss.

**498.** FEDOROVA, ELENA. Interdependence of emerging Eastern European stock markets. 2012. Diss.

**499.** SHAH, SRUJAL. Analysis and validation of space averaged drag model for numerical simulations of gas-solid flows in fluidized beds. 2012. Diss.

**500.** WANG, YONGBO. Novel methods for error modeling and parameter identification of redundant hybrid serial-parallel robot. 2012. Diss.

**501.** MAXIMOV, ALEXANDER. Theoretical analysis and numerical simulation of spectral radiative properties of combustion gases in oxy/air-fired combustion systems. 2012. Diss.

**502.** KUTVONEN, ANTERO. Strategic external deployment of intellectual assets. 2012. Diss.

**503.** VÄISÄNEN, VESA. Performance and scalability of isolated DC-DC converter topologies in low voltage, high current applications. 2012. Diss.

**504.** IKONEN, MIKA. Power cycling lifetime estimation of IGBT power modules based on chip temperature modeling. 2012. Diss.

**505.** LEIVO, TIMO. Pricing anomalies in the Finnish stock market. 2012. Diss.

**506.** NISKANEN, ANTTI. Landfill gas management as engineered landfills – Estimation and mitigation of environmental aspects. 2012. Diss.

**507.** QIU, FENG. Surface transformation hardening of carbon steel with high power fiber laser. 2012. Diss.

**508.** SMIRNOV, ALEXANDER. AMB system for high-speed motors using automatic commissioning. 2012. Diss.

**509.** ESKELINEN, HARRI, ed. Advanced approaches to analytical and systematic DFMA analysis. 2013.

**510.** RYYNÄNEN, HARRI. From network pictures to network insight in solution business – the role of internal communication. 2013. Diss.

**511.** JÄRVI, KATI. Ecosystem architecture design: endogenous and exogenous structural properties. 2013. Diss.

**512.** PIILI, HEIDI. Characterisation of laser beam and paper material interaction. 2013. Diss.

**513.** MONTO, SARI. Towards inter-organizational working capital management. 2013. Diss.

**514.** PIRINEN, MARKKU. The effects of welding heat input usability of high strength steels in welded structures. 2013. Diss.

**515.** SARKKINEN, MINNA. Strategic innovation management based on three dimensions diagnosing innovation development needs in a peripheral region. 2013. Diss.

**516.** MAGLYAS, ANDREY. Overcoming the complexity of software product management. 2013. Diss.

**517.** MOISIO, SAMI. A soft contact collision method for real-time simulation of triangularized geometries in multibody dynamics. 2013. Diss.

**518.** IMMONEN, PAULA. Energy efficiency of a diesel-electric mobile working machine. 2013. Diss.

**519.** ELORANTA, LEENA. Innovation in a non-formal adult education organisation – multi-case study in four education centres. 2013. Diss.